Towards a More Quantitative Understanding of Intermolecular Interactions: Biologically Significant Intermolecular Clusters

Thesis by

Sakae Suzuki

In Partial Fulfillment of the Requirements
for the Degree of
Doctor of Philosophy

California Institute of Technology
Pasadena, California

1996

(Submitted July 31, 1995)

Acknowledgements

There are many to thank for my satisfying six years at Caltech. First, I would like to thank my advisor, Prof. Geoff Blake, for his generous support, guidance, ideas, inspiration, and, yes, much patience. The daily flash-flood of ideas from Geoff's mouth was difficult to ride at first, but once I learned to catch the wave, the rides took me down canyons full of new perspectives. Much of my enjoyment as a graduate student is tied to his spirit of enjoying science: An image of excited Geoff skipping down the hallway after letting out a free-flowing string of new ideas to improve an experiment is burnt into my memory.

Endless thanks go to my co-worker Paul Stockman for putting up with me for six years in the "Arctic" FIR lab, the "Tropical" roof-top vacuum pump room with fiberglass insulation and frequent oil spills (both anthropogenic and "natural"), and in our office. I learned many valuable lessons from Paul, and enjoyed his company. He generously and graciously contributed to much of the work contained in the thesis. His support throughout the time here has been invaluable. I will also cherish the time spent at his home with Kirsten and, more recently, Hans. I am grateful for their generosity and hospitality.

I owe much to other members of the Blake group. I thank former post-docs Roger Bumgarner for teaching me much about spectroscopy, and Peter Green for teaching me, in addition to science, how to Tele-ski and sharing about his expeditions. I still wouldn't know a thing about football had it not been for my roommate for three years, Dave Rodham, who answered all my questions about American football. Pin Chen's bottom-less capacity for food and willingness to go eat added excitement to eating sessions–lunch, dinner, or snack. Thanks to Jim Kubicki for our trips to Starbucks "Mecca" coffee shop.

I had the privilege of working with many outstanding scientists: Dr. Siddharth Dasgupta kindly taught me how to use *Gaussian 92*. Drs. Jon Hougen, Rick Suenram,

Frank Lovas and Gerry Fraser at NIST were always generous and willing to teach me about spectroscopy. Jennifer Loeser, Matt Elrod, Kun Liu and others in the Berkeley Saykally lab extended to me their wisdom in FIR-VRT spectroscopy. In addition to giving us the DMC simulation codes, Pablo Sandler and Victoria Buch visited us to carefully instruct us on the use of the code. Their generosity is deeply appreciated.

I would like to thank the chemistry faculty for contributing to my education here, especially my committee members who taught me through candidacy and proposal exams, and the thesis defense: Professors Mitchio Okumura, Doug Rees, Ahmed Zewail, Vincent McKoy and Harry Gray.

Much thanks go to the Chemistry staff: Dian Buchness for guiding me through all the requirements; Guy Duremberg for teaching me how to machine, and often making parts absolutely necessary for the experiments in a rush; Tom Dunn for letting me borrow equipment; and Jesse Miller and Darryl Riley for teaching me about vacuum pumps. I received much generous help from the Geology staff: Jan Haskell patiently helped me as the group secretary, Annette McCusker slogged through computer problems with me, and Vick Nenow taught me about electronics and built devices for our group.

Not all of my time was spent in the lab, thanks to my hiking, camping and skiing friends Teri Longin, Matt and Karin Johnson, Jack Hwang, Stew Fisher, and Elaine Marzluff. My sanity was kept intact by these and other friends who took me outside to roam the hills. My life at Caltech has been enriched by friends: Chrissy Nelson and Jennifer Herek, who explored L.A. with me, and Sherrie Campbell, John Marohn, and the Wing trio, Ariel and Marni Anbar and Hari Nair, who shared with me the various joys and concerns of being here. Much thanks go to the members of CETF "Trash Club" with whom I worked to bring recycling to Caltech. Support from a long-time friend kept me going at rough times; thanks to Jill for constant moral support. And, much thanks is due to Koko for love, understanding, patience and IV's of encouragement.

Finally, none of this would have been possible without the love and support of my parents. They have made countless sacrifices and effort for my 22 years of formal

education. This thesis is dedicated to them. My aunt, Mitsuko, has generously supported my education and giventhe freedom to study what I enjoy.

Abstract

Intermolecular potential energy surfaces (IPS's) of weakly bound clusters with potential applications to the interpretation of biological and other natural phenomena, namely Ar-D_2O, Ar-DOH, C_6H_6-H_2O, C_6H_6-D_2O, C_6H_6-DOH, and $(D_2O)_3$, were studied with fully rotationally resolved spectroscopy, *ab intio* calculations and diffision Monte Carlo simulations. These results contributed to the characterization of the Ar-water, benzene-water and water trimer IPS's and reinforced the need to treat complete the complex dynamics of intermolecular forces.

The Caltech tunable far-infrared spectrometer (TuFIR) was used to observe the $\Sigma^+_{0_{00}} \rightarrow \Pi_{1_{11}}$ transition at 19.32 cm^{-1} and the $\Sigma^+_{0_{00}} \rightarrow \Sigma^+_{1_{11}}$ transition at 20.65 cm^{-1} for Ar-D_2O, and the $\Sigma^+_{0_{00}} \rightarrow \Pi_{1_{01}}$ transition at 19.9 cm^{-1} for Ar-HDO. These transitions probed previously unexplored regions of the Ar-water IPS and enabled the generation of an improved multi-dimensional IPS for this simplest model system of hydrophobic-polar interactions.

The Caltech direct absorption microwave spectrometer was used to record the symmetric top rotational spectrum for the J=4 $\rightarrow$ 5 to 9 $\rightarrow$ 10 transitions in the $m = 0$ and $m = \pm 1$ manifold of C_6H_6-H_2O, C_6H_6-D_2O, and C_6H_6-DOH, to examine the nature of "aromatic-polar" interactions. The rotational constants from the three isotopomers demonstrated unambiguously that water is positioned above the benzene plane in nearly free internal rotation with the hydrogen atoms pointing toward the benzene π-electron cloud. A D_0 of 1.9 kcal/mol was estimated based on the spectra. *Ab initio* calculations supported the aromatic-π-H bond geometry and predicted a binding energy of $D_e \geq 1.78$ kcal/mol. Diffusion Monte Carlo simulations on the *ab initio* surface were performed to visualize the large amplitude motions in this dimer. The TuFIR was also employed to measure a C_6H_6-D_2O intermolecular vibrational band at 19.5 cm^{-1}. The symmetric top pattern and *l*-type doubling in the excited state revealed a strong coupling between the internal rotation and bending

coordinates.

Finally, a previously unpredicted c-type FIR band of $(D_2O)_3$ centered at 41.1 cm^{-1} was observed, which prompted the replacement of a simple one-dimensional model with a more realistic analysis of the $(D_2O)_3$ dynamics.

Contents

Acknowledgements ii

Abstract v

1 Introduction 1

Bibliography 13

2 Experimental Methods 19

2.1 Microwave Techniques 19

2.1.1 FTMW at NIST 22

2.1.2 DAMW at Caltech 23

2.1.3 Comparison of the two microwave techniques 32

2.2 The Caltech tunable FIR spectrometer 33

2.2.1 FIR laser 37

2.2.2 Mixing microwaves and FIR radiation 37

2.3 Summary 39

Bibliography 41

3 Ar-water clusters: Ar-D_2O and Ar-HDO 44

3.1 Experimental 44

3.2 Data analysis 45

3.3 Results 51

3.4 Summary 52

Bibliography 57

4 Benzene-Water 59

4.1 Motivation 59
4.2 The benzene-water ground state structure 63
4.2.1 Microwave data 63
4.2.2 Analysis 63
4.2.3 Structural analysis 66
4.2.4 Summary 69
4.3 Calculations 70
4.3.1 *Ab initio* 70
4.3.2 DMC 75
4.3.3 Summary 80
4.4 FIR Spectra 80
4.4.1 FIR experiment and data 80
4.4.2 Analysis 82
4.4.3 Summary 91
4.5 Conclusion 91

Bibliography **101**

5 Pseudorotation in $(D_2O)_3$ **106**
5.1 Introduction 106
5.2 Experiment and data 109
5.3 Results 112
5.4 Conclusion 117

Bibliography **123**

6 Conclusions and future directions **127**

Bibliography **130**

Appendix A: Microwave experimental procedure **131**

Appendix B: TuFIR experimental procedure **133**

Bibliography **136**

Appendix C: Repair hints **137**

.1 Vacuum pumps 137

.1.1 Complete overhaul 137

.2 Lasers 140

.2.1 Laser alignment 140

.2.2 Notes on laser repair 142

.3 Cooling units 143

Appendix D: PI theory for benzene-water **147**

Bibliography **155**

Appendix E: Fitting programs **156**

Appendix F: *Gaussian 92* and DMC **198**

Appendix G: PI theory for $(D_2O)_3$ **217**

Bibliography **230**

List of Figures

1.1 Cluster IPS to macroscopic properties 2

1.2 HF *vs.* $(HF)_2$: Radial potentials and wavefunctions 4

1.3 A depiction of an arbitrary intermolecular radial potential and various experimental probes that can be used to study it. 6

2.1 Schematic of the original Balle-Flygare FTMW spectrometer. 21

2.2 The Caltech direct absorption microwave spectrometer 24

2.3 Slit nozzle design. 27

2.4 Stark plates attached to the slit nozzle 30

2.5 The Stark modulation power supply. 31

2.6 Caltech TuFIR spectrometer 35

3.1 Ar-H_2O energy level diagram. 47

3.2 Σ and Π states of Ar-H_2O with $j_{water} = 1_{11}$. 48

3.3 Σ and Π states of Ar-H_2O with $j_{water} = 1_{01}$. 50

3.4 Structural parameters θ and ϕ for Ar-water 53

4.1 The benzene-water coordinate system and structure 62

4.2 Spectra in the J=6 $\rightarrow$ 7 region for the benzene-water isotopomers. . . 65

4.3 Benzene-water structure fit 69

4.4 *G92* radial potential. 72

4.5 *G92* potential along θ and ϕ. 73

4.6 Distribution over potential energy cut, R. 77

4.7 Distribution over potential energy cut, θ 78

4.8 Distribution over potential energy cut, χ. 79

4.9 Stick spectrum of the observed and assigned 19.5 cm^{-1} band in bz-D_2O. 83

4.10 Stick spectrum of lowest Q-branch lines 84

4.11 G92 frequency calculations and normal mode vectors for the benzene-H_2O intermolecular modes. 88
4.12 G92 frequency calculations and normal mode vectors for the benzene-D_2O intermolecular modes. 89
4.13 Water replaced by a symmetric top above the benzene plane. 90

5.1 Feasible motions in $(D_2O)_3$. 110
5.2 $(D_2O)_3$ energy level diagram based on a one dimensional model. . . . 111
5.3 $(D_2O)_3$ spectrum near 41 cm^{-1} 113
5.4 Coordinates used in pseudorotation analysis 118
5.5 Water trimer energy levels calculated by Klopper and Schütz 119

.1 Alignment of the lasers. 145
.2 Alignment targets. 146
.3 Benzene-water notation used in PI theory. 148
.4 General flow chart for the spectral fitting program 157
.5 QCLUSTER flow chart 207
.6 Water trimer in its planar structure and labeling convention used. . . 218

List of Tables

3.1 Fitted Ar-D_2O and HDO constants 51

3.2 Observed Ar-D_2O lines 55

3.3 Observed Ar-HDO lines 56

4.1 Benzene-water structural *para*meters. 70

4.2 V_n parameters used to fit the potentials. 74

4.3 FIR lines used for benzene-water transition search. 81

4.4 Termination patterns of the assigned sets of P, Q, and R branches. . . 82

4.5 Stark shifts expected and observed. 85

4.6 Constants fit to FIR C_6H_6-D_2O lines. 86

4.7 Benzene-H_2O m=0 microwave line list. 92

4.8 Benzene-H_2O m=1 microwave line list. 93

4.9 Benzene-H_2O m=1 line list, continued. 94

4.10 Benzene-D_2O microwave line list. 95

4.11 Benzene-HDO microwave line list. 96

4.12 Fitted microwave rotational constants. 97

4.13 Dipole moment measurements for benzene-H_2O 97

4.14 Benzene-D_2O FIR lines observed near 19.5 cm^{-1}. 98

4.15 Benzene-D_2O FIR line list, continued. 99

4.16 Benzene-D_2O FIR line list, continued. 100

5.1 Correlation among C_6, S_6, C_{3h}, and G_{48} groups. 109

5.2 $(D_2O)_3$ spectroscopic constants. 114

5.3 Fitted $(D_2O)_3$ line list near 41 cm^{-1} 121

5.4 $(D_2O)_3$ line list near 41 cm^{-1} continued 122

.1 G_{24} character table 150

.2 Direct product multiplication rules used in Appendix D. 153

.3 Direct product table continued. 154
.4 C_{3h} character table 218
.5 D_{3h} character table 221
.6 C_3 character table 222
.7 The character table for the point group T_h. 224
.8 Character table for the direct product $C_2 \otimes C_2 \otimes C_2$. 225
.9 One-dimensional characters of $C_3 \otimes$ "C_2" 226
.10 Characters for each of the AAB type three-dimensional representations. 226

Chapter 1 Introduction

The main goal of this work is to obtain a quantitative understanding of *inter*molecular interactions. *Intra*molecular chemical bonds have been studied extensively and the results of this research, particularly those over the last century, have been used to systematize our understanding of chemistry. The investigation of *inter*molecular bonds also has a very long history, but they are weaker and more collective, and hence less rigorously studied. They have been crudely quantified via bulk properties such as melting point, boiling point, heat capacity, viscosity, friction, density, and tensile strength. As our microscopic understanding has emerged, concepts such as steric hindrance, valence shell electron pair repulsion theory, and electrostatics have been applied to explain molecular interactions, reaction rates and branching ratios in bulk chemical reactors. Intermolecular potential energy surfaces (IPS's) quantitatively unify these concepts. That is, once an accurate IPS is obtained for a molecular interaction, all the bulk properties and chemical reactions pertaining to the molecules whose IPS is understood can be quantified based on the IPS (see Figure 1.1). This thesis is a part of the ongoing effort to obtain IPS's for model chemical systems. Here, a particular focus is made for those interactions of potential biological significance, namely, Ar-water, benzene-water and the water trimer.

A complete IPS describes the interaction energy of a system in all degrees of freedom, and as such, is essential in quantifying intermolecular interactions. Figure 1.2 compares HF monomer *intra*molecular and HF dimer *inter*molecular radial potential energy surfaces. The monomer bond is much stronger, hence deeper, and is narrower, allowing only a limited range of interatomic distance (R) values for the wavefunction of the intramolecular bond. The monomer potential is nearly harmonic at the ground state level, and the first excited state is $\sim$4000 cm^{-1} above the zero-point energy. At ambient temperature, essentially all of the population is in the ground state. Thus, one can say that the structure of a monomer is reasonably well characterized with

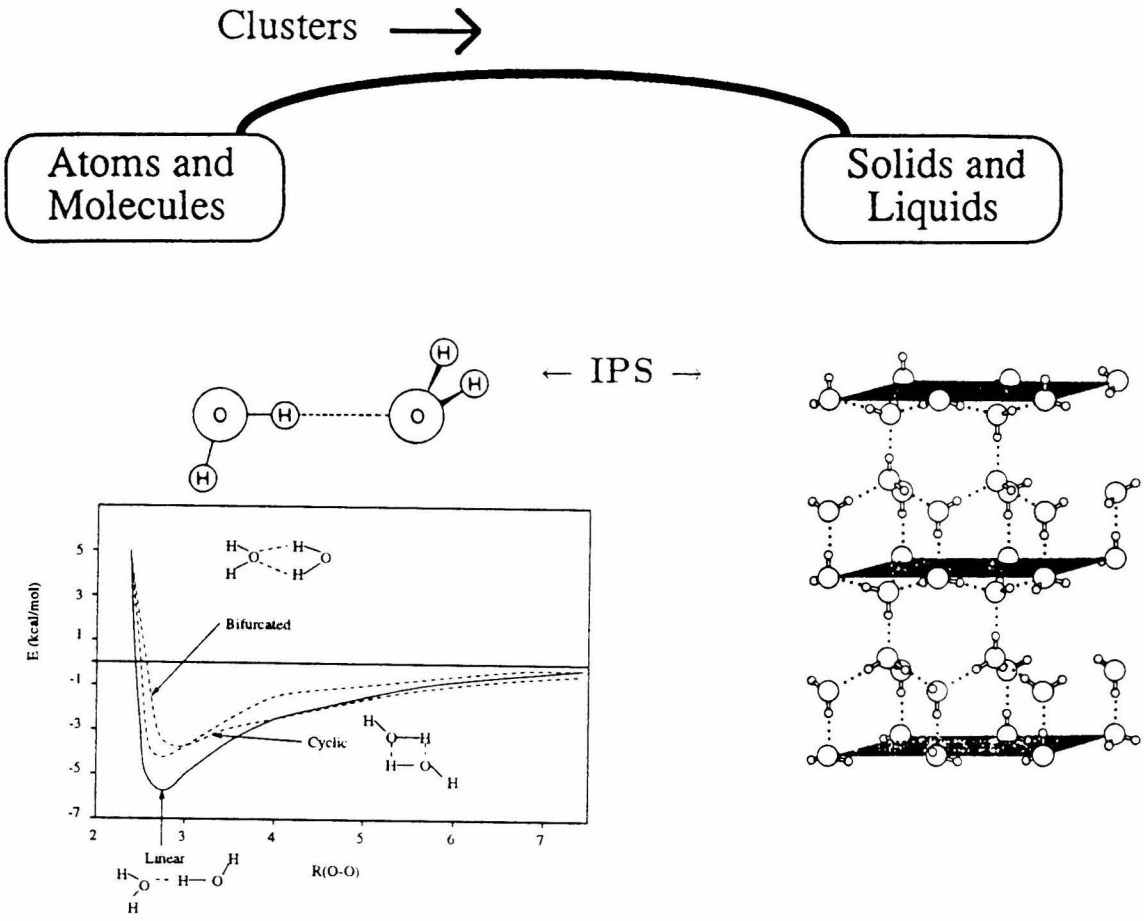

Figure 1.1: A graphical depiction of the relationship of the cluster IPS to macroscopic properties, illustrating how the IPS obtained from intermolecular clusters is expected to yield a detailed understanding of macroscopic properties. It is not yet clear how large a cluster must be studied in order to make realistic extrapolations to macroscopic properties, but dimer surfaces alone are certainly not sufficient. Dimer potentials are based on calculations by Jorgensen [16].

a single R value close to the equilibrium value, R_e. These basic concepts are the bedrock on which much of modern spectroscopy rests.

On the other hand, the dimer intermolecular potential surface is shallow and broad. It is a much weaker bond. The asymmetrically broad potential indicates a large degree of anharmonicity, and a much larger range of R values are allowed for the wavefunction. Thus, in the case of the dimer, <R> is averaged over a much wider range, and is often significantly different from R_e even in the ground state. Furthermore, although the angular coordinate is omitted in the simplified picture given in Figure 1.2, a slight change in the orientations of the two HF monomers changes the bond strength for a given R, i.e., there is a significant *coupling* between the degrees of freedom. In addition, there are potentially several equivalent structures resulting in multiple minima. Tunneling among such multiple minima give rise to unique vibration-rotation-tunneling (VRT) dynamics. IPS's describe these motions as well. Complete IPS's are therefore complex and multi-dimensional, but have many uses. A detailed description of the orientation effects of amino acids in protein folding, for example, can be obtained from a thorough study of such multidimensional IPS's and the subsequent improvement of force fields used in computer simulations [2]. Alternatively, an attractive potential channel between two molecules can explain why a reaction between two molecules favors one product over another [3, 4].

The second virial coefficient in the van der Waals equation of state includes in it both the effects of energy transfer in inelastic collisions as well as longer range attractive forces such as the electrostatic and dispersion interactions which are included in the IPS's. Thus, a complete description of the delicate balance between the various attractive and repulsive forces among all the coordinates is vital to our understanding of intermolecular interactions, material properties and natural phenomena. Simple descriptions of equilibrium structures and bond strengths are inadequate for intermolecular bonds. In this sense, an IPS is much like the higher energy regions of chemically reactive potential energy surfaces for which many interactions and degrees of freedom must be rigorously accounted.

Initially, macroscopic thermodynamic properties, which are manifestations of mi-

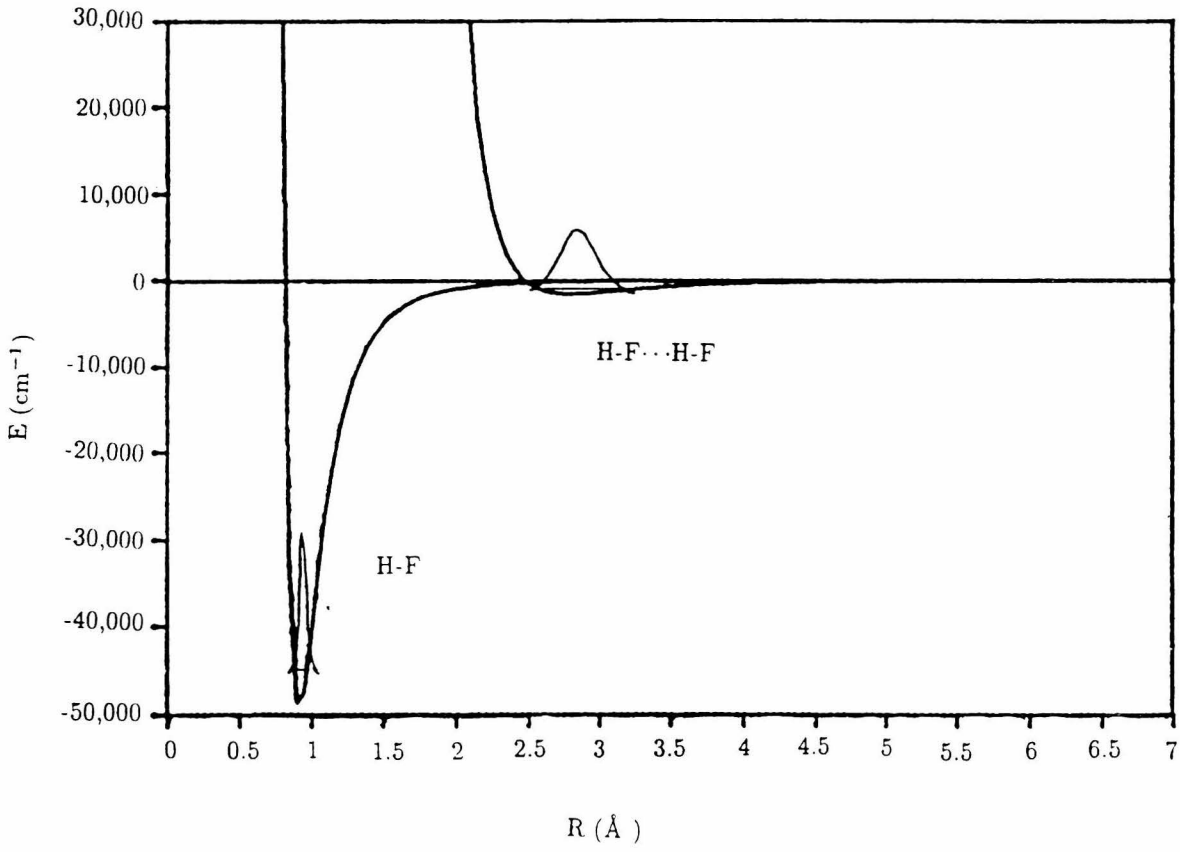

Figure 1.2: HF *vs.* $(HF)_2$: Radial potentials and wavefunctions

croscopic intermolecular interactions, were used to delineate certain aspects of intermolecular forces. In order to study the interactions between two molecules in some detail, deviations from the ideal gas model were investigated under low pressure conditions. Rotational and vibrational spectroscopy were subsequently used to make state resolved measurements of intermolecular interactions via pressure broadening cross sections. Such measurements, however, were average over many intermolecular collisions, and detailed descriptions of the IPS dependent on all degrees of freedom could not be obtained.

Much effort has been expended over the last two decades to improve or create new experimental measurement methods which can characterize intermolecular forces. Instead of the low pressure gas cells used initially to measure pressure broadening effects, molecular beam methods were introduced to truly isolate molecules and, in some cases, to control the energy and orientation of each molecule in the collision. This advancement took us from bulk phase studies to the investigation of isolated molecules. Crossed-beam apparati have been used to measure isolated molecular collisions. These studies provided information primarily on the high energy repulsive region of the IPS, a region difficult to access with state-resolved techniques based on spectroscopy (see Figure 1.3). Although each collision may be isolated, however, such measurements still described properties averaged over many collisions.

Microwave spectroscopy was subsequently used to investigate species in molecular beams. Molecular clusters, where one or several atoms or molecules are bound non-covalently to another, were formed in the expansion region of supersonic molecular beams, and their rotational spectra collected. In molecular clusters, it is possible to observe one-on-one interactions. Dyke's measurement of the water dimer microwave absorption spectrum [5] clearly established the general aspects of the water dimer geometry, for which three structures had been proposed in the matrix isolation study of Pimentel and co-workers [1]. Microwave spectroscopy of molecular beams yield, through rotational and distortion constants, electric dipole moments, and nuclear quadrupole coupling constants, highly sensitive information on the intermolecular bond strengths and interaction geometries for clusters in their ground states. Ground

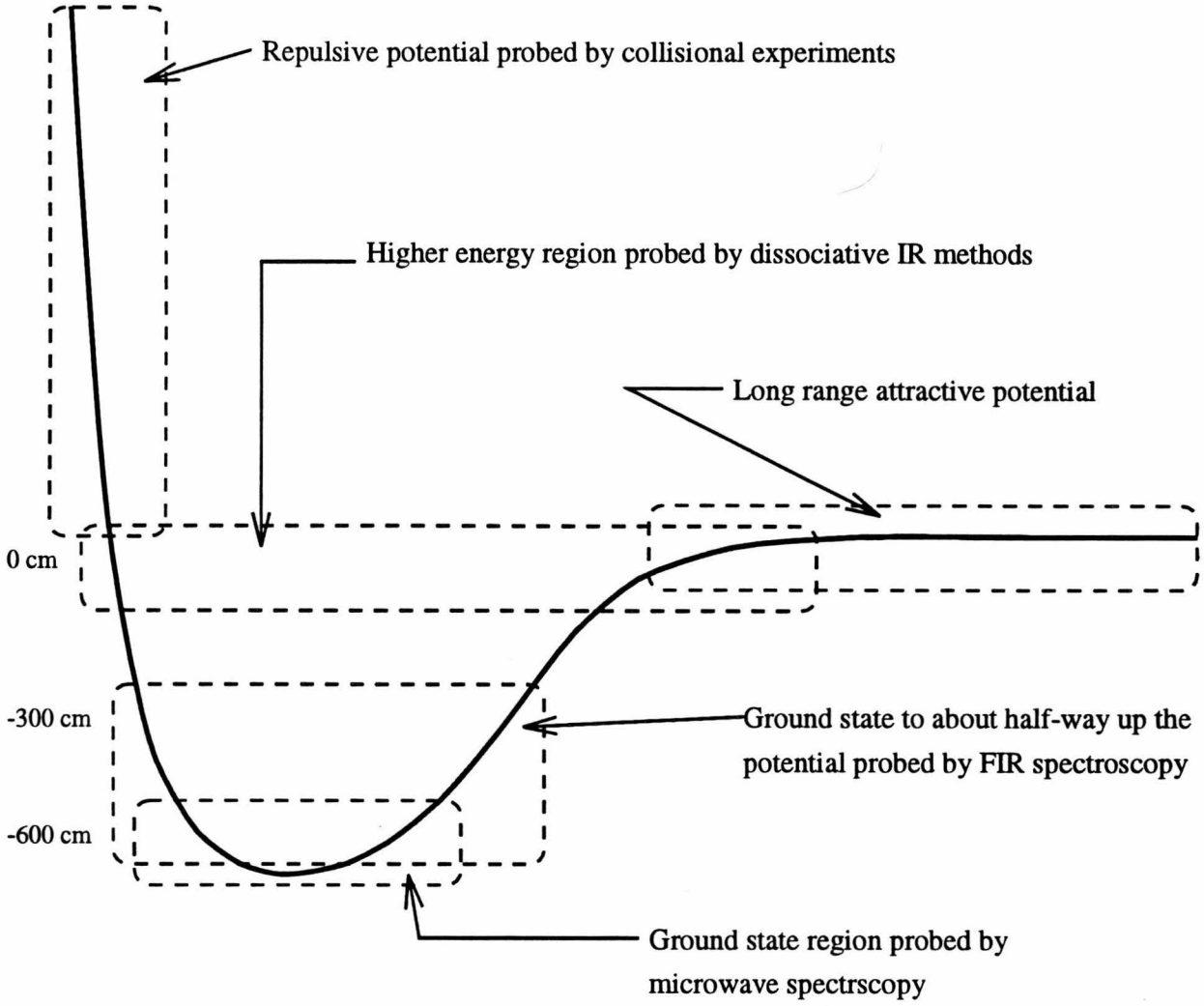

Figure 1.3: A depiction of an arbitrary intermolecular radial potential and various experimental probes that can be used to study it.

state measurements, unfortunately, limit the range of intermolecular interactions investigated to the region close to the IPS minimum, even in the most weakly bound clusters (see Figure 1.3). Recent reviews concerned with the microwave spectroscopy of clusters have been provided by Novick *et al.* [7] and by Dyke [8].

A more recent development is the use of infrared (IR) spectroscopy to observe the fundamental and combination bands of *intra-* and *inter*molecular vibrations in molecules bound to other molecules. Here, monomer vibrational energy, far in excess of the intermolecular binding energy, is put into the cluster. The large difference in vibrational energy between the monomer and the intermolecular modes leaves the energy isolated in the monomer for some time, an extention of Born-Oppenheimer approximation. This method, unlike microwave spectroscopy, can probe the higher energy region of the IPS, yielding anharmonicity of the IPS sometimes near the dissociation limit; but typically only for the IPS of the vibrationally excited state of the intramolecular mode (see Figure 1.3). In addition, the spectral resolution is typically coarse enough to miss the very detailed information available in fine and hyperfine interactions. Detailed reviews of these IR probes of molecular clusters are given by Nesbitt [9] and Miller [10].

Zwier and co-workers cleverly studied clusters where one of the monomers is a visible photon chromophore by coupling intermolecular modes with an electronic transition. Resonance enhanced multiphoton ionization (REMPI) and time of flight (TOF) mass spectrometry were used to probe numerous clusters. This efficient, sensitive method was used to study clusters, for example, benzene with 1 to 8 water molecules [5, 12]. By rotational contour fitting, low resolution structural information was obtained. The drawback to this method is that the intermolecular vibrations probed are in electronically excited states, and so while excellent excited state information can be obtained, information on the ground state, which is more relevant to interpretation of natural phenomena, is only inferred.

Recently, P.M. Felker and co-workers have obtained Raman vibration-rotation spectra of weakly bound clusters (private communication). It probes transitions not easily observed by IR-vibrational spectroscopy; thus, it yields complementary infor-

mation to these methods. However, the low resolution presently available does not allow a more precise determination of eigenstates involved in the observed vibrations. Thus, we see that the study of clusters has evolved from the effort to further isolate intermolecular interactions to that between two energetically controlled molecules, and the probes have become increasingly sophisticated, advancing from a thermometer used in melting point measurements to laser-based high resolution spectrometers.

A typical intermolecular cluster has a binding energy of ~0.5 to 5 kcal/mol. The transition energy for vibrational motion along the intermolecular mode is ~10-300 cm^{-1}, much less than that for covalent bonds, and corresponds to the far-infrared (FIR) region (see Figure 1.3). This is also the range of energy available at ambient temperature. If an intermolecular vibrational transition is measured with rotational resolution, then the ground state structure as well as the vibrationally excited (intermolecular mode) cluster structure, which is at an energy level pertinent to most natural systems at room temperature, can be observed. There would be no dependence on monomer chromophore or the Born-Oppenheimer approximation. Such an interrogation would yield a great deal of information about the cluster energetics, structural changes, and hence, a detailed understanding of the IPS from the ground state to roughly halfway up the IPS, even if only the lowest excited states are excited. Thus, FIR spectroscopy is an ideal method for characterizing weak interactions. Yet, until recently, FIR region has been known as "the gap in the electromagnetic spectrum"; there was simply no sensitive method available to perform spectroscopy in the FIR. FIR spectroscopy of van der Waals clusters with rotational resolution finally became available nearly a decade ago [13, 14, 15]. One such approach, tunable FIR direct absorption with a supersonic slit jet expansion, will be used in this thesis. Review articles regarding this approach have been written by Saykally [16], Hutson [3], Cohen and Saykally [18], and Saykally and Blake [19].

Experimental measurements do not automatically yield an IPS. A necessarily limited number of measurements on the IPS cannot uniquely predict an IPS possessing infinite number of points on it's surface. However, experimental observables are all predictable given a complete and accurate IPS. Thus, the acquisition of an

IPS involves adjustment of a theoretical or empirical IPS to predict experimental measurements. Calculational methods, beginning with *ab initio* approaches, Monte Carlo and molecular dynamics simulations of bulk properties, and various methods of spectral inversion to fit the measured intermolecular eigenvalues must be employed for a detailed understanding. This is no small feat, but through the extensive research efforts, a few highly refined potentials have been obtained to date: for example, Hutson's H6 potential for Ar-HCl [20], Cohen and Saykally's AW2 potential for Ar-water [1], and more recently, $(HCl)_2$ potentials by Braly *et al.* [22], and Elrod and Saykally [23], and $(HF)_2$ IPS's by Necoechea and Truhlar [24], Quack and Suhm [25, 4], and Bunker *et al.* [26]. Extensive discussions on how the various calculational methods are used and how they compare with each other are given by the above authors as well as in review articles by Cohen and Hutson [27, 28].

A brief history of the Ar-HCl IPS research will be given below to illustrate how our understanding has evolved and what efforts were necessary to bring about the complete characterization of a "simple" IPS.

Rare gas-hydrogen halides form a relatively straight-forward system where the main attractive force is clearly electrostatic: the dipole-induced dipole term. In order to quantify the details of such an interaction, rotational and rovibrational line pressure broadening coefficients for HCl in an Ar gas sample were measured in the 1960's [29]. Later in 1973, Neilsen and Gordon [30] ingeneously fit the pressure broadening cross sections and additional proton relaxation measurements made with NMR [31] to obtain interaction potential parameters. They found significant radial-angular coupling in the potential, which, as we will see, was qualitatively correct. The more controlled environment of a molecular beam was used with microwave photons by Klemperer's group in the 1970's and further refined the model potential surface near the IPS minimum [32, 33]. In the 1980's, Hutson and Howard produced several potential surfaces including both the bulk property and molecular beam measurements, i.e, pressure broadening values, second virial coeffiecients, and microwave constants [34, 35]. These test potentials, M3 and M5, were different from each other in that M3 had only one minimum, an Ar$\cdots$H-Cl linear geometry, while M5 had two minima at

the Ar···H-Cl and Ar···Cl-H orientations.

Howard and Pine attempted to test these potentials by using infrared photons to measure higher regions of the surface in cooled cells, which may allow the cluster to sample the second minimum had it existed [36]. Unfortunately, they were not able to resolve the difference. Experimental techniques were developed to enable high resolution measurements within molecular beams in the infrared and FIR regions in the 1980's [37]. The Klemperer and Saykally groups developed a far-infrared spectroscopy technique which enabled accurate measurements of the Ar-HCl cluster [13, 15, 38, 39, 40]. The Berkeley measurements clearly established the existence of a secondary minimum [15]. Further experimental measurements were accomplished with a different FIR technique by Busarow *et al.* [14], and with near-IR combination band measurements by Lovejoy and Nesbitt [41]. These and other measurements were included in obtaining a now quite accurate IPS for Ar-HCl by Hutson, called H6 [20].

Thus, nearly fifteen years of work by various researchers was required to substantially improve the first estimate of the interaction potential by Neilson and Gordon to an essentially quantitative description of the IPS. Initially, before Neilson and Gordon's potential, there was a simple pseudodiatomic model of electrostatic interactions described by a Morse or Lennard-Jones function. Here, the interaction potential was treated as isotropic. Neilson and Gordon's results showed radial-angular coupling in the potential. A more detailed IPS revealed that the potential is highly anisotropic, and that, in addition to electrostatic interactions such as the dipole-induced dipole interaction in Ar-HCl, which play a major role, there is a delicate balancing of many forces which contribute to the *details* of the anisotropy. After much study, Hutson and others concluded that the secondary minimum is not a secondary attractive minimum, but that the repulsive force is lower when the Cl is pointing towards the Ar because the electron density is lower on the Cl directly opposite of the H.

The simple electrostatic properties, such as dipole moment, polarizability and quadrupole moments, for each of the molecules studied in this thesis are well known. A zeroth-order understanding of the intermolecular interaction is therefore known, or can be guessed with some qualitative accuracy. However, just as a pressure broaden-

ing measurement can not produce a full IPS, without a complete IPS, macroscopic properties cannot be predicted with high accuracy. The complete characterization of a suite of "representative" IPS's is the main goal of the research in Prof. Blake's laboratory; this thesis presents a range of results directed toward this goal. Microwave and FIR spectroscopy will be used as well as *ab initio* calculations. As in the case of Ar-HCl, tunable FIR spectroscopy is a powerful tool which probes the intermolecular modes directly, and thus, leads to a detailed mapping of the IPS. Yet, as seen above, much effort and time is needed to completely characterize the IPS. The goal of this thesis is practically limited to contributing to the extensive body of work by other researchers in pursuit of IPS's.

Among the unlimited clusters to be studied, this work is directed towards understanding molecular interactions which have direct influence on our understanding of nature. Work on three clusters are presented in here: Ar-water, benzene-water and water trimer. Water is the solvent of choice in biological systems. We also learned recently that aromatic moieties in biological systems interact with ionic and polar entities, in contrast to the traditionally held view of little interactions between polar and non-polar molecules. For example, amino acids with aromatic side chains preferentially bind to amino and hydroxyl groups within proteins [11, 10, 12], and aromatic rings stabilize ions used as stimulants or repressors in biological systems [14]. Ar-water is the simplest model system for such an interaction. Benzene-water clusters in a molecular beam isolate an aromatic group and a polar group. Intermolecular vibrations of an isolated aromatic-π-hydrogen bonded cluster structure without any external force acting on it were observed for the first time. The study of water trimer contributes to a better understanding of solvent systems. Simulations performed by Warshel and co-workers have shown that pairwise forces alone do not accurately reproduce bulk water properties [15]. Indeed, as found in a recent series of papers by Elrod and Saykally, and by Cooper and Hutson, the Ar_2-HCl trimer is not a simple extension of the individual dimer IPS's [47, 48, 49, 50, 51]. Such three-body forces and larger scale many-body interaction terms must be understood before cluster information can be extended to analyzing bulk properties at the molecular level.

The organization of the remaining chapters is as follows: The majority of this work is experimental and the measurements were made primarily on the Caltech microwave spectrometer and on the Caltech tunable far-infrared spectrometer. An overview of these instruments will be given in Chapter 2. There are three companion appendices for Chapter 2: In Appendix A, the experimental procedure for microwave absorption spectroscopy is outlined; Appendix B outlines the FIR experimental procedure; and Appendix C describes repair methods for various experimental systems. Chapter 3 is a study of a model hydrophobic interaction in the Ar-water dimer, which sets the stage for the larger clusters to follow. Extensive work had been done by Cohen and Saykally on this cluster. Their IPS, called AW1, was already complete at the time of this work. However, there were still pertinent transitions to be measured for Ar-H_2O and its deuterated isotopomers. Such measurements were made and were used to constrain Cohen and Saykally's more refined AW2 potential. Appendix E contains descriptions of the programs used to fit spectroscopic measurements in this and subsequent chapters.

Chapter 4 describes the work on the benzene-water dimer, which serves as a model for aromatic-water interactions in aqueous media and proteins. A comparison will be made with the Ar-water interaction since water is bound to a "hydrophobic" entity which differs in size and anisotropy. How might these size and electrostatic differences change the interaction potential? Appendix D details the permutation inversion (PI) group theory needed to understand the benzene-water spectra, and Appendix F contains notes regarding the use of an *ab initio* code, *Gaussian 92*, and diffusion Monte Carlo simulation package called QCLUSTER. Chapter 5 describes the first Blake group trimer study, that of $(D_2O)_3$. Measurements taken at Caltech and by the Saykally group are combined with calculational efforts by theorists to gain a better understanding of the water trimer and to shed light on the nature of three-body forces. Appendix G details the PI theory for this cluster.

Bibliography

[1] W.L. Jorgensen. Transferable Intermolecular Potential Functions of Water, Alcohols, and Ethers. Application to Liquid Water. *J. Am. Chem. Soc.*, 103:335, 1981.

[2] M. Karplus and G.A. Petsko. Molecular Dynamics Simulations in Biology. *Science*, 347:631, 1990.

[3] D.G. Truhlar and M.S. Gordon. From Force Fields to Dynamics: Classical and Quantal Paths. *Science*, 249:492, 1990.

[4] M. Quack and M.A. Suhm. Potential-Energy Surfaces, Quasi-Adiabatic Channels, Rovibrational Spectra, and Intramolecular Dynamics of $(HF)_2$ and Its Isotopomers from Quantum Monte-Carlo Calculations. *J. Chem. Phys.*, 95:28, 1991.

[5] T.R. Dyke, K.M. Mack, and J.S. Muenter. The Structure of Water Dimer from Molecular Beam Electric Resonance Spectroscopy. *J. Chem. Phys.*, 66:498, 1977.

[6] M. van Thiel, E.D. Becker, and G.C. Pimentel. Infrared Studies of Hydrogen Bonding of Water by the Matrix Isolation Technique. *J. Chem. Phys.*, 27:486, 1957.

[7] S. Novick, K. Leopold, and W. Klemperer. *Atomic and Molecular Clusters.* Elsevier, Amsterdam, 1990.

[8] T.R. Dyke. Microwave and Radiofrequency Spectra of Hydrogen Bonded Complexes in the Vapor Phase. *Topics in Curr. Chem.*, 120:85, 1984.

[9] D.J. Nesbitt. High-Resolution Infrared Spectroscopy of Weakly Bound Molecular Complexes. *Chem. Rev.*, 88:843, 1988.

[10] R.E. Miller. The Vibrational Spectroscopy and Dynamics of Weakly Bound Neutral Complexes. *Science*, 240:447, 1988.

[11] A.J. Gotch and T.S. Zwier. Multiphoton Ionization Studies of Clusters of Immiscible Liquids: 1. C_6H_6-$(H_2O)_n$, n=1,2. *J. Chem. Phys.*, 95:3388, 1992.

[12] A.W. Garrett and T.S. Zwier. Multiphoton Ionization Studies of Clusters of Immiscible Liquids: 2. C_6H_6-$(H_2O)_n$, n= 3-8 and $(C_6H_6)_2$-$(H_2O)_{1,2}$. *J. Chem. Phys.*, 96:3402, 1992.

[13] M.D. Marshall, A. Charo, H.O Leung, and W. Klemperer. Characterization of the Lowest-Lying Π-Bending State of Ar-HCl by Far Infrared Laser-Stark Spectroscopy and Molecular-Beam Electric Resonance. *J. Chem. Phys.*, 83:4924, 1985.

[14] K.L. Busarow, G.A. Blake, K.B. Laughlin, R.C. Cohen, Y.T. Lee, and R.J. Saykally. Tunable Far Infrared Laser Spectroscopy of van der Waals Bonds: Extended Measurements on the Lowest Σ Bend of ArHCl. *J. Chem. Phys.*, 89:1268, 1988.

[15] R.L. Robinson, D-H. Gwo, D. Ray, and R.J. Saykally. Evidence for a Secondary Minimum in the ArHCl Potential Surface from Far Infrared Laser Spectroscopy of the Lowest Σ Bending Vibration. *J. Chem. Phys.*, 86:5211, 1987.

[16] R.J. Saykally. Far-Infrared Laser Spectroscopy of Van Der Waals Bonds: A Powerful New Probe of Intermolecular Forces. *Acct. Chem. Res.*, 22:295, 1989.

[17] J.M. Hutson. Atom-Asymmetric Top Van Der Waals Complexes: Angular Momentum Coupling in Ar-H_2O. *J. Chem. Phys.*, 92:157, 1990.

[18] R.C. Cohen and R.J. Saykally. Vibration-Rotation-Tunneling Spectroscopy of the Van Der Waals Bond: A New Look at Intermolecular Forces. *J. Phys. Chem.*, 96:1024, 1992.

[19] R.J. Saykally and G.A. Blake. Molecular Interactions and Hydrogen Bond Tunneling Dynamics: Some New Perspectives. *Science*, 259:1570, 1993.

[20] J.M. Hutson. The Intermolecular Potential of Ar-HCl: Determination from High-Resolution Spectroscopy. *J. Chem. Phys.*, 89:4550, 1988.

[21] R.C. Cohen and R.J. Saykally. Determination of an Improved Intermolecular Global Potential Energy Surface for Ar-H_2O from Vibration-Rotation-Tunneling Spectroscopy. *J. Chem. Phys.*, 98:6007, 1993.

[22] L.B. Braly, R.J. Saykally, and C.L. LeForestier. Wigner DVR: A New Method for the Calculation of VRT Dynamics of Van Der Waals Clusters. *OSU Molecular Spectroscopy Symposium Abstracts*, TI:07, 1995.

[23] M.J. Elrod and R.J. Saykally. *J. Chem. Phys.*, in press, 1995.

[24] W.C. Necoechea and D.G. Truhlar. A Converged Full-Dimensional Calculation of the Vibrational-Energy Levels of $(HF)_2$. *Chem. Phys. Lett.*, 224:297, 1994.

[25] M. Quack and M.A. Suhm. Accurate Quantum Monte-Carlo Calculations of the Tunneling Splitting in $(HF)_2$ on a 6-Dimensional Potential Hypersurface. *Chem. Phys. Lett.*, 234:71, 1995.

[26] P.R. Bunker, M. Kofranek, H. Lischka, and A. Karpfen. An Analytical 6-dimensional Potential-Energy Surface for $(HF)_2$ from *Ab Initio* Calculations. *J. Chem. Phys.*, 89:3002, 1988.

[27] R.C. Cohen. Multidimensional Intermolecular Potential Surfaces from Vibration-Rotation-Tunneling (VRT) Spectra of Van Der Walls Complexes. *Annu. Rev. Phys. Chem.*, 42:369, 1991.

[28] J.M. Hutson. Intermolecular Forces From the Spectroscopy of Van Der Waals Molecules. *Annu. Rev. Phys. Chem.*, 41:123, 1990.

[29] D.H. Rank, D.P. Eastman, B.S. Rao, and T.A. Wiggins. Breadths and Shifts of Molecular Band Lines Due to Perturbation by Foreign Gases. *J. Mol. Spect.*, 10:34, 1963.

[30] W.B. Neilsen and R.G. Gordon. On a Semiclassical Study of Molecular Collisions. II. Application to HCl-Argon. *J. Chem. Phys.*, 58:4149, 1973.

[31] A.M. Leonardi-Cattolica, K.O.l Prins, and J.S. Waugh. Proton Spin-Lattice Relaxation in HCl-Ar mixtures. *J. Chem. Phys.*, 54:769, 1971.

[32] S.E. Novick, P. Davies, S.J. Harris, and W. Klemperer. Determination of the Structure of ArHCl. *J. Chem. Phys.*, 59:2273, 1973.

[33] S.L. Holmgren, M. Waldman, and W. Klemperer. Internal Dynamics of Van Der Waals Complexes. II. Determination of a Potential Energy Surface for ArHCl. *J. Chem. Phys.*, 69:1661, 1978.

[34] J.M. Hutson and B.J. Howard. The Intermolecular Potential Energy Surface of ArHCl. *Mol. Phys.*, 43:493, 1981.

[35] J.M. Hutson and B.J. Howard. Anisotropic Intermolecular Forces I. Rare Gas-Hydrogen Chloride Systems. *Mol. Phys.*, 45:769, 1982.

[36] B.J. Howard and A.S. Pine. Rotational Predissociation and Libration in the Infrared Spectrum of Ar-HCl. *Chem. Phys. Lett.*, 122:1, 1985.

[37] D. Ray, R.L. Robinson, D-H. Gwo, and R.J. Saykally. Vibrational Spectroscopy of Van Der Waals Bonds: Measurement of the Perpendicular Bend of ArHCl by Intracavity Far Infrared Laser Spectroscopy of a Supersonic Jet. *J. Chem. Phys.*, 84:1171, 1986.

[38] R.L. Robinson, D-H. Gwo, and R.J. Saykally. An Extended Study of the Lowest Π Bending Vibration-Rotation Spectrum of Ar-HCl by Intercavity Far Infrared Laser/Microwave Double Resonance Spectroscopy. *J. Chem. Phys.*, 87:5149, 1987.

[39] R.L. Robinson, D-H. Gwo, and R.J. Saykally. The High-Resolution Far Infrared Spectrum of a Van Der Waals Stretching Vibration: The ν_3 Band of Ar-HCl. *J. Chem. Phys.*, 87:5156, 1987.

[40] R.L. Robinson, D-H. Gwo, and R.J. Saykally. Far Infrared Laser Stark Spectroscopy of the Σ Bending Vibration of ArHCl. Strong Evidence for a Double Minimum Potential Surface. *Mol. Phys.*, 63:1021, 1988.

[41] C.M. Lovejoy and D.J. Nesbitt. Infrared-Active Combination Bands in ArHCl. *Chem. Phys. Lett.*, 146:582, 1988.

[42] S.K. Burley and G.A. Petsko. Amino-Aromatic Interactions in Proteins. *FEBS Lett.*, 203:139, 1986.

[43] S.K. Burley and G.A. Petsko. Aromatic-Aromatic Interaction: A Mechanism of Protein Structure Stabilization. *Science*, 229:23, 1985.

[44] S.K. Burley and G.A. Petsko. Weakly Polar Interactions in Proteins. *Adv. Prot. Chem.*, 39:125, 1988.

[45] M. Dennis, J. Giraudat, F. Kotzyba-Hibert, M. Goeldner, C. Hirth, J-Y. Chang, C. Lazure, M. Chretien, and J-P. Changeux. Amino Acids of the *Torpedo marmorata* Acetylcholine Receptor α Subunit Labeled by a Photoaffinity Ligand for the Acetylcholine Binding Site. *Biochem.*, 27:2346, 1988.

[46] S. Kuwajima and Arieh Warshel. Incorporating Electric Polarizabilities in Water-Water Interaction Potentials. *J. Phys. Chem.*, 94:460, 1990.

[47] M.J. Elrod, D.W. Steyert, and R.J. Saykally. Tunable Far Infrared Laser Spectroscopy of a Ternary Van Der Waals cluster Ar_2HCl: A Sensitive Probe of Three-Body Forces. *J. Chem. Phys.*, 94:58, 1991.

[48] M.J. Elrod, D.W. Steyert, and R.J. Saykally. An Investigation of Three-Body Effects in Intermolecular Forces. II. Far-Infrared Vibration-Rotation-Tunneling Laser Spectroscopy of Ar_2HCl. *J. Chem. Phys.*, 95:3182, 1991.

[49] M.J. Elrod, J.G. Loeser, and R.J. Saykally. An Investigation of Three-Body Effects in Intermolecular Forces. III. Far Infrared Laser Vibration-Rotation Tun-

neling Spectroscopy of the Lowest Internal Rotor States of Ar_2HCl. *J. Chem. Phys.*, 98:5352, 1993.

[50] M.J. Elrod, R.J. Saykally, A.R. Cooper, and J.M. Hutson. Non-Additive Intermolecular Forces from the Spectroscopy of Van Der Waals Trimers: Far-Infrared Spectra and Calculations of Ar_2-DCl. *Molec. Phys.*, 81:579, 1994.

[51] A.R. Cooper and J.M. Hutson. Nonadditive Intermolecular Forces from the Spectroscopy of Van Der Waals Trimers: Calculations on Ar_2HCl. *J. Chem. Phys.*, 98:5337, 1993.

Chapter 2 Experimental Methods

Intermolecular interactions are studied at two levels in this thesis. Cluster "structure determination" is pursued with microwave spectroscopy, and the direct probe of the intermolecular potential energy surface (IPS) eigenvalues is performed with direct absorption far-infrared(FIR) spectroscopy. In this chapter, the two microwave spectrometers and the FIR spectrometer used to conduct the measurements presented in this thesis are described. Since some of the instruments were developed elsewhere, the reader is referred to appropriate articles, review papers and theses of other researchers for more detailed explanations of the instruments. This chapter will include a general overview of the instruments and major repairs and modifications made on the instruments during 1990-1995. Detailed operation manuals for the Caltech instruments are given in Appendices A and B. Hints on repairing the FIR spectrometer are given in Appendix C.

2.1 Microwave Techniques

Microwave spectroscopy has been widely used to probe molecular structures since the 1930's [1]. Molecular cluster geometries have been probed since the 1960's when dimers in static cells were investigated at 20 MHz resolution. In the 1970's and the 1980's, microwave spectroscopy techniques were developed such that the resolution improved to 1 - 20 kHz [2, 3]. Such drastic improvements were made possible by the use of molecular beam techniques and by the development of advanced electronics needed for Fourier transform spectroscopy. Molecular beam electric resonance spectroscopy (MBER) and Balle-Flygare Fourier transform spectroscopy (FTMW) are the two primary techniques which utilized these innovations and enabled high resolution, high sensitivity spectroscopy [2, 3, 4]. The 1-20 kHz line widths obtained with these techniques correspond to a formal structural precision of, for example, 0.0001

Å out of 4.1107 Å in the case of Kr-HCl clusters [4]. MBER was first applied to cluster spectroscopy in 1972 by Klemperer and co-workers in their study of the HF dimer [2]. In addition to rotational constants, Stark coefficients and polarizability are obtained with MBER. MBER was used by Klemperer and co-workers in the so-called "flop-out" mode, that is microwave absorption corresponds to signal dips in the mass spectrometer output. This leads to inherently low signal-to-noise ratios. On the other hand, Fourier transform microwave spectrometry (FTMW), developed by Balle and Flygare in 1980, affords better signal-to-noise and comparable resolution [3, 4]. The schematic of the original instrument is shown in Figure 2.1. In general, an adiabatically expanded pulsed (100-500μs) molecular beam is directed into a Fabry-Perot cavity into which a polarized microwave pulse (0.5 to 3 μs) is also injected. By tuning the distance between the mirrors of the Fabry-Perot, different microwave frequencies with $\sim$1 MHz bandwidth can be brought into resonance with the cavity. The excited and aligned molecules inside the cavity emit coherently and this emission is detected in the time domain. This emission is digitized, averaged, background subtracted, and Fourier transformed on a computer to obtain the emission spectrum in the frequency domain. The detection of the emitted signal occurs after the dissipation of the initial microwave pulse. This affords high signal-to-noise ratios. Although the cavity bandwidth is about 1 MHz, the Fourier transform of the time domain emission spectrum obtained over a period of $\sim$ 10 msec yields a resolution of $\leq$ 10 kHz. High signal-to-noise ratios, narrow linewidths, and the use of collision-free rotationally-cold molecular beams have made this a popular method in obtaining cluster rotational spectra.

Thus, rotational spectroscopy has been used for decades to determine molecular structures. Microwave data are also indispensable in FIR studies where ground state information is used to aid in the assignment and fitting of the spectra. Recent advances in technology have increased the sensitivity and the resolution with which cluster structures are studied in detail. The two microwave spectroscopy techniques used in this thesis to probe molecular clusters, FTMW and direct absorption microwave spectroscopy (DAMW), are described in further detail below.

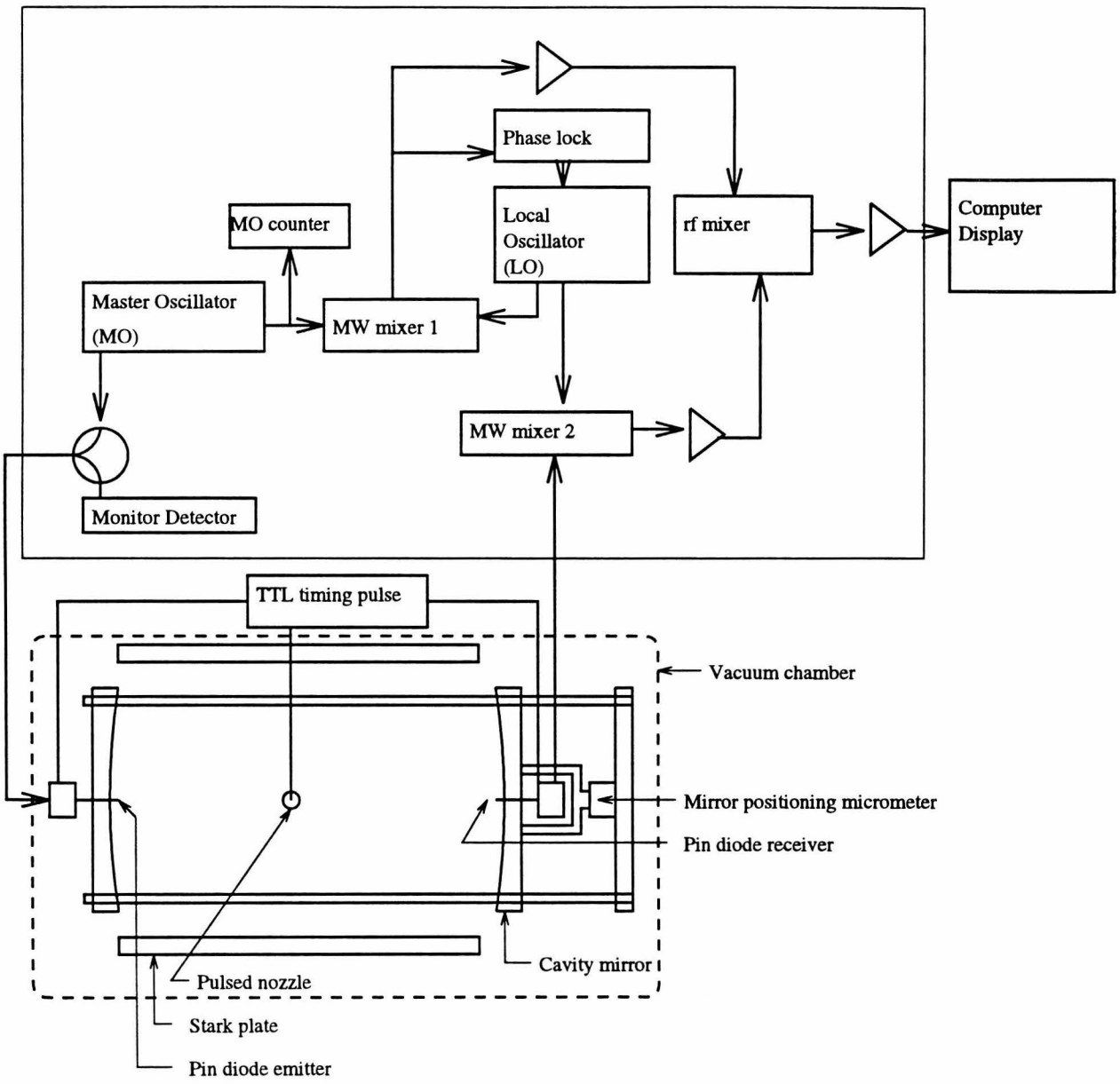

Figure 2.1: Schematic of the original Balle-Flygare FTMW spectrometer.

2.1.1 FTMW at NIST

Some of the information in this thesis was collected using a Balle-Flygare type FTMW at the National Institute of Standards and Technology (NIST). A brief overview of the instrument is given below; for a complete description, readers are referred to the NIST researchers and accounts written by them [5, 5].

The cylindrical vacuum chamber has a diameter of 56 cm and length of 1.2 m. The cylinder is placed horizontally and a diffusion vacuum pump with pumping speed of 8000 l/s backed by a 90 ft^3/min mechanical pump is attached at the center bottom. The base pressure inside the chamber is about $2x10^{-7}$ Torr.

Two concave mirrors constructed from aluminum disks, each with a 35.6 cm diameter and a radius of curvature of 87 cm, are placed near the ends of the cylinder, facing each other. The mirrors are mounted on a rigid assembly of four 3/4 inch diameter stainless steel rods which are fastened to the ends of the cylindrical vacuum chamber. Each mirror is attached to the four stainless steel rods with linear motion bearings so that the mirror separation distance may be easily adjusted. The micrometer used to move one of the mirrors can be controlled to better than 1 μm. (A typical microwave frequency used is 20 GHz, or $\nu = \frac{2}{3}cm^{-1}$, $\lambda = 1.5$ cm.)

A pin-hole molecular beam source with an $\sim$80 μm orifice diameter is placed between the two mirrors, about 15 cm away from the cavity axis. The sample gases are premixed and supplied to the pulsed nozzle with a backing pressure ranging from 0.5 to 2 atm.

The molecular beam pulse is timed with the microwave pulse and signal detection gate so as to allow background subtraction and detection of the free induction decay signal for each molecular beam pulse. Here, the microwave source used was the single-microwave-source configuration described by Suenram *et al* [5]. First, a background measurement is performed by switching the microwave power on for 0.5 μs to 3 μs. This is followed by a short delay of about 2 μs to allow the excess cavity radiation to dissipate. The detection circuit is then opened to digitize the background signal for a period of $\sim$10 ms at a 1-10 MHz sampling rate. This sequence is followed by the

molecular absorption signal collection sequence which begins with a molecular beam pulse of approximately 300 μs, followed by a delay of about 500 μs to allow the gas to expand into the Fabry-Perot cavity. A short microwave pulse of identical length to that used in background signal collection is then emitted into the cavity. The delay time and the digitizing time is identical with the background signal collection. This sequence is repeated at about 30 Hz. A user selected number of pulse sequences are averaged before the cavity length and the microwave frequency are altered. The data collected are in the time domain and are digitized so that the background subtraction and Fourier transform can be performed by a computer.

Two parallel Stark plates ~26 cm apart are placed perpendicularly to the mirrors. Static fields of up to ~10 kV or ~ 835 V/cm are produced for dipole moment measurements. A well-characterized molecule such as OCS is used to calibrate the fields strength.

2.1.2 DAMW at Caltech

The DAMW spectrometer at Caltech was developed as a simple modification of the tunable far-infrared sideband spectrometer (TuFIR), which is described in detail below.

A schematic of the instrument is shown in figure 2.2. The instrument consists of a microwave source, a function generator for microwave modulation, coaxial and horn waveguides, a fast solid state detector, a lock-in amplifier, and a PC that controls the microwave synthesizer, gas flow controllers and data collection. The sample gas is expanded through a slit jet expansion into a vacuum chamber.

Microwave source and detection scheme

The microwave radiation source is a Wiltron 6747A-20 phase-locked frequency synthesizer (+18 dBm output in the range 10 MHz - 20 GHz). A doubler, triplers and an amplifier are used to extend the range of the microwaves available. (Watkins-Johnson(WJ) model SMD180 doubler (18-40 GHz output), WJ Q2300N tripler (40-60

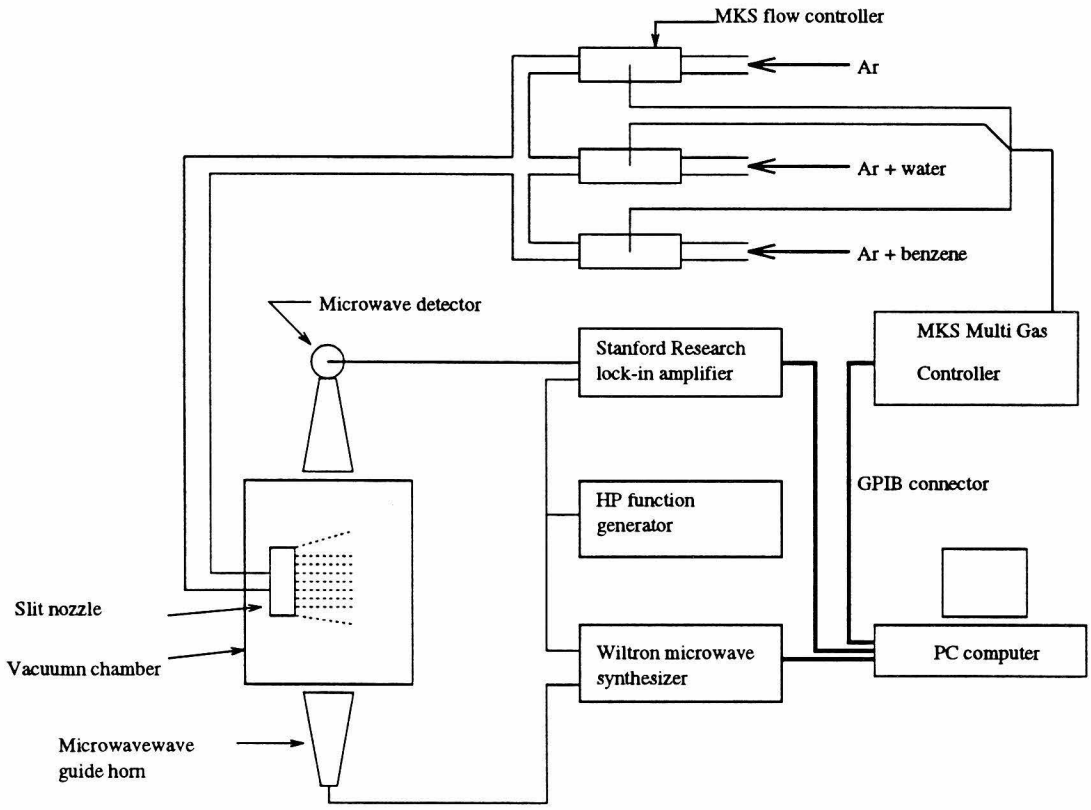

Figure 2.2: The Caltech direct absorption microwave spectrometer

GHz output), Millitech MU7-12 tripler (60-90 GHz output), MITEQ AMF-60-200265-15P amplifier; +15 V power supply required.) The microwave signal is carried via a K-connectored coaxial cable and emitted into space with an appropriately sized waveguide horn. The output is aligned perpendicular to the beam expansion and parallel to the plane of the slit nozzle. A Wiltron model 75KC50 Schottky diode detector (for frequencies below 43 GHz) or a Hewlett-Packard HO6-R422A detector is placed on the other side of the chamber. The microwave synthesizer is frequency modulated at a rate of $\leq$50 kHz with a total modulation depth of 200 to 400 kHz. The detector output is phase sensitive detected by a Stanford Research System SR510 lock-in amplifier. While the microwave synthesizer is frequency modulated at $f\simeq$50 kHz, the detector reference is modulated at $2f\simeq$100 kHz. Thus, the resulting lineshape obtained by the lock-in amplifier is a second derivative. Therefore, an absorption "dip" looks like a "peak". Typical line widths (FWHM) are about 0.8 MHz.

Gas sample preparation

The gas mixing apparatus consists of four Swagelok inlet ports. The gas flow through each of the four lines is controlled by an MKS model 1259B mass flow controller. The amount of flow through each controller is monitored by an MKS Instruments model 147B mass flow programmer, and the proportionality of the amount of gas mixed $\sim$1 meter upstream from the nozzle is continuously maintained by the MKS controller. For example, in the case of the C_6H_6-H_2O experiment described below, 3 ports were used. Port 1 supplied Ar at 1.4 standard liters per minute (SLM), port 2 supplied Ar gas bubbled through room temperature H_2O at a flow rate of 4.2 SLM, and port 3 supplied Ar gas passed over benzene at a flow rate of 750 standard centiliters per minute. These flow rates were determined by maximizing a microwave absorption signal due to the C_6H_6-H_2O dimer. This mass flow system allows gas compositions to be changed by simply adjusting gas flow rates. Similarly, sample chemistry tests can be easily accomplished by turning certain gas flows on or off. This system affords real-time gas composition adjustment that is difficult for MBER or FTMW spectrometers.

The gas is expanded into a vacuum chamber pumped by a Roots blower system

with pumping speed at the expansion nozzle of 1800 cfm. (The pumping system used is an Edward pumping station consisting of an EH4200 roots blower and two E2M275 mechanical backing pumps.)

Supersonic adiabatic expansions have been used extensively in gas phase spectroscopy [7, 8, 9]. Both pin hole and slit jets have been well characterized by other researchers. The following is a brief summary of advantages in using a slit nozzle instead of a pin hole nozzle: First, a slit nozzle has an inherently longer cross section for a laser probing perpendicular to the direction of the expansion and parallel to the slit. Thus, the number of absorbing species is increased.

Second, unlike the particles emitted from a pin hole nozzle which diverge in two dimensions, the bulk of the molecules coming out of a slit nozzle diverge only along the dimension perpendicular to the slit and parallel to the face of the nozzle. By probing the jet with a laser perpendicular to the expansion jet and parallel to the slit, most molecules interrogated by the laser have very little velocity components towards or away from the light source. Hence, the line widths are sub-doppler.

Third, since the gas diverges only in one dimension for the slit expansion, the drop-off of gas density with increasing distance from the nozzle is proportional to $1/r$, unlike the two dimensional divergence of a pin hole expansion whose gas density fall-off is proportional to $1/r^2$. This slower drop-off contributes to slower translational cooling, but also to a better chance of cluster formation and a better equilibration of the rotational and vibrational temperatures with the translational temperature. Thus, the spectrum obtained will be further simplified compared to a pin hole expansion.

The first application of a slit nozzle to gas phase spectroscopy was made by Amirav, Even and Jortner [10]. They observed a 3 order of magnitude improvement in sensitivity by using a slit nozzle instead of a circular nozzle. For aniline, they observed T_{trans} = 6 - 8 K, T_{vib} = 20 K. T_{rot} is expected to lie between T_{trans} and T_{vib}. The slit jet cooled more slowly and achieved less ultimate cooling than a circular nozzle.

Sulkes, Jouvet and Rice found that a slit nozzle with aspect ratio of 5:1 affords cooling not very different from a circular nozzle, and that slit nozzles with aspect ratios of greater than 20:1 give performance expected of an infinite slit source [11].

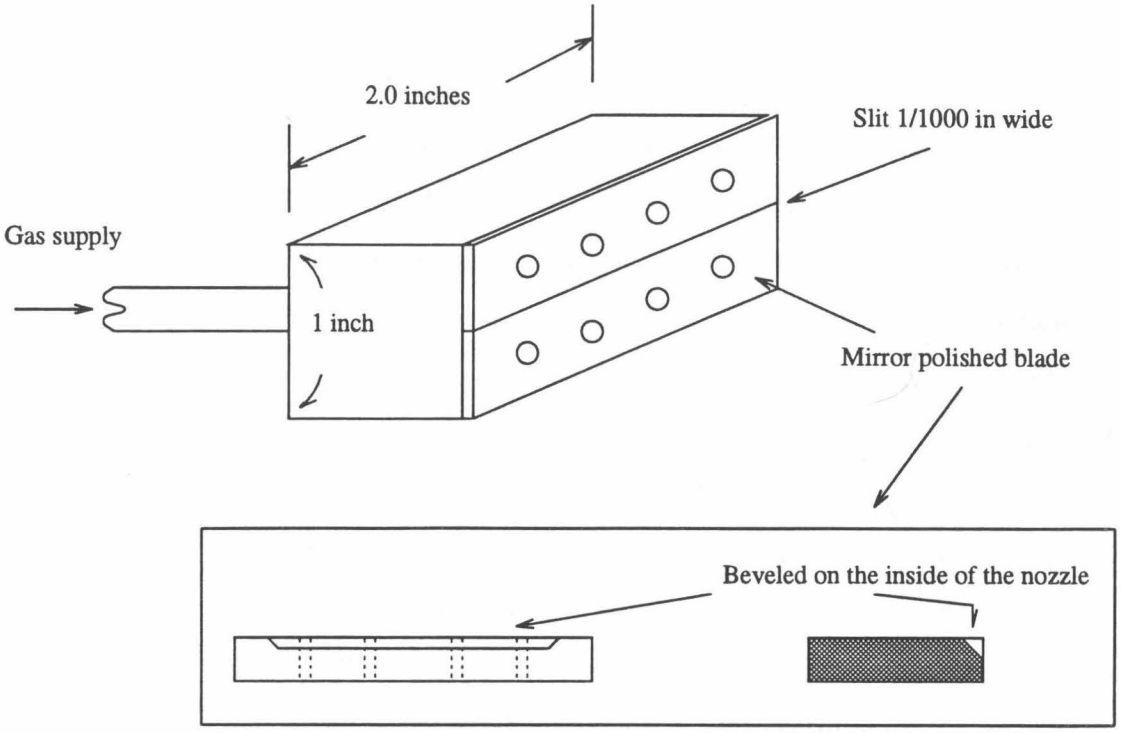

Figure 2.3: Slit nozzle design.

A nozzle with an aspect ratio of 5:1 would be ideal for situations requiring circular nozzle-like cooling but a longer path length. Since our experiment benefits from cooling properties much like those of an infinite slit, a nozzle with a large aspect ratio will be employed.

Specifically, the slit nozzle used is 2 inches long with a slit width of 1/1000″ (see figure 2.3). This nozzle design was optimized by the Saykally group at UC Berkeley. A detailed account is given by Busarow [9].

Hagena has characterized the performances of pin hole and slit nozzles. The following equations are obtained from Hagena's paper [7]:

$$T_x = T_o 0.341 \left(\frac{2.5 \times 10^{-3}}{x}\right)^{2/3}$$

$$M = 2.957 \left(\frac{x}{2.5 \times 10^{-3}}\right)^{1/3}$$

where T_x (K) is the temperature at a distance x (cm) from the nozzle, T_o is the gas temperature in the nozzle reservoir, 2.5×10^{-3} cm is the width of our slit jet, and M is

the Mach number at a distance x (cm) from the nozzle. Sulkes, Jouvet and Rice's [11] data for a slit jet with aspect ratio 20:1 indicates that the terminal Mach number is reached at approximately 60 times the slit width, or 1.5 mm in our application. The translational temperature at that point is approximately 6.5 K. These temperature values agree with that observed by Jortner's group [10]. Experimentally, we observed T_{rot} = 3.6 K (Blake lab notebook no. 3, p. 132), while Busarow reported T_{rot} = 2.9 ± 0.6 K for the nozzles she constructed. The experimental measurements may have had a large systematic error, however, as they are based on intensity differences between two regions in a spectrum, and this is not always highly reliable in the FIR. In any case, adequate cooling was obtained through the nozzle. According to Busarow [9], the Mach disk, the point along the expansion where the density becomes too low to prevent the warm background gas from entering the jet and heating it up, is at $x_{Mach} = 0.67d(\frac{P_B}{P_0})^{0.5}$ for a pin-hole expansion. Since we have a slit nozzle of area $2.5 \times 10^{-3} cm \times 5cm$, the effective radius is $(2.5 \times 10^{-3} \times 5)^{0.5} = 0.063$ and $x_{Mach} = 4.2cm$. Thus, the region 1.7 mm to 4.2 cm away from the nozzle should be examined. Usually, our best results for cluster study were obtained when the FIR beam skimmed the surface of the nozzle.

Stark modulation spectroscopy

In order to improve the S/N for molecules with first order Stark effects, a pair of Stark plates and a Stark modulation (SM) driver box were built (see Fig. 2.4). The $2 \times 3 \times \frac{1}{4}$ inch aluminum Stark plates were polished by hand to low grade optical quality. The plates were placed above and below the planar jet. Two pieces of Plexiglas and threaded nylon rods were used to attach the plates to the nozzle with a 4.825 cm separation and in electrical isolation, as shown in Figure 2.4. The simple electrical circuit used to apply the modulated Stark field is shown in Figure 2.5. High-voltage, high slew-rate operational amplifiers (model PA85; 450 V, 1000 V/μs) were purchased from Apex Microtechnologies. The input signal is a 0.2-5 V, 100 kHz square wave generated by an HP function generator (model 3312A). The outputs are also square waves, one positive and the other negative relative to the nozzle and the rest of the

instrument, which are tied to ground. Although the total voltage that can be supplied by the circuit is 450 V (+225 V and -225 V), our typical operating pressure in the vacuum chamber is ~100 mTorr, which results in a measured break down voltage of about 200 V. In addition, this voltage is limited by the dual power supply that is currently available (± 50 V). Typical FWHM observed with frequency modulation is about 0.5 MHz to 1.0 MHz. With Stark modulation, we observed line widths of about 0.7 MHz to 1.4 MHz in the microwave region. The field inhomogeneity and the amplitude of the Stark shift contribute to this line width. In the Stark modulation mode, most scanning parameters are the same as in FM, *viz.* a step size of 40 kHz, a dwell time of 200 ms, and a lock-in time constant of 1 s; but the modulation frequency, which is limited by the lock-in amplifier, was increased to 100 kHz for $1f$ detection. One significant difference is that SM plus phase sensitive lock-in detection does not require a separate background subtraction scan; thus, the scanning time is halved. The typical field strength used was 70 V. Acetonitrile served as the test molecule, which revealed that the effective plate separation was increased to 5.245 cm by the field inhomogeneity. Our weak field does not allow some Stark components to be shifted beyond the boundary of the parent peak. With a larger field, the composite line could resolve all the Stark components, and thereby reduce the FWHM.

SM is particularly powerful in enhancing the S/N during microwave spectroscopy, which suffers greatly from resonances in the sample cavity. For the benzene-water spectrum taken near 40 GHz, the S/N of SM spectra taken at 100 kHz modulation, 25 V/cm field strength and 10 scan averaging was about 3 times better than that of an FM spectrum taken at 50 kHz modulation and summed over 60 scans. Thus, the S/N for the SM is $3 \times 6^{1/2} \times 3^{1/2} = 10$ times better than FM.

Later, when SM was applied to far-infrared (FIR) spectroscopy, the S/N for each scan for FM and SM was very similar. However, Stark modulation takes half the time since no background subtraction scan is needed. Thus, the effective S/N was increased by a factor of 2. Also, the weak Stark field limits the clusters observed to those with a first order Stark effect, i.e., systems which are symmetric tops or have degeneracies. This was particularly useful when scanning for benzene-water peaks in

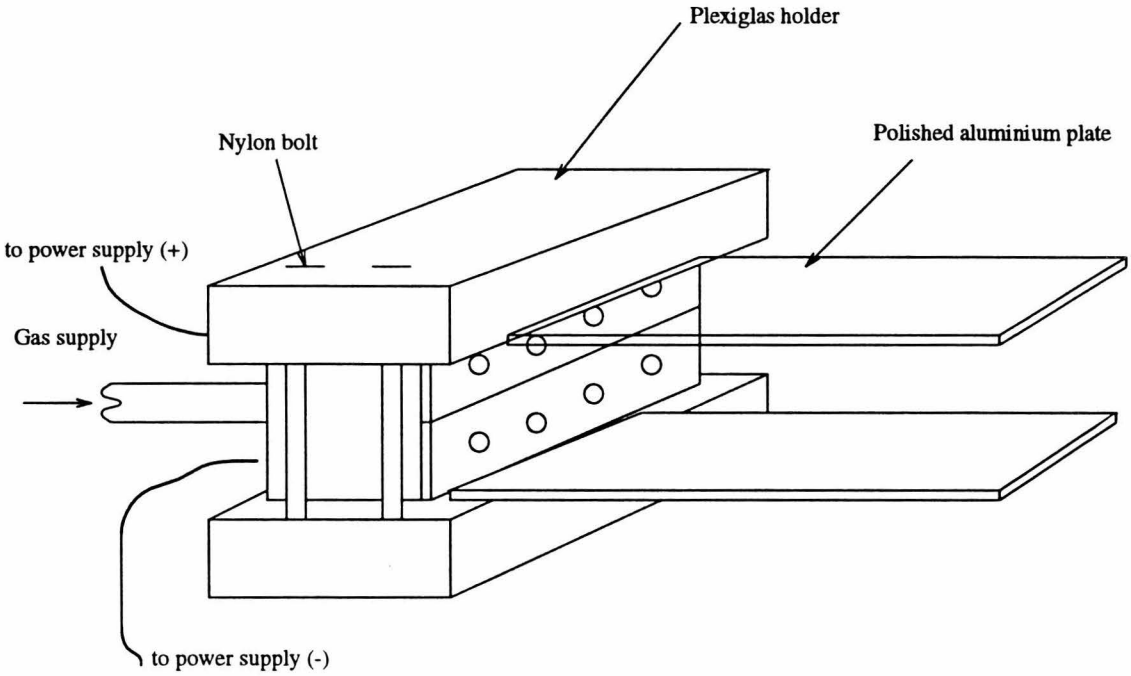

Figure 2.4: Stark plates attached to the slit nozzle

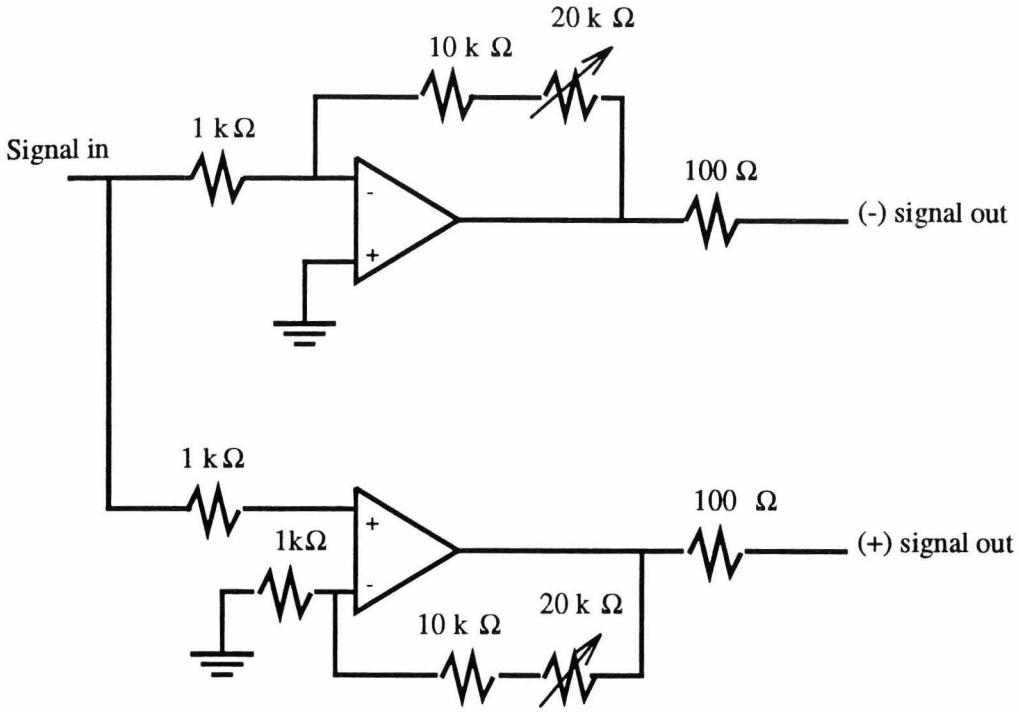

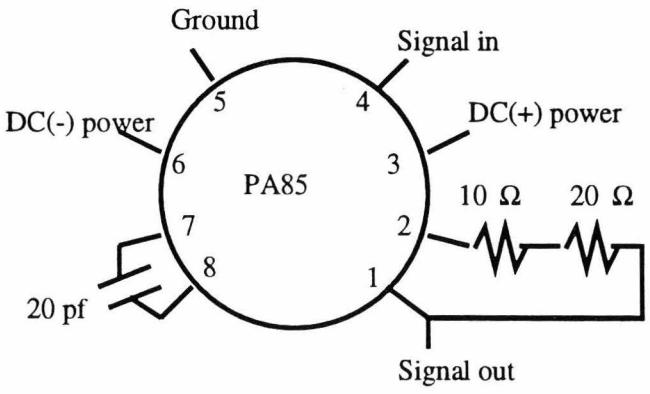

Figure 2.5: The Stark modulation power supply.

the FIR, where there are many absorption lines from monomer water and Ar-water clusters. Both the monomer and Ar-water cluster lines were removed from the spectra automatically. Thus, SM has been helpful in increasing the S/N and in simplifying spectra.

The lower bound for the necessary Stark shift to be observable with the Stark modulation spectrometer was determined to be 0.5 MHz. With the limited field strength of 40 V/cm that is available, this implies that a 0.0125 MHz/(V/cm) Stark coefficient is necessary to be observable.

2.1.3 Comparison of the two microwave techniques

A comparison of the DAMW spectrometer at Caltech and the FTMW instrument at NIST will be made to illustrate the advantages of each method. FTMW requires a carefully constructed resonance cavity, where as DAMW simply requires a molecular beam nozzle and a vacuum chamber. The microwave source and the detection scheme in FTMW requires various electronic devices and mixers in addition to the microwave synthesizer, while DAMW uses a commercially available lock-in amplifier, a diode detector, and a microwave synthesizer. Indeed, the DAMW system was quite simply transported in an afternoon to the University of Southern California where we characterized a nozzle and a vacuum chamber there.

The frequency range surveyed by FTMW is lower than that available for DAMW: 4 to 26 GHz for FTMW *vs.* 20 to 40 GHz (possibly up to 60 GHz) for DAMW. FTMW is limited by the resonance cavity geometry and the available microwave electronics. DAMW is limited in the low frequency range by poor S/N. By observing transitions with higher energy, DAMW is capable of probing higher up the potential well of these weakly bound clusters, i.e., energy levels with higher distortion, providing useful IPS information.

The resolution of FTMW is $\sim$ 1 to 30 kHz while that for DAMW is $\sim$ 0.5 to 1 MHz. Thus, FTMW is capable of resolving finer hyperfine splittings than the DAMW is capable of, and therefore, provides additional information such as quadrupole and

spin-spin coupling constants, and dipole moments.

FTMW consumes far less sample ($\sim$ 0.02 SLM) since it uses a pulsed circular nozzle as compared to the continuous slit nozzle ($\sim$ 10 SLM) used in DAMW. This is an advantage and a disadvantage to each method. By having a much smaller throughput, FTMW can be used to study compounds with rare isotopes that are prohibitively expensive for DAMW and its continuous source. Because of the large throughput, however, compounds with facile isotopic exchange, namely hydroxyl groups with deuterium (D) substitution, can be used with DAMW. In FTMW, prolonged D exchange of the gas line is necessary to ensure that the observed species is a D substituted compound, not one which exchanged the D for ^{1}H. By using a mass flow controller to adjust gas composition on-the-fly, DAMW is capable of quick chemistry tests, including isotopic substitutions. FTMW requires cumbersome and time consuming changes of the various gas mix cylinders.

Thus, the DAMW is a simple system that is easily transported and set-up. It yields useful information quickly; however, it does not have as high a resolving power or sensitivity does FTMW, which is a more complicated system capable of providing detailed information useful in structural analyses. Detail instructions on setting up the microwave experiment at Caltech are given in Appendix A.

2.2 The Caltech tunable FIR spectrometer

Intermolecular potential energy surfaces (IPS's) describe in detail the energetics of molecular association. A well characterized IPS can yield information regarding the reaction dynamics, bulk properties, and other matters of chemical and material interests. Hence, the elucidation of IPS's have been pursued by many researchers in the past, as has been described in some detail in the introductory chapter.

As noted previously, in this thesis intermolecular bonds are probed directly in the naturally occurring state, i.e., the ground vibrational and electronic states. Thus, far-infrared photons, which correspond to intermolecular vibrational energies, are used with full rotational resolution for detailed investigation of both the ground and the

vibrationally excited state.

The first tunable far-infrared sideband spectrometer (TuFIR) applied to the study of intermolecular clusters was built at the University of California at Berkeley. Several previously existing technologies were combined to construct the TuFIR instrument: a CO_2 laser-pumped FIR gas laser source, FIR sideband production in GaAs Schottky diodes, a slit jet, and an appropriate detector. A detailed description of the original TuFIR is given by Blake *et al* [12, 13].

The basic design and construction of the Caltech TuFIR are nearly the same as those described by Blake *et al.* The following paragraphs present specifics for the Caltech system (see figure 2.6).

CO_2 laser

The CO_2 laser used to optically pump the FIR laser was purchased from Apollo (model 150). Since then, numerous changes and repairs have been made. The CO_2 gas mix was purchased from Matheson Gas, and recycled through a platinum catalyst column. However, the catalyst column was eventually contaminated. The catalytic element was not successfully replaced, and hence, the gas could no longer be recycled. In order to reduce the laser gas cost, we began to mix the three gases (N_2, He, CO_2) in real-time using a gas flow mixer. The flow ratio was first adjusted to match the recommended gas composition and later fine tuned to maximize the CO_2 laser power output. In 1990, the CO_2 output was greater than 100 W for most lines. However, for some unresolved reasons, the power has declined to range between 45 and 80 W. We do not have difficulties producing sufficient FIR laser intensity, and in fact continue to observe previously seen peaks with significant signal-to-noise ratio increases. Thus, we have not spent much effort to correct this problem, which may be a simple calibration error of the power meter.

Initially, there was a noticeable drift in the CO_2 laser power accompanying the cooling/heating cycle of the CO_2 laser cooling water circulator. By purchasing a new circulator with temperature control of $\pm$ 0.1 °C, the laser power seems to stabilize after some time ($\sim$ 2 hours); the laser may be stable continuously for several hours in the late evenings and early mornings, requiring no manual adjustments of the laser

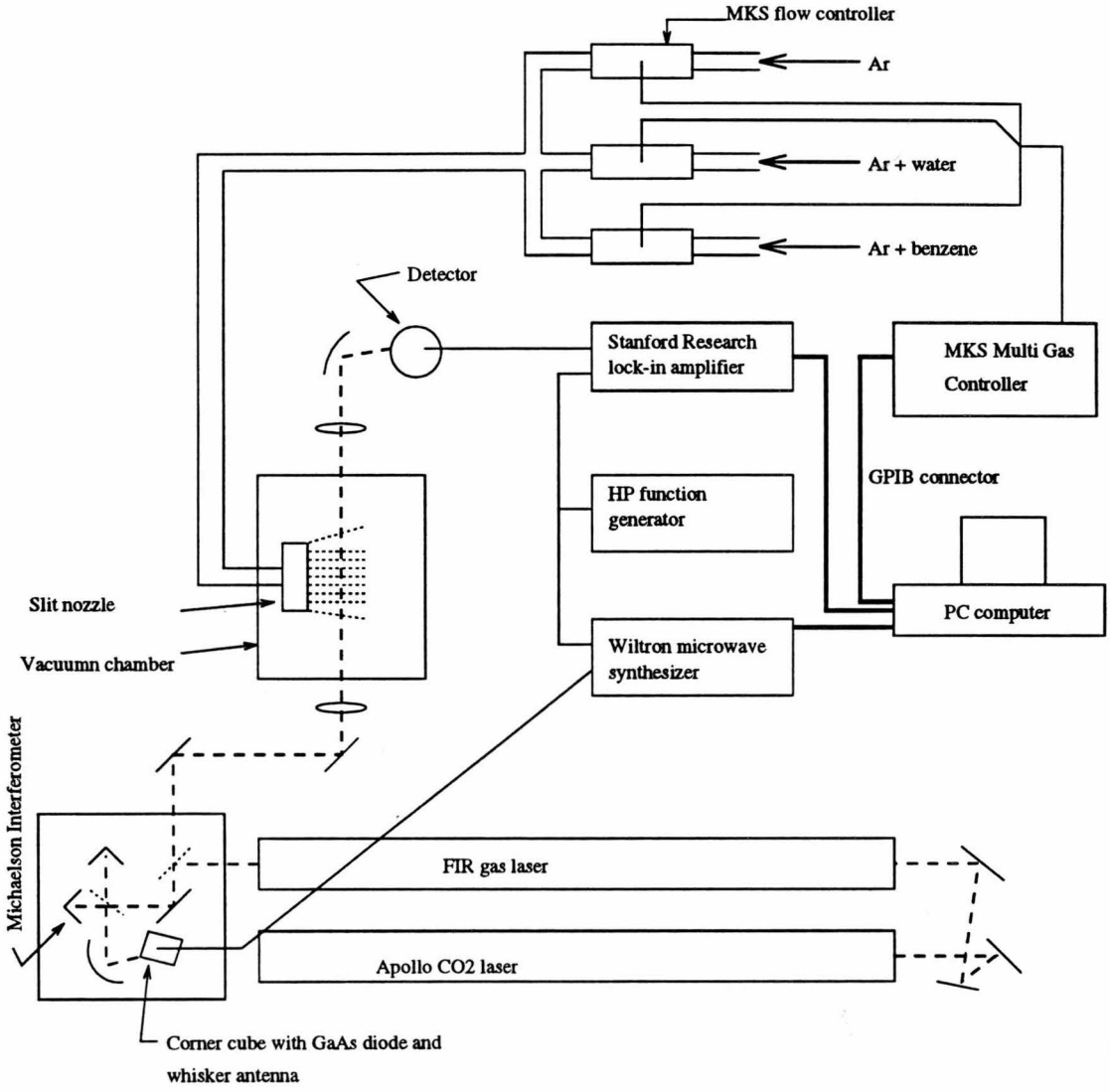

Figure 2.6: Caltech TuFIR spectrometer

cavity.

The CO_2 laser power supply fails occasionally. The high voltage transformers have failed three times and have been replaced. The high voltage regulator zener diodes burnt out twice and were also replaced. These diodes on the bottom side of the pull out tray are easily exchanged. Degradation of the laser parts occasionally pose serious problems. The diffraction grating was replaced once, and if the laser cavity is contaminated by O_2 or H_2O the grating may become pitted and in need of replacement. The anodes deteriorated once and these parts were machined based on the measurements taken of the partially disintegrated original steel parts. This steel part must be acid washed to remove all oil and carbonaceous material. Similarly, the inside of the cathode housing had to be rebuilt to correct damage created by arcing inside the housing assembly. Both cooling water and oil are in the cathode housing, and thus, partial damage to the cathode housing may lead to a water and/or oil leak which causes severe damage to the entire laser system. This problem was noted by the Berkeley group, also. However, we have not experienced the cathode oil leakage back in to the laser power supply that they also noted.

The laser housing parts made of aluminum seem to degrade over time. This leads to the accumulation of metal particles in the cooling tube surrounding the lasing tube itself, which eventually clogs the circulating water and thereby leading to several problems: pressure build-up causing circulator failure; water leakage into the laser cavity; or heating of the stagnant cooling water leading to a meltdown of the laser's outer cooling tube. The aluminum deposits are removed as necessary. The laser is disassembled with little difficulty, but the detachment of the laser cavity quartz tube from the holders must be performed with great caution. With proper care to avoid breaking the tube, the bored tube can be removed and installed without serious difficulty. Whenever the laser is disassembled, it should be realigned using a He:Ne laser. (See Appendix C for repair hints and alignment instructions.)

2.2.1 FIR laser

The optically pumped FIR gas laser, described in detail elsewhere [13, 14], has been slightly modified. The gold coating on the original cavity mirrors eventually eroded. We learned that chromium coating available at a local electroplating company would work as well as the gold coating and was claimed to be more robust. The electrocoated chromium eventually eroded as well, however. A local brass polishing and chrome coating shop was used to recoat the mirrors, but in-house resurfacing was needed. The mirrors were lapped over number 200, 400, 500, 600 sand paper and then with a 1 μm diamond grit mirror polishing kit. Since the resulting bare copper mirror surfaces looked quite good optically, we surmised that they should be good FIR reflectors as well. The copper mirrors ($\sim$ \$ 50 each) were directly placed in the FIR laser. For nearly three years, the bare copper mirrors have functioned just as well as the chromium plated and gold coated mirrors.

2.2.2 Mixing microwaves and FIR radiation

The FIR laser radiation is coupled with microwave radiation using a Schottky- barrier diode. The process of mixing and separating the TuFIR photons and the unmixed carrier is described elsewhere [15, 16, 17, 18]. A brief description is given below with some useful parameters for the Caltech instrument.

The microwave source is a Wiltron 6747A-20 phase-locked frequency synthesizer (+18 dBm output in the range 10 MHz-20GHz), the same source used in the microwave spectrometer described above. The microwave radiation and the FIR laser radiation are coupled onto and mixed in a whisker contacted GaAs Schottky-barrier diode located at the apex of a rooftop, or corner cube, reflector [16, 17]. The diode responds non-linearly to the electric fields it is subjected to. Typically, a 100 to 1000 mV change in the diode bias occurs when microwave or FIR radiation is coupled onto the diode. Oscillating electric fields at frequencies

$$n \cdot (laser frequency) \pm m \cdot (microwave frequency)$$

where $n, m = 1, 2, 3, \ldots$, flow through the diode. These frequencies are radiated by the whisker antenna along the incoming path of the FIR laser. Thus, the FIR laser, the sums and the differences of the FIR laser and microwave harmonics, and harmonics of the microwave radiation are produced. According to Zmuidzinas [16], it is best to maintain the whisker antenna length at $L \geq \lambda_{FIR}$. The position of the antenna and the diode are adjusted within the corner cube, whose overall geometry rotation angle is optimal when

$$\theta_{max} = cos^{-1}[1 - 0.37101\frac{\lambda_{FIR}}{L}]$$

and

$$s = 0.485\frac{\lambda_{FIR}}{sin\theta_{max}}$$

where θ_{max} is the angle between the FIR laser and the whisker and s is the distance between the antenna and the corner cube roof top mirror [16]. Whenever λ_{FIR} is changed, θ_{max} is calculated and the corner cube is adjusted to that angle. Then, the position of the roof top mirror is adjusted to produce the best coupling, i.e., s is not calculated but empirically adjusted. The uncoupled FIR laser radiation travels reversibly through the Martin-Puplett polarizing interferometer, re-entering the FIR laser cavity. The lengths of the interferometer arms are adjusted to maximize the amount of first harmonic sideband ($\nu_{laser} \pm \nu_{microwave}$) and to minimize the FIR fundamental that are passed to the sample chamber and the detector. Ideally, this means that the following equation holds true: $2l = 2n\lambda_{laser} \cong (2m+1)\lambda_{sideband}$, where n and m are integers and l is the path length difference of the two arms. Typically there are small misalignments in the interferometer so that the best approach is to maximize on a spectroscopic signal.

The amount of laser radiation, microwave radiation, and current should be adjusted to yield the best molecular absorption signal. The molecular absorption signal-to-noise seems to be best when the diode voltage is between 300 to 600 mV. Thus, the diode current is increased until the diode voltage is in this range. If the microwave or the FIR radiation is too strong to allow the diode voltage into this range, the radiation strengths are reduced. As the current on the diode is increased, the noise

level also increases. However, in most cases the signal-to-noise ratio increased as the diode current was increased until the diode voltage was between 300 and 600 mV.

The detector employed is a $He_{(l)}$-cooled InSb hot electron bolometer (Cochise Instruments), used in either the Rollin mode (zero field) or the Putley mode (2.7 to 5.5 kG external magnetic field). The responsivity of InSb as a function of the magnetic field has been studied by Brown [19]. Samarium-cobalt magnets obtained from the local Magnet Sales Company are used to obtain various field strengths. The geometric configuration of the detection element is such that the field strength could not be increased to greater than 5.5 kG even with additional magnets. New detector designs and new magnets are being considered to increase the field strength.

The original Cochise Instruments apparatus was equipped with 20 AA battery holders. Twenty AA batteries usually lasted for $\sim$ 20 hours. The cost of batteries and the excess hazardous wasted produced prompted us to modify the power supply to consist of four 8 V fork lift batteries. With an appropriate circuit, these batteries performed well and for over a year of normal operation. A small power supply was constructed by the department staff to re-charge the batteries over night once a month to prolong the battery life indefinitely.

The gas flow control, slit jet nozzle and the vacuum chamber are the same as those used in DAMW. The TuFIR spectrometer is a high resolution, high sensitivity instrument, and provides measurements of the intermolecular vibrational modes of weakly bound clusters at rotational resolution for the first time.

2.3 Summary

A brief description of the instruments used were given above. The Caltech DAMW, which was developed as a simple modification of the TuFIR instrument, resulted in an effective microwave spectrometer, capable of scanning regions not readily accessible by other microwave designs. Its S/N was increased with the addition of a Stark modulation adapter. The high resolution FTMW spectrometer at NIST was used to obtain detailed information helpful in structure determination for certain clusters.

The Caltech TuFIR spectrometer is similar to those used at University of California at Berkeley and the Jet Propulsion Laboratory. The Stark modulation developed for the DAMW is directly applicable to the TuFIR.

For more practical details of operation, the reader is referred to the appendices: Appendix A for the microwave experiment, Appendix B for the FIR experiment and Appendix C for the TuFIR and other hardware repair.

Bibliography

[1] C.H. Townes and A.L. Schawlow. *Microwave Spectroscopy.* Dover Publications, Inc., New York, NY 10014, 1975.

[2] T.R. Dyke, B.J. Howard, and W. Klemperer. Radiofrequency and Microwave Spectrum of the Hydrogen Fluoride Dimer; a Nonrigid Molecule. *J. Chem. Phys.*, 56:2442, 1972.

[3] T.J. Balle, E.J. Campbell, M.R. Keenan, and W.H. Flygare. A New Method for Observing the Rotational Spectra of Weak Molecular Complexes: KrHCl. *J. Chem. Phys.*, 71:2723, 1979.

[4] T.J. Balle, E.J. Campbell, M.R. Keenan, and W.H. Flygare. A New Method for Observing the Rotational Spectra of Weak Molecular Complexes: KrHCl. *J. Chem. Phys.*, 72:922, 1980.

[5] F.J. Lovas and R.D. Suenram. Pulsed Beam Fourier Transform Microwave Measurements on OCS and Rare Gas Complexes of OCS with Ne, Ar, and Kr. *J. Chem. Phys.*, 87:2010, 1987.

[6] R.D. Suenram, F.J. Lovas, G.T. Fraser, J.Z. Gilles, C.W. Gilles, and M. Onda. Microwave-Spectrum, Structure, and Electric-Dipole Moment of Ar-CH_3OH. *J. Mol. Spect.*, 137:127, 1989.

[7] O.F. Hagena. Nucleation and Growth of Clusters in Expanding Nozzle Flows. *Surf. Sci.*, 106:101, 1981.

[8] R.E. Smalley, L. Wharton, and D.H. Levy. Molecular Optical Spectroscopy with Supersonic Beams and Jets. *Acct. Chem. Res.*, 10:139, 1977.

[9] Kerry Lynn Busarow. *Tunable Far Infrared Laser Spectroscopy of Van Der Waals Molecules in a Planar Supersonic Jet Expansion.* Ph.D. thesis, University of California at Berkeley, Berkeley, CA, December 1990.

[10] A. Amirav, U. Even, and J. Jortner. Absorption Spectroscopy of Ultracold Large Molecules in Planar Supersonic Expansions. *Chem. Phys. Lett.*, 83:1, 1981.

[11] M. Sulkes, C. Jouvet, and S.A. Rice. Theoretical and Experimental Characterization of Supersonic Expansions from Slit Sources. *Chem. Phys. Lett.*, 87:515, 1982.

[12] G.A. Blake, K.B. Laughlin, R.C. Cohen, K.L. Busarow, D-H. Gwo, C.A. Schmuttenmaer, D.W. Steyert, and R.J. Saykally. Tunable Far Infrared Laser Spectrometers. *Rev. Sci. Instrum.*, 62:1693, 1991.

[13] G.A. Blake, K.B. Laughlin, R.C. Cohen, K.L. Busarow, D-H. Gwo, C.A. Schmuttenmaer, D.W. Steyert, and R.J. Saykally. The Berkeley Tunable Far Infrared Laser Spectrometers. *Rev. Sci. Instrum.*, 62:1701, 1991.

[14] T.Y. Chang and T.J. Bridges. Laser Action at 452, 496, and 541 μm in Optically Pumped CH_3F. *Opt. Commun.*, 1:423, 1970.

[15] J. Farhoomand, G.A. Blake, M.A. Frerking, and H.M. Pickett. Generation of Tunable Laser Sidebands in the Far-Infrared Region. *J. Appl. Phys.*, 57:1763, 1985.

[16] J. Zmuidzinas, A.L. Betz, and R.T. Borenko. A Corner-Reflector Mixer Mount for Far Infrared Wavelengths. *Infrared Phys.*, 29:119, 1989.

[17] E.N. Grossman. The Coupling of Submillimeter Corner-Cube Antennas to Gaussian Beams. *Infrared Phys.*, 29:875, 1989.

[18] H. Kräutle, E. Sauter, and G.V. Schultz. Antenna Characteristics of Whisker Diodes Used as Submillimeter Receivers. *Infrared Phys.*, 17:477, 1977.

[19] Elliott R. Brown. *Investigation of Bulk Indium Antimonide as Heterodyne Detector for the Submillimeter Wavelength Region.* Ph.D. thesis, California Institute of Technology, Pasadena, CA 91125, May 1985.

Chapter 3 Ar-water clusters: Ar-D_2O and Ar-HDO

As described in the Introduction, the study of intermolecular interactions began with simple systems. One such system was rare gas-(polar bond) interactions such as the Ar-HCl dimer, which was investigated extensively by numerous researchers. The next step up in complexity is atom-triatom complexes. Following the rare gas-polar motif, Ar-H_2O was among the first of these dimers to be investigated. Water is an ubiquitous polar solvent, and Ar-water serves as the simplest, some may say trivial, model for "hydrophobic" interactions.

Before the work presented here was initiated, Ar-H_2O had been investigated using microwave and FIR spectroscopy as well as by calculational methods. Extensive surveys using an FIR sideband spectrometer at UC Berkeley were performed by Cohen and Saykally [1, 2]. The vibration-rotation-tunneling(VRT) motions were subsequently interpreted and fit to model potentials [3, 2].

In this work, deuterated isotopomers of Ar-water were investigated to obtain experimental details which complement those obtained by Cohen and Saykally [1, 2] and to test the AW1 potential surface obtained by these authors [2].

3.1 Experimental

FIR spectra were obtained for Ar-D_2O and Ar-DOH in the 490 - 720 GHz range with formic acid lasers at 584.4 and 693.0 GHz providing the FIR carrier frequencies. Gas mixtures of Ar and H_2O/D_2O/DOH were prepared by passing Ar gas over a 50/50 mixture of H_2O and D_2O at room temperature. Flow rates of the gas mixture were 2.9 standard liters per minute (SLM) of Ar and 4 SLM of Ar bubbled through water. A total of 179 lines were found, of which 110 were assigned to Ar-DOH or Ar-D_2O, 69 remain unassigned. Lines due to H_2O/D_2O monomers and dimers were removed

by chemistry tests, while those due to Ar-H_2O were removed based on assignments made by Cohen *et al* [1, 2]. Ar-DOH and Ar-D_2O transitions were differentiated by using pure D_2O and by assignment based on ground state microwave data and combination-differences [5]. Lists of the observed and assigned transition frequencies are given in Tables 3.2 and 3.3.

3.2 Data analysis

The transitions observed (broken arrows) as well as those states coupled by Coriolis interactions (double-headed solid arrows) are shown in Figure 3.1, whose notation follows that of Cohen *et al.* [2]. For Ar-D_2O, two distinct bands at 579.7 and 619.6 GHz were observed. The lower energy transition consisted of P, Q and R branches, while the higher energy transition contained only P and R branches. Furthermore, the P and R branches and the Q branch of the lower energy transition seemed to behave slightly differently, indicating that the origin or the terminating states are different. The energy level correlation diagram produced by Cohen *et al.* [2] was then consulted (see Figure 3.1). Cohen *et al.* concluded that case (b) in Figure 3.1 was the correct interpretation of the degree of anisotropy in the Ar-water potential. The set of P, Q and R and the set of P and R transitions have an average transition energy of 599.65 GHz, very close to the free D_2O $0_{00} \rightarrow 1_{11}$ rotational transition at 607.3 GHz. Thus, these bands are likely to be the $\Sigma_{0_{00}} \rightarrow \Pi_{1_{11}}$ and $\Sigma_{0_{00}} \rightarrow \Sigma_{1_{11}}$ transitions in the *para* manifold of Ar-D_2O. Analogous to the existence of metastable states in H_2 and D_2 that arise because of the forbidden exchange of fermions and bosons, there are two flavors of water, *para* and *ortho*, corresponding to symmetric and antisymmetric states, which do not interchange because of nuclear spin statistics. It is as though there were two types of Ar-H_2O clusters and two types of Ar-D_2O clusters in the molecular beam. The $\Sigma_{0_{00}} \rightarrow \Pi_{1_{11}}$ band within the *para* manifold can be further split into two components (see Figure 3.1): The P and R branches of the lower energy transition are assigned to the $\Sigma^+ \rightarrow \Pi^+$ transition, and the Q branch, which requires a change in parity, is assigned to the $\Sigma^+ \rightarrow \Pi^-$ transition.

The higher energy band corresponds to the $\Sigma^+_{0_{00}} \rightarrow \Sigma^+_{1_{11}}$ transition, but does not have a Q branch, just as expected due to the lack of a parity change. These bands are not stretching vibrations of the pseudodiatomic system but arise from the nearly free internal rotation of the water subunit. We say that it is nearly free because the average transition energy is slightly less than that of a free D_2O monomer, and because the m_j degeneracy of the D_2O 1_{11} E level is split by the interaction of the water rotation with the overall rotation. The splitting in the $\Pi_{1_{11}}$ level arises from the Coriolis interaction of the water rotation with the complex frame. As explained in detail by Cohen *et al.* [2], the Σ and Π labels denote the projection of the internal rotation onto the pseudodiatomic axis. Σ has no projection onto the axis and Π possesses one quantum, as shown in Figure 3.2. The $\Sigma^+_{1_{11}}$ and $\Pi^+_{1_{11}}$ states are connected by the Coriolis interaction, causing the $\Pi^+_{1_{11}}$ level to move further away from $\Sigma^+_{1_{11}}$ level than $\Pi^-_{1_{11}}$ level. Note that the $\Pi_{1_{11}}$ states are lower in energy than the $\Sigma_{1_{11}}$ state, contrary to the interpretation of Hutson's Ar-H_2O potential [3, 6]. Figure 3.1 has the correct energy ordering.

The assigned transitions were fit with the Hamiltonian given by Cohen *et al.*[2] including Coriolis coupling:

$$H(\Sigma) = \nu + B(J(J+1)) - D(J(J+1))^2 + H(J(J+1))^3 + L(J(J+1))^4 + ...$$

$$H(\Pi) = \nu + B(J(J+1) - l^2) - D(J(J+1) - l^2)^2 + H(J(J+1) - l^2)^3 + ...$$

$$H_{Coriolis} = \beta(J(J+1))^{1/2}$$

where $H_{Coriolis}$ couples the Σ^+ state to the Π^+ state and is arranged in the Hamiltonian matrix as

$$\begin{vmatrix} \Sigma^+ & H_{Coriolis} & 0 \\ H_{Coriolis} & \Pi^+ & 0 \\ 0 & 0 & \Pi^- \end{vmatrix}$$

See Appendix E for the fitting program and its explanation.

For Ar-DOH, only P and R branches were found at 597.0 GHz. Based on ground

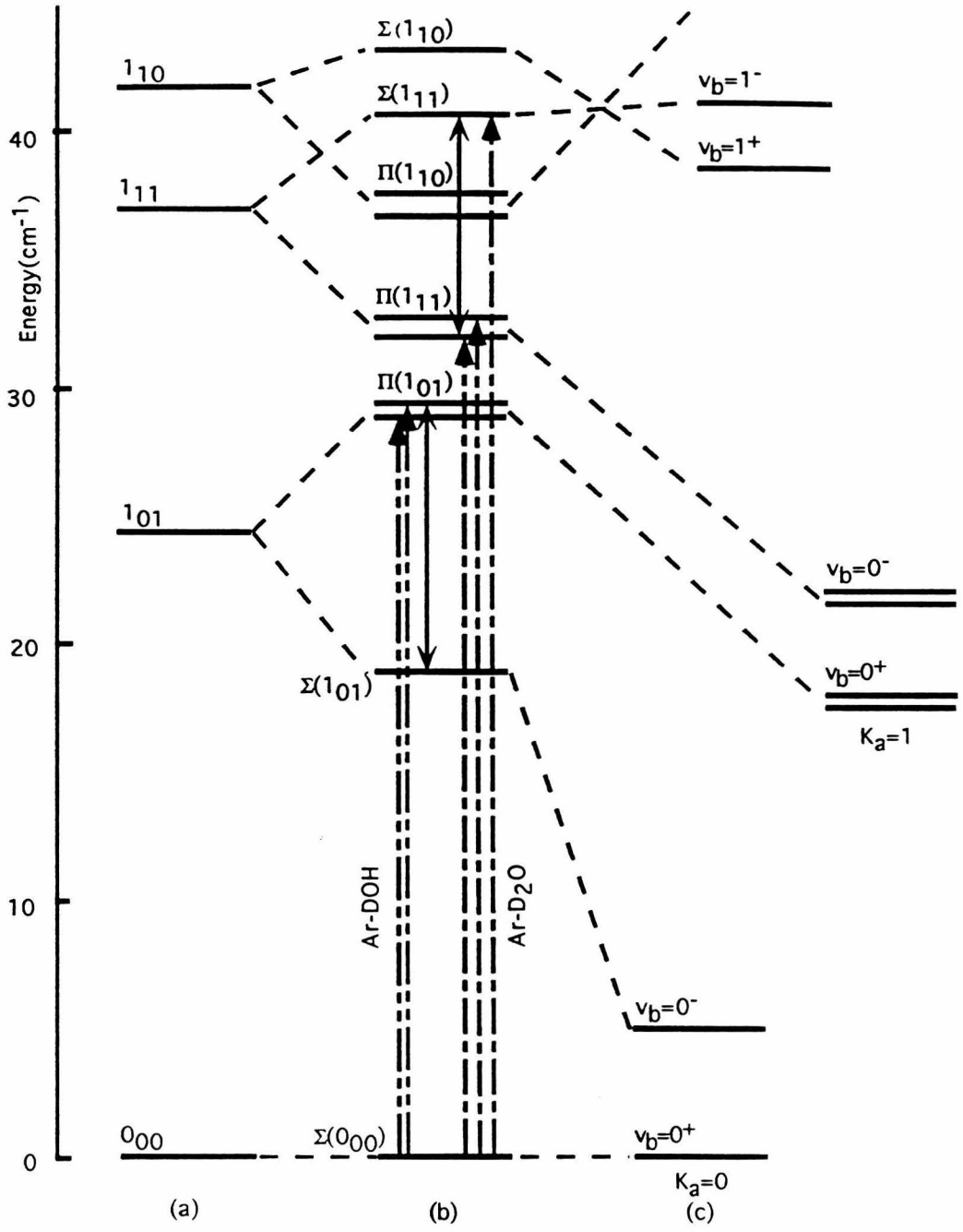

Figure 3.1: Ar-water energy level diagram: a) The free rotor limit for water; b) a slightly hindered rotor; and c) the near rigid-rotor limit.

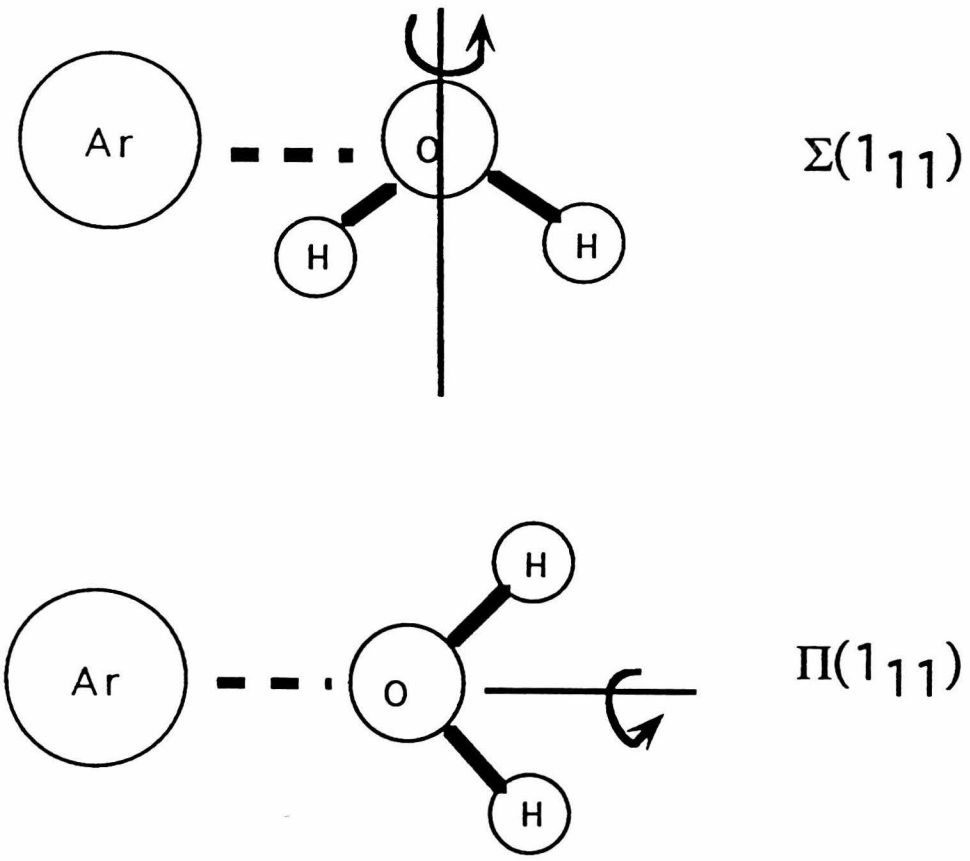

Figure 3.2: Σ and Π states of Ar-H_2O with $j_{water} = 1_{11}$.

state information obtained from Fraser *et al.* [5], we knew that this transition originated from the $\Sigma_{0_{00}}$ ground state. We also noted that the P and R branches fit differently from the Q branch in a preliminary fit. This situation is similar to the case for Ar-D_2O. Considering the free rotational energy of HDO, this is unlikely to be the $0_{00} \rightarrow 1_{11}$ transition, which lies at 893638.67 MHz. Since HDO does not have ortho and para manifolds, there is no separation of states by spin statistics in HDO. A ground state transition from $0_{00} \rightarrow 1_{01}$ is therefore reasonable. (The free HDO $0_{00} \rightarrow 1_{01}$ transition lies at 464924.52 MHz.) As seen in Figure 3.1, the free water 1_{01} level is split into $\Sigma_{1_{01}}$ and $\Pi_{1_{01}}$ states, similar to the Ar-D_2O case. These motions correspond to those shown in Figure 3.3, with the $\Pi_{1_{01}}$ split further by Coriolis interaction with the $\Sigma^+_{1_{01}}$ state. We did not observe a set of transitions without a Q branch, that is, we did not observe the $\Sigma^+_{0_{00}} \rightarrow \Sigma^+_{1_{01}}$ transition. Thus, in the fitting of the $\Sigma^+_{0_{00}} \rightarrow \Pi^{\pm}_{1_{01}}$ transitions, we estimated the $\Sigma^+_{1_{01}}$ energy level, which is required for the Coriolis constant, based on the prediction of Lascola and Nesbitt from near-IR spectroscopy [7].

The fitted constants for both isotopomers are given in Table 3.1. Several assumptions were made in the fitting procedure. For Ar-D_2O, the constants were fit simultaneously, forcing ν and B for Π^+ and Π^- to be the same and allowing D, H, L to vary. For the Ar-DOH spectrum, where the $\Sigma^+_{0_{00}} \rightarrow \Sigma^+_{1_{01}}$ band was not observed, we have used predicted values of 9.06 cm^{-1} for the $\Sigma^+_{1_{01}}$ state energy [7]. The results are summarized in Table 3.1. In order to estimate the effect of errors in the location of the $\Sigma^+_{1_{01}}$ state on β, values ± 1 cm^{-1} from that predicted were substituted and the parameters adjusted to fit the observed line frequencies. The Coriolis coupled constants obtained for each value of $\nu(\Sigma^+_{0_{00}} \rightarrow \Sigma^+_{1_{01}})$ are 5662.35(62), 5414.55(59), and 5160.76(56) MHz for ν = 8, 9.06, and 10 cm^{-1}. Adopting the error of 0.1 cm^{-1} predicted theoretically [7], β can be determined to about ± 25 MHz.

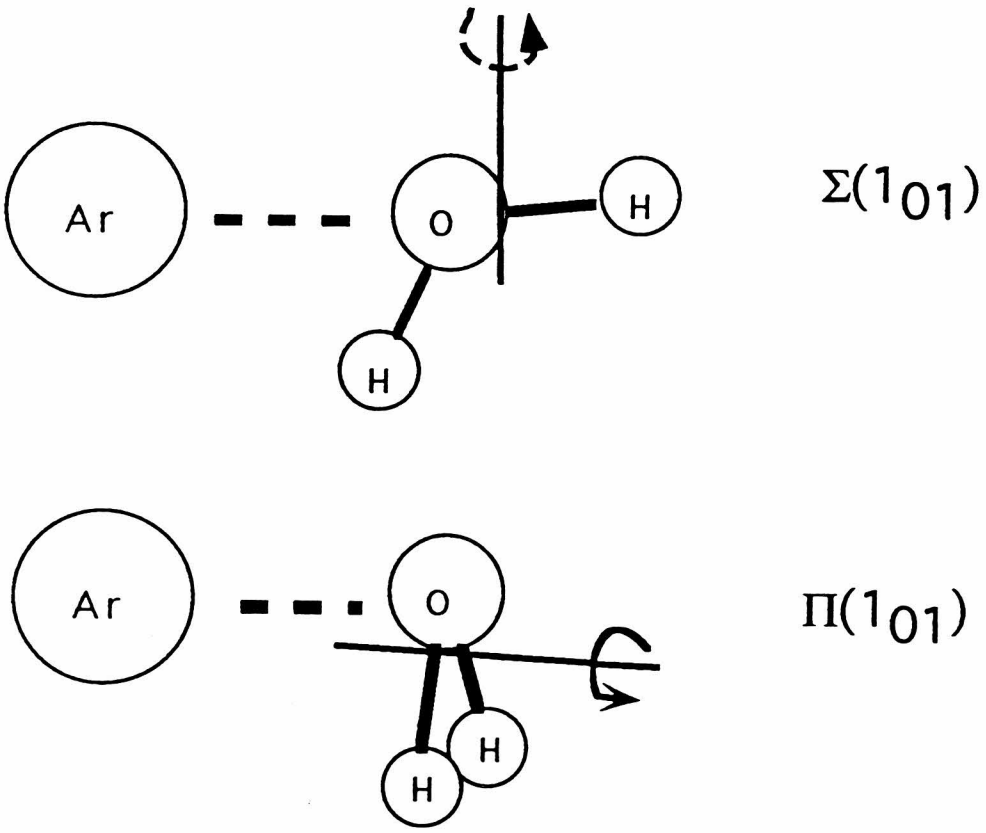

Figure 3.3: Σ and Π states of Ar-H_2O with $j_{water} = 1_{01}$.

Table 3.1: Fitted Ar-D_2O and HDO constants. All values are in MHz.

Ar-D_2O Constants	$\Sigma^+(0_{00})$	$\Sigma^+(1_{11})$	$\Pi^+(1_{11})$	$\Pi^-(1_{11})$
ν	0.0(fixed)*	619643.47(34)	579652.75(32)	579652.75(32)
B	2795.93(fixed)*	2808.409(30)	2793.526(22)	2793.526(22)
D	0.078137(fixed)*	0.13624(85)	0.01384(74)	0.07906(33)
H	-2.406E-6(fixed)*	-2.33(69)E-5	-1.49(58)E-6	-1.7(1.3)E-6
L	...	-0.84(18)E-7	1.40(14)E-7	...
β	5141.09(12)			
Ar-DOH Constants	$\Sigma^+(0_{00})$	$\Sigma^+(1_{01})$	$\Pi^+(1_{01})$	$\Pi^-(1_{01})$
ν	0.0(fixed)*	270336.6#(fixed)	597037.51(28)	597037.51(28)
B	2889.919(42)	2880.0&(fixed)	2856.472(37)	2856.472(37)
D	0.087322(64)	0.0&(fixed)	0.12373(54)	0.10767(60)
H	-8.8(3.0)E-6	0.0&(fixed)	-2.65(22)E-5	...
β	5414.55(60)			

* These values were determined from microwave data on the ground state. # This value is that predicted by fits to near-IR and FIR data by Lascola and Nesbitt [7]. & These values were estimated by analogy with Ar-H_2O.

3.3 Results

Several findings from the present study are noteworthy. The extensive work by the Saykally group. had no torsional band measured in the *para*-manifold. The transition we observed for Ar-D_2O was the first band to probe strictly torsional transitions in the *para*-manifold and the $j_{water} = 1_{11}$ state. Saykally and co-workers were also unable to experimentally determine the relative positions of $\Sigma_{1_{11}}$ and $\Pi_{1_{11}}$ for Ar-H_2O. These states, which correspond to $j_{water} = 1_{11}$, and therefore, differ in the projection of the angular momentum on the pseudodiatomic axis, sensitively probe the anisotropy in the in-plane *vs.* out-of-plane motions. Our data places $\Pi_{1_{11}}$ state (in-plane rotation) below the $\Sigma_{1_{11}}$ state (out-of-plane rotation) with a difference of 39.99072 GHz ($\sim$ 1.33 cm^{-1}). The locations of these Ar-D_2O bands were near the free rotor value as predicted by Cohen and Saykally [2]. The $\Sigma_{0_{00}} \rightarrow \Pi_{1_{01}}$ transition measured for Ar-DOH probes a region in the potential inaccessible via studies of H_2O and D_2O species because of spin statistics. Furthermore, the heavier species have lower zero-

point energies, thereby placing them near the in-plane internal rotation barrier height but well below the out-of-plane internal rotation barrier. Thus, these data points are also sensitive probes of the out-of-plane barrier location and height and the locations of various potential minima.

By incorporating the Ar-D_2O data presented here and those of Zwart and Meerts [8], Ar-H_2O data recorded by Lascola and Nesbitt [7], and Cohen and Saykally [9], plus microwave data by Fraser *et al.* [5], Cohen and Saykally refined the AW1 potential previously obtained and constructed the AW2 potential, which reproduced VRT data to within less than 1% error [1]. Cohen and Saykally noted the following salient features regarding AW2: The minimum was found at R=3.636 Å, θ=74.3°, and ϕ = 0° with D_e=142.98 cm^{-1} (see Figure 3.4 for coordinate definitions). As was found in the AW1 potential, the linear H-bonded structure, θ=54.7° was not the global IPS minimum. At long range, the linear H-bonded geometry was indeed favored. However, as R decreases from 3.8 Åto 3.5 Å, θ increases from 55° to 74.3° at the IPS minimum near 3.6 Å, and then to 120° at R=3.5 Å. There is significant radial-angular coupling, rejecting Hutson's "reversed adiabatic" approximation, an assumption in his potential calculation that there is very little radial-angular coupling [3].

Cohen and Saykally estimate that the AW2 IPS is correct in relative energies to better than ±5 cm^{-1}. Given this error range, the minimum of the potential spans over R=3.55 to 3.8 Å, θ= 50° to 105°, and ϕ = -20° to +20°. Furthermore, at R_e, the entire space spanned by (θ, ϕ) the potential varies by only 50 cm^{-1}, clearly showing the broad IPS region accessible even to the lowest energy states in Ar-H_2O.

3.4 Summary

We obtained VRT spectra in the FIR for Ar-D_2O and Ar-DOH. These were assigned to internal rotation of the water within the complex. The Ar-D_2O spectra probed a region of the IPS previously unexplored, providing a sensitive test for a proposed empirical IPS. The Ar-DOH eigenvalues provided information linking the *para* and *ortho* metastable states in Ar-H_2O and Ar-D_2O. Data from Ar-D_2O were incorporated

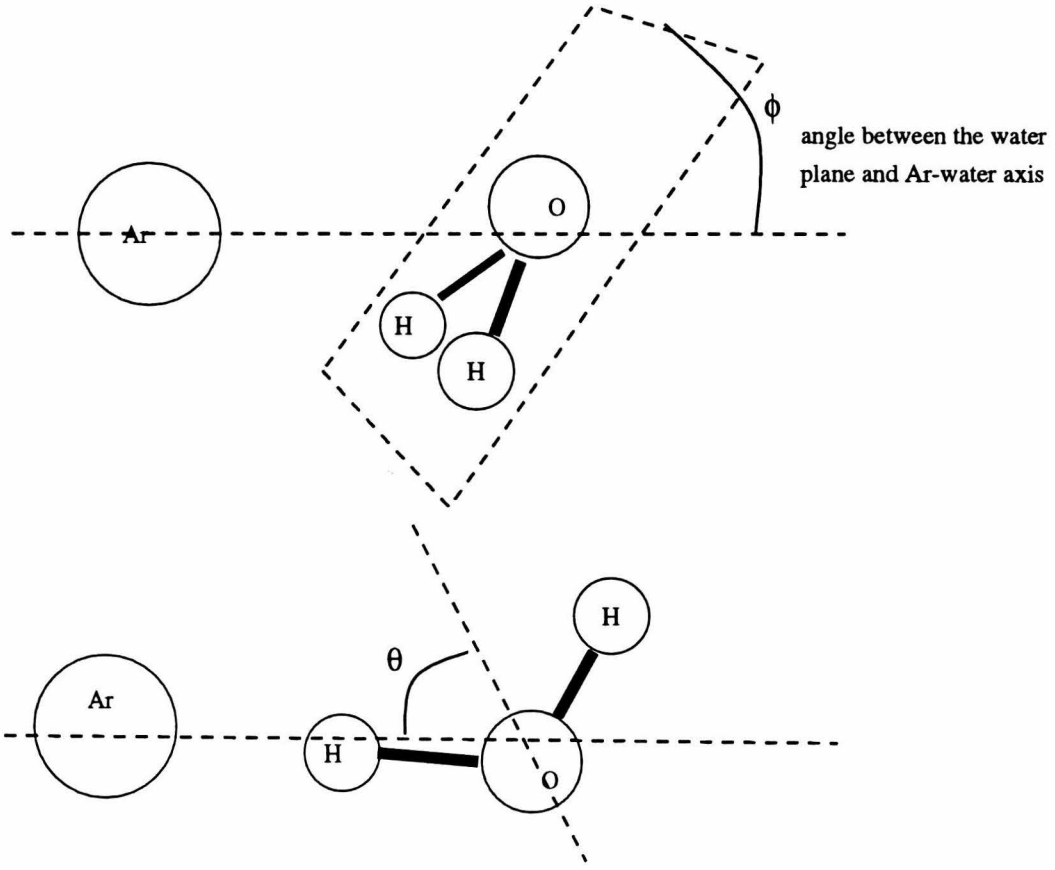

Figure 3.4: Structural parameters θ and ϕ for Ar-water

into the extensive calculation by Cohen and Saykally to produce a highly accurate IPS, called AW2. It was the first multidimensional cluster IPS to be obtained.

It is interesting to note, however, that despite the highly refined AW2 IPS showing that a symmetric minimum exists along ϕ at ϕ=0, Germann and Gutowsky concluded from very high resolution microwave data that the average ground state structure has $< \phi > \neq 0$ [11]. Perhaps the high resolution spectra were misinterpreted or the AW2 is not accurate. While constructing the AW2 potential, Cohen and Saykally found that near the minimum, the attractive and repulsive anisotropies are nearly equally large but opposite in sign. The IPS may, therefore, have very small (< 5 cm^{-1}) bumps caused by the delicate balance of large opposing forces thereby leading to a slight tilting of the water along ϕ. In addition, this delicate balancing of strong forces along one coordinate varies rapidly as other coordinates change: there is a significant radial-angular coupling. This may also contribute to a slightly out-of-plane "average structure". On the other hand, the IPS may be as smooth and flat as AW2 suggests, yet owing to the broadness near the minimum, $< \phi >$ may not have been interpreted correctly with the simple models used to analyze the microwave data. Yet another view point is that this discrepancy is a manifestation of the inappropriateness of the idea of a cluster "structure" when such large region of the IPS are accessible even to the ground state.

Table 3.2: Observed Ar-D_2O lines

$\Sigma^+_{0_{00}} \rightarrow \Sigma^+_{1_{11}}$			$\Sigma^+_{0_{00}} \rightarrow \Pi^+_{111}$		
Observed	Calculatec	Assignment	Observed	Calculated	Assignment
593671.56	593672.41	P(15)	529456.94	529456.92	P(6)
594125.10	594123.86	P(14)	538944.20	538944.16	P(5)
594617.34	594617.15	P(13)	548068.80	548068.03	P(4)
595159.22	595159.91	P(12)	564472.24	564472.47	P(2)
595761.68	595762.56	P(11)	581244.48	581245.26	R(0)
596438.86	596438.99	P(10)	587181.98	587182.63	R(2)
597208.18	597207.87	P(9)	589211.88	589211.82	R(3)
598095.30	598094.95	P(8)	590861.04	590860.71	R(4)
599137.41	599136.72	P(7)	592246.68	592246.65	R(5)
600387.39	600386.26	P(6)	593449.38	593448.49	R(6)
601924.22	601922.26	P(5)	594518.75	594519.28	R(7)
603862.02	603861.76	P(4)	595494.34	595495.25	R(8)
606374.16	606374.63	P(3)	596401.33	596401.67	R(9)
609688.76	609687.96	P(2)	597256.58	597256.52	R(10)
614050.94	614051.91	P(1)	598073.14	598072.98	R(11)
626461.13	626460.74	R(0)	598861.05	598860.95	R(12)
634322.63	634323.02	R(1)	599628.49	599628.08	R(13)
642975.68	642976.36	R(2)	600380.64	600380.37	R(14)
652188.92	652189.92	R(3)	601122.42	601122.38	R(15)
661789.14	661790.05	R(4)	601856.02	601856.96	R(16)
671655.74	671655.90	R(5)	602584.84	602584.37	R(17)
681704.80	681704.98	R(6)	576424.08	576424.07	Q(13)
691879.92	691880.38	R(7)	576488.93	576488.91	Q(12)
702141.48	702141.73	R(8)	576548.01	576548.08	Q(11)
712459.36	712459.41	R(9)	576601.72	576601.70	Q(10)
722811.14	722810.80	R(10)	576649.90	576649.89	Q(9)
733178.48	733178.07	R(11)	576692.81	576692.77	Q(8)
...	...	...	576730.48	576730.47	Q(7)
...	...	...	576763.12	576763.13	Q(6)
...	...	...	576790.88	576790.88	Q(5)
...	...	...	576813.78	576813.81	Q(4)
...	...	...	576832.02	576832.03	Q(3)
...	...	...	576845.60	576845.62	Q(2)
...	...	...	576854.64	576854.64	Q(1)

Table 3.3: Observed Ar-HDO lines

$\Sigma^{+}_{0_{00}} \rightarrow \Pi^{\pm}_{1_{01}}$

Observed	Calculated	Assignment
536746.97	536747.13	P(11)
541468.70	541467.91	P(10)
546270.56	546271.25	P(9)
551164.24	551164.73	P(8)
561249.32	561248.72	P(6)
566450.64	566450.31	P(5)
571763.79	571764.04	P(4)
577193.04	577192.85	P(3)
591031.70	591031.70	Q(9)
591685.96	591686.07	Q(8)
592257.72	592257.71	Q(7)
592750.33	592749.97	Q(6)
593165.84	593165.92	Q(5)
593508.47	593508.24	Q(4)
593778.67	593779.24	Q(3)
593980.40	593980.82	Q(2)
594114.26	594114.39	Q(1)
600074.82	600074.85	R(0)
606079.20	606079.80	R(1)
612192.20	612191.05	R(2)
618402.58	618402.61	R(3)
624707.90	624707.24	R(4)
637560.05	637561.02	R(6)
644089.88	644090.15	R(7)
650672.60	650672.49	R(8)
657296.08	657295.72	R(9)
663947.10	663946.84	R(10)
670611.90	670612.15	R(11)

Bibliography

[1] R.C. Cohen, K.L. Busarow, K.B. Laughlin, G.A. Blake, M. Havenith, Y.T. Lee, and R.J. Saykally. Tunable Far Infrared Laser Spectroscopy of Van Der Waals Bonds: Vibration-Rotation-Tunneling Spectra of Ar-H_2O. *J. Chem. Phys.*, 89:4494, 1988.

[2] R.C. Cohen, K.L. Busarow, Y.T. Lee, and R.J. Saykally. Tunable Far Infrared Laser Spectroscopy of Van Der Waals Bonds: The Intermolecular Stretching Vibration and Effective Radial Potentials for Ar-H_2O. *J. Chem. Phys.*, 92:169, 1990.

[3] J.M. Hutson. Atom-Asymmetric Top Van Der Waals Complexes: Angular Momentum Coupling in Ar-H_2O. *J. Chem. Phys.*, 92:157, 1990.

[4] R.C. Cohen and R.J. Saykally. Extending the Collocation Method to Multidimensional Molecular Dynamics: Direct Determination of the Intermolecular Potential of Ar-H_2O from Tunable Far-Infrared Laser Spectroscopy. *J. Phys. Chem.*, 94:7991, 1990.

[5] G.T. Fraser, F.J. Lovas, R.D. Suenram, and K. Matsumura. Microwave Spectrum of Ar-H_2O: Dipole Moment, Isotopic Studies, and ^{17}O Quadrupole Coupling Constants. *J. Mol. Spect.*, 144:97, 1990.

[6] Ronald Carl Cohen. *Determination of Multidimensional Intermolecular Potential Energy Surfaces.* Ph.D. thesis, University of California at Berkeley, Berkeley, CA, June 1991.

[7] R. Lascola and D.J. Nesbitt. Slit-Jet Near-Infrared Spectroscopy and Internal Rotor Dynamics of the ArH_2O Van Der Waals Complex: An Angular Potential-Energy Surface for Internal H_2O Rotation. *J. Chem. Phys.*, 95:7917, 1991.

[8] E. Zwart and W.L. Meerts. The Submillimeter Rotation-Tunneling Spectrum of Ar-D_2O and Ar-NH_3. *Chem. Phys.*, 151:407, 1991.

[9] R.C. Cohen and R.J. Saykally. Multidimensional Intermolecular Dynamics from Tunable Far-Infrared Laser Spectroscopy–Angular-Radial Coupling in the Intermolecular Potential of Argon-H_2O. *J. Chem. Phys.*, 95:7891, 1991.

[10] R.C. Cohen and R.J. Saykally. Determination of an Improved Intermolecular Global Potential Energy Surface for Ar-H_2O from Vibration-Rotation-Tunneling Spectroscopy. *J. Chem. Phys.*, 98:6007, 1993.

[11] R.C. Germann and H.S. Gutowsky. Nuclear Hyperfine Interactions and Dynamic State of the H_2O in Ar-H_2O. *J. Chem. Phys.*, 98:5235, 1993.

Chapter 4 Benzene-Water

4.1 Motivation

A natural extension of the atom-triatom case presented in the previous chapter is a diatomic-diatomic or diatomic-triatomic interaction. Indeed, research on N_2-H_2O, CO-H_2O is in progress in Prof. Blake's laboratory and other groups [1, 2, 3], and diatomic-diatomic clusters, such as $(HF)_2$ and H_2-HF, have been extensively studied elsewhere [4, 5, 6, 7]. This work jumps to benzene-water, a much larger cluster, which may be considered as a pseudoatom-triatom system if benzene is modeled as an aggregate of electrons. There is also a thematic motivation to study biologically significant interactions such as those manifested in benzene-water clusters.

Benzene and water form an example of a pair whose immiscibility is often construed as evidence for little or no intermolecular interaction between the two molecules. Likewise, amino acids with aromatic side chains have been traditionally classified as hydrophobic, and expected to not interact strongly with polar groups or ions and to be confined to the hydrophobic core of proteins.

In the past decade, many biological structural motifs have surfaced which indicate that non-polar aromatic groups interact with polar groups. Tüchsen and Woodward found such an example in a high resolution pancreatic trypsin inhibitor structure [8], in which the benzene ring of a phenylalanine was sandwiched between two polar groups, amides, each of them closer than the van der Waals contact distance. Levitt and Perutz calculated the bonding energy for the amides and the benzene ring and concluded that each "hydrogen bond" was about half as strong as a regular hydrogen bond [9]. Burley and Petsko searched through the resolved protein crystallographic data base and discovered that amides and hydroxyl groups in a protein are preferentially bound to the face of the aromatic ring in such interactions [10, 11, 12].

Several experiments reported in the literature corroborate the binding

between non-polar aromatic rings and a polar group. For example, Atwood and co-workers found that a molecular cavity consisting of aromatic rings binds several water molecules within it, and that the O-H bond dipoles point directly to the face of the aromatic rings [13]. Dennis *et al.* found aromatic rings are placed near hydrophilic binding regions in proteins [14]. This agrees with other findings that cation-π election interactions are important in protein ion channels [15]. Indeed, anionic side chains are in many senses less desirable for binding cations than are aromatic moieties [16].

When Linus Pauling suggested that H-bonds are important in biological systems, he stressed the need for biological bonds to be broken with some ease at ambient temperature [17]. The benzene-ion or -polar interaction is one such case where these bonds may be far more suitable for biological functions than a much stronger ion-ion bond. The lower binding energy in the aromatic-ion interaction provides sufficient stability to favor and maintain the cation-protein bond, yet it is easily broken at ambient temperature when there is a functional need to do so. Ion-ion bond strengths can be far in excess of the energy available at biological temperatures.

In addition to being a prototype for such biochemical interactions, a better understanding of the benzene-water bond will illuminate many other processes as well. For example, aromatic substitution reactions are highly influenced by the polarizability of the aromatic ring. An understanding of the benzene-water intermolecular force field will provide valuable insight to such studies. Currently, aromatic compounds released from human activities are a major component of urban pollution. Investigation of the interaction between such compounds and aerosol particles is currently underway [18]. Similar species, polycyclic aromatic hydrocarbons (PAHs), trapped in ice mantles are an important part of the carbon distribution in cosmochemistry. Thus, benzene-water clusters serve as prototypes of numerous interactions.

A search through literature showed that very few experimental results were available for the benzene-water dimer. Engdahl and Nelander conducted matrix isolation studies where they produced benzene-water dimers in an Ar matrix [19, 20], and probed the IR intramolecular vibrational modes of the water and benzene. They concluded that there was some interaction. However, they did not have conclusive

results for the dimer structure. In fact, they observed nearly free rotation of the water relative to the benzene. Similar systems studied at full rotational resolution include benzene-HCl probed with FTMW [21, 22] and benzene-HF probed with MBER [23]. In both aromatic-dipole interactions, the polar group was found to lie above the plane of the benzene with the positive end of the dipole pointing toward the aromatic π-electron cloud. The benzene center-of-mass (cm) to H distance was 2.35 Å for benzene-HCl and 2.25 Å for benzene-HF. The expectations for the benzene-water dimer based on these similar systems is to have water above the plane of benzene with a center-of-mass separation of about 3.5 Å (see figure 4.1).

In the first molecular beam work, Bernstein and co-workers studied benzene-water systems using two color time-of-flight mass spectroscopy [24]. Based on spectral shifts in vibronic spectra, modeled with Lennard-Jones potentials, a benzene-water structure with a benzene-oxygen separation of 3.2 Å, a benzene-H distance of 3.0 Å, and a binding energy of 505 cm^{-1}, were suggested. However, these spectra lacked the resolution needed to obtain rotational information, and thus, do not provide accurate structural constraints.

In this study, the benzene-water clusters are investigated in the gas phase, removed from interference by external forces, using three methods. Microwave spectroscopy was used initially to obtain the ground state "structure" and estimates on various IPS parameters. *Ab initio* and diffusion Monte Carlo methods were used to computationally simulate the IPS which was then compared and fitted to the microwave parameters, and used to predict intermolecular vibrational transitions. Lastly, FIR spectroscopy was used to probe these intermolecular vibrational transitions, which give us a more direct view of the IPS. Results from each of these approaches are summarized below.

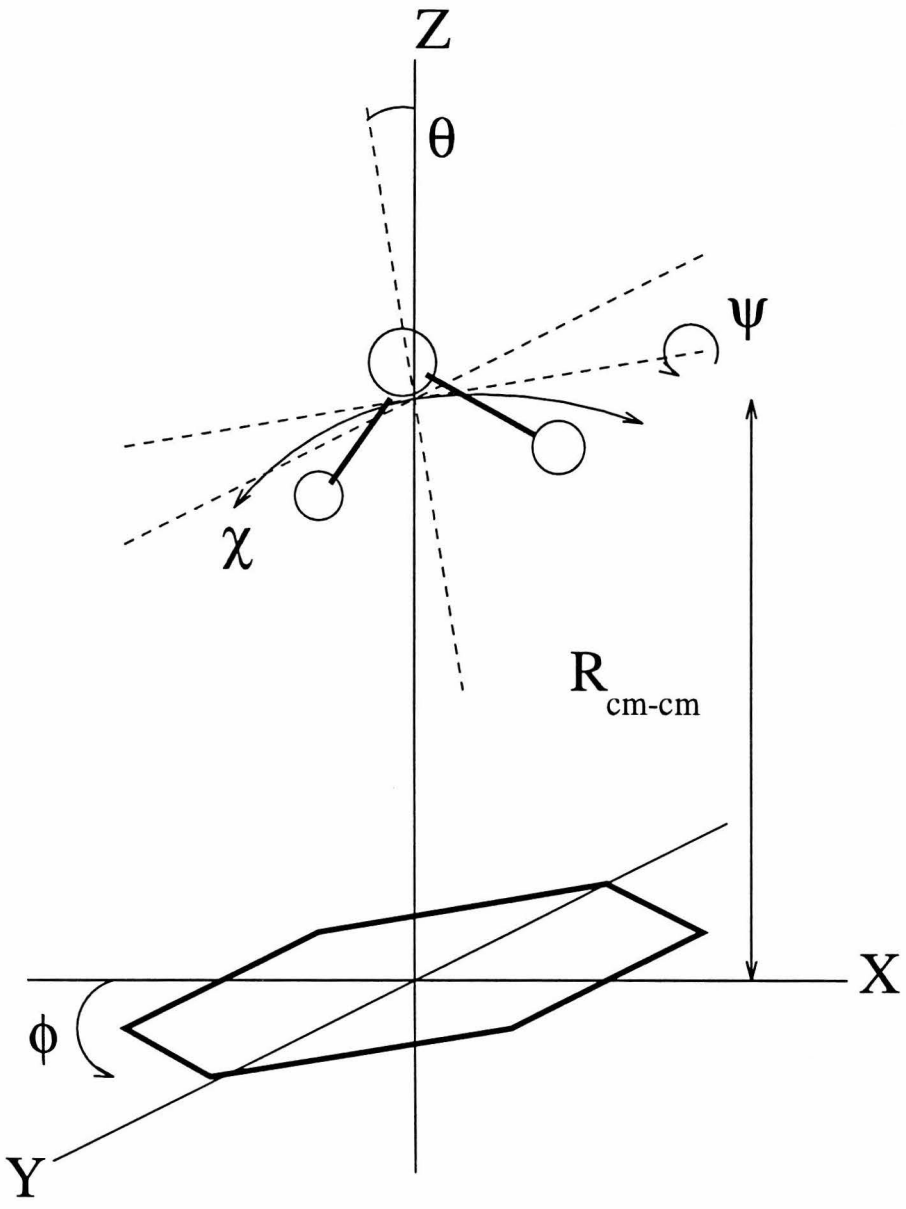

Figure 4.1: The benzene-water coordinate system and structure

4.2 The benzene-water ground state structure

4.2.1 Microwave data

Microwave spectra for C_6H_6-H_2O (bz-H_2O), bz-D_2O and bz-HDO were collected using several methods. Initially, frequency modulation (FM) using the direct absorption microwave spectrometer (DAMW) at Caltech was used. Spectra for the three isotopomers were first obtained in the range from 19 GHz to 40 GHz (the J= 5 $\leftarrow$ 4 to J= 10 $\leftarrow$ 9 transitions). The Stark modulation adapter was then built to increase the S/N of these spectra for more detailed study. Dipole moment measurements were subsequently taken at NIST, using the Fourier transform microwave spectrometer(FTMW). The data obtained are summarized below: Tables 4.7, 4.8 and 4.9 list all bz-H_2O lines observed with assignments where appropriate; Table 4.10 lists all bz-D_2O lines; Table 4.11 lists all bz-HDO lines; Table 4.13 lists results from the bz-H_2O dipole moment measurements; and Table 4.12 lists the fitted rotational constants.

There were four noticeable features in the spectra. First, there are symmetric top-like patterns separated by $\sim$ 2 GHz. Second, each of the symmetric top-like patterns has close to them a set of irregular patterns at slightly lower frequency. Third, the intensity ratios for the regular symmetric top-like pattern to the irregular pattern are approximately reversed between the H_2O and D_2O isotopomers. Fourth, no irregular pattern was observed for the bz-HDO species.

4.2.2 Analysis

A qualitative interpretation of the spectral patterns noted above are as follows. (See Figure 4.2.) The patterns marked A, A′ and A″, the symmetric top-like patterns in each isotopic species, are suspected to belong to benzene-water complexes with $j_{K_pK_o}(water) = 0_{00}$. The patterns marked B and B′, but not present in the bz-HDO spectrum, are suspected to belong to $j_{K_pK_o}(water) = 1_{01}$ clusters. The $j_{K_pK_o}(water) = 1_{01}$ state is metastable, analogous to the *ortho* state of H_2 and D_2. Since the hydrogens in HDO are not identical, the $j_{K_pK_o}(water) = 1_{01}$ state in HDO is not

metastable, and this state is cooled to a negligible population by the supersonic expansion. (The $j_{K_pK_o}(water) = 1_{01}$ state energy is approximately 23.8 cm^{-1} for H_2O, 12.1 cm^{-1} for D_2O and 15.5 cm^{-1} for HDO.) This explains the presence of two types of patterns in the H_2O and D_2O species but only one pattern for bz-HDO. This is also supported by the reversal of the relative intensity between the A and B pair and the A′ and B′ pair. The $j_{K_pK_o}(water) = 0_{00}$ state is expected to form ~1/3 of the population of the $j_{K_pK_o}(water) = 1_{01}$ state in bz-H_2O based on spin statistics. On the other hand, $j_{K_pK_o}(water) = 0_{00}$ is expected to have twice as large a population as the $j_{K_pK_o}(water) = 1_{01}$ state in D_2O. Lastly, a simple symmetric top-like pattern fits the A, A′ and A″ parts of the spectra of the three isotopic species. However, a more complicated pattern is expected in a system with coupling between the internal rotation of the water corresponding to the $j_{K_pK_o}(water) = 1_{01}$ state and the over all dimer rotation, and is assigned to the B and B′ pattern. Thus, qualitatively, we observed "two" clusters for bz-H_2O and bz-D_2O, corresponding to the $j_{K_pK_o}(water) = 0_{00}$ and $j_{K_pK_o}(water) = 1_{01}$. These two internal rotor states will be referred to as m =0 for $j_{K_pK_o}(water) = 0_{00}$, and m =± 1 for $j_{K_pK_o}(water) = 1_{01}$.

The permutation inversion (PI) group for benzene-water was determined and the spin statistics were calculated. The result of PI analysis agrees with the analogy made above with the *para* and *ortho* states of H_2 and D_2. As derived in Appendix D, the full PI group of benzene-water is G_{24}. The direct product of six-fold permutation from benzene and two-fold permutation of water give rise to a twelve-fold permutation, which, when combined with inversion, results in G_{24}.

The energy level expressions consisting of two symmetric tops have been discussed by Fraser *et al.*[25], and the transition energy is described by the following formula:

$$\nu = 2(J+1)[B - D_{JK}K^2 - D_{Jm}m^2 - D_{JKm}Km - H_{JKm}m^2K^2] - 4(J+1)^3D_J.$$

When the spectroscopic data are fit to this equation, we obtain an rms within experimental error for the $m = 0$ states and a slightly higher root-mean-square error for the $m = \pm 1$ data. (See Tables 4.7 to 4.12.) The $m = 0$ data are fit by a symmetric

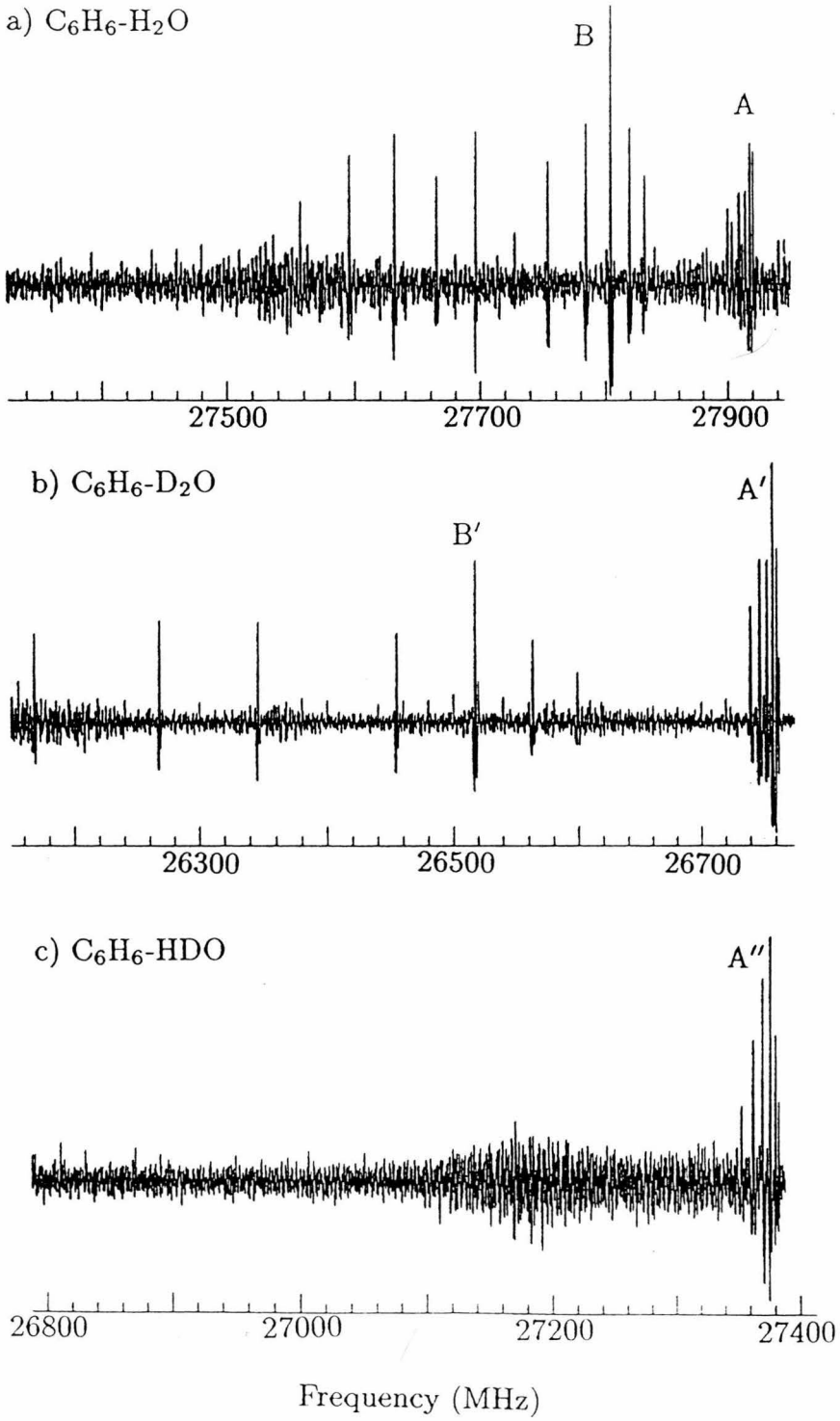

Figure 4.2: Spectra in the J=6 → 7 region for the benzene-water isotopomers.

top formula, i.e., the transition frequencies are given by

$$\nu \;=\; 2(J+1)[B - D_{JK}K^2] \;-\; 4(J+1)^3 D_J.$$

The assignment for the m=±1 state is based on a thorough study of various isotopomers and hyperfine splittings using FTMW by Gutowsky and co-workers [26]. We are confident of the qualitative description of the spectra assigned as m=0 and m=±1 bands; however, residuals in the fit which are slightly larger than experimental error informs us of the incompleteness of the analysis. The use of large number of distortion constants will likely produce a reasonable fit; thus, we consider this rough fit as an indication of the floppiness of the cluster.

4.2.3 Structural analysis

The fitted rotational constants and the symmetric top patterns observed eliminate cases where the water is not above the plane of benzene ring. Based on previous *ab initio* calculations and the microwave results for C_6H_6-HCl and C_6H_6-HF, the protons are expected to lie between the centers-of-mass (cm) of the monomers.

A cursory examination of a benzene-water structure with water above the plane of benzene confirms that any instantaneous geometry of the cluster is not a symmetric top and that it has at most a 2-fold symmetry axis.(See Figure 4.1. The cluster has a 2-fold axis when $\theta = 0$.) The symmetric top pattern obtained despite the C_{2v} symmetry group of rigid benzene-water suggests highly floppy motions of the water above the benzene, such that on the time scale of a dimer rotational period the cluster is symmetric. Indeed, the Zwier group study of the benzene water dimer using electronic transitions confirms that the molecular symmetry is six-fold [5].

The floppy nature of the cluster leads to significant complications in the understanding of the cluster "structure". Often, a molecular structure is described by average distances and angles, or equilibrium distances and angles. Since the motions of the atoms in molecules are more localized, one can speak of, for example, a two-fold symmetry of water above the six-fold symmetric benzene. However, since the water

orientation is "smeared" over the face of benzene within the experimental time scale, it is not possible to freeze a rigid water molecule above a rigid benzene. Thus, in our "structural" interpretation of the benzene-water cluster data, one must keep in mind that we will not obtain an equilibrium structure and that the frozen vibrationally averaged structure must be considered only as a first step in the characterization of the cluster. A true understanding of the cluster will only come with a complete unraveling of the IPS.

The general structure of the water above the benzene plane was recognized by Zwier's group in concurrent work on the same cluster with resonance ionization [5]. Our initial contribution, the high resolution microwave spectra of the three isotopomers and dipole moment measurements, is the elucidation of more precise ground state properties. Three progressively more involved approaches were taken to gain such an understanding. Each approach is limited by the assumptions made and the relative paucity of experimental data.

The zeroth-order approximation is the rigid diatomic model. Using the relations I $= \mu\ r^2$ and I=$h/(8\pi^2 B)$, we obtain $R_{(cm-cm)}$ values of 4.1608 Å, 4.1102 Åand 4.0727 Åfor bz-H_2O, bz-HDO and bz-D_2O. The similar constants tells us that the traditional assumption that isotopomers of the same chemicals have the same structure may be "reasonable". Note that these values are most likely to be upper bounds for the true $R_{(cm-cm)}$, in that by assuming a point mass for benzene and another for H_2O, the reduced mass is underestimated.

The next two approaches used a structural fitting program called STRFTQ written by R.H. Schwendenman [28], which was later revised by F. Lovas (see Appendix E for annotated input files). First, $\theta = 0$ was assumed (see Figure 4.1). The $R_{(cm-cm)}$'s obtained were 3.3239(1), 3.3103(1) and 3.2811(1) Å for the H_2O, HDO and D_2O species. The error values listed are those given by STRFTQ as the standard deviation to the fit of the rotational constants. The R_{cm-cm} values are well within the values obtained by Zwier's group, 3.4(2) Åfor bz-HDO and 3.32(7) Åfor bz-D_2O [5].

Using STRFTQ, the next approach allowed a fit of bz-H_2O, -D_2O and -HDO to the same structure. With three isotopomeric rotational constants, two structural

parameters were fitted: $R_{(cm-cm)}$ = 3.341(4) Å and θ = 18(13). The large relative uncertainty in θ was initially attributed to an expected slight preference for deuterium to "bind" to benzene in the bz-HDO cluster, since deuterium is often preferentially H-bonded in other water clusters [29, 30, 3]. Thus, the same parameters were fit using only the rotational constants of bz-H_2O and bz-D_2O, yielding $R_{(cm-cm)}$ = 3.333(8) Åand θ = 38(16)°. The θ values are the same within error, and the error value in the θ fit is equally large in both cases. Perhaps then, the large uncertainly is indicative of large amplitude vibration in at least the θ coordinate.

In the last method, if one assumes a vibrationally averaged value of $< \psi >$=0, places the H_2O cm on the benzene C_6 axis, and integrates over the sixfold internal rotation potential in ϕ, i.e., include the free internal rotation of water into consideration, the vibrationally averaged value of $< \theta >$ can be expressed in relation to $R_{(cm-cm)}$ and the moments of inertia, I, of the monomers and the complex as

$$I_{bb(C_6H_6-H_2O)} = \mu R^2_{(cm-cm)} + \frac{I_{aa(H_2O)}}{2} < 1 + \cos^2\theta > + \frac{I_{bb(H_2O)}}{2} < \sin^2\theta > + I_{bb(C_6H_6)},$$

where $\mu = m_{C_6H_6} \cdot m_{H_2O}/(m_{C_6H_6} + m_{H_2O})$ [25]. H_2O is substituted by D_2O or HDO in the other two isotopomers. Assuming that the distance from the oxygen atom to the benzene plane was identical for all three isotopomers led to an independent constraint on R and θ. (See figure 4.3.) The derived constants clearly demonstrated that the water protons must be pointing toward the benzene. Mathematically, $R_{(O-bz)}$=3.411 and θ=20°, but the model is consistent with a range of ±0.005 Åfor $R_{(O-bz)}$ and ±15° for θ_0^{expt}. In terms of cm separation, $R_{(cm-cm)}$ = 3.347(1) Åfor H_2O, 3.304(1) Åfor D_2O and 3.342(1) Åfor HDO. Again, our results agree well with $R_{(cm-cm)}$ reported by Gotch and Zwier [5].

A simple analysis of the dipole moment measurement using the equation

$$\begin{aligned} \mu_{complex} &= \mu_{bz\ induced} + \mu_{H_2O} cos\theta \\ &= \frac{2 \cdot \alpha \cdot \mu_{H_2O} \cdot cos\theta}{R^3} + \mu_{H_2O} cos\theta \end{aligned}$$

with a benzene polarizability of α=10.32 Å^{-3}, R=3.347 Å, μ_{H_2O}= 1.86 D, and $\mu_{complex}$=2.20(4) D, yields θ=40°, qualitatively consistent with the tilted structure.

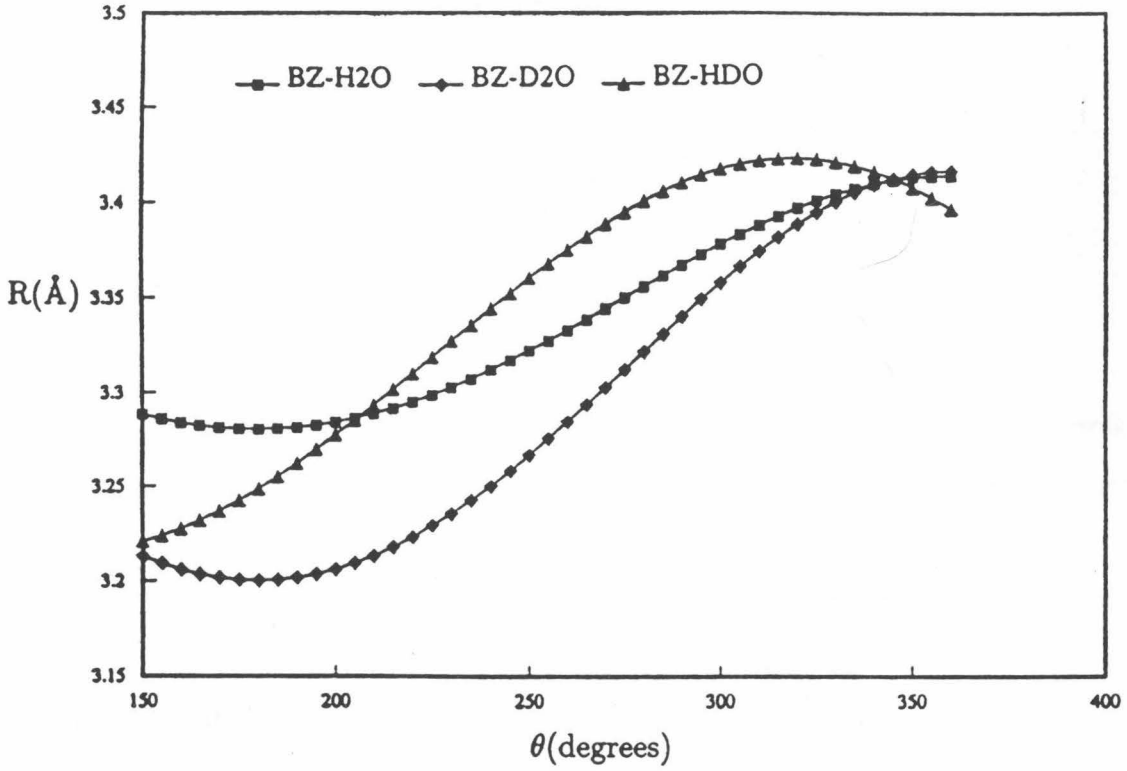

Figure 4.3: The benzene-water structural parameters, $R_{(cm-cm)}$ and θ, calculated by including the free internal rotor effect.

4.2.4 Summary

Using microwave spectroscopy, we confirmed the hydrogen bond between the water protons and the benzene π-electrons. The bond energy estimated from the D_J distortion constant is 1.9 kcal/mol. This agrees with the 1.63 < D_0 < 2.78 kcal/mol boundaries given by Gotch and Zwier [5]. Structural parameters obtained by this work and by Gutowsky's group [26] are summarized in Table 4.1.

The average of the $R_{(cm-cm)}$ found in this work for the three isotopomers agrees with that found by Gutowsky's group. The θ angle agrees within experimental error except for the bz-DOH species. The large value of the error in our work and the

Table 4.1: Benzene-water structural *para*meters determined by this work and by Gutowsky's group.

	R (Å, cm-cm)	θ(deg)
This work		
bz-H_2O	3.347(5)	20(15)
bz-D_2O	3.308(5)	20(15)
bz-HDO	3.322(5)	20(15)
Gutowsky		
bz-H_2O, m=1	3.329	0
bz-D_2O, m=0	3.329	15
bz-D_2O, m=1	3.329	29
bz-DOH	3.329	56

scattered distribution in θ found from quadrupole hyperfine splittings by Gutowsky's group suggests a low resistance to the change in θ angle along the potential energy surface.

Though the H-bonding between water and benzene is confirmed, a detailed characterization of the structure is not possible at this stage. Rather, there are several indications that the benzene-water interaction is governed by a relatively shallow potential and the notion of a frozen ground state "structure" may not exist for this cluster. Surely the IPS must be characterized in detail for a better understanding.

4.3 Calculations

4.3.1 *Ab initio*

The *Gaussian 92* (G92) suite of programs [31] were used to calculate the benzene-water IPS as a next step in characterizing the dimer interaction. We also use the *ab initio* IPS calculated to estimate vibrational transition energies and as a first guess in fitting observables to an empirical IPS.

Calculations were initially performed in collaboration with the Goddard group at Caltech and later on the IBM RISC 6000 370 workstation in Prof. Blake's laboratory. Though there is a G92 instruction manual [31], the specific input files and additional

notes made concerning potential problems are given in Appendix F. All calculations except for frequency calculations were performed at HF-MP2 level using 6-31 G** basis sets. Frequency calculations were performed without the MP2 perturbation treatment. Basis set superposition error (BSSE) corrections were made in all potential energy cuts described below.

A fully optimized C_6H_6-H_2O structure with frozen intramolecular coordinates was calculated first. The water center of mass was found on the benzene C_6 axis above the benzene plane: $R_{e(cm-cm)}$=3.168 Å and $\theta_e = \pm 21°$. Several potential energy cuts were made based on this equilibrium structure. R was varied with θ fixed at 21°, θ was varied with R fixed at 3.168 Å, ψ was varied with θ fixed at 0° and R fixed at 3.168 Å, and χ was varied with θ fixed at 21° and R fixed at 3.168 Å. These potential slices are shown in Figures 4.4 and 4.5. The R potential was fit to a Morse function, yielding D_e = 633(30) cm^{-1}, α = 2.06(10) $Å^{-1}$, and R_e=3.12(1) Å. The minimum of $R_{(cm-cm)}$ potential is underestimated by the *ab initio* calculation.

The θ, ψ and χ potentials were fit to

$$V = \sum_n \frac{V_n}{2}(1 - cosn\theta)$$

expansions. (See Appendix E for descriptions of the programs.) The V_n parameters are summarized in Table 4.2. The energy difference obtained for staggered and eclipsed geometries of water above benzene (ϕ=0 and 30°) was 0.17 cm^{-1}. Given that the rotational energy of water about it's *b*-axis is at about 37 cm^{-1}, the zero point energy assuming free rotation is about 19 cm^{-1}, well above this small barrier.

The *ab initio* potential energy cuts agree qualitatively with the experimental observations. The potential is shallow along the θ coordinate, rising only to 50 cm^{-1} by ±50°, and θ_e is within error of the θ_o observed. However, the θ coordinate potential energy rises more sharply past ±50°, reaching 180 cm^{-1} at ±70°. The potential surface along the ϕ coordinate is steeper still, rising to 100 cm^{-1} by ±25°.

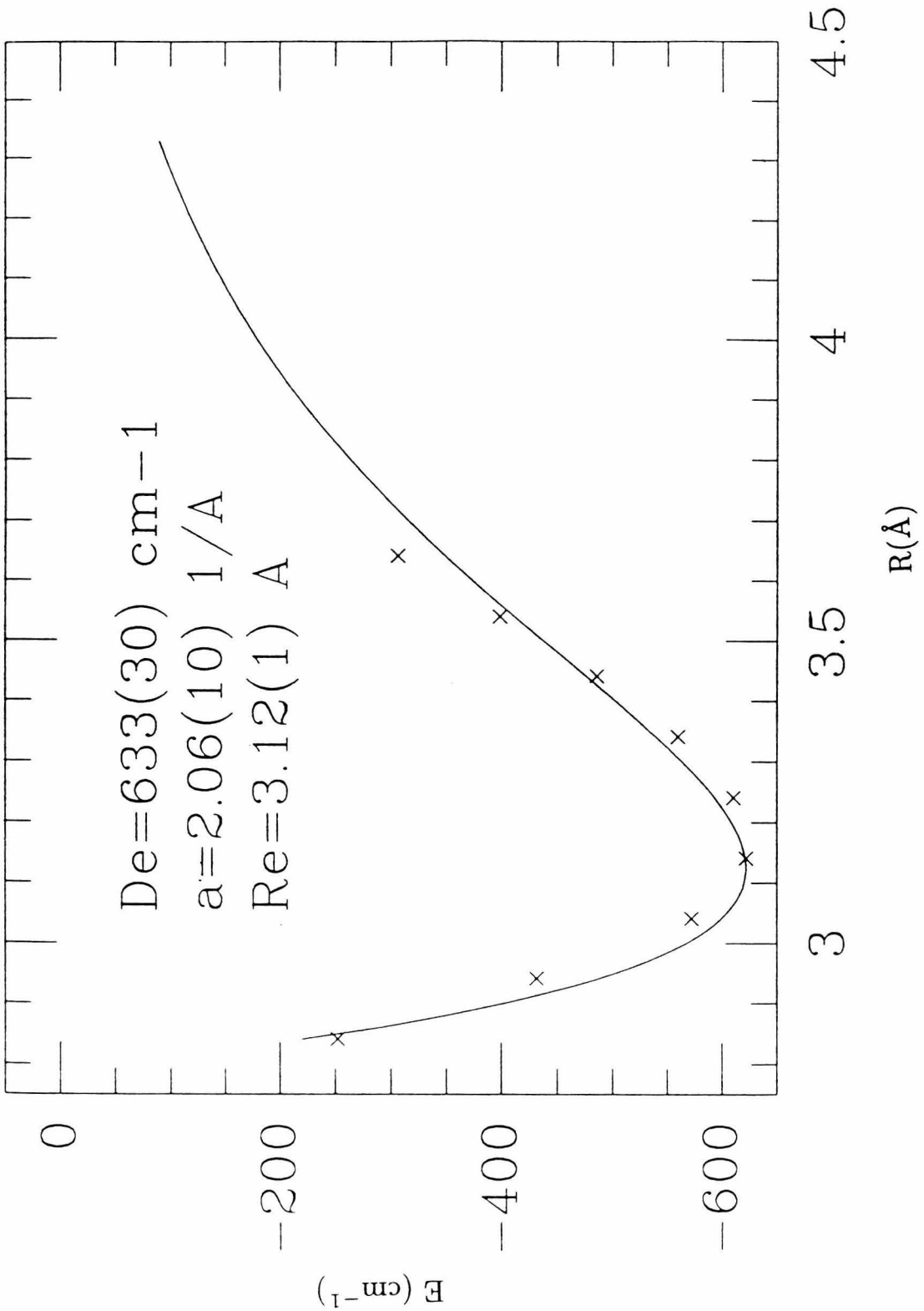

Figure 4.4: *G92* 6-31g** MP2 (BSSE corrected) C_6H_6-H_2O potential cut along $R_{(cm-cm)}$.

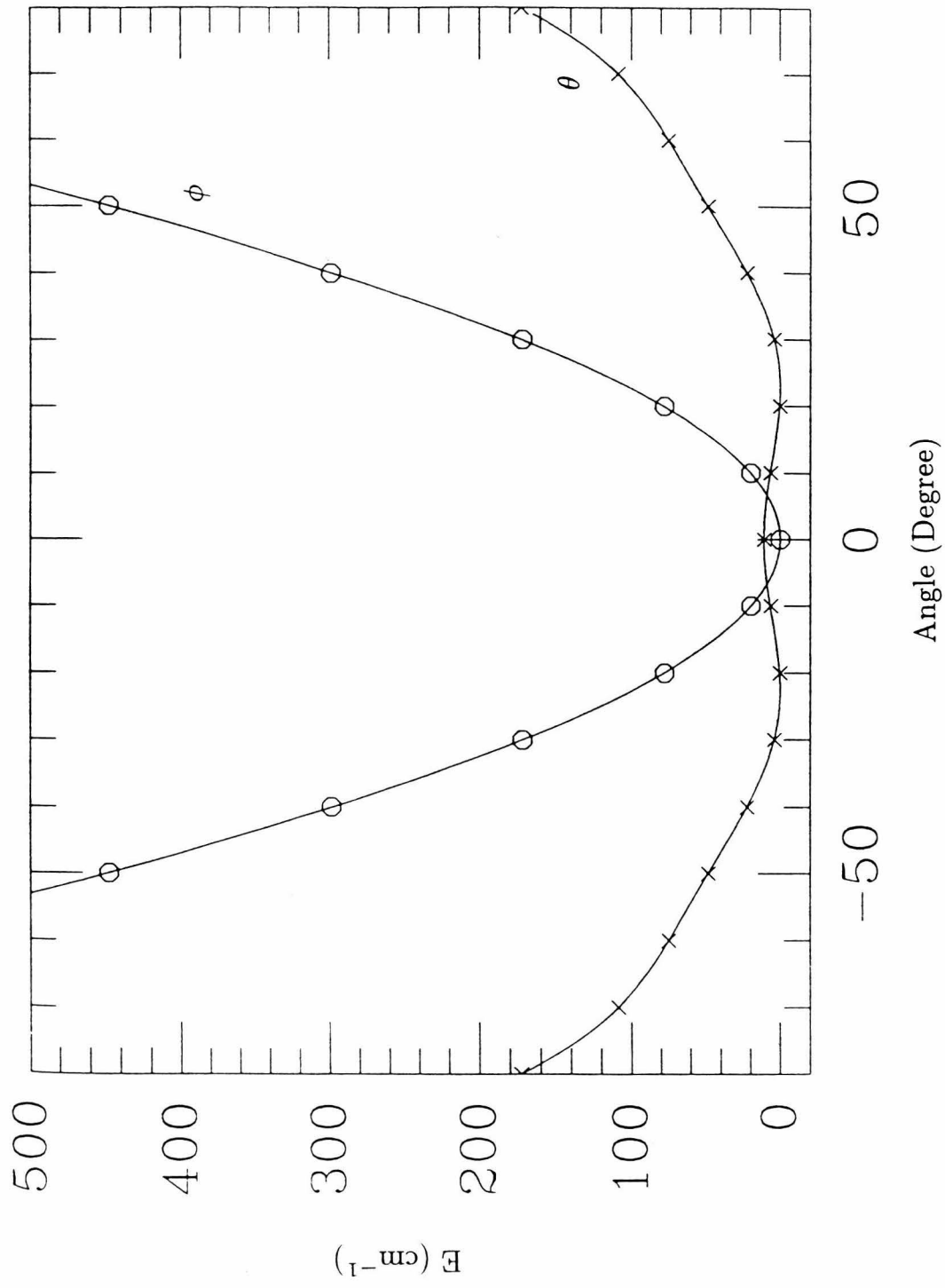

Figure 4.5: *G92* 6-31g** MP2 level C_6H_6-H_2O potential slice along θ and ϕ.

Table 4.2: V_n parameters used to fit the potentials.

Coordinate	V_n	Value(cm^{-1})
θ	V_1	-3916(476)
	V_2	3347(335)
	V_3	-2040(182)
	V_4	822(73)
	V_5	-175(19)
	V_6	-15(3)
	E level	H_2O
	Ground	12
	First	58.2
		D_2O
	Ground	5.6
	First	35.4
ψ	V_1	2027(38)
	V_2	146(11)
	E level	H_2O
	Ground	132
	First	390
		D_2O
	Ground	98.7
	First	292.9
χ	V_1	19600(129)
	E level	H_2O
	Ground	20.2
	First	60.7
		D_2O
	Ground	19.4
	First	58.3

4.3.2 DMC

Diffusion Monte Carlo (DMC) simulation methods were subsequently employed to better understand the IPS. This random walk method for solving Schrödinger's equation to obtain wavefunctions was developed by Anderson [32, 33] and later applied to clusters by Watts [34] and by Buch [35, 36]. Essentially, the method takes many particles, each of which designates coordinate definitions for the cluster, distributes them arbitrarily over an IPS, and allows a random walk of the particles that are either eliminated or multiplied. After a sufficiently large number of random walk steps, the distribution of the particles indicates the wavefunction of the cluster, from which average structural parameters such as $< \psi^* | r | \psi >$ and $< \psi^* | \theta | \psi >$, rotational constants, and hyperfine splittings may be calculated. We will use this program to constrain an IPS with ground state information obtained by microwave spectroscopy.

Various spectral inversion methods currently in use, for example that used to obtain the Ar-water potential described in chapter 3, require large amounts of FIR data and extensive computational power to map out the multi-dimensional IPS. DMC simulations yield IPS information that can be compared with microwave data, and do not require extensive memory. Since there is no matrix diagonalization, the memory requirement scales as N, the number of atoms, unlike other methods which typically scale by N^2 or N^3. Of course there are disadvantages. DMC is very difficult to apply to vibrational transitions and it lacks precision. Thus, it is most useful in obtaining first-order approximations of the IPS near the ground state by iteratively adjusting the potential parameters as they are fit to experimental measurements. Also, while studying weakly bound clusters with large amplitude motions, such as benzene-water, it is helpful to be able to visualize how wide the large amplitude motions may be. In this work, the wavefunctions were calculated using DMC to obtain this type of information.

Currently, a collaboration with C. Dykstra is being arranged to better adapt the iterative fitting scheme to a large number of clusters. The molecular mechanics for clusters (MMC) developed by Dykstra and co-workers [37] is a fast, moderately

accurate method of calculating an IPS based on electrostatics and other empirically determined parameters. One point on an IPS is calculated on the time scale of a second for benzene-water on an IBM RISC 6000 workstation, not hours as it is the case for G92. Thus, parameters used in MMC package to calculate the IPS can be fit to the experimental observations in the ground state within reasonable time. In this approach, the DMC simulations will be the most time consuming step.

The wavefunctions were calculated using the G92 potentials along R, θ and χ. Clearly, three coordinates are less than the six coordinates, R, θ, χ_x and χ_y, ϕ and ψ, needed to fully describe the intermolecular motions. The numbers of variables were reduced to simplify the calculation using the following reasoning. Since ϕ (internal rotation) is a nearly flat potential, it was removed. The assumed free internal rotation along ϕ makes χ_x and χ_y equivalent. Thus, χ_x and χ_y were combined to yield χ. Any motion along ψ is quickly converted to that along θ by the fascile internal rotation in ϕ as well. Thus, ψ is ignored in this initial calculation. The rotational constants calculated were A=2837.33 MHz, B=2197.20 MHz, and C=2180.98 MHz. The distribution function along R, θ, χ, and ϕ are shown in Figures 4.6, 4.7, and 4.8.

The R_o^{DMC} calculated is close to R_e^{G92} and lower than the measured quantity. This is one reason for the 10 % error in the calculated rotational constants. Simple adjustment of R_e to R_e=R_0^{expt}=3.347 Ågave A=2832 MHz , B= 2014 MHz and C= 2002 MHz. $\frac{B+C}{2}$ = 2008 MHz is within 1% of the measured value, as expected. The A value is close to the free benzene C rotational constant ($C_{free\ bz}$ = 2835.2 MHz).

There has been some dispute as to what the "structure" of benzene-water may be, and regarding the extent of the large amplitude motion. DMC calculations shed light on such large amplitude motions by providing distribution functions of the cluster geometry.

The distribution function over the R coordinate is, as expected, maximized close to R_e. The χ coordinate distribution is also as expected with a maximum at χ=0 (see Figure 4.8). The distribution along θ should to be broader and cover the region with θ= $\pm$20 with near equal probability because of the low barrier in this coordinate. As it can be seen in Figure 4.7, θ = 0 is not a maximum, reflecting the slight double

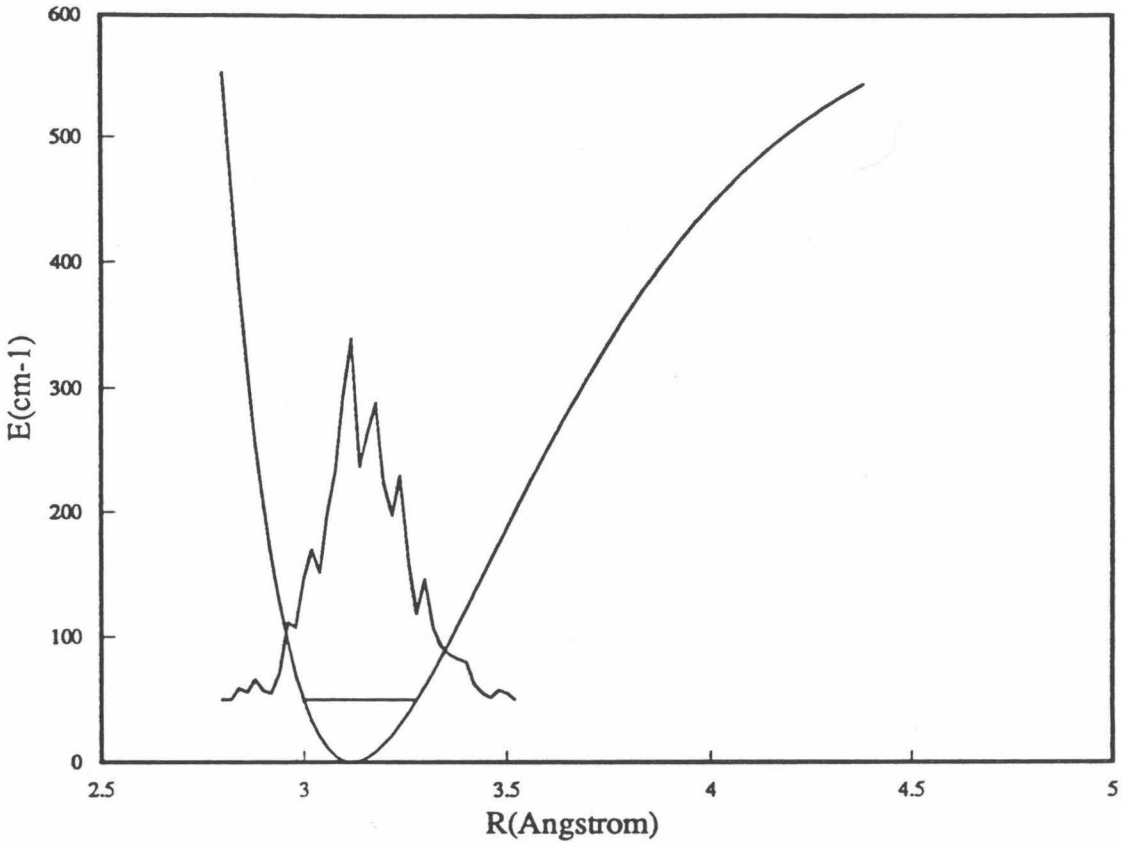

Figure 4.6: Distribution over potential energy cut, R. Note that the discrete nature and the limited sample size in the simulation causes the "discontinuity" in the distribution curve.

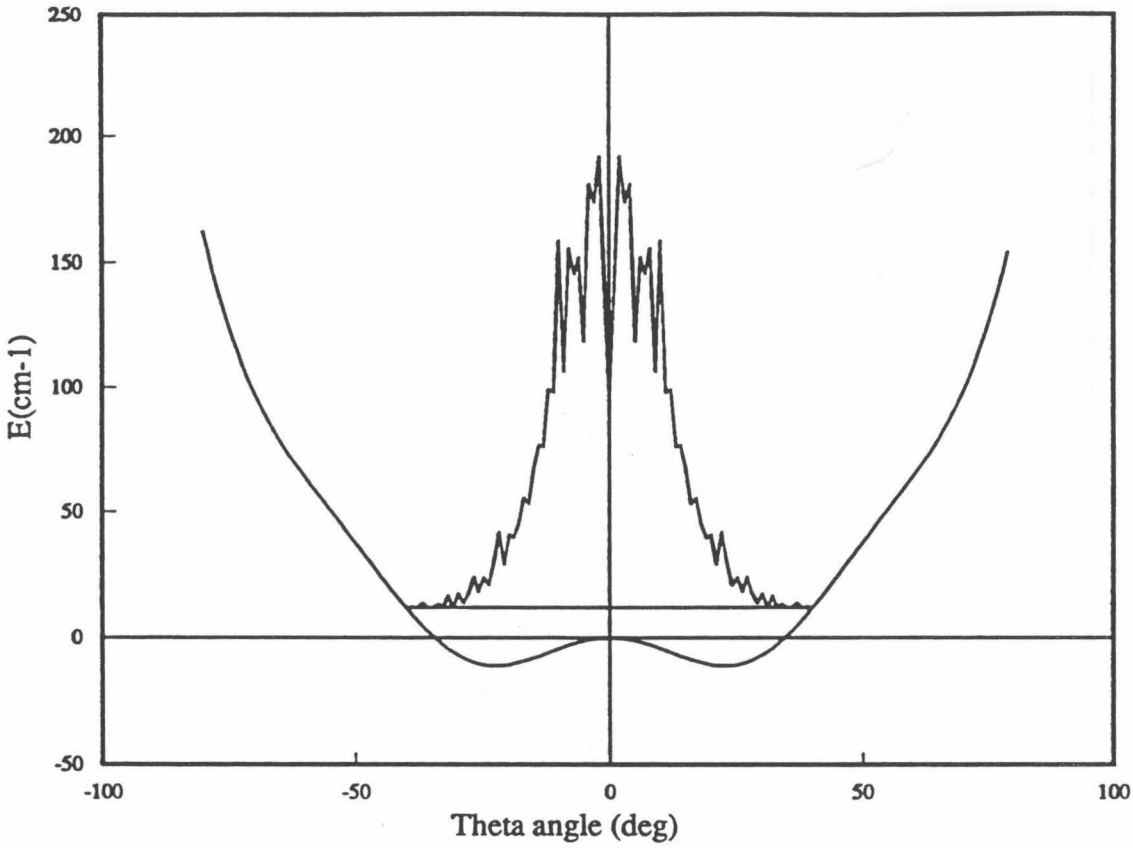

Figure 4.7: Distribution over potential energy cut, θ

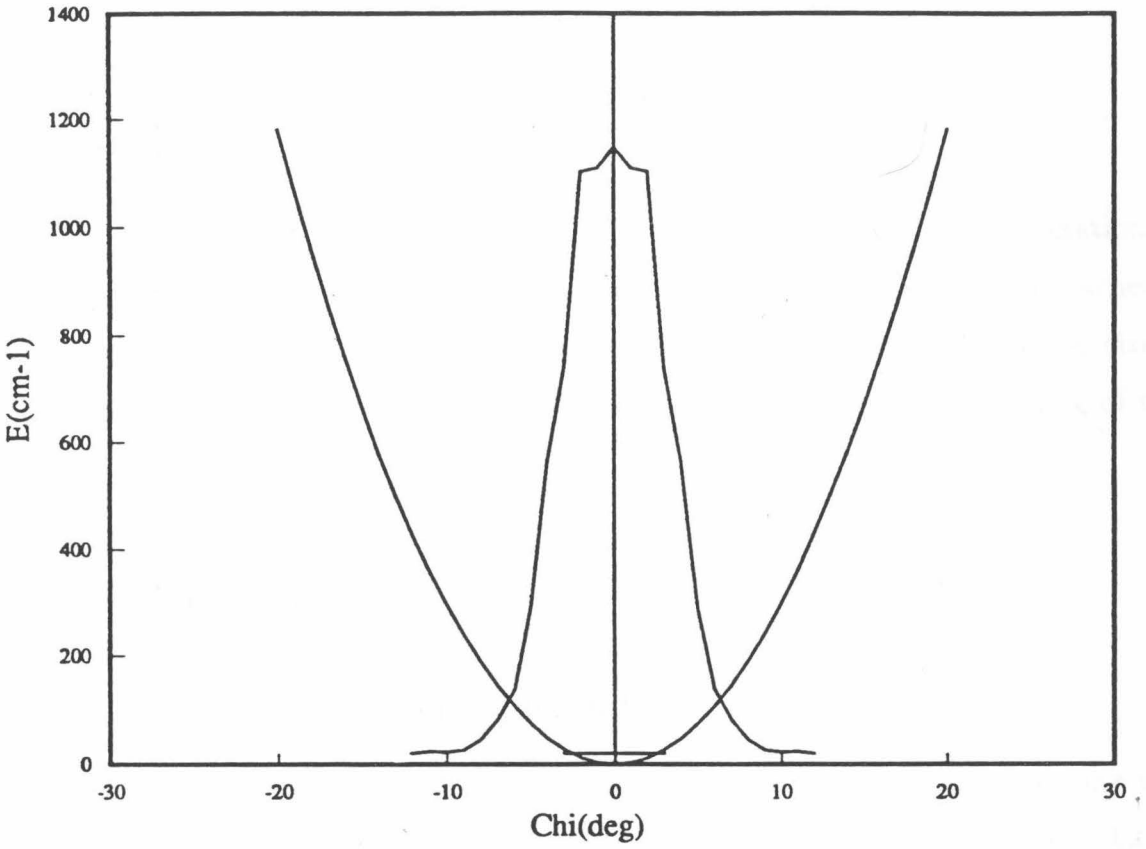

Figure 4.8: Distribution over potential energy cut, χ.

minimum potential, and the θ distribution is indeed broader than that of the χ distribution. The average θ value over this distribution, $< \theta >_{ave} = \pm 17°$, is in qualitative agreement with experimental observation, but the experimental values are uniformly larger than this calculated value, perhaps implying that the true θ potential is even shallower and broader, and/or the small barrier at 0° is actually higher than that predicted.

4.3.3 Summary

Ab initio calculations provided us with a model IPS to aid us in the interpretation of the experimental observations. Furthermore, by coupling the IPS generation scheme with DMC calculations, we plan to fit the IPS to the ground state data. A visual representation of the wavefunction was obtained to aid in the understanding of the IPS and the FIR spectra obtained from such clusters.

4.4 FIR Spectra

4.4.1 FIR experiment and data

FIR spectroscopy was finally used to explore the IPS in more detail. Scanning was started at 43.4 cm^{-1}, slightly below the predicted bending frequency of 47 cm^{-1} based on the one dimensional *ab initio* θ cut. P. Felker's group was kind enough to provide low resolution Raman spectra of benzene-water clusters in the ground state (private communication). Subsequently, we searched in the region where they observed Raman transitions, expecting some IR activity in the Raman-active modes. Since there was a higher density of bands among the H_2O, HDO and D_2O isotopomers between 43 and 52 cm^{-1}, and because this matched the expected frequency range of bending motions in θ with a large change in dipole moment derivative (and hence, IR activity), all known strong FIR laser lines in this region were used to search for transitions. The lines used in this search are given in Table 4.3. No benzene-water band was observed using laser lines ranging from 1267081.6 MHz to 1626602.6 MHz, although each of

these lines produced spectra for one or more of the N_2-H_2O, CO-H_2O, and $(D_2O)_3$ clusters. Although this is not a definitive null-result, it supports the conclusion that the bands between 43 and 52 cm^{-1} observed by Raman spectroscopy are not strongly IR active, and are most likely tied to a reorientation of the benzene monomer.

Table 4.3: FIR lines used for benzene-water transition search.

ν(MHz)	ν(cm^{-1})	Pump CO_2	Gas
420403.7	14.02316	10R34	DCOOH
584388.2	19.49309	9R28	HCOOH
604297.3	20.15719	9P20	CH_3F
1267081.6	42.26529	9R6	CH_2F_2
1299996.9	43.363229	9P6	CH_3OD
1397118.4	46.602854	9R34	CH_2F_2
1546083.4	51.571791	9R22	CH_2F_2
1626602.6	54.257622	9R32	CH_2F_2

Although the band near 20 cm^{-1} observed by Felker's group for benzene-D_2O was not expected to be strongly IR active, but rather a rotation of water about it's *b*-axis, we searched in this region. We initially scanned using a sample gas mixture containing H_2O, HDO and D_2O in various ratios, but transitions were only observed when D_2O was mixed in the sample gas. A total of 430 lines were observed. Stark modulation at 100 kHz, $\pm$40 V, was used to increase the signal-to-noise ratio (2$\times$ including the effect of shorter scan time) and to eliminate asymmetric top species from the spectrum, as described in the experimental section. For example, a water monomer line with S/N=10^5 was barely visible with Stark modulation. Other typical scanning parameters are: 40 kHz stepsize, 2 scan average, 1 second time constants, and daily adjusted flow rates of approximately $\sim$1 SLM of Ar+C_6H_6, $\sim$6 SLM of Ar+D_2O.

The DCOOH FIR laser line at 14.0 cm^{-1} was also used to search for the 14.3 cm^{-1} transition observed by Felker's group for benzene-HDO, but none was found. Since the 14.0 cm^{-1} FIR laser line is much weaker than the 19.5 cm^{-1} line, it is possible that our sensitivity was too low to observe this transition.

Although Felker group's spectra were of low resolution and Raman active, they

were extremely helpful in the FIR spectra search. This clearly illustrates the value of a lower resolution FIR spectrometer with wide coverage. Such a spectrometer is currently under construction in the Blake lab.

4.4.2 Analysis

The observed FIR spectrum (Figure 4.9) was analyzed in the following manner. The congested spectrum was combed for some recognizable pattern. A series of Q-branch like patterns were found with spacings between the lines being multiples of ~70 MHz. Combination differences using the ground state constants obtained from microwave spectra were used to predict P and R branches that went along with the observed Q-branches. (See Appendix E for the program.) Predictions with m=±1 resulted in no match in the spectrum. When the ground state was assumed to be m=0, P- and R-branches were predicted within experimental error (~2 MHz). Since the parity of D_2O cannot be changed by vibration, we assigned the transitions as originating and terminating in states with m=0. The accuracy of the P and R branches predicted by combination difference strongly supports the assignment in the J quantum numbers, which were tentatively assigned based on Q-branch spacing patters.

Figure 4.10 shows a stick spectrum of the lowest J Q-branch line from each set of PQR bands observed. The lowest P, Q and R for each set is tabulated in Table 4.4.

Table 4.4: Termination patterns of the assigned sets of P, Q, and R branches.

PQR set	Lowest P	Lowest Q	Lowest R	Tentative K″ →K′
A		Q5	R4	4→5
B		Q4	R3	3→4
C		Q4	R2	2→3
D	P3	Q2	R1	1→2
E	P1	Q1	R1	1→0
F	P2	Q2	R2	2→1
G	P3	Q3	R3	3→2
H	P4	Q4	R4	4→3
I	P5	Q5		5→4
J	P8	Q6		6→5

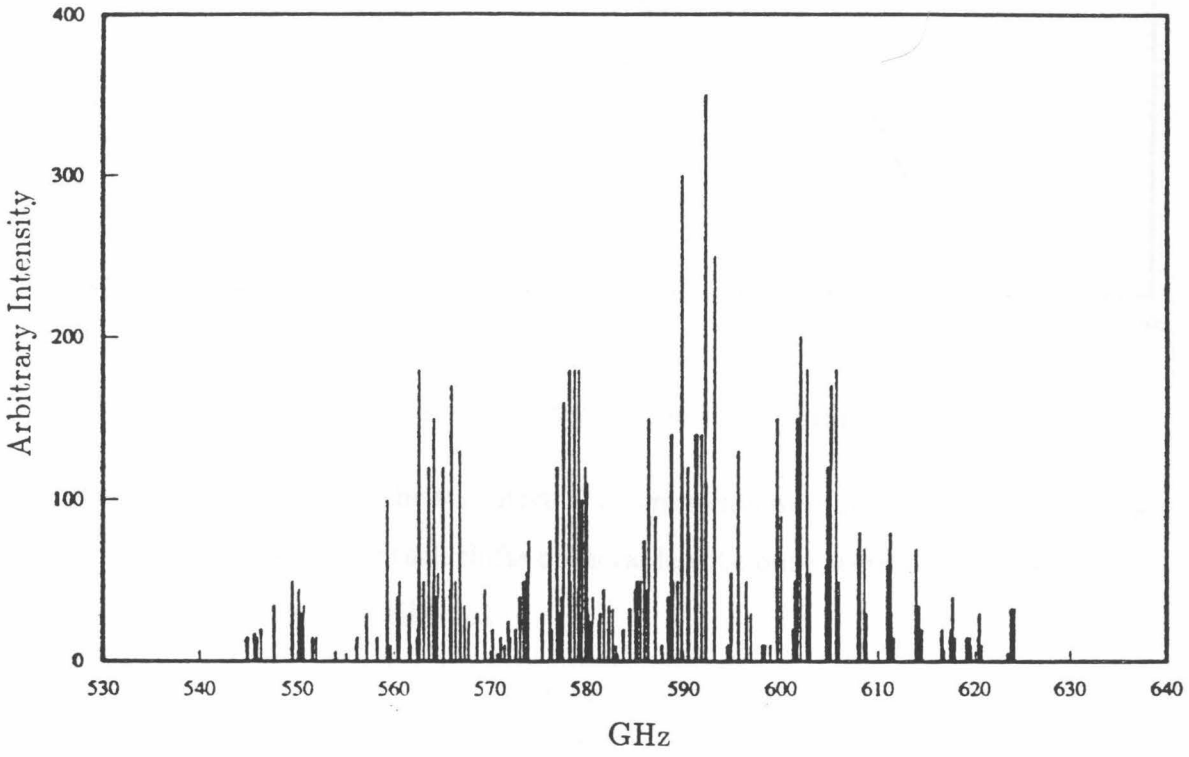

Figure 4.9: Stick spectrum of the observed and assigned 19.5 cm^{-1} band in bz-D_2O.

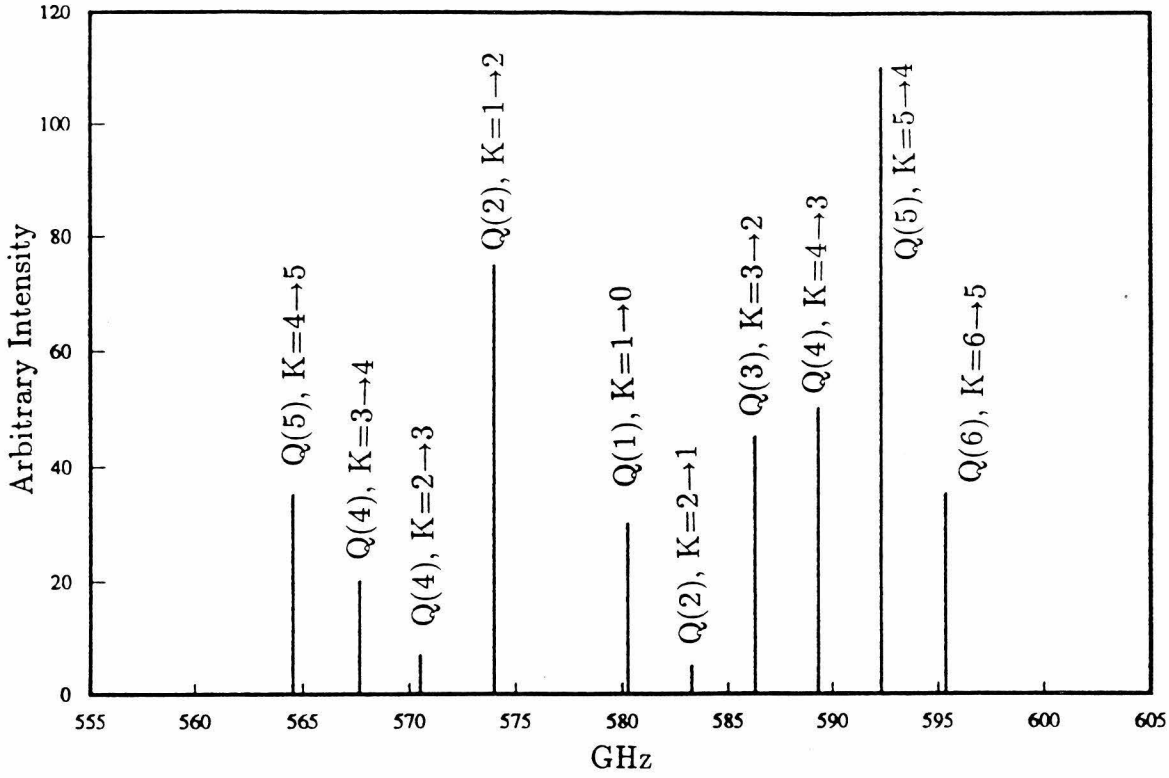

Figure 4.10: Stick spectrum of lowest Q branch lines

The J assignments and the tentative K assignments were compared with the Stark shift patterns. First order Stark shifts observable with our spectrometer give displacements in energy levels described as:

$$\Delta \mathrm{E} = \frac{-\mu E K M_J}{J(J+1)} = \alpha \frac{K M_J}{J(J+1)}.$$

Stark splittings were observed in PQR set E for Q(1), Q(2), R(1), R(2), P(1) and P(2) lines. An incomplete set of shifts was recorded for the PQR set D. Stark shifts in set E, which was tentatively assigned to K=1→0, is only consistent with a $\Delta M_J = \pm 1$, K=1→0 assignment. (See Table 4.5.) Since the FIR sideband radiation contains a significant fraction of its polarization perpendicular to the applied Stark field, $\Delta M_J = \pm 1$ is reasonable. Thus, set E is assigned conclusively to K=1→0 transition. It is assumed that the K assignments based on termination patterns are correct for set F, G, H, I and J based on these data.

The Stark splittings for the lower band are inconclusive. Only the R(1) line of

Table 4.5: Stark shifts expected and observed.

	Expected		Observed(MHz)	
M_J	1	2	1	2
Q(1)	$\alpha''/2$		3.22	
Q(2)	$\alpha''/6$	$\alpha''/3$	1.14	2.12
R(1)	$\alpha''/2$		3.3	
R(2)	$\alpha''/6$	$\alpha''/3$	1.18	2.28
P(1)	$\alpha''/2$		3.31	
P(2)	$\alpha''/6$	$\alpha''/3$	1.12	2.22

set D showed Stark splittings. The K assignments were, therefore, made based on termination patterns.

When individual sets are fitted with these assignments, each K structure (i.e., each set) fit nicely with a symmetric top Hamiltonian.

There are several qualitative observations to be made. First, we note that: 1) the transitions are between $m = 0$ states, and the upper state behaves as a symmetric top; 2) we observed ΔK = -1 at a higher frequency than ΔK = +1, which is the opposite of what is typically expected. Based on these observations, the following symmetric top Hamiltonian with l-type doubling, given by Gordy and Cook, was used to fit the spectra [38]:

$$\begin{aligned} \mathrm{E}_{JK} \;=\; & h\{B_v J(J+1) + (A_v - B_v)K^2 - 2A_v K l\zeta \\ & -D_J J^2(J+1)^2 - D_{JK} J(J+1)K^2 - D_K K^4 \\ & +2((2D_J + D_{JK})J(J+1) + (2D_K + D_{JK})K^2)Kl\zeta \\ & +P(J,K,l)\} \end{aligned}$$

where for K=l=$\pm$1 $P = \pm\frac{1}{2}J(J+1)q$, $q \simeq 2B^2/\omega$, and ω is the fundamental bending vibrational frequency. For K$\neq l = \pm 1$,

$$P = \pm\frac{(J(J+1) - K(K \mp 1))(J(J+1) - (K \mp 1)(K \mp 2))}{8(K \mp 1)((1-\zeta)A_v - B_v)}q^2.$$

A degenerate vibration giving rise to l-type doubling was needed to explain the "re-

versed" ΔK assignment. Usually, $\Delta K < 0$ is expected to be lower in frequency than $\Delta K > 0$ bands. Our K assignments are exactly the reverse of this expected pattern. The fitted constants and the line list are shown in Tables 4.6 and 4.14, 4.15 and 4.16. The ground state A rotational constant was fitted for the first time. The value is within 4% of the free benzene C rotational constant (2835.2 MHz), but lower as expected because of the coupling of the water motion onto this axis. The A value simulated by DMC calculation is 2832 MHz, which is essentially the same as the C constant in the free benzene. Although a 4% error may be permissible, the coupling of the benzene frame and the water rotor in the simulation needs to be reconsidered.

Table 4.6: Constants fit to FIR C_6H_6-D_2O lines.

Constant	Fit(MHz)	Std Dev
A	2737	5
B	1912.1	0.1
D_J	0.005	0.002
D_{JK}	0.040	0.007
D_K	4.0	0.5
A_U	2721	8
B_U	1872.5	0.2
E_v	581156	6
D_{Jl}	-0.026	0.004
D_{Ju}	0.009	0.002
D_{JKl}	-0.65	0.07
D_{JKu}	0.29	0.01
H_{JJKl}	0.0023	0.0007
H_{JJKu}	-0.0007	0.0002
D_{Kl}	3.7	0.4
D_{Ku}	4.1	0.5
H_{JKKl}	0.006	0.002
H_{JKKu}	-0.003	0.001
ζ (fixed)	0.87549	

Another qualitative observation is that in the Raman spectra taken by the Felker group, we noticed that there is not a peak in the C_6H_6-H_2O or C_6H_6-HDO species in the 19.5 cm^{-1} region. If the transition involved a motion of the entire water molecule and benzene, the reduced mass for that coordinate would have been similar for all three isotopomers. For example, Figures 4.11 and 4.12 show the G92 6-31G**

Hartree-Fock level frequency calculations. The motions that involve the entire water at 38.747 cm^{-1} for C_6H_6-H_2O have reduced masses for the H_2O and D_2O species differing by less than 1 %. Other motions that involve large amplitude motions in the hydrogen atoms and much less motion of the oxygen and benzene have very different reduced masses for the H_2O and D_2O species. Since there are no similar bands at 19.5 cm^{-1} for bz-H_2O and -HDO, we conclude that the motion involves a large amplitude motion of the hydrogen atoms.

We assigned the splitting in the spectrum to *l*-type doubling. This implies that there are at least two degenerate vibrational modes perpendicular to each other, and that the motion must have components perpendicular to the symmetry axis of the benzene-water cluster. Such normal modes are not predicted by the double harmonic G92 frequency calculations. We have already seen that the internal rotation is free or nearly free and that the water effectively becomes a symmetric top in the microwave spectra. The bending motion at 46.28, 67.44 and 259.43 cm^{-1} in the G92 frequency calculations for the H_2O species require the water to be in a certain position, and are not accurate descriptions. Thus, the rigid structure interpretation that was invalid for structural analysis using the microwave spectroscopy is, not surprisingly, inadequate for vibrational analyses as well. If the water molecule is replaced by a symmetric top as shown in Figure 4.13, then there are two perpendicular motions of the water bending, one along the X-axis and another along the Y-axis, as drawn. Recent reports by Zwier and co-workers support this interpretation. Their model potential required θ and ϕ coordinates to be closely coupled to each other [39].

In order to obtain such perpendicular vibrations, four out of six intermolecular normal modes shown in the Figures 4.11 and 4.12 must be combined. In the H_2O case, the 9.66, 46.28, 67.44 and 259.43 cm^{-1} modes must be combined. This may result in a four-fold degenerate mode, or two sets of two-fold degenerate modes, corresponding to geared and anti-geared motions. Full VRT spectra for the three isotopic species are needed to test this hypothesis. It will be of great interest to study the FIR spectra of the C_6H_6-NH_3 complex and its isotopomers since these consist of truly symmetric tops with a similar geometry.

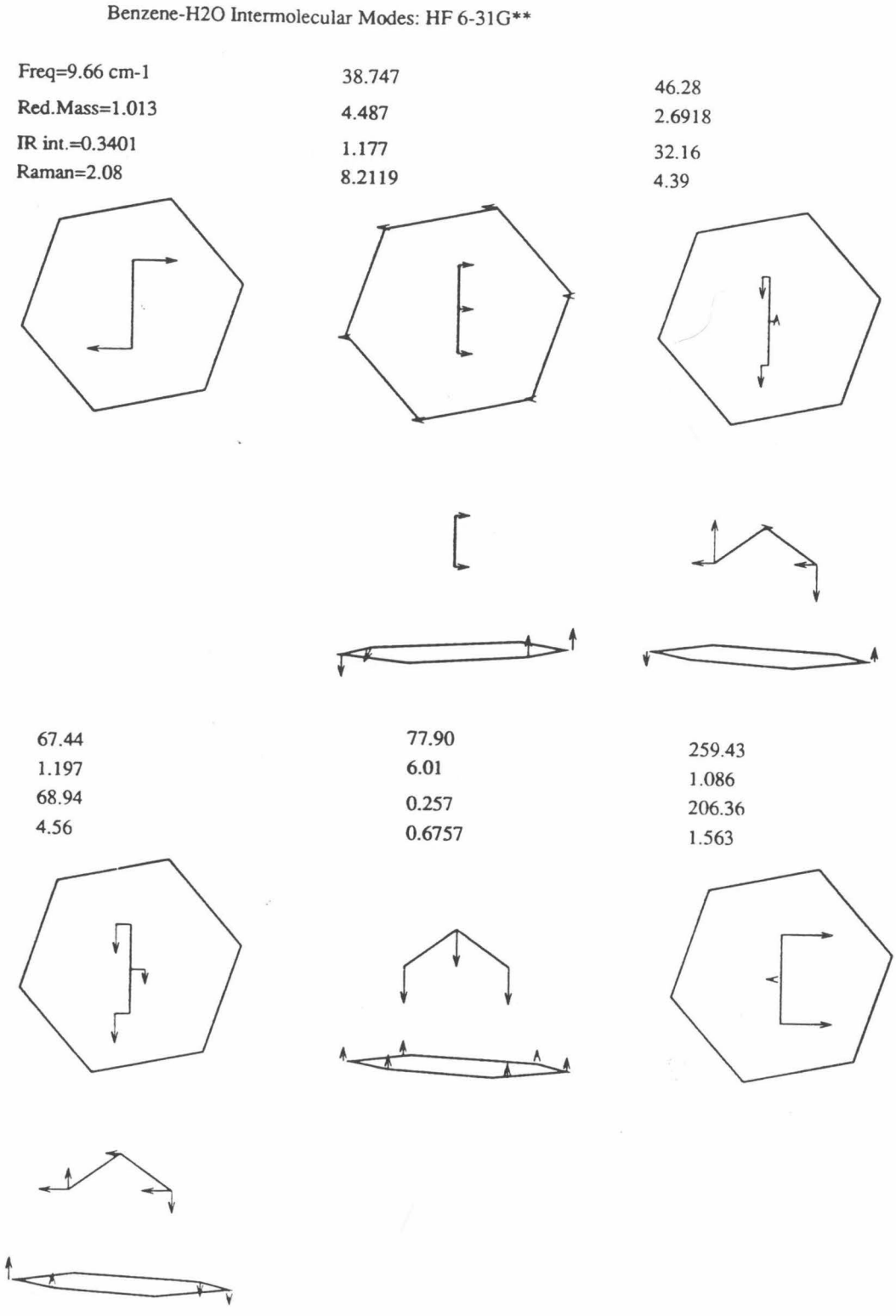

Figure 4.11: G92 frequency calculations and normal mode vectors for the benzene-H_2O intermolecular modes.

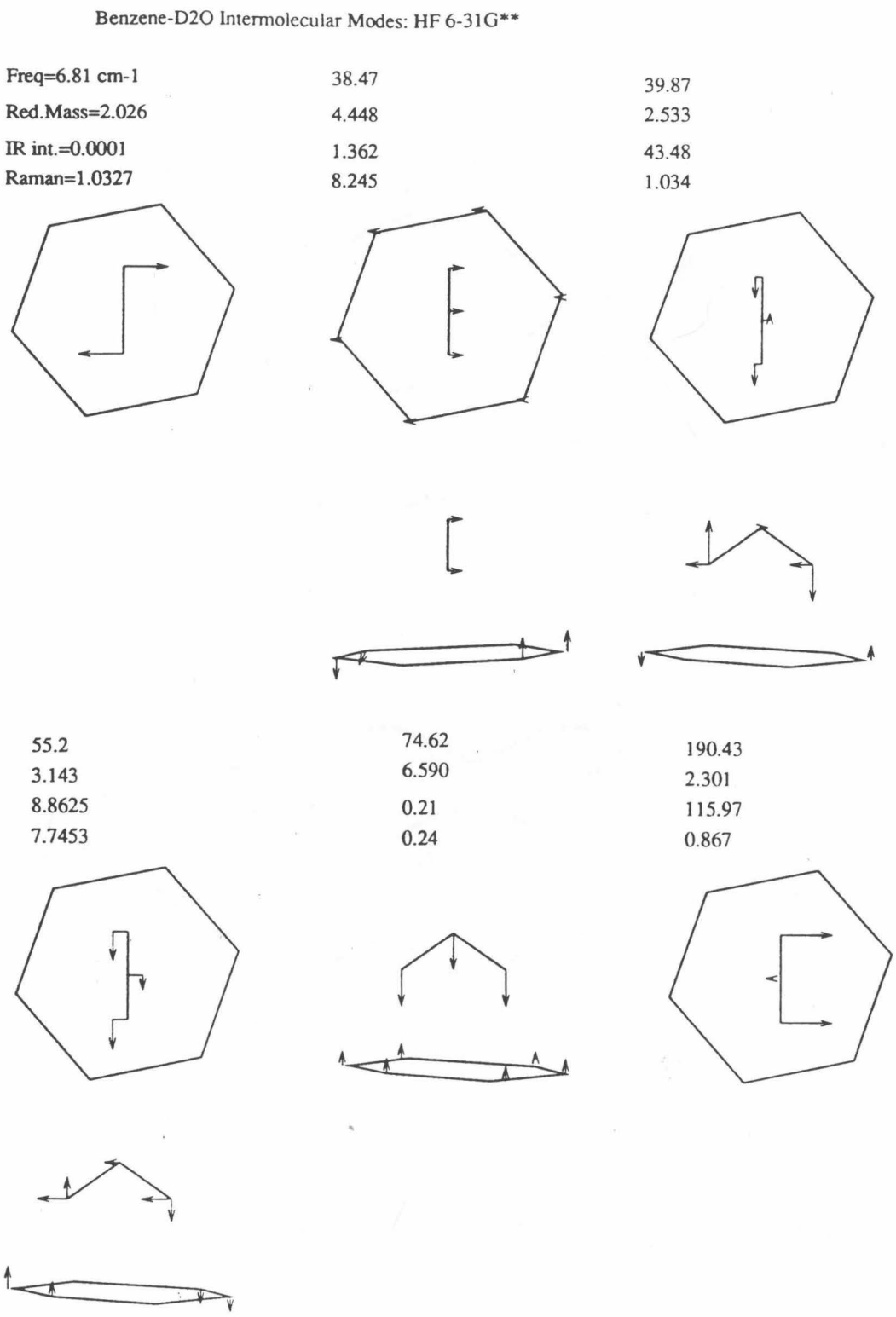

Figure 4.12: G92 frequency calculations and normal mode vectors for the benzene-D_2O intermolecular modes.

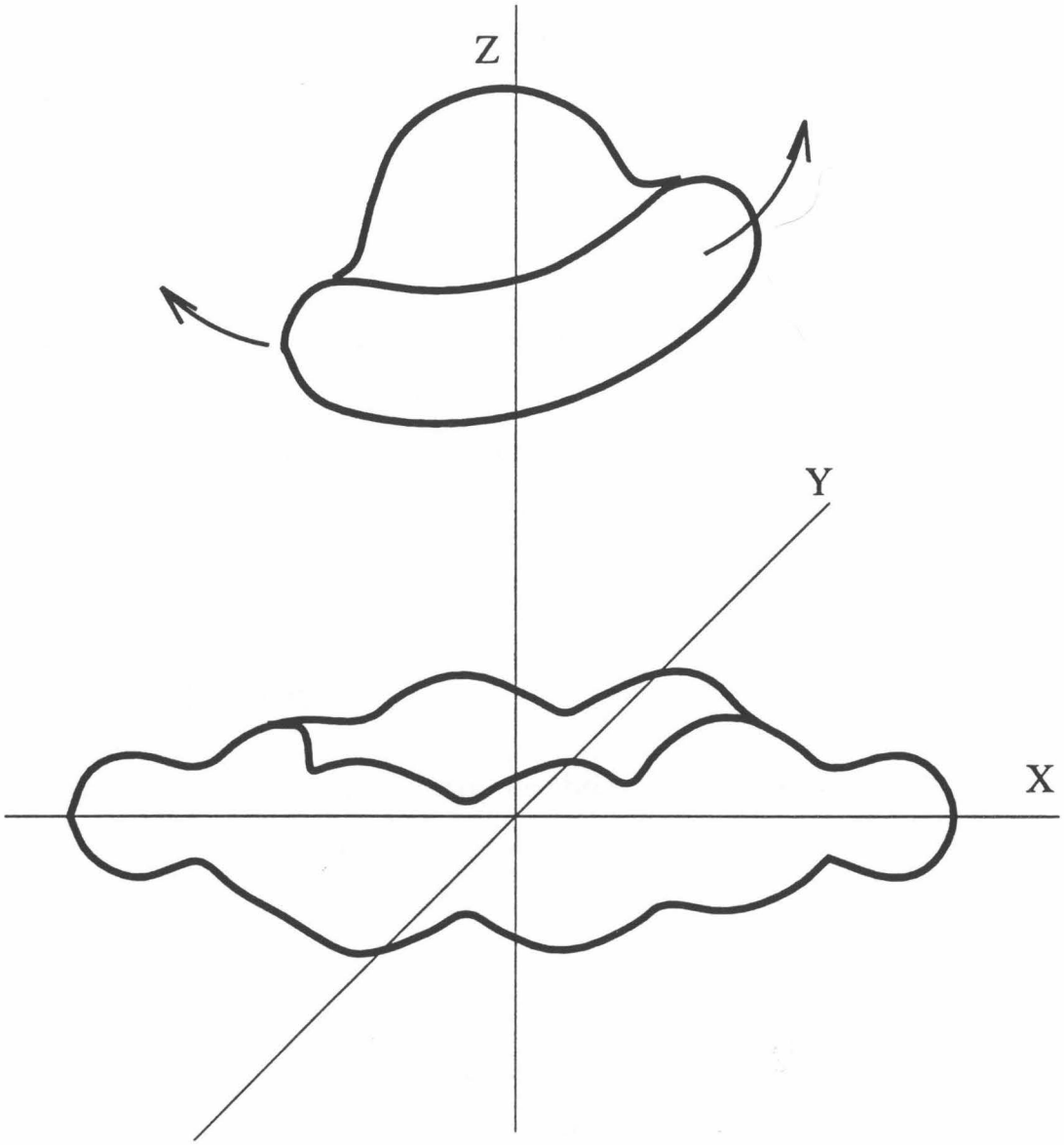

Figure 4.13: Water replaced by a symmetric top above the benzene plane.

The ζ term describes the proportion of the vibrational motion perpendicular to the symmetry axis. If $\zeta = 1$, then the motion is entirely perpendicular to the symmetry axis. The ζ we obtained suggests that 88% of the motion is perpendicular to the symmetry axis, leaving 12% of the motion to be along the symmetry axis. This qualitatively agrees with the motion described above, which has dipole derivative components perpendicular and parallel to the symmetry axis.

4.4.3 Summary

An FIR spectrum for C_6H_6-D_2O centered at 19.5 cm^{-1} was obtained. The proposed vibrational motion for this transition is a bending motion that is mostly perpendicular to the symmetry axis. The spectrum dictates that this motion is at least two-fold degenerate, giving rise to *l*-type doubling. In this interpretation, we see that the traditional concept of rigid structure is not applicable and an interpretation based on an IPS is required.

4.5 Conclusion

In both the microwave and FIR spectra, we observed a symmetric top spectrum for a cluster considered to be at most C_{2v} in the point group designation. The cluster is considered here as belonging to the G_{24} PI group. The vibrational spectrum obtained is better explained with a model of a cluster consisting of two symmetric tops. We have found that benzene-water is similar to Ar-water in some ways and quite different in others. They both include "hydrogen bonded" water with a polarizable object. However, the water in Ar-water can be considered as a water molecule with a slight perturbation by a point charge. The benzene is much larger and is no longer a small perturbation. For example, the benzene-water θ potential is shallow, similar to Ar-water between $\pm 50°$, but the potential increases as θ increases restricting free rotation about water *c*-axis. In the ϕ coordinate, the water is strictly confined to a narrow harmonic well, far from being a free rotor. Benzene-water has large amplitude motions similar to Ar-water, but the intermolecular bond is much stronger and restrictive.

Table 4.7: Benzene-H_2O m=0 microwave line list. Observed and calculated lines are given with the assignments.

J″	K''_P	K''_O	J′	K'_P	K'_O	Obs. (MHz)	Calc. (MHz)	O-C (MHz)
4	4	0	5	4	0	19941.0(10)	19940.5	0.5
4	3	0	5	3	0	19943.7(10)	19943.1	0.5
4	2	0	5	2	0	19945.4(10)	19945.0	0.3
4	1	0	5	1	0	19946.5(10)	19946.2	0.3
5	5	0	6	5	0	23923.4(10)	23923.6	-0.2
5	4	0	6	4	0	23927.5(10)	23927.6	-0.1
5	3	0	6	3	0	23930.7(10)	23930.8	-0.1
5	2	0	6	2	0	23933.0(10)	23933.1	-0.1
5	1	0	6	1	0	23934.3(10)	23934.4	-0.1
6	6	0	7	6	0	27903.6(10)	27903.7	-0.1
6	5	0	7	5	0	27909.4(10)	27909.5	-0.1
6	4	0	7	4	0	27914.2(10)	27914.3	-0.1
6	3	0	7	3	0	27917.9(10)	27918.0	-0.1
6	2	0	7	2	0	27920.4(10)	27920.6	-0.2
6	1	0	7	1	0	27922.1(10)	27922.2	-0.1
7	6	0	8	6	0	31888.2(10)	31888.3	-0.1
7	5	0	8	5	0	31894.9(10)	31894.9	0.0
7	4	0	8	4	0	31900.3(10)	31900.3	0.0
7	3	0	8	3	0	31904.6(10)	31904.6	0.0
7	1	0	8	1	0	31909.4(10)	31909.4	0.0
8	6	0	9	6	0	35872.1(10)	35872.1	0.0
8	5	0	9	5	0	35879.5(10)	35879.6	-0.1
8	4	0	9	4	0	35885.5(10)	35885.7	-0.2
8	3	0	9	3	0	35890.3(10)	35890.4	-0.1
8	2	0	9	2	0	35893.7(10)	35893.8	-0.1
8	1	0	9	1	0	35895.8(10)	35895.9	0.0
9	8	0	10	8	0	39834.1(10)	39834.1	0.0
9	7	0	10	7	0	39845.4(10)	39845.4	0.1
9	6	0	10	6	0	39855.3(10)	39855.2	0.1
9	5	0	10	5	0	39863.6(10)	39863.5	0.1
9	4	0	10	4	0	39870.3(10)	39870.3	0.0
9	3	0	10	3	0	39875.7(10)	39875.6	0.1
9	2	0	10	2	0	39879.4(10)	39879.3	0.1
9	1	0	10	1	0	39881.7(10)	39881.6	0.1

Table 4.8: Benzene-H_2O m=1 microwave line list. Observed and calculated lines are given with the assignments.

J″	K''_P	K''_O	J′	K'_P	K'_O	Obs. (MHz)	Calc. (MHz)	O-C (MHz)
4	-4	1	5	-4	1	19737.6(10)	19735.9	1.7
4	-3	1	5	-3	1	19760.0(10)	19760.6	-0.6
4	-2	1	5	-2	1	19782.4(10)	19783.5	-1.1
4	-1	1	5	-1	1	19803.0(10)	19804.6	-1.5
4	1	1	5	1	1	19835.8(10)	19841.3	-5.5
4	2	1	5	2	1	19853.0(10)	19857.0	-4.0
4	3	1	5	3	1	19865.4(10)	19870.8	-5.4
5	-5	1	6	-5	1	23653.7(10)	23651.8	1.8
5	-4	1	6	-4	1	23684.0(10)	23683.6	0.4
5	-3	1	6	-3	1	23712.4(10)	23713.2	-0.8
5	-2	1	6	-2	1	23739.0(10)	23740.7	-1.7
5	-1	1	6	-1	1	23764.8(10)	23766.0	-1.2
5	1	1	6	1	1	23819.4(10)	23810.1	9.4
5	2	1	6	2	1	23835.3(10)	23828.9	6.4
5	3	1	6	3	1	23847.8(10)	23845.5	2.2
6	-6	1	7	-6	1	27557.4(10)	27554.9	2.5
6	-5	1	7	-5	1	27595.9(10)	27594.5	1.4
6	-4	1	7	-4	1	27631.7(10)	27631.6	0.1
6	-3	1	7	-3	1	27665.1(10)	27666.1	-1.0
6	-2	1	7	-2	1	27696.7(10)	27698.2	-1.5
6	-1	1	7	-1	1	27728.1(10)	27727.7	0.4
6	1	1	7	1	1	27784.8(10)	27779.1	5.7
6	2	1	7	2	1	27804.4(10)	27801.1	3.3
6	3	1	7	3	1	27819.7(10)	27820.5	-0.8
6	4	1	7	4	1	27831.9(10)	27837.4	-5.4
7	-7	1	8	-7	1	31447.0(10)	31444.1	2.9
7	-6	1	8	-6	1	31494.3(10)	31492.3	2.1
7	-5	1	8	-5	1	31538.2(10)	31537.5	0.7
7	-4	1	8	-4	1	31579.4(10)	31579.9	-0.5
7	-3	1	8	-3	1	31618.0(10)	31619.4	-1.4
7	-2	1	8	-2	1	31655.1(10)	31656.0	-0.9
7	-1	1	8	-1	1	31692.6(10)	31689.7	2.9
7	1	1	8	1	1	31748.0(10)	31748.5	-0.5
7	2	1	8	2	1	31772.1(10)	31773.6	-1.5
7	3	1	8	3	1	31790.3(10)	31795.8	-5.4
7	4	1	8	4	1	31816.2(10)	31815.0	1.2

Table 4.9: Benzene-H_2O m=1 line list continued.

J″	K''_P	K''_O	J′	K'_P	K'_O	Obs. (MHz)	Calc. (MHz)	O-C (MHz)
8	-6	1	9	-6	1	35431.0(10)	35430.0	1.1
8	-5	1	9	-5	1	35471.4(10)	35480.9	-9.5
8	-4	1	9	-4	1	35527.3(10)	35528.6	-1.2
8	-3	1	9	-3	1	35571.4(10)	35573.0	-1.5
8	-2	1	9	-2	1	35614.1(10)	35614.2	0.0
8	-1	1	9	-1	1	35658.5(10)	35652.1	6.4
8	1	1	9	1	1	35717.1(10)	35718.2	-1.2
8	2	1	9	2	1	35737.6(10)	35746.4	-8.8
8	3	1	9	3	1	35776.2(10)	35771.4	4.8
9	-8	1	10	-8	1	39244.9(10)	39244.1	0.7
9	-7	1	10	-7	1	39308.6(10)	39307.9	0.6
9	-6	1	10	-6	1	39367.8(10)	39368.1	-0.3
9	-5	1	10	-5	1	39423.4(10)	39424.7	-1.3
9	-4	1	10	-4	1	39475.6(10)	39477.6	-2.0
9	-3	1	10	-3	1	39525.3(10)	39527.0	-1.7
9	-2	1	10	-2	1	39574.0(10)	39572.8	1.2
9	2	1	10	2	1	39726.8(10)	39719.7	7.1
9	3	1	10	3	1	39746.5(10)	39747.5	-1.0
9	4	1	10	4	1	39773.6(10)	39771.6	2.0
9	7	1	10	7	1	39821.4(10)	39822.3	-0.9

Table 4.10: Benzene-D_2O microwave line list.

J″	K''_P	K''_O	J′	K'_P	K'_O	Obs. (MHz)	Calc. (MHz)	O-C (MHz)
4	1	0	5	1	0	19118.6(10)	19118.3	0.2
4	2	0	5	2	0	19117.1(10)	19116.9	0.2
4	3	0	5	3	0	19115.0(10)	19114.6	0.3
4	4	0	5	4	0	19111.7(10)	19111.4	0.4
5	1	0	6	1	0	22941.0(10)	22941.0	0.0
5	2	0	6	2	0	22939.4(10)	22939.3	0.1
5	3	0	6	3	0	22936.6(10)	22936.5	0.1
5	4	0	6	4	0	22932.6(10)	22932.6	0.0
5	5	0	6	5	0	22927.7(10)	22927.6	0.1
6	6	0	7	6	0	26740.0(10)	26740.3	-0.3
6	5	0	7	5	0	26747.8(10)	26747.4	0.4
6	4	0	7	4	0	26753.1(10)	26753.3	-0.2
6	3	0	7	3	0	26757.6(10)	26757.8	-0.2
6	2	0	7	2	0	26760.9(10)	26761.1	-0.2
6	1	0	7	1	0	26762.8(10)	26763.1	-0.3
7	7	0	8	7	0	30548.7(10)	30548.8	-0.1
7	6	0	8	6	0	30558.3(10)	30558.4	-0.1
7	5	0	8	5	0	30566.5(10)	30566.6	-0.1
7	4	0	8	4	0	30573.2(10)	30573.3	-0.1
7	3	0	8	3	0	30578.4(10)	30578.5	-0.1
7	2	0	8	2	0	30582.1(10)	30582.2	-0.2
7	1	0	8	1	0	30584.3(10)	30584.5	-0.2
8	7	0	9	7	0	34365.0(10)	34365.0	0.1
8	6	0	9	6	0	34375.8(10)	34375.9	0.0
8	5	0	9	5	0	34385.0(10)	34385.1	0.0
8	4	0	9	4	0	34392.6(10)	34392.6	0.0
8	3	0	9	3	0	34398.5(10)	34398.5	0.0
8	2	0	9	2	0	34402.6(10)	34402.6	0.0
8	1	0	9	1	0	34405.2(10)	34405.2	0.0
9	8	0	10	8	0	38166.5(10)	38166.4	0.1
9	7	0	10	7	0	38180.4(10)	38180.4	0.0
9	6	0	10	6	0	38192.4(10)	38192.4	0.0
9	5	0	10	5	0	38202.7(10)	38202.7	0.0
9	4	0	10	4	0	38211.1(10)	38211.1	0.1
9	3	0	10	3	0	38217.6(10)	38217.6	0.0
9	2	0	10	2	0	38222.3(10)	38222.2	0.1
9	1	0	10	1	0	38225.2(10)	38225.0	0.2

Table 4.11: Benzene-HDO microwave line list.

J″	K''_P	K''_O	J′	K'_P	K'_O	Obs. (MHz)	Calc. (MHz)	O-C (MHz)
4	4	0	5	4	0	19552.6(10)	19552.1	0.6
4	3	0	5	3	0	19556.8(10)	19556.3	0.4
4	2	0	5	2	0	19559.6(10)	19559.3	0.3
4	1	0	5	1	0	19561.4(10)	19561.2	0.3
5	5	0	6	5	0	23454.9(10)	23455.0	-0.1
5	4	0	6	4	0	23461.4(10)	23461.5	-0.1
5	3	0	6	3	0	23466.5(10)	23466.6	-0.1
5	2	0	6	2	0	23470.2(10)	23470.2	-0.1
5	1	0	6	1	0	23472.3(10)	23472.4	-0.1
6	6	0	7	6	0	27353.4(10)	27353.5	-0.1
6	5	0	7	5	0	27362.8(10)	27362.8	0.0
6	4	0	7	4	0	27370.4(10)	27370.5	-0.1
6	3	0	7	3	0	27376.3(10)	27376.4	-0.1
6	2	0	7	2	0	27380.6(10)	27380.6	-0.1
6	1	0	7	1	0	27383.0(10)	27383.2	-0.1
7	7	0	8	7	0	31246.8(10)	31246.9	-0.1
7	6	0	8	6	0	31259.4(10)	31259.4	0.0
7	5	0	8	5	0	31270.0(10)	31270.1	-0.1
7	4	0	8	4	0	31278.7(10)	31278.8	-0.1
7	3	0	8	3	0	31285.5(10)	31285.6	0.0
7	2	0	8	2	0	31290.3(10)	31290.4	-0.1
7	1	0	8	1	0	31293.2(10)	31293.3	-0.1
7	1	0	8	1	0	31293.2(10)	31293.3	-0.1
8	8	0	9	8	0	35134.2(10)	35134.2	0.1
8	7	0	9	7	0	35150.4(10)	35150.5	-0.1
8	6	0	9	6	0	35164.5(10)	35164.6	-0.2
8	5	0	9	5	0	35176.5(10)	35176.6	-0.1
8	4	0	9	4	0	35186.3(10)	35186.4	-0.1
8	3	0	9	3	0	35193.9(10)	35194.0	-0.1
8	2	0	9	2	0	35199.4(10)	35199.5	0.0
8	1	0	9	1	0	35202.7(10)	35202.7	0.0
8	0	0	9	0	0	35203.9(10)	35203.8	0.1
9	9	0	10	9	0	39014.8(10)	39014.6	0.2
9	8	0	10	8	0	39035.3(10)	39035.2	0.1
9	7	0	10	7	0	39053.2(10)	39053.3	-0.1
9	6	0	10	6	0	39069.0(10)	39069.0	-0.1
9	5	0	10	5	0	39082.3(10)	39082.3	0.0
9	4	0	10	4	0	39093.3(10)	39093.2	0.1
9	3	0	10	3	0	39101.8(10)	39101.7	0.1
9	2	0	10	2	0	39107.9(10)	39107.7	0.2
9	1	0	10	1	0	39111.5(10)	39111.4	0.1
9	0	0	10	0	0	39112.7(10)	39112.6	0.1

Table 4.12: Fitted microwave rotational constants.

Complex	B(MHz)	D_J(kHz)	D_{JK}(kHz)	σ(MHz)
m=0				
C_6H_6-H_2O	1994.83(2)	3.58(6)	37.87(26)	0.27
C_6H_6-HDO	1956.357(7)	3.641(12)	60.48(5)	0.11
C_6H_6-D_2O	1912.068(8)	3.877(27)	46.41(7)	0.13
	D_{Jm}(MHz)	D_{JKm}(MHz)	H_{JKm}(kHz)	σ(MHz)
m=1				
C_6H_6-H_2O	12.49(5)	1.650(8)	58.9(25)	3.9

Table 4.13: Dipole moment measurements for benzene-H_2O

	M_J=0	M_J=1	M_J=2
m=0	2.07(18)	2.14(65)	2.07(23)
m=1	2.13(20)	2.15(67)	2.12(23)

Table 4.14: Benzene-D_2O FIR lines observed near 19.5 cm^{-1}.

l''	J''	K''	l'	J'	K'	Obs. (MHz)	Calc. (MHz)	O-C (MHz)
0	1	1	-1	0	0	576511.0(10)	576511.5	-0.5
0	2	1	-1	1	0	572611.0(10)	572608.6	2.4
0	3	1	-1	2	0	568625.2(10)	568627.1	-1.9
0	4	1	-1	3	0	564566.0(10)	564567.5	-1.5
0	5	1	-1	4	0	560428.0(10)	560430.4	-2.4
0	6	1	-1	5	0	556214.0(10)	556216.6	-2.6
0	7	1	-1	6	0	551930.0(10)	551927.3	2.7
0	1	1	-1	2	0	587747.0(10)	587746.6	0.4
0	2	1	-1	3	0	591333.0(10)	591334.0	-1.0
0	3	1	-1	4	0	594842.0(10)	594843.1	-1.1
0	4	1	-1	5	0	598274.0(10)	598274.5	-0.5
0	5	1	-1	6	0	601633.0(10)	601628.9	4.1
0	6	1	-1	7	0	604920.0(10)	604907.4	12.6
0	1	1	-1	1	0	580259.0(10)	580256.5	2.5
0	2	1	-1	2	0	580100.0(10)	580098.7	1.3
0	3	1	-1	3	0	579862.0(10)	579862.4	-0.4
0	4	1	-1	4	0	579547.0(10)	579548.1	-1.1
0	5	1	-1	5	0	579156.0(10)	579156.7	-0.7
0	6	1	-1	6	0	578693.0(10)	578688.9	4.1
0	2	2	-1	2	1	583280.0(10)	583272.8	7.2
0	3	2	-1	3	1	583035.0(10)	583031.7	3.3
0	4	2	-1	4	1	582709.0(10)	582710.3	-1.3
0	5	2	-1	5	1	582306.0(10)	582309.1	-3.1
0	6	2	-1	6	1	581824.0(10)	581828.1	-4.1
0	7	2	-1	7	1	581264.0(10)	581267.7	-3.7
0	2	2	-1	1	1	575796.0(10)	575786.3	9.7
0	3	2	-1	2	1	571809.0(10)	571802.0	7.0
0	4	2	-1	3	1	567741.0(10)	567737.7	3.3
0	5	2	-1	4	1	563593.0(10)	563593.8	-0.8
0	6	2	-1	5	1	559368.0(10)	559370.5	-2.5
0	7	2	-1	6	1	555063.0(10)	555068.2	-5.2
0	2	2	-1	3	1	594506.0(10)	594502.6	3.4
0	3	2	-1	4	1	598003.0(10)	598004.3	-1.3
0	4	2	-1	5	1	601423.0(10)	601425.6	-2.6
0	5	2	-1	6	1	604762.0(10)	604766.7	-4.7
0	6	2	-1	7	1	608025.0(10)	608027.7	-2.7
0	3	3	-1	3	2	586298.0(10)	586296.8	1.2
0	4	3	-1	4	2	585965.0(10)	585966.2	-1.2
0	5	3	-1	5	2	585550.0(10)	585553.3	-3.3
0	6	3	-1	6	2	585055.0(10)	585058.5	-3.5
0	7	3	-1	7	2	584478.0(10)	584481.9	-3.9

Table 4.15: Benzene-D_2O FIR line list, continued.

l''	J''	K''	l'	J'	K'	Obs. (MHz)	Calc. (MHz)	O-C (MHz)
0	3	3	-1	2	2	575082.2(10)	575075.2	7.0
0	4	3	-1	3	2	571007.0(10)	571004.4	2.6
0	5	3	-1	4	2	566851.0(10)	566851.6	-0.6
0	6	3	-1	5	2	562614.0(10)	562617.1	-3.1
0	7	3	-1	6	2	558298.0(10)	558301.4	-3.4
0	3	3	-1	4	2	601258.0(10)	601258.6	-0.6
0	4	3	-1	5	2	604665.0(10)	604667.9	-2.9
0	5	3	-1	6	2	607991.0(10)	607994.7	-3.7
0	6	3	-1	7	2	611237.0(10)	611239.1	-2.1
0	4	4	-1	4	3	589318.0(10)	589320.7	-2.7
0	5	4	-1	5	3	588893.0(10)	588894.2	-1.2
0	6	4	-1	6	3	588384.0(10)	588383.7	0.3
0	7	4	-1	7	3	587793.0(10)	587789.7	3.3
0	4	4	-1	3	3	574369.2(10)	574372.4	-3.2
0	5	4	-1	4	3	570207.0(10)	570208.9	-1.9
0	6	4	-1	5	3	565961.0(10)	565961.4	-0.4
0	7	4	-1	6	3	561631.0(10)	561630.5	0.5
0	8	4	-1	7	3	557220.0(10)	557217.0	3.0
0	4	4	-1	5	3	608004.0(10)	608006.0	-2.0
0	5	4	-1	6	3	611317.0(10)	611316.5	0.5
0	6	4	-1	7	3	614546.0(10)	614542.9	3.1
0	5	5	-1	5	4	592336.0(10)	592338.8	-2.8
0	6	5	-1	6	4	591816.0(10)	591812.7	3.3
0	7	5	-1	6	4	565068.2(10)	565064.5	3.7
0	6	5	-1	5	4	569409.2(10)	569410.3	-1.1
0	6	5	-1	7	4	617958.2(10)	617950.2	8.0
0	6	6	-1	6	5	595352.2(10)	595356.5	-4.3
0	7	6	-1	7	5	594734.2(10)	594733.8	0.4
0	8	6	-1	8	5	594030.2(10)	594029.1	1.1
0	9	6	-1	9	5	593241.2(10)	593245.1	-3.9
0	8	6	-1	7	5	564175.2(10)	564173.9	1.3
0	9	6	-1	8	5	559653.2(10)	559652.2	1.0
0	3	1	1	2	2	562518.0(10)	562527.5	-9.5
0	6	1	1	5	2	550126.0(10)	550121.5	4.5
0	7	1	1	6	2	545836.0(10)	545835.6	0.4
0	1	1	1	2	2	581637.7(10)	581647.1	-9.4
0	2	1	1	3	2	585231.0(10)	585235.2	-4.2
0	3	1	1	4	2	588748.0(10)	588745.7	2.3
0	4	1	1	5	2	592185.0(10)	592179.3	5.7
0	5	1	1	6	2	595540.0(10)	595537.2	2.8
0	6	1	1	7	2	598812.0(10)	598820.6	-8.6

Table 4.16: Benzene-D_2O FIR line list, continued.

l''	J''	K''	l'	J'	K'	Obs. (MHz)	Calc. (MHz)	O-C (MHz)
0	2	1	1	2	2	573989.0(10)	573999.1	-10.1
0	3	1	1	3	2	573759.0(10)	573763.6	-4.6
0	4	1	1	4	2	573453.0(10)	573450.8	2.2
0	5	1	1	5	2	573066.0(10)	573061.6	4.4
0	6	1	1	6	2	572599.0(10)	572597.2	1.8
0	6	2	1	6	3	569711.2(10)	569707.6	3.6
0	5	2	1	5	3	570159.2(10)	570155.6	3.6
0	4	2	1	4	3	570531.2(10)	570530.0	1.2
0	5	2	1	4	3	551415.2(10)	551413.4	1.8
0	6	2	1	5	3	547220.2(10)	547217.0	3.2
0	2	2	1	3	3	582299.2(10)	582301.1	-1.9
0	3	2	1	4	3	585824.7(10)	585824.0	0.7
0	4	2	1	5	3	589275.2(10)	589272.2	3.0
0	5	2	1	6	3	592650.2(10)	592646.2	4.0
0	6	2	1	7	3	595946.7(10)	595946.6	0.1
0	4	3	1	4	4	567676.0(10)	567673.3	2.7
0	5	3	1	5	4	567316.0(10)	567316.4	-0.4
0	6	3	1	6	4	566882.0(10)	566885.7	-3.7
0	3	3	1	4	4	582969.0(10)	582965.7	3.3
0	4	3	1	5	4	586429.0(10)	586431.0	-2.0
0	5	3	1	6	4	589818.0(10)	589821.9	-3.9
0	6	3	1	7	4	593134.0(10)	593137.1	-3.1
0	4	4	1	5	5	583645.0(10)	583644.4	0.6
0	5	4	1	6	5	587047.0(10)	587049.4	-2.4
0	6	4	1	7	5	590378.0(10)	590373.8	4.2
0	5	4	1	5	5	564533.0(10)	564532.7	0.3
0	6	4	1	6	5	564115.0(10)	564116.5	-1.5
0	8	2	-1	8	1	580630.0(10)	580628.4	1.6

Bibliography

[1] R.E. Bumgarner, S. Suzuki, P.A. Stockman, P.G. Green, and G.A. Blake. Microwave and Tunable Far-Infrared Laser Spectroscopy of OC-H_2O–Investigation of the Water Tunneling Potential. *Chem. Phys. Lett.*, 176:123, 1991.

[2] D. Yaron, K.I. Peterson, D. Zolandz, W. Klemperer, F.J. Lovas, and R.D. Suenram. Water Hydrogen-Bonding–The Structure of the Water Carbon-Monoxide Complex. *J. Chem. Phys.*, 92:7095, 1990.

[3] H.O. Leung, M.D. Marshall, R.D. Suenram, and F.J. Lovas. Microwave-Spectrum and Molecular-Structure of the N_2-H_2O Complex. *J. Chem. Phys.*, 90:700, 1989.

[4] Z.S. Huang, K.W. Jucks, and R.E. Miller. The Vibrational Predissociation Lifetime of the HF Dimer upon Exciting the "Free-H" Stretching Vibration. *J. Chem. Phys.*, 85:3338, 1986.

[5] E.J. Bohac, M.D. Marshall, and R.E. Miller. Initial State Effects in the Vibrational Predissociation of Hydrogen Fluoride Dimer. *J. Chem. Phys.*, 96:6681, 1992.

[6] C.M. Lovejoy, Jr. D.D. Nelson, and D.J. Nesbitt. Hindered Internal Rotation in Jet Cooled H_2HF Complexes. *J. Chem. Phys.*, 87:5621, 1987.

[7] C.M. Lovejoy, Jr. D.D. Nelson, and D.J. Nesbitt. The Infrared Spectrum of D_2HF. *J. Chem. Phys.*, 89:7180, 1988.

[8] E. Tüchsen and C. Woodward. Assignment of Asparagine-44 Side-Chain Primary Amide ^1H NMR Resonances and the Peptide Amide N^1H Resonance of Glycine-37 in Basic Pancreatic Trypsin Inhibitor. *Biochemistry*, 26:1918, 1987.

[9] M. Levitt and M.F. Perutz. Aromatic Rings Act as Hydrogen Bond Acceptors. *J. Mol. Biol.*, 201:751, 1988.

[10] S.K. Burley and G.A. Petsko. Aromatic-Aromatic Interaction: A Mechanism of Protein Structure Stabilization. *Science*, 229:23, 1985.

[11] S.K. Burley and G.A. Petsko. Amino-Aromatic Interactions in Proteins. *FEBS Lett.*, 203:139, 1986.

[12] S.K. Burley and G.A. Petsko. Weakly Polar Interactions in Proteins. *Adv. Prot. Chem.*, 39:125, 1988.

[13] J.L. Atwood, F. Hamada, K.D. Robinson, G.W. Orr, and R.L. Vincent. X-ray Diffraction Evidence for Aromatic π Hydrogen Bonding to Water. *Nature*, 349:683, 1991.

[14] M. Dennis, J. Giraudat, F. Kotzyba-Hibert, M. Goeldner, C. Hirth, J-Y. Chang, C. Lazure, M. Chretien, and J-P. Changeux. Amino Acids of the *Torpedo marmorata* Acetylcholine Receptor α Subunit Labeled by a Photoaffinity Ligand for the Acetylcholine Binding Site. *Biochem.*, 27:2346, 1988.

[15] R.A. Kumpf and D.A. Dougherty. A Mechanism for Ion Selectivity in Potassium Channels: Computational Studies of Cation-π Interactions. *Science*, 261:1708, 1993.

[16] J.L. Sussman, M. Harel, F. Frolow, C. Oefner, A. Goldman, L. Toker, and I. Silman. Atomic Structure of Acetylcholinesterase from *Torpedo californica*: A Prototypic Acetylcholine-Binding Protein. *Science*, 253:872, 1991.

[17] L. Pauling. *The Chemical Bond.* Cornell University Press, Ithaca, NY, 1967.

[18] J.H. Seinfeld. Urban Air Pollution: State of the Science. *Science*, 243:745, 1989.

[19] A. Engdahl and B. Nelander. A Matrix Isolation Study of the Benzene-Water Interaction. *J. Phys. Chem.*, 89:2860, 1985.

[20] A. Engdahl and B. Nelander. A Matrix Isolation Study of the Interaction between Water and the Aromatic π-Electron System. *J. Phys. Chem.*, 91:2253, 1987.

[21] W.G. Read, E.J. Campbell, and G. Henderson. The Rotational Spectrum and Molecular Structure of the Benzene-Hydrogen Chloride Complex. *J. Chem. Phys.*, 78:3501, 1983.

[22] W.G. Read, E.J. Campbell, G. Henderson, and W.H. Flygare. Identification and Structure of Benzene-Hydrogen Chloride Complex from Microwave Spectroscopy. *J. Am. Chem. Soc.*, 103:7670, 1981.

[23] F.A. Baiocchi, J.H. Williams, and W. Klemperer. Molecular Beam Studies of C_6F_6, $C_6F_3H_3$, and C_6H_6 Complexes of HF. The Rotational Spectrum of C_6H_6-HF. *J. Phys. Chem.*, 87:2079, 1983.

[24] J. Wanna, J.A. Menapace, and E.R. Bernstein. Hydrogen Bonded and Non-Hydrogen Bonded Van Der Waals Clusters: Comparison Between Clusters of Pyrazine, Pyrimidine, and Benzene with Various Solvents. *J. Chem. Phys.*, 85:1795, 1986.

[25] G.T. Fraser, F.J. Lovas, R.D. Suenram, Jr. D.D. Nelson, and W. Klemperer. Rotational Spectrum and Structure of CF_3H-NH_3. *J. Chem. Phys.*, 84:5983, 1986.

[26] H.S. Gutowsky, T. Emilsson, and E. Arunan. Low-J Rotational Spectra, Internal-Rotation, and Structures of Several Benzene-Water Dimers. *J. Chem. Phys.*, 99:4883, 1993.

[27] A.J. Gotch and T.S. Zwier. Multiphoton Ionization Studies of Clusters of Immiscible Liquids: 1. C_6H_6-$(H_2O)_n$, n=1,2. *J. Chem. Phys.*, 95:3388, 1992.

[28] R.H. Schwendenman. *Critical Evaluation of Chemical and Physical Structural Information.* National Academy of Sciences, Washington, D.C., 1974.

[29] S. Suzuki, R.E. Bumgarner, P.A. Stockman, P.G. Green, and G.A. Blake. Tunable Far-Infrared Laser Spectroscopy of Deuterated Isotopomers of Ar-H_2O. *J. Chem. Phys.*, 94:824, 1991.

[30] D. Yaron, K.I. Peterson, D. Zolandz, W. Klemperer, F.J. Lovas, and R.D. Suenram. Water Hydrogen-Bonding–The Structure of the Water Carbon-Monoxide Complex. *J. Chem. Phys.*, 92:7095, 1990.

[31] M.J. Frisch, G.W. Trucks, M. Head-Gordon, P.M.W. Gill, M.W. Wong, J.B. Foresman, B.G. Johnson, H.B. Schlegel, M.A. Robb, E.S. Replogle, R. Gomperts, J.L. Andres, K. Raghavachari, J.S. Binkley, C. Gonzalez, R.L. Martin, D.J. Fox, D.J. Defrees, J. Baker, J.J.P. Stewart, and J.A. Pople. *Gaussian 92, Revision A.* Gaussian, Inc., Pittsburgh, PA, 1992.

[32] J.B. Anderson. A Random-Walk Simulation of the Schrödinger Equation: H_3^+. *J. Chem. Phys.*, 63:1499, 1975.

[33] J.B. Anderson. Quantum Chemistry by Random Walk. H ^2P, H_3^+ $D_{3h}^1A_1$, H_2 $^3\Sigma_u^+$, H_4 $^1\Sigma_g^+$, Be ^1S. *J. Chem. Phys.*, 65:4121, 1976.

[34] M.A. Suhm and R.O. Watts. Quantum Monte Carlo Studies of Vibrational States in Molecules and Clusters. *Physics Reports*, 204:293, 1991.

[35] V. Buch. Treatment of Rigid Bodies by Diffusion Monte Carlo: Application to the Para-H_2...H_2O and Ortho-H_2...H_2O Clusters. *J. Chem. Phys.*, 97:726, 1992.

[36] P. Sandler, J. oh Jung, M.M. Szczesniak, and V. Buch. The Complex of N_2 with H_2O, D_2O, and HDO: A Combined *Ab Initio* and Diffusion Monte Carlo Study. *J. Chem. Phys.*, 101:1378, 1994.

[37] C.E. Dykstra. Electrostatic Interaction Potentials in Molecular-Force Fields. *Chem. Rev.*, 93:2339, 1993.

[38] W. Gordy and R.L. Cook. *Microwave Molecular Spectra.* John Wiley & Sons, New York, New York, 1984.

[39] R.N. Pribble, A.W. Garrett, K. Haber, and T.S. Zwier. Resonant Ion-Dip Infrared Spectroscopy of Benzene-H_2O and Benzene-HOD. *J. Chem. Phys.*, submitted.

Chapter 5 Pseudorotation in $(D_2O)_3$

5.1 Introduction

Water is ubiquitous in nature, is present in all organisms, and takes part in many natural reactions. The interactions of water with reactant molecules are of immense interest, and the first two experiments described in this thesis pertain to water interacting with other entities. The interactions between water molecules themselves are also of great fundamental importance. For example, the significant ecological effect that the structural difference between liquid and solid water causes in the spring thawing and natural convection of lakes is described in many introductory text books. Introductory chemistry texts describe how intermolecular bond strengths in water contribute to the high enthalpy of fusion and evaporation, and the high heat capacity of water. Mankind has long observed the macroscopic manifestations of the intermolecular forces in water, but a microscopic understanding has eluded us. One of the earliest observation of water-water interactions on the molecular level was made by van Thiel and Pimentel in 1957 through an N_2 matrix isolation of water molecules [1]. Microwave structural determinations for $(H_2O)_2$ and $(D_2O)_2$ [2, 3, 4, 5], FIR probes of intermolecular modes [6, 7, 8, 9] and a near-IR probe of dimer bonds [10] followed as further experimental attempts to understand the water pair-pair interaction. Theoretical investigations have been pursued with similar enthusiasm using Monte Carlo and molecular dynamics simulations, and *ab initio* calculations [11, 12, 13, 14].

Further work to connect these findings with macroscopic observables ensued [15, 16]. Difficulties in extending dimer interaction potentials to macroscopic properties became evident early on [11, 12]. While the body of knowledge for water dimer is extensive, an understanding of the difference between the two-body interaction and many body forces has remained elusive. Hence, many calculations have been performed on water trimers to investigate the difference between three-body and two-

body interactions in water [17, 18, 19, 20, 21]. *Ab initio* calculations have revealed that there is about a 10% "three body" contribution to the trimer binding energy, that the O-O distance in a trimer is shorter than in a dimer, and that the intermolecular vibrational frequencies are on the average higher in a trimer. Yet, it is uncertain whether the widespread work on three-body interactions can be extended to larger size clusters and to bulk properties. Once the differences between dimers and trimers are qualitatively understood, the direction of such studies must be re-evaluated. It is clear, however, that a solid understanding of the water dimer and trimer entail full characterizations of their IPS's.

We sought an opportunity to contribute to this effort, namely to conduct spectroscopy on the water-trimer system which will further our understanding on non-pairwise interaction energetics. Saykally and co-workers had been actively searching for VRT transitions for water trimers and had recorded two $(D_2O)_3$ bands and one $(H_2O)_3$ band [1, 3]. (Recently, R.P. McLaughlin *et al.* reported a higher frequency H_2O trimer band at 523 cm^{-1} [24].) The $(H_2O)_3$ band was lower in energy than the $(D_2O)_3$ band. D_2O, being heavier than H_2O, often forms clusters possessing transitions at approximately half the energy as those in the H_2O isotopomer. The existence of an $(H_2O)_3$ band at 87 cm^{-1} suggested the existence of a $(D_2O)_3$ band roughly between 40 and 50 cm^{-1}. Theoretical work by Schütz *et al.* supported this estimation [25]. Fortuitously, our laser system was operating at 1299996.9 MHz (43.3 cm^{-1}) where we had been searching for benzene-water cluster transitions. We scanned this region and did indeed find a $(D_2O)_3$ band.

Before describing our findings, a brief explanation of the information on the water trimer "structure" available at that time is given below. As predicted by theory [20, 21, 26, 18, 17, 15, 27, 28, 25] and confirmed by experiments [1, 3], the IPS minimum is found to be cyclic, with each monomer acting as *both* a hydrogen bond donor and acceptor. As with many other weakly bounded clusters studied to date, large amplitude motions were predicted and observed. The full permutation-inversion (PI) group is G_{96} as reported by Pugliano and Saykally [1], yet the data of Liu *et al.*[3] show that there are only two "feasible" pathways which manifest themselves at current

experimental resolution, constraining the PI group to G_{48}. These two permutation pathways are that of a six-fold pseudorotation (flipping of the unbound hydrogens) which is predicted to have a very low barrier and which produces the exact oblate symmetric top nature of the ground state VRT spectra despite the asymmetric top character of any fixed combination of three water monomers; and a donor exchange motion, which has a higher barrier and is responsible for a quartet splitting pattern spanning $\sim$ 5 MHz [29, 1, 3].

In the minimum energy structure, one O-H bond from each monomer contributes to one side of an approximately equilateral triangle (see Figure 5.1). Of the remaining unbound hydrogens, two are on one side of the face of the triangle (side A), while one is on the other side (B) of the plane. Flipping describes the motion of one unbounded hydrogen from side A to side B (Figure 5.1). A series of six flipping motion returns the trimer to the original structure, hence the term pseudorotation [25]. As noted by Pugliano and Saykally, individual flipping motion changes the chirality of the trimer [1]. Chirality is prevalent in biological molecules, and the fact that water clusters also possess chirality has piqued interest in their energetics, i.e., the IPS's of these systems [30].

The donor exchange motion is the exchange of an unbonded hydrogen with the bonded hydrogen on a given water monomer, along with a flipping motion of water to which the original hydrogen was bound. The barrier for this motion is thought to be similar to a corresponding tunneling pathway in the water dimer, about 600-700 cm^{-1} [29], and in the D_2O trimer it is the *difference* in the tunneling patterns of the lower and upper state which are recorded experimentally [3].

Further analysis of the large amplitude motions of the water trimer species can be found elsewhere [25, 29, 3]; here we simply note that they do not allow a quantitative estimate of the geometry to be deduced from "standard" analyses of the VRT spectra. A detailed examination and derivation of the G_{48} group is presented in Appendix G. The result is that pseudorotation gives rise to the energy level diagram outlined in Figure 5.2. The selection rules are $a \leftrightarrow e_2$, $b \leftrightarrow e_1$ and $e_2 \leftrightarrow e_1$ for a ΔK=1, a-type transition, and $a \leftrightarrow b$ for a ΔK=0, c-type transition.

Table 5.1: Correlation among C_6, S_6, C_{3h}, and G_{48} groups. Refer to this table when comparing Figures 5.2 and 5.5.

C_6	S_6	C_{3h}	G_{48}
a	a_g	a'	$A_1^+, B_1^+, F_A^+, F_B^+$
b	a_u	a''	$A_1^-, B_1^-, F_A^-, F_B^-$
e_1	e_g	e'	$A_{2,3}^+, B_{2,3}^+, F_A^+, F_B^+$
e_2	e_u	e''	$A_{2,3}^-, B_{2,3}^-, F_A^-, F_B^-$

Table 5.1 lists the correlation among the different symmetry notations used by Schütz *et al.* [25], Klopper and Schütz [31], and in Appendix G of this work.

5.2 Experiment and data

The CH_3OD FIR laser line at 1299996.9 MHz pumped by the 9P6 CO_2 laser transition, and the CH_3OH line at 1193729.3 MHz pumped by 10R38 were used to record the $(D_2O)_3$ spectrum between 39.1 and 44.2 cm^{-1}. The gas mixture used for $(D_2O)_3$ was 2 SLM of Ar and 7 SLM of Ar bubbled through D_2O at 10 psig. Following Pugliano and Saykally [1], the identity of the suspected $(D_2O)_3$ lines was verified by monitoring the intensity change as the mole fraction of the D_2O was varied by successive dilution with H_2O. The mole fraction of D_2O and the intensity then have the following relation:

ln[fractional intensity] $\cong$ N ln [mole fraction of D_2O],

where N would be 4 for a cluster containing two D_2O subunits and 6 for a cluster containing three D_2O subunits. We found N = 5.52, σ=0.37 from the above equation, similar to that found by Pugliano and Saykally [1]. Furthermore, the tunneling pattern described in the next section closely resembled that observed by Pugliano and Saykally, and the lower state rotational constants derived from the spectra reproduced those obtained by Liu *et al.*[3]. Thus, the spectrum was unambiguously assigned to $(D_2O)_3$.

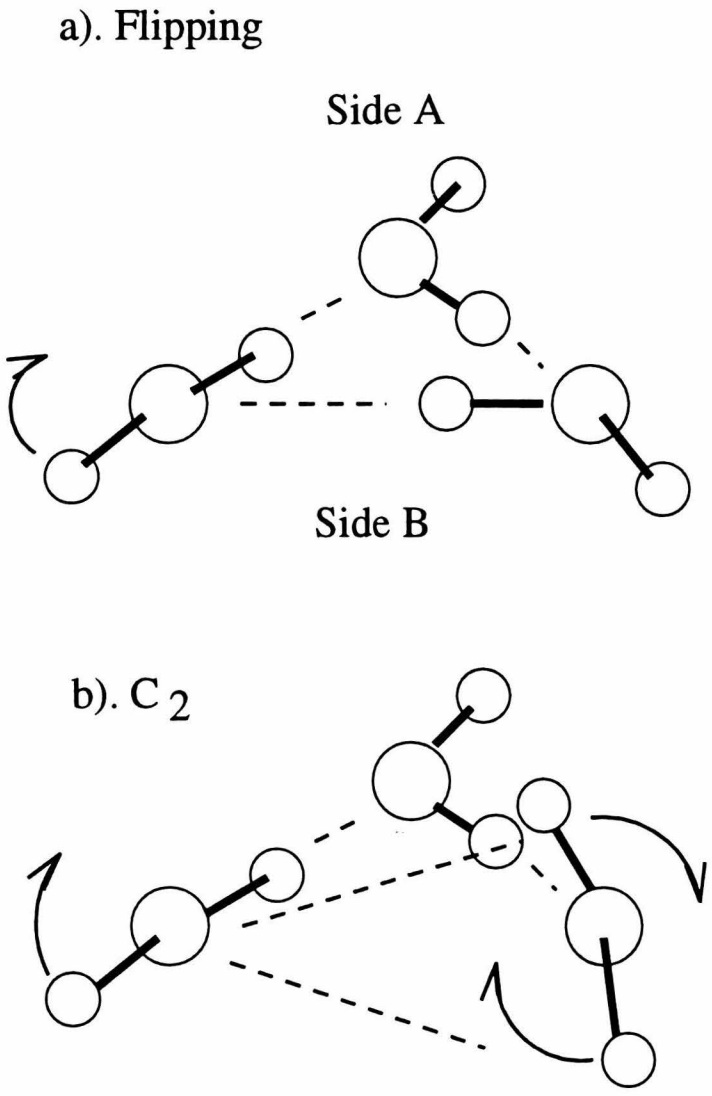

Figure 5.1: Feasible motions in $(D_2O)_3$. a). The facile flipping motion. b). The high barrier C_2 or "donor exchange" motion, giving rise to tunneling motion and the quartet splitting pattern.

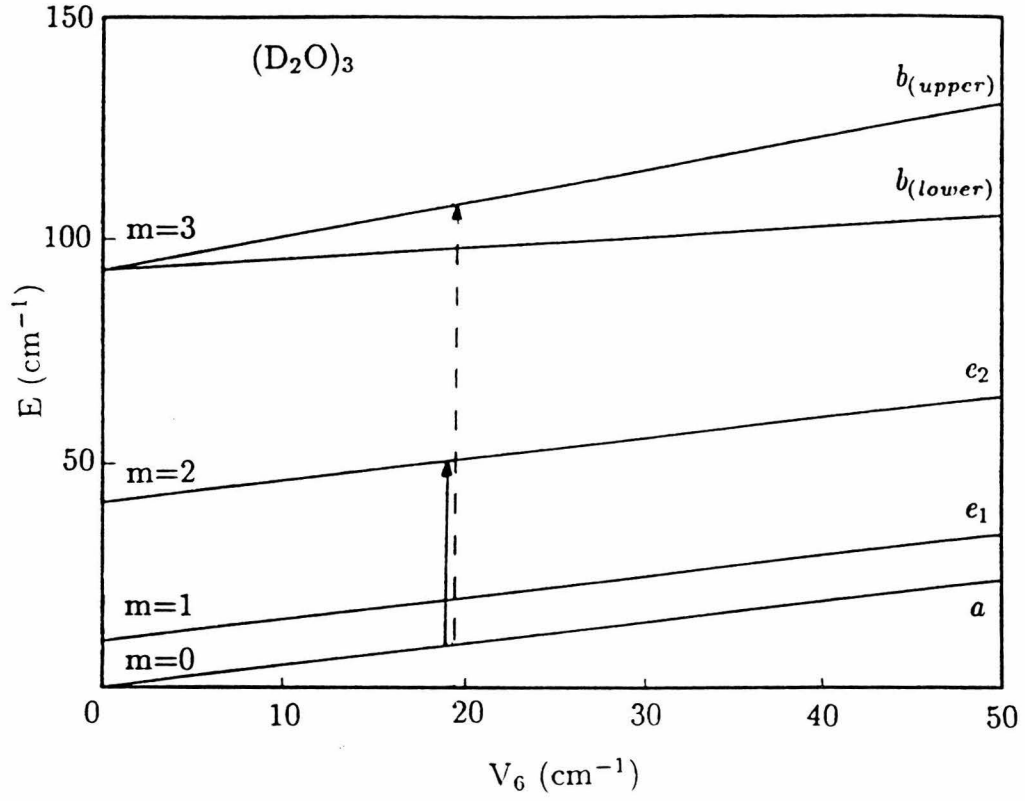

Figure 5.2: $(D_2O)_3$ energy level diagram based on Schütz *et al* [25]. Cf. Table 5.1 for symmetry notations.

5.3 Results

We initially observed a set of transitions consisting of quartets spanning $\sim$ 4.5 MHz, that is, the spacing between individual lines within the quartet was $\sim$ 1.5 MHz, similar to those reported by Pugliano and Saykally [1] and Liu *et al.*[3]. These quartets exhibited symmetric rotor-type patterns with (J+1) lines in clusters separated by $\sim$ 11.5 GHz. The value of the B rotational constant for the R branch lines was similar to that calculated for the 98 cm^{-1} a-type band reported by Liu *et al.* By constraining the ground state constants to those found by Liu *et al.*, a fit to the R branch lines enabled the prediction and detection of P and Q branch lines within 1 MHz of the initial prediction. The strongest line from each quartet is tabulated in Tables 5.3 and 5.4. An overall view of the band and an expanded presentation of the $4_2 \leftarrow 3_2$ quartet is presented in Figure 5.3.

Low S/N in the 39.1 cm^{-1} to 41.1 cm^{-1} region made complete scanning impractical. Based on the accuracy of the predictions, the P branch lines near 41.1 cm^{-1} were assigned and fitted to a c-type spectrum. Thus, concurrent fitting of our c-type lines and the Saykally group a-type lines [1] was necessary to constrain the upper and lower state C rotational constants separately and obtain the constants given in Table 5.2. The Hamiltonian used for the fit was as follows:

$$H = \nu + BJ(J+1) + (C-B)K^2 - D_J J^2(J+1)^2 - D_{JK} J(J+1)K^2,$$

with B, C, D_J, and D_{JK} being specific to each vibrational state. The accuracy of the fit strongly suggests that both 41.1 cm^{-1} and 98.0 cm^{-1} bands originate from the same lower state, while the intensity behavior of these bands with changing expansion conditions is consistent with them arising from the $(D_2O)_3$ ground state. The ground state rotational constants obtained closely match those predicted by *ab initio* calculations [20, 25]; this concurrence supports the proposed cyclic geometry of the water trimer.

As we have seen in the previous chapters, detailed information concerning the IPS cannot be determined simply based on a few VRT transitions. Hence, our present

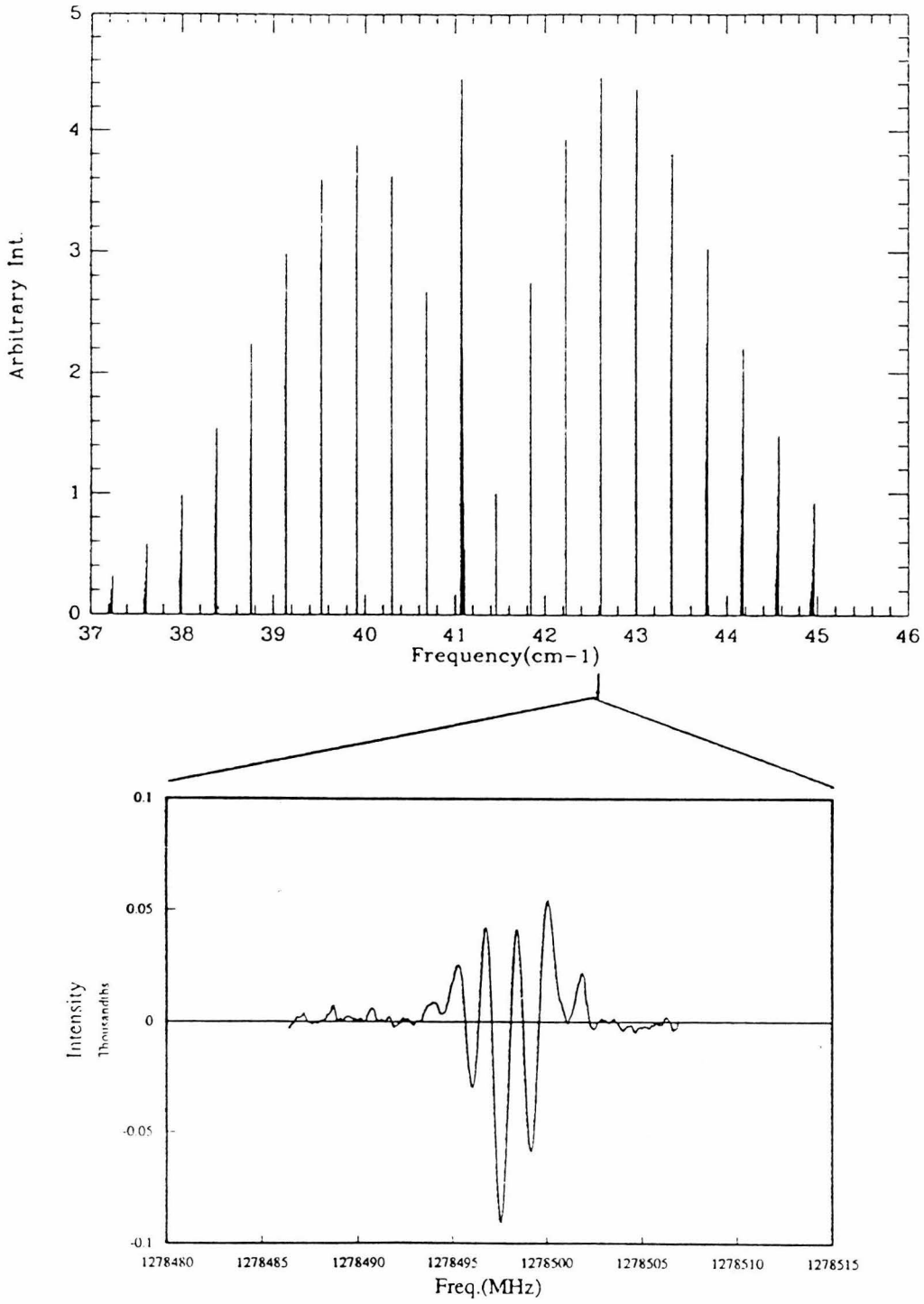

Figure 5.3: Simulated $(D_2O)_3$ spectrum near 41 cm^{-1} with an expanded view of the recorded $4_2 \leftarrow 3_2$ quartet.

Table 5.2: $(D_2O)_3$ spectroscopic constants.

Constant	Ground State	Upper State
B(MHz)	5796.34(8)	5792.91(7)
C(MHz)	3088.5(1)	3100.1(1)
Δ_J(kHz)	27.8(16)	26.0(11)
Δ_{JK}(kHz)	-30.7(19)	-35.2(16)
ν (MHz)		1232140.2(7)

focus is to investigate the spectroscopic manifestations of the large amplitude trimer dynamics, which will ultimately provide a quantitative probe of the intermolecular forces involved. As mentioned above, several theoretical calculations have been used to predict the IPS, and while our data verifies to some extent the accuracy of these predictions, they also reveal inconsistencies that must be adjusted to yield a quantitative surface.

The current experimental information relating to the D_2O trimer IPS is as follows: an 89.6 cm^{-1} c-type band, a 98.0 cm^{-1} a-type band, and a 41.1 cm^{-1} c-type band. The 41.1 and 98.0 cm^{-1} bands have the same lower state, the 89.6 cm^{-1} band has both lower and upper states that differ from the other two bands. Consistent with this interpretation of the ground state nature of the 98.0 and 41.1 cm^{-1} bands, Liu *et al.* [3] found the 89.6 cm^{-1} band to be a hot band.

Here we compare the one dimensional six-fold pseudorotation energy level pattern predicted by Schütz *et al.*[25] to the available experimental findings. In this work, *ab initio* theory was used to examine the permutation/tunneling pathways of the water trimer, with the pseudorotation energy levels obtained in the low barrier limit by assuming that only the planar transition state D or H atom motion contributes to the kinetic energy, resulting in internal rotation constants of $F_{(D_2O)} = 11.75$ cm^{-1} and $F_{(H_2O)} = 23.49$ cm^{-1} [25]. Accordingly, these estimates are likely to form *upper* bounds to the true F values, and we indeed find that further modeling of the one-dimensional V_6 and F constants is necessary. For small barriers, the pseudorotation levels appear near Fm^2 (m=the pseudorotational quantum number, see Figure 5.2), and a physically meaningful interpretation of the experimental data (i.e. positive

values of both V_6 and F) is possible only when the 41.1 cm^{-1} and 98.0 cm^{-1} bands are assigned to the $e_2 \leftarrow a$ and $b_{(upper)} \leftarrow a$ transitions. Numerically, we find F_{D_2O} = 10.3(1) cm^{-1} and V_6 = 19.1(1) cm^{-1} can fit the two transitions to within 0.5 cm^{-1}; this model also predicts the 87.0 cm^{-1} $(H_2O)_3$ band to be the $e_2 \leftarrow a$ transition with F values close to that noted above.

These assignments are based solely on energetics, however, are *not* consistent with the $C_{3h}(M)$ dynamical symmetry of the pseudorotation motion or with the overall G_{48} selection rules. In the pseudorotational manifold, the dominant selection rules are those for which $\Delta(m+K) = 3$, meaning that the lowest energy transition having a c-type selection rule is the $b_{(lower)} \leftarrow a$ band. The lowest allowed $\Delta K = \pm 1$ band is the $e_2 \leftarrow a$ transition. In the free-rotor limit (V_6=0), the observed frequencies require $F_{(D_2O)} = h/8\pi^2 c I_{(D_2O)}$ = 4.6 cm^{-1}, a value much smaller than that calculated by Schütz *et al.* and one that would require substantial motion of the water oxygen. Furthermore, the $b_{(lower)} \leftarrow a$, or $m = 3_{(lower)} \leftarrow 0$, transition acquires appreciable intensity only if m is not a good quantum number. Both of these observations suggest that V_6 must be substantially larger than F, or that the model constructed by Schütz *et al.* is insufficient. Assuming the model by Schütz *et al.*, and with 11.75 cm^{-1} as a likely upper bound for $F_{(D_2O)}$, and $0 \leq V_6 \leq 375$ cm^{-1}(upper bound implied by assigning 41.1 cm^{-1} to $b_{lower} \leftarrow a$), it is found that the $e_2 \leftarrow a$ transition lies between 18.3 cm^{-1} and 27.6 cm^{-1}, while the $b_{(upper)} \leftarrow a$ transition is much more sensitive to barrier height, lying between 41.1 cm^{-1} and 226.1 cm^{-1}.

The 98.0 cm^{-1} a-type transition, which has the same ground state rotational constants as the 41.1 cm^{-1} transition, does not fit into the pseudorotational manifold with the above assignment, nor does the 89.6 cm^{-1} hot band. A possible explanation is that these transitions terminate in a different vibrational state. As suggested by Liu *et al.* [3], the 89.6 cm^{-1} band may originate from the e_1, or $m = 1$, level and involve as its upper state a vibrational mode outside of the pseudorotational manifold built upon the true trimer ground state. In the models of Schütz *et al.* [25], this vibration is calculated to be another low frequency torsional mode which is approximately orthogonal to the pseudorotation coordinate, but which is strongly allowed and of

c-type symmetry. The double harmonic approximation gives a frequency of ~104 cm^{-1} for the hot band transition, which as expected is to the blue of the observed band position.

By analogy, if the 87.0 cm^{-1} $(H_2O)_3$ c-type band is also assigned to the $b_{(lower)} \leftarrow a$ transition, then with the $V_6 \leq 375$ cm^{-1} upper bound, a range of 38.7 - 55.1 cm^{-1} is predicted for the $e_{(lower)} \leftarrow a$ band. The $F_{(H_2O)}$ values obtained for these ranges give $F_{(H_2O)}/F_{(D_2O)}$ ratios near the predicted ratio of two only in the low barrier limit, but their absolute magnitudes are much smaller than expected. At higher barriers, the F values are larger, but the ratio is near 1.5, again suggesting that the pseudorotation motion does not simply involve only the free proton/dueteron. Confirmation of the assignment of the $(D_2O)_3$ c-type 41.1 cm^{-1} and the $(H_2O)_3$ c-type 87 cm^{-1} bands to the $b_{(lower)} \leftarrow a$ transition must be made before continuing this line of analysis.

The interpretation of the present data with Schütz's one-dimensional pseudorotation model, therefore, remains unconfirmed. Klopper and Schütz recently improved their model to include a two-dimensional analysis [31]. In the one-dimensional analysis of Schütz *et al.*, the "flipping" motion was treated as a pseudorotation, that is, the coordinate ϕ used in the model potential function,

$$V(\phi) = V_6(1 - cos6\phi)/2,$$

is the "rotation" of the cyclic trimer about a six-fold symmetry axis. (See Figure 5.4.) The "flipping" motion actually consists of motions along three torsional angles of the free hydrogens (ω_1, ω_2 and ω_3 in Figure 5.4). Thus, in the one-dimensional model, three variables are reduced to one variable.

In the two-dimensional analysis by Klopper and Schütz [31], the three torsional angles are used to form symmetry adapted linear combination coordinates which are then transformed into spherical coordinates to utilize spherical harmonic basis functions in the analysis. This effectively transforms the $V(\omega_1, \omega_2, \omega_3)$ potential function to $V(\vartheta, \varphi, R)$ where the R coordinate is a fixed variable. Thus, for a given R, the potential becomes $V(\vartheta, \varphi)$, i.e., two-dimensional. The advantage of this model is that

the wavefunctions obtained have the full S_6 symmetry appropriate for the pseudorotation motion. The energy levels obtained using this model are shown in Figure 5.5. Using $F_{red(D_2O)_3} = 12$ cm^{-1}, as in the original work by Schütz *et al.*, the energy levels predicted are 40.9 cm^{-1} for $a_u^{lower} \leftarrow a_g$ (which correlates to $b \leftarrow a$), 91.4 cm^{-1} for $e_g^{upper} \leftarrow e_u$, and 97.8 cm^{-1} for $e_g^{upper} \leftarrow a_g$ for $(D_2O)_3$. These correspond closely in both transition energies and selection rules with the observed transitions at 41.1, 89.6 and 98.1 cm^{-1}. The $(H_2O)_3$ band observed at 87.1 cm^{-1} also corresponds well with the $a_u^{lower} \leftarrow a_g$ band calculated to be at 88.6 cm^{-1}. This nice agreement between predictions and observations illustrates the importance of a fully coupled dynamics treatment in the simulation of VRT spectra.

5.4 Conclusion

We observed high resolution VRT spectra for the water-trimer species. As the number of molecules in the weakly bound cluster increases, it becomes increasingly difficult to extract valuable information from the complex spectra. Through collaborative efforts with theorists and other experimentalists, the assignment of the water trimer spectra is improving. Our understanding is not at the level of a complete characterization of the IPS. However, we have so far distilled the following information. 1) The flipping motion is very facile. 2). Donor exchange motion results in tunneling splittings indicating that the barrier lies above the zero point energy. 3). The observed transitions lead to $F_{red(D_2O)_3} = 12$ cm^{-1}, indicating that the motion is essentially a flipping of the hydrogens alone. 4). There are now several observed bands in this pseudorotation manifold that are well predicted by a two-dimensional model [31].

The IPS of water trimer is expected to be complex and shallow with multiple minima. The successful model of the trimer produced by Klopper and Schütz demands that the ground state description include the flipping motions. A frozen "structural" description is not appropriate. An approximation of the flipping motion as a one-dimensional "hindered rotation" consisting of two of the three free hydrogens moving from oneside of the O-O-O plane to the other was also not appropriate. In the two-

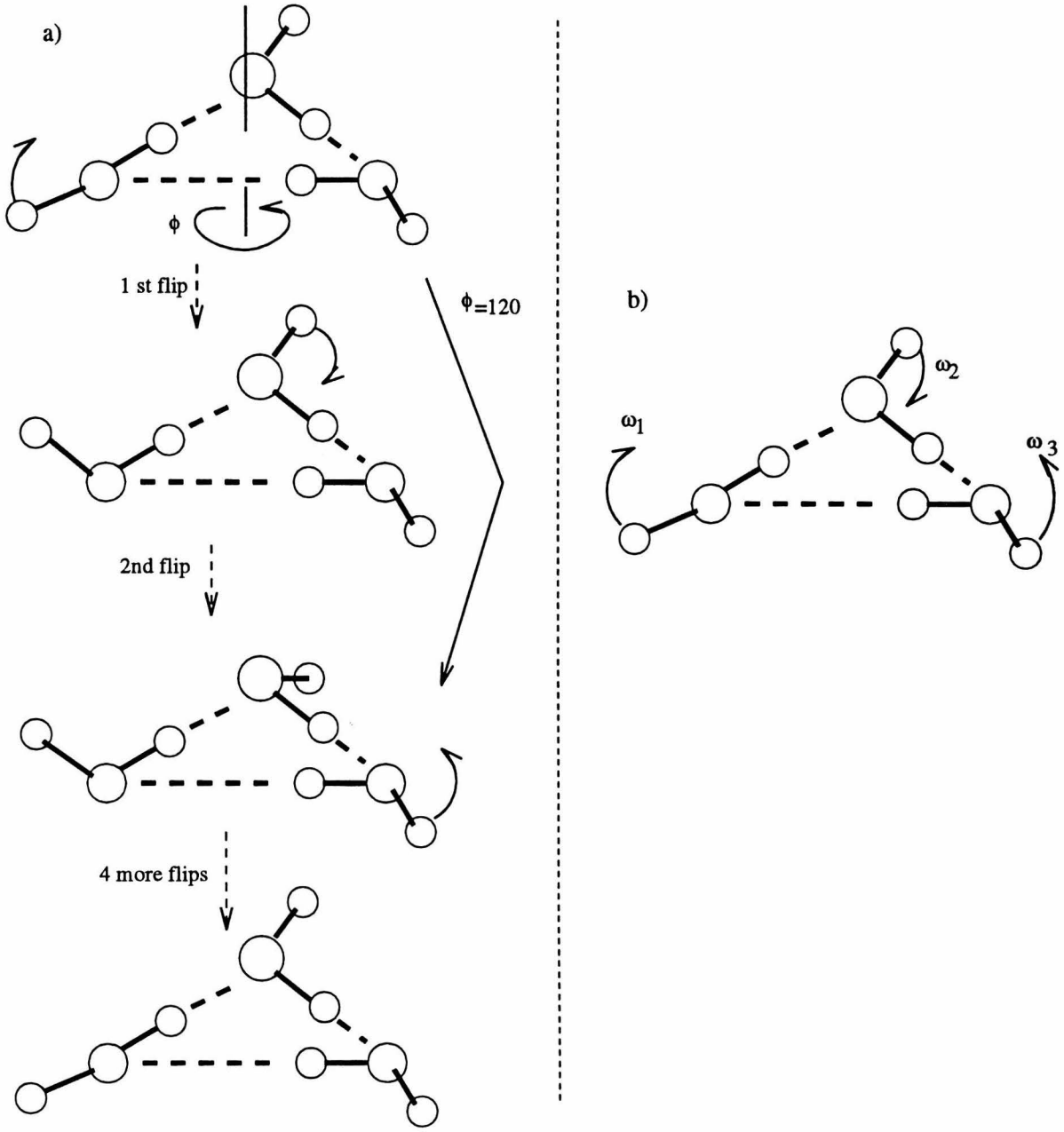

Figure 5.4: Two coordinate systems used in pseudorotation analysis. a). One dimension, ϕ is used to describe the pseudorotation. b). Symmetry adapted linear combination coordinates of ω_1, ω_2 and ω_3 to produce two variable coordinates, ϑ and φ, and one fixed coordinate, R.

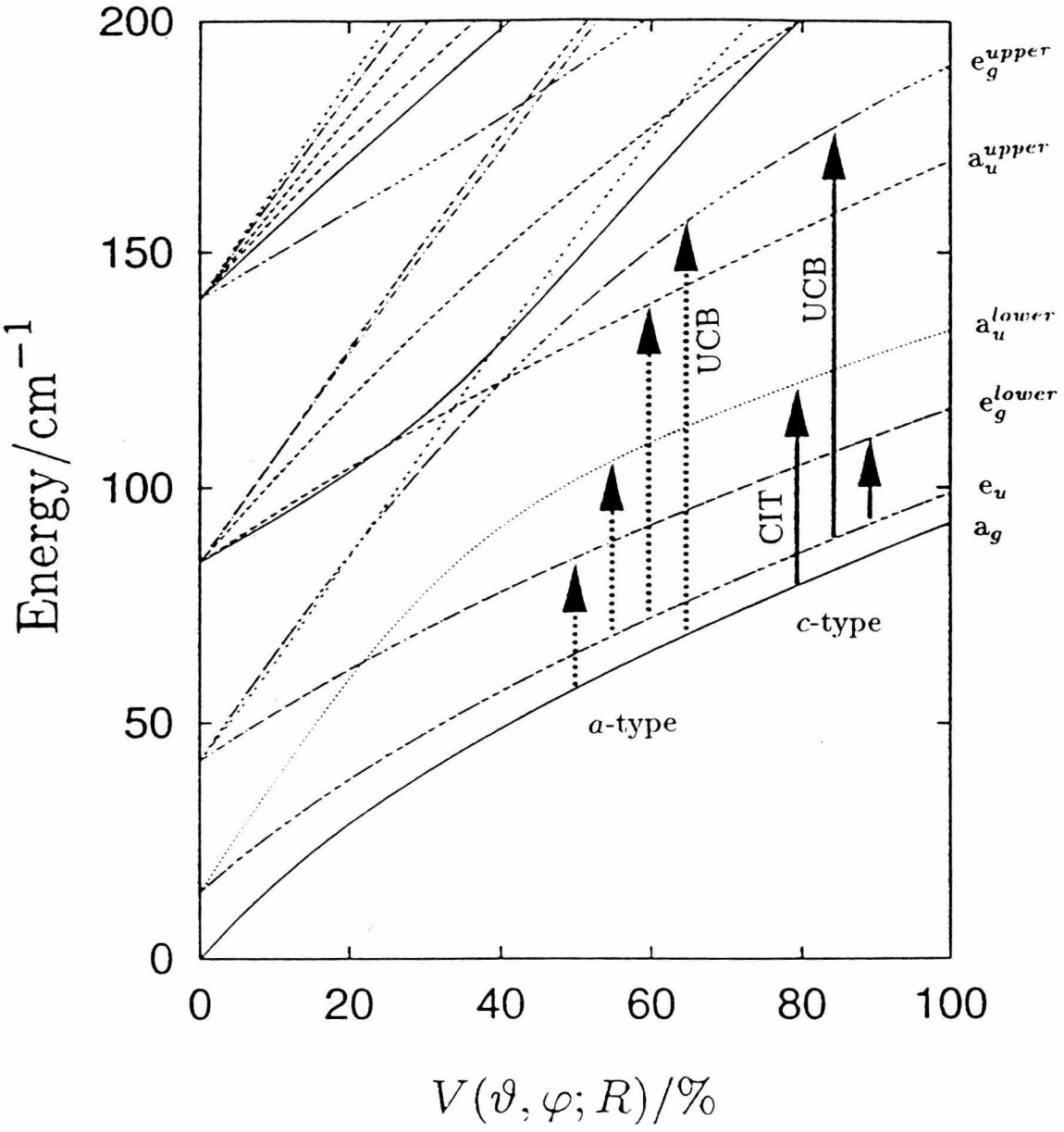

Figure 5.5: Water trimer energy levels calculated by Klopper and Schütz [31]. The x-axis corresponds to the percentage of V assumed as the barrier in the calculations. The predictions when 100% of V was assumed matched the observed transitions. The $(D_2O)_3$ band presented in this thesis is marked "CIT", and those recorded by Pugliano and Saykally [1], and Liu *et al.* [3] are marked "UCB". Cf. Table 5.1 for symmetry notations.

dimensional model, the flipping motion was treated as wavefunctions consisting of linear combinations of three torsional coordinates, and their behavior was determined by an entirely *ab initio* IPS. The lowest energy level occupied by this wavefunction is symmetric, in perfect agreement with the VRT spectra observed.

Table 5.3: Fitted $(D_2O)_3$ line list near 41 cm^{-1}

v″	J″	K''_O	v′	J′	K'_O	Obs. (MHz)	Calc. (MHz)	O-C (MHz)
0	5	4	1	4	4	1174361.8(10)	1174360.5	1.3
0	5	3	1	4	3	1174256.7(10)	1174256.4	0.3
0	5	2	1	4	2	1174182.3(10)	1174182.1	0.1
0	5	1	1	4	1	1174137.3(10)	1174137.5	-0.2
0	5	0	1	4	0	1174122.6(10)	1174122.7	0.0
0	4	0	1	3	0	1185735.1(10)	1185735.6	-0.5
0	4	1	1	3	1	1185750.2(10)	1185750.5	-0.3
0	4	2	1	3	2	1185795.2(10)	1185795.1	0.1
0	4	3	1	3	3	1185869.6(10)	1185869.6	0.0
0	6	1	1	6	1	1232014.9(10)	1232014.3	0.6
0	6	4	1	6	4	1232243.1(10)	1232243.3	-0.3
0	6	6	1	6	6	1232545.5(10)	1232548.7	-3.2
0	5	2	1	5	2	1232100.7(10)	1232099.6	1.1
0	5	4	1	5	4	1232282.1(10)	1232282.2	-0.1
0	5	5	1	5	5	1232418.3(10)	1232419.1	-0.8
0	4	1	1	4	1	1232087.3(10)	1232087.4	-0.1
0	4	3	1	4	3	1232209.9(10)	1232208.7	1.2
0	4	4	1	4	4	1232314.6(10)	1232314.9	-0.3
0	3	2	1	3	2	1232158.8(10)	1232159.8	-1.0
0	3	3	1	3	3	1232234.9(10)	1232235.4	-0.5
0	2	2	1	2	2	1232179.0(10)	1232180.1	-1.0
0	1	1	1	1	1	1232147.3(10)	1232148.4	-1.1
0	0	0	1	1	0	1243725.8(10)	1243725.9	-0.1
0	1	0	1	2	0	1255305.4(10)	1255304.1	1.3
0	1	1	1	2	1	1255320.9(10)	1255319.3	1.6
0	3	0	1	4	0	1278434.9(10)	1278435.8	-0.9
0	3	1	1	4	1	1278450.6(10)	1278451.2	-0.6
0	3	2	1	4	2	1278498.1(10)	1278497.5	0.7
0	3	3	1	4	3	1278576.3(10)	1278574.5	1.7
0	4	0	1	5	0	1289986.9(10)	1289988.2	-1.3
0	4	1	1	5	1	1290002.8(10)	1290003.8	-1.0
0	4	2	1	5	2	1290050.1(10)	1290050.3	-0.2
0	4	3	1	5	3	1290128.7(10)	1290127.9	0.7
0	4	4	1	5	4	1290238.2(10)	1290236.6	1.6
0	6	0	1	7	0	1313062.4(10)	1313064.0	-1.6
0	6	1	1	7	1	1313079.5(10)	1313079.8	-0.2
0	6	2	1	7	2	1313126.5(10)	1313127.0	-0.6
0	6	3	1	7	3	1313206.2(10)	1313205.8	0.3
0	6	4	1	7	4	1313317.4(10)	1313316.2	1.3
0	6	5	1	7	5	1313459.7(10)	1313458.0	1.7
0	6	6	1	7	6	1313632.1(10)	1313631.4	0.7

Table 5.4: $(D_2O)_3$ line list near 41 cm^{-1} continued

v″	J″	K''_O	v′	J′	K'_O	Obs. (MHz)	Calc. (MHz)	O-C (MHz)
0	7	0	1	8	0	1324585.3(10)	1324586.5	-1.2
0	7	1	1	8	1	1324601.2(10)	1324602.4	-1.2
0	7	2	1	8	2	1324650.7(10)	1324650.1	0.6
0	7	3	1	8	3	1324729.6(10)	1324729.6	0.0
0	7	4	1	8	4	1324842.1(10)	1324840.8	1.2
0	7	5	1	8	5	1324985.8(10)	1324983.9	1.9
0	7	6	1	8	6	1325159.4(10)	1325158.7	0.7
0	7	7	1	8	7	1325363.1(10)	1325365.3	-2.2

Bibliography

[1] M. van Thiel, E.D. Becker, and G.C. Pimentel. Infrared Studies of Hydrogen Bonding of Water by the Matrix Isolation Technique. *J. Chem. Phys.*, 27:486, 1957.

[2] J.A. Odutola, T.A. Hu, D. Prinslow, S.E. Odell, and T.R. Dyke. Water Dimer tunneling States with K=0. *J. Chem. Phys.*, 88:5352, 1988.

[3] L.H. Coudert, F.J. Lovas, R.D. Suenram, and J.T. Hougen. New Measurements of Microwave Transitions in the Water Dimer. *J. Chem. Phys.*, 87:6290, 1987.

[4] G.T. Fraser, R.D. Suenram, L.H. Coudert, and R.S. Frye. Electric-Resonance Optothermal Spectrum of $(H_2O)_2$: Microwave Spectrum of the K=1 - 0 Subband for the $E_2^{\pm}$ State. *J. Mol. Spect.*, 137:244, 1989.

[5] R.D. Suenram, F.J. Lovas, G.T. Fraser, J.Z. Gilles, C.W. Gilles, and M. Onda. Microwave-Spectrum, Structure, and Electric-Dipole Moment of Ar-CH_3OH. *J. Mol. Spect.*, 137:127, 1989.

[6] Kerry Lynn Busarow. *Tunable Far Infrared Laser Spectroscopy of Van Der Waals Molecules in a Planar Supersonic Jet Expansion.* Ph.D. thesis, University of California at Berkeley, Berkeley, CA, December 1990.

[7] E. Zwart, J.J. Termeulen, and W.L. Meerts. The Submillimeter Rotation Tunneling Spectrum of $(D_2O)_2$. *Chem. Phys. Lett.*, 173:115, 1990.

[8] E. Zwart and W.L. Meerts. The Submillimeter Rotation-Tunneling Spectrum of Ar-D_2O and Ar-NH_3. *Chem. Phys.*, 151:407, 1991.

[9] N. Pugliano, J.D. Cruzan, J.G. Loeser, and R.J. Saykally. Vibrational and K_a' Dependencies of the Multidimensional Tunneling Dynamics in the 82.6 cm^{-1} Intermolecular Vibration of the Water Dimer-d_4. *J. Chem. Phys.*, 98:6600, 1993.

[10] Z.S. Huang and R.E. Miller. Sub-Dopper Resolution Infrared-Spectroscopy of Water Dimer. *J. Chem. Phys.*, 88:8008, 1988.

[11] J.A. Barker and R.O. Watts. Structure of Water; a Monte Carlo Simulation. *Chem. Phys. Lett.*, 3:144, 1969.

[12] A. Rahman and F.H. Stillinger. Molecular Dynamics Study of Liquid Water. *J. Chem. Phys.*, 71:2703, 1979.

[13] D. Feller. Application of Sytematic Sequences of Wave-Functions to the Water Dimer. *J. Chem. Phys.*, 96:6104, 1992.

[14] O. Hess, M. Caffarel, C. Huiszoon, and P. Claverie. Second-Order Exchange Effects in Intermolecular Interactions. The Water Dimer. *J. Chem. Phys.*, 92:6049, 1990.

[15] S. Kuwajima and Arieh Warshel. Incorporating Electric Polarizabilities in Water-Water Interaction Potentials. *J. Phys. Chem.*, 94:460, 1990.

[16] W.L. Jorgensen. Transferable Intermolecular Potential Functions of Water, Alcohols, and Ethers. Application to Liquid Water. *J. Am. Chem. Soc.*, 103:335, 1981.

[17] G. Chalasinski, M.M. Szczesniak, P. Cieplak, and S. Scheiner. *Ab Initio* Study of Intermolecular Potential of H_2O Trimer. *J. Chem. Phys.*, 94:2873, 1991.

[18] E. Honegger and S. Leutwyler. Intramolecular Vibrations of Small Water Clusters. *J. Chem. Phys.*, 88:2582, 1988.

[19] K. Laasonen, M. Parrinello, R. Car, C. Lee, and D. Vanderbilt. Structures of Small Water Clusters Using Gradient-Corrected Density Functional Theory. *Chem. Phys. Lett.*, 207:208, 1993.

[20] S.S. Xantheas and Jr. T.H. Dunning. The Structure of the Water Trimer from *Ab Initio* Calculations. *J. Chem. Phys.*, 98:8037, 1993.

[21] S.S. Xantheas and Jr. T.H. Dunning. *Ab Initio* Studies of Cyclic Water Clusters $(H_2O)_n$, n=1-6.I. Optimal Structures and Vibrational Spectra. *J. Chem. Phys.*, 99:8774, 1993.

[22] N. Pugliano and R.J. Saykally. Measurement of Quantum Tunneling Between Chiral Isomers of the Cyclic Water Trimer. *Science*, 257:1937, 1992.

[23] K. Liu, M.J. Elrod, J.G. Loeser, J.D. Cruzan, N. Pugliano, M.G. Brown, J. Rzepiela, and R.J. Saykally. Far-IR Vibration-Rotation Tunneling Spectroscopy of the Water Trimer. *Faraday Dis.*, 97:35, 1994.

[24] R.P. McLaughlin, R.S. Fellers, M.R. Vivant, and R.J. Saykally. VRT Spectroscopy of Jet Cooled Water Clusters with Far-Infrared Diode Lasers. *Ohio State University Molecular Symposium Abstract*, TL:06, 1995.

[25] M. Schütz, T. Bürgi, S. Leutwyler, and H.B. Bürgi. Fluxionality and Low-Lying Transition Structures of the Water Trimer. *J. Chem. Phys.*, 99:5228, 1993.

[26] S.S. Xantheas. *Ab Initio* Studies of Cyclic Water Clusters $(H_2O)(N)$, N=1-6. II. Analysis of Many-Body Interactions. *J. Chem. Phys.*, 100:7523, 1994.

[27] E. Clementi, F. Cavallone, and R. Scordamaglia. Analytical Potential from "ab Initio" Computations for the Interaction between Biomolecules. 1. Water with Amino Acids. *J. Am. Chem. Soc.*, 99:5531, 1977.

[28] J. Tiradorives, D.S. Maxwell, and W.L. Jorgensen. Molecular-Dynamics and Monte-Carlo Simulations Favor the α-Helical form for Alanine-Based Peptides in Water. *J. Am. Chem. Soc.*, 115:11590, 1993.

[29] D.J. Wales. Theoretical-Study of Water Trimer. *J. Am. Chem. Soc.*, 115:11180, 1993.

[30] N.A. Bulenkov. On the Possible Role of Hydration as a Leading Integrational Factor in the Organization of Biosynthesis at Different Levels of Hierarchy. *Biofizika*, 36:181, 1991.

[31] W. Klopper and M Schütz. 2-Dimensional Model Treatment of Torsional Motions in the Water Trimer. *Chem. Phys. Lett.*, 237:536, 1995.

Chapter 6 Conclusions and future directions

It is the goal of this thesis to contribute to the acquisition of complete IPS's. In this work, three molecular clusters whose IPS's are important models for our understanding of natural phenomena, in particular biological systems, were studied using both spectroscopic and theoretical tools.

Our FIR spectra recorded for the Ar-D_2O and Ar-HDO dimers contributed to the most recent complete potential for the Ar-water interaction (AW2) [1] and served as an exacting test for the previous IPS (AW1) constructed by Cohen and Saykally [2]. These benchmark potentials for Ar-H_2O serve as a quantitative model for further studies of water-containing clusters.

The ground state "structure" of the benzene-water dimer was obtained by microwave spectroscopy on the C_6H_6-H_2O, C_6H_6-D_2O and C_6H_6-HDO dimers. The measurements clearly showed that the water lies above the plane of the benzene and that there are large amplitude motion within the dimer. The estimated bond strength of (benzene-water) at 1.9 kcal/mol is nearly 5 times as large as the well depth of AW2, D_e=0.41 kcal/mol, and $\frac{1}{3}$ of the strong water-water bond at 5.4 kcal/mol [3]. To a first-order approximation, the large polarizability of benzene is responsible for the strong intermolecular forces. The details of the interaction based on *ab initio* potential slices deserve some attention. Although the potential curvature is suspected to be shallower than that of Ar-water near the minimum, the edges of the IPS are found to be much steeper, "localizing" the water molecule to have its hydrogens pointed towards the benzene, in contrast to Ar-water where water behaves more as a free rotor. Benzene is, thus, a more favorable hydrogen bond acceptor than Ar for a variety of reasons. This reinforces the biological observations that aromatic rings are often found to line channels where polar and ionic compounds travel. An FIR spectrum was obtained for the C_6H_6-D_2O species, and confirmed the microwave observations of a symmetric top-like cluster with large amplitude motions in the ground state. The

cluster with one quantum of intermolecular vibrational excitation remains symmetric at our resolution limit of $\leq$1 MHz. Much work remains to be done on this cluster; the work presented here serves as the foundation for future work. Of similar interest is the study of benzene-ammonia dimer whose ground state microwave spectrum and resonance-enhanced two-photon ionization cross sections have also been collected in Prof. Blake's laboratory [4].

An intermolecular transition of $(D_2O)_3$ was observed with the tunable FIR spectrometer. Our observations have brought the understanding of water trimer one step closer to a full IPS. Specifically, we observed a band at a frequency lower than any predicted by theoretical calculations, thereby effecting a reconsideration of the trimer dynamics. A collaborative effort with several research groups is in progress.

The acquisition of IPS's clearly benefits our understanding of natural phenomena. In order to characterize more IPS's, extensive laboratory measurements and improvements in spectroscopic and computational methods are necessary. As seen in a relatively simple system, Ar-H_2O, all the VRT modes of a cluster must be investigated to yield an accurate IPS. There are seemingly an infinite number of clusters and VRT modes to be measured. More chemically interesting clusters, such as the water dimer, have stronger bonds than Ar-H_2O resulting in deeper potential minima and higher frequency transitions. This requires the capability to scan at a higher frequency range ($\sim$100-500 cm^{-1}) than can be accessed with the laser sideband instrument. One nascent technique that may reach this range involves FIR generation by mixing radiation from infrared diode lasers in low temperature GaAs, which is being developed at MIT Lincoln Labs and in Prof. Blake's laboratory. The FIR generated in this fashion will have much faster scan rates and broader coverage than the tunable FIR sideband spectrometer currently in use. This will aid greatly, and perhaps retire, the slower, high resolution tunable FIR sideband instrument. We see in water trimer that the three-body force is a small but significant fraction of the two-body force. Such small differences require highly accurate IPS's for meaningful quantitative understanding, which in turn maintain the demand for high resolution spectroscopy. Thus, the next generation spectrometers must have broad range, high

scanning speed, and high resolution.

Clusters of greater chemical interest also have strong bonds between a large number of atoms, and thus, have many deep potential minima among which tunneling can occur. In order to interpret increasingly complex experimental data, our theoretical understanding of the relationship between multi-dimensionally coupled VRT spectra and IPS's must be refined, and faster algorithms for spectral inversion are desperately needed. Both algebraic and computational theorists are pushing back the frontiers in these directions. Improved computational algorithms for spectral inversion to be performed on future generations of computational hardware are being pursued by various research groups, many mentioned in the preceding chapters. The quantitative IPS's, in combination with the new experimental and theoretical tools developed, will enable many chemical and biological processes to examined at the molecular level for the first time.

Bibliography

[1] R.C. Cohen and R.J. Saykally. Determination of an Improved Intermolecular Global Potential Energy Surface for Ar-H_2O from Vibration-Rotation-Tunneling Spectroscopy. *J. Chem. Phys.*, 98:6007, 1993.

[2] R.C. Cohen and R.J. Saykally. Extending the Collocation Method to Multidimensional Molecular Dynamics: Direct Determination of the Intermolecular Potential of Ar-H_2O from Tunable Far-Infrared Laser Spectroscopy. *J. Phys. Chem.*, 94:7991, 1990.

[3] L.A. Curtiss, D.J. Frurip, and M. Blander. Studies of Molecular Association in H_2O and D_2O Vapors by Measurement of Thermal Conductivity. *J. Chem. Phys.*, 71:2703, 1979.

[4] D.A. Rodham, S. Suzuki, R.D. Suenram, F.J. Lovas, S. Dasgupta, W.A. Goddard III, and G.A. Blake. Hydrogen Bonding in the Benzene-Ammonia Dimer. *Nature*, 362:735, 1993.

Appendix A: Microwave experimental procedure

The following is a general procedure often used to start a microwave scan.

1. The first step is to place and align the two microwave horns on opposite sides of the slit nozzle. One horn should be connected to the Wiltron microwave source, and the other should be connected to a microwave detector. The horns are first aligned by eye, and then by maximizing the amplitude modulated (AM) microwave throughput. Note that the amplitude modulation on the Wiltron is not perfect, and hence, maximum AM signal is not when the power is the greatest. Often, the ~11 dBm setting gave the largest AM signal. The AM signal is observed by connecting the detector output to the lock-in amplifier (LIA) or to the oscilloscope. When using the LIA, $1f$ detection should be used.

2. Once the horns are adjusted for the maximum through-put, adjust the slit nozzle position such that the nozzle body barely occludes the microwave through-put. This is achieved by pulling out the nozzle feed-through from the chamber, and then pushing it back in towards the microwave until there is a slight decrease in the microwave through-put.

3. The set-up is now ready for spectroscopy. However, a known absorption line should be scanned to make sure that the system is aligned properly. The known absorption signal should be maximized with minor adjustments of the horn positions, nozzle position, and the gas flow rate. Some strong monomer absorption lines are cataloged at JPL. On-line access via a browser is at

"`http://spec.jpl.nasa.gov/cgi-bin/catform/`".

For frequency modulation scans. Change the LIA detection scheme to $2f$, and adjust the phase to maximize an absorption signal. This can be done by changing the phase and simply maximizing the signal, or, by first adjusting the phase until the signal is zero and then changing the phase by 90 degrees.

For Stark modulation scans. The nozzle must be equipped with the Stark plates,

as shown in Chapter 2. The leads to the Stark plates should be connected with the vacuum feed-through to the Stark modulation power supply, which is simply the high voltage amplification of a function generator signal. The modulation power supply itself must be connected to a DC power supply. The function generator used to trigger and control the Stark voltage should be set to 100 kHz (the LIA limit). The output of the Stark modulation power supply should be monitored using an oscilloscope. A 10× probe is connected to the red wires attached near the BNC output of the modulation power supply. The shape of the modulated voltage should be adjusted to be as close to a square wave as possible with one output giving a positive pulse, and the other giving a negative pulse. The amplification factor control knobs (resistor pots on the modulation power supply), function generator signal voltage, function generator offset knob, and the function generator symmetry knob are used to obtain two opposing square waves on the oscilloscope. The modulation voltage is usually limited by the DC power supply which must supply nearly 0.045 Amp for operation at $\pm$ 50 V, for each polarity.

Appendix B: TuFIR experimental procedure

The following is a general procedure often used to start a far-infrared scan.

Finding the FIR laser line.

1. Consult *Millimetre and Submillimetre Wavelength Lasers* [1] or the green three ring binder titled *Berkeley Laser Line List* to choose the appropriate laser gas and CO_2 laser pump line. A list of FIR laser lines used for this thesis is given in Chapter 4.

2. Tune the CO_2 laser to the appropriate laser line and maximize the output power.

3. Fill the FIR laser cavity with the appropriate gas. The pressure inside the laser cavity varies depending on the laser line and the gas species. In general, 60 to 200 mTorr above the background pressure of the tube seems to work well. Once a laser line is found, the pressure should be adjusted to maximize the FIR laser output. A list of laser gas and parameters are recorded in a laboratory notebook titled "FIR Laser Lines".

4. Place a chopper in front of and centered near the FIR laser output. The chopper frequency should be set at $\sim$ 200-400 Hz. Adjust the first polarizer to reflect the laser radiation. Monitor the voltage change on the corner cube mixer using the lock-in amplifier (LIA) and/or the oscilloscope while the FIR laser cavity length is scanned and the CO_2 laser cavity length is modulated by hand; the piezo output coupler control knob is turned from one end to the other end at approximately 0.5 Hz. The laser power output will be seen as a spike on the LIA or the sudden appearance of a square wave on the oscilloscope. If a laser signal is not detected after scanning the FIR laser cavity for several λ_{FIR}, then change one of the following and try again: the Michelson interferometer arm length, the corner cube rooftop mirror position, the corner cube angle, or the FIR laser cavity pressure. When nothing seems to work, try a strong FIR laser line such as the 584 GHz HCOOH line or the 692 GHz CH_2F_2 line to tweak the laser system. If these two lines do not work, it is time for

realignment.(See Appendix C.)

Maximize the FIR laser radiation onto the whisker antenna.

First, adjust the chopper position and make sure that the FIR radiation is coming out near the center of the laser output window. Then adjust all mirror angles and positions. The corner cube angle and the roof top mirror position should be adjusted next. Finally, the off-axis mirror, Michelson arm lengths, other mirrors including those guiding the CO_2 laser into the FIR laser cavity, the CO_2 and FIR laser gas pressures, their cavity lengths, and the CO_2 laser current should all be optimized.

Alignment of the FIR sideband.

1. Connect the InSb detector to the oscilloscope and maximize the chopped FIR laser signal while adjusting mirrors and lens positions. Usually, the InSb output ranges from 10 to 20 V for the chopped FIR laser leakage. The FIR leakage does not travel the same path as the sidebands, but it is close enough to the sideband path to provide a rough alignment.

2. Connect the microwave source to the corner cube. When the microwave source is amplitude modulated (AM), the detector sees the chopped FIR and AM sideband signal (AM at about 50 kHz). The AM sideband signal should be maximized by adjusting all mirrors inside and outside the Michelson box. The Michelson interferometer, corner cube angle and rooftop mirror position should be readjusted to maximize the sideband strength. On a good laser line, >1 V of sideband is detected. The nozzle position should be adjusted such that the nozzle body slightly occludes the sideband radiation.

3. Use a strong monomer absorption line in the region to fine tune the alignment of the tunable far-infrared sidebands. The JPL line list is a useful source of such monomer absorption frequencies. The Blake lab has a microfiche of the JPL absorption line catalog. However, the on-line catalog is much more convenient. Use a browser, such as *mosaic* and access the http site "http://spec.jpl.nasa.gov/cgi-bin/catform/". This site provides an interactive search of the JPL line catalog. Change the microwave source to frequency modulation, LIA to $2f$ detection, adjust the phase and microwave power, as well as all optics' positions.

4. Once the monomer absorption is maximized, use a known cluster line to maximize the alignment as well as the nozzle position. Often the monomer species and the cluster species have different optimal nozzle positions.

Bibliography

[1] N.G. Douglas. *Millimetre and Submillimetre Wavelength Lasers: A Handbook of cw Measurements.* Springer-Verlag, Berlin, Germany, 1989.

Appendix C: Repair hints

This appendix contains helpful hints and information for repairing the instruments used for the thesis work.

.1 Vacuum pumps

Edwards mechanical pumps: E2M275

The large vacuum pumps for the slit nozzle chamber require one routine and several need-based maintenance operations. The routine maintenance is the oil change. This is done every 4 to 8 weeks of continuous operation. If the gas sample used is particularly corrosive, the oil is changed more frequently. If a toxic or corrosive sample is used, the pumps are left on with a small amount of Ar gas flowing overnight to prevent the oil from "freezing". This is particularly important before an oil change when the residual chemical in the oil may surprise the maintenance crew – choking, near vomiting, coughing, and near fainting are some of the potential side effects if this step is neglected.

One need-based maintenance step is the exchange of the oil pump filter. The oil pressure gauge on the side of the mechanical pump should be periodically inspected to make sure that it is not clogging up. If it does clog up and the pressure gauge indicates a need for filter exchange, drain the pump oil, remove the part counting the pressure gauge, and replace the cylindrical filter element. Replacement parts can be purchased from Edwards, or from a less expensive parts supplier, Precision Plus Vacuum Parts, Inc., 30 Troy Road, Whippany, NJ, 07981, (800) 526-2707.

.1.1 Complete overhaul

According to the Saykally group at UC Berkeley and the engineers at Edwards, the gaskets inside the E2M275 pumps last for about 3 to 5 years. As the gaskets wear

out, the pumping speed will decrease. This is when the gaskets and the vanes need to be replaced. Below are notes made after the first such overhaul in March 1993. The first overhaul took a week, but the second overhaul performed in 1994 following the use of corrosive samples was performed over two days.

1. Darryl Riley at Unilab Technologies was the person whom we hired to fix the pumps. He charged the least and was also local and willing to work on site. He used to work for the chemistry department. As of March 1993, Unilab Technologies was located at, 5340 Temple City Blvd., Temple City, CA 91780 (818)287-8316. Jesse Miller also worked for the chemistry department and now has a repair shop of his own: Miller Scientific (818)301-9965. These two were sources of helpful advice during the first and the second overhauls.

2. The refurbishing kit can be purchased from Edwards or from Precision Plus. Precision Plus has the advantage of charging only half as much as Edwards for the kit. When the first overhaul was done, Edwards sent us defective parts which destroyed the stator of the pump. Edwards replaced the internal parts of the pump. Precision Plus claims to not have the defective parts. However, they are not inclined to replace the internal parts damaged from defective parts. The defective part was the main pump vanes. They should not have springs and pins, but rather should rely on centrifugal force for the sealing of the vanes against the stator wall. The abrasion of the spring against the fiberglass/asbestos vanes broke the vanes and allowed the springs and the pins to gouge the inside of the stator. Beware.

3. You may chose to fix the pumps your self. The Edwards pumps are modular and the alignment is fixed by several pins. To take it apart, remove the top plate, then the front plate and proceed to dismantle. All the bolts will eventually come loose, i.e., none are glued in. In order to get the main rotor out, you must remove the whole stator from the pump case first. While doing so, **DO NOT** to remove the back plate of the stator since that is what aligns the whole pump. The main stator can be removed without loosening the back plate. The back plate is circular and is attached to the outside of the oil tank, between the oil tank wall and the motor. It places the rotor shaft so that it is aligned with the motor shaft.

4. Clean all the surfaces and replace the gaskets. Effective cleaning agents are Scotchbright^{TM}, firm bristle brushes, cotton tip applicators, and squirt bottles with solvents. Hexane and acetone are effective solvents. Put the pump back together the way it came apart. It is best to keep all foreign particles out when you clean the pump, i.e., **DO NOT** use sand blasting. Though all the holes and small cavities may be plugged up before sand blasting, there will be a lot of sand which will manage to get into the pump. Unless the pump parts are cleaned with extraordinary care and thoroughness, there will be damage made to the insides of the stator by the small sand particles.

5. If you work continuously and make no major mistakes, disassembling the pump will take about half a day to a day depending on how dirty the pump is. Cleaning up all the gunk on the pump will take another 1 to 2 days. Putting the pump back together should take half a day to a full day. So, with nothing going wrong, it will take a week to do the job. (With experience, it will take only a couple of days. In either case, doing the overhaul by yourself will be faster than sending the pumps back to Edwards.)

6. There are no tricky parts to take apart or put together. The bolts may be difficult to loosen. The vanes may be hard to put in place–a lot of greasing up and some sanding down with a sand paper will help. Taking out the heavy stator requires at least two people. Pulleys and leverage are the tools to be used. When prying apart parts, remember there may be pins that should not get bent.

7. Rags are useful to have. Rags work better than paper towels. Ice cream at the end of each day is good.

Small mechanical pumps

Small mechanical pumps can be repaired in one afternoon provided all the replacement parts are available. As with the large Edwards' pumps, it is faster to repair the pumps in house. However, if there are replacements readily available, Darryl at Unilab Technologies or Jesse at Miller Scientific are good people to send out the pumps to for repair(see above for phone numbers). Sergeant Welch pumps require teflon sealant, a white paste to be placed between different sections which cures in about

24 hours. Several teflon sealants are available at hardware stores, but the one that worked after trying a few was made by Permatex Industrial, and it is called "Seals Pipes". Fixing a small pump is a good practice for the inevitable overhaul of the big puppies.

.2 Lasers

The FIR laser and the CO_2 laser system occasionally fail. Here are some examples of past failures: 1) misalignment of the folding mirrors guiding the CO_2 laser output into the FIR laser; 2) misalignment of the cavity mirrors inside the FIR laser; 3) leakage of the FIR cavity mirror cooling water; and 4) leakage of water or air into the CO_2 laser cavity. In all of these cases, the lasers must be realigned. The more damaging failures must be repaired before the lasers are aligned. One should not be apprehensive about opening the lasers and realigning the system. Once one becomes accustomed to the process, the realignment of the FIR laser cavity mirrors and the CO_2 beam path can be performed in less than an hour. In the case of damaging failures, such as examples 3 and 4, it is essential that the laser cavities be opened and cleaned as soon as possible to prevent further damage. In cases such as 1 and 2, it is more efficient to take one hour to realign the lasers than to search blindly through the multidimensional of parameter space mirror angles. Following is a list of instructions for aligning the lasers.

.2.1 Laser alignment

FIR laser

This step is essentially the alignment of the cavity mirrors.

1. Remove the plexi-glass tops from the input and the output boxes. Remove the

input coupler (ZeSn window) and the output lens (poly lens). Remove the input and output mirrors.

2. Place 1 mm diameter constriction appatures made of anodized aluminum where the input and output windows were attached.

3. Using two mirrors, guide the HeNe laser light in through the input end and out the output end. Make sure that there are no reflections inside the FIR laser tube. Turning off the room lights helps to identify the locations of internal reflection.

4. Place and secure a flat 2 inch diameter mirror in the gimble mount where the output mirror/coupler was located. At the input end, check to see if the mirror placed at the output end is reflecting the HeNe laser beam back. The center of the reflected beam should overlap with in incoming HeNe beam. Make sure there are no reflections. If the output mirror is not aligned, adjust the gimble mount so that the reflected beam from the mirror at the output end overlaps with the incoming beam. Make sure that the tip of the micrometer is in contact with the gimble mount. Once the reflected beam overlaps the incoming beam, the output gimble is aligned. Remove the 2 inch mirror.

5. Move the HeNe laser and the two mirrors to the output end and guide the HeNe beam in through the 1 mm diameter aperture at the output end and then out through the input end. Place a flat 2 inch diameter mirror into the gimble mount and adjust for gimble angles so that the reflected beam overlaps the incoming beam. Once the beams overlap, remove the 2 inch mirror.

Folding mirrors

Once the FIR laser cavity mirrors are aligned, the folding mirrors should be aligned so that the HeNe radiation coming through the FIR laser goes into the CO_2 laser and is observed on the grating (look through the window where the CO_2 laser radiation comes out for the spectrum analyzer.)

CO_2 laser

In the event the CO_2 laser needs realignment, continue with the following instructions after completing the FIR laser alignment.

1. Remove the grating housing. Remove the CO_2 laser cavity tubes.

2. Place a "Space Invader" target near each end of the CO_2 laser. Adjust the HeNe laser height so that it is 7.75 inches above the laser table at both ends of the laser. Adjust the horizontal position of the HeNe so that it crosses the targets at the center of the laser. To insure that each support block is centered, one may place a transparency graph paper with concentric circles.

3. Once the HeNe beam is aligned, replace the attachments and the laser tubes for the grating end of the CO_2 laser. Using the stainless steel laser cavity plug, adjust the position of the laser cavity tube so that it is centered on the HeNe laser beam. Once the grating end is put in place and secured, do likewise for the output end of the CO_2 laser.

4. Once the tubes are in place, attach the remaining parts of the laser. Check to make sure that the HeNe is coming through all the way to the grating by looking in through the window allowing the zeroth order diffracted beam to exit the CO_2. If a fuzzy red spot on the grating is not observed, there is something wrong with the alignment. Otherwise, this will serve as a qualitative reference for checking the FIR alignment as noted above.

Now the two lasers should be aligned well. It should require only minor tweaking to maximize the FIR laser power, once the FIR radiation is detected.

.2.2 Notes on laser repair

Disassembly and re-assembly of the lasers is not difficult. The construction of the lasers is straightforward, and the alignment process is tedious but its outcome certain (mostly successful alignment). A careful step-by-step process is recommended since there are fragile parts. In particular, the inner bored cavity tube of the CO_2 laser purchased from Wilmad Glass is easily chipped. When removing the tubes, a slow

gentle tug with a twisting motion is helpful. Do not pull or squeeze or bend the tubes too hard. A very small amount of grease on the parts outside of the laser cavity will facilitate the placement of the bored cavity tubes.

The inside of the cavity tubes are cleaned with large doses of volatile solvents, usually an acetone rinse is followed by a final dose of distilled water rinse. It is then wiped dry and air dried.

Laboratory tissue-paper is made into a ball soaked with solvent, and passed through the cavity to clean the FIR laser cavity. The FIR laser cavity rarely becomes dirty, however.

Some of the FIR laser lines are produced by corrosive chemicals, such as formic acid. In such cases, a liquid nitrogen trap is placed before the FIR laser cavity pump. This prolongs the FIR mechanical vacuum pump life immensely.

Eric Müller at University of Massachusetts at Lowell is familiar with the Apollo laser systems and the original designer. Alain Semet may be contacted for further guidance at (818) 222-2495.

.3 Cooling units

There are several cooling units used in the Blake lab. The cooling unit for the CO_2 laser was purchased from Bay-Voltex and it controls the temperature to $\pm$ 0.1 °C. All the other cooling units were purchased from Neslab. The part that fails the most on these units is the water pump. In particular, the key that connects the motor and the pump breaks often. The water pump in these units are made by Procon, model 10153. Procon has been helpful in providing us with free samples of the key, and their delivery of the water pump is timely. They are located in Murfeesboro, TN.

The Bay-Voltex is equipped with an external water filter to remove all the sludge that is developed by the CO_2 aluminum blocks. The filter element should be cleaned or replaced periodically (3-6 months).

The plastic cooling water jacket around CO2 laser, with a trade name Excelon, can be purchased from Ryan Herco in Burbank. This tube melts and deforms easily when

the cooling water temperature increases–perhaps a safety feature against superheating or damage to the laser cavity. It can be bent back in place by heating the tube with a heating gun.

McCarthy Scientific Co is where we get the mirror polishing kit to polish the FIR mirrors. P.O. Box 5332, Fullerton, CA 92635, (714) 526-2742, Fax (714) 526-29927.

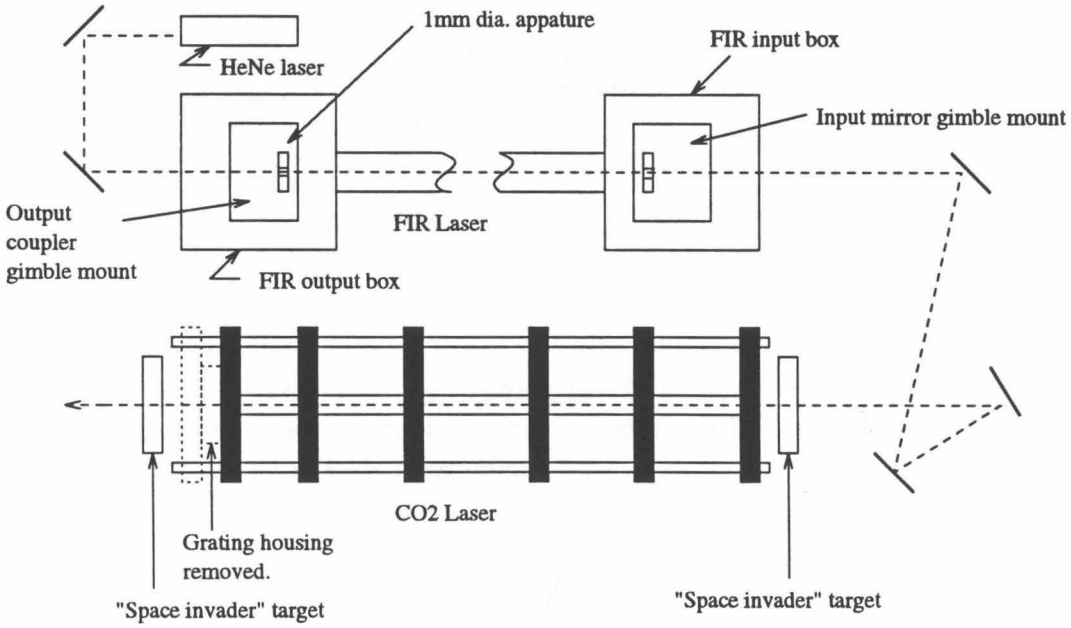

Figure .1: The HeNe laser beam is guided through the output end of the FIR laser, through the FIR input, reflected by the folding mirrors, and aligned through the CO_2 laser cavity.

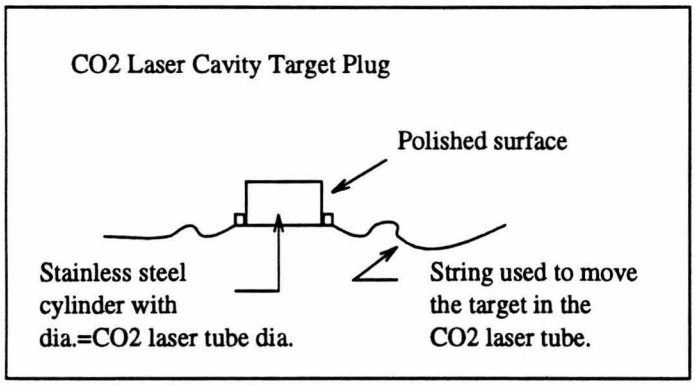

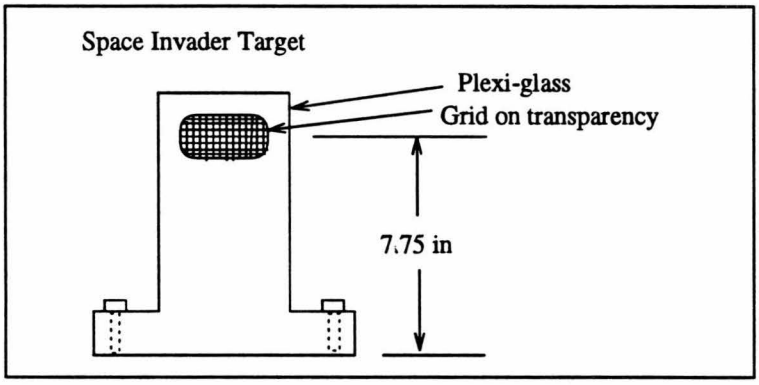

Figure .2: These targets aid in aligning the CO_2 laser cavity. The "Space Invader" targets are used to ascertain the correct height and horizontal position of the HeNe laser used to align the CO_2 laser cavity.

Appendix D: PI theory for benzene-water

The permutation inversion (PI) group for benzene-water, along with the character table and statistical weights are derived below.

References consulted for this work are monographs by Bunker, *Molecular symmetry and spectroscopy* [6], and by Cotton, *Chemical Applications of Group Theory* [5], articles by Wilson [7], Balasubramanian [4], and Gotch and Zwier [5], and the Ph.D. thesis of Gotch [6].

The character table and statistical weights presented by Gotch and Zwier [5] contains a small error in the table, and the spin statistics seem to differ slightly from my calculations. The derivation below is meant to assist anyone who may wish to examine the difference further. The following calculations are simpler than those given by Gotch in his thesis [6]. Especially, the spin statistics calculated using the method outlined by Balasubramanian [4] is simpler than the method that Gotch used.

The benzene molecule can be notated as in Figure .3. The permutation operations possible on benzene are:

C_{6v}	PI	$Classsize$
E	E	1
C_6	(123456)	2
C_3	(135)(246)	2
C_2	(14)(23)(36)	1
σ_d	(16)(25)(34)*	3
σ_v	(15)(24)*	3

The total number of operations is 12. The PI group is isomorphic with the C_{6v} point group.

The two permutations possible on water are E and (78).

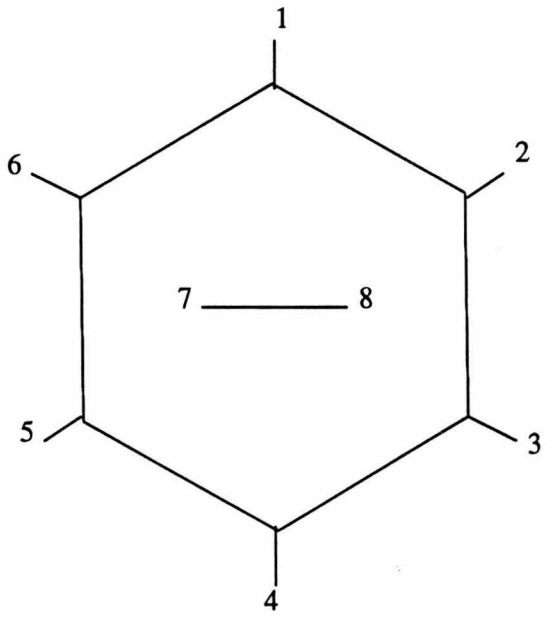

Figure .3: Benzene-water notation used in the PI theory calculation. In this simplified diagram, the numbers denote hydrogen atoms. In the PI theory for benzene-water, the C-H and O-H bonds are not broken; thus, this shorthand notation concerning the atoms with spins is quite useful.

The permutations and the class sizes for benzene-water are, therefore:

Class number	*PI*	*Class size*
1	E	1
2	(123456)	2
3	(135)(246)	2
4	(14)(23)(36)	1
5	(16)(25)(34)*	3
6	(15)(24)*	3
7	(78)	1
8	(123456)(78)	2
9	(135)(246)(78)	2
10	(14)(23)(36)(78)	1
11	(16)(25)(34)(78)*	3
12	(15)(24)(78)*	3

The order of this group is 24, hence G_{24}. The character table for the group is obtained by taking the direct product of the C_{6v} character table for benzene and C_2 for water.

C_2	E	(78)
A	1	1
B	1	-1

The direct product is easily produced by replicating the C_{6v} character table in the pattern below:

$C_{6v} \otimes C_2$		
	C_{6v}	C_{6v}
	C_{6v}	$-C_{6v}$

The G_{24} character table is given in Table .1, using the class numbers outlined above to denote the PI operations

As described by Wilson, the direct product $\Gamma^{nuc} \otimes \Gamma^{tor} \otimes \Gamma^{rot}$ must be B_1^- or B_2^-

Table .1: G_{24} character table

Operations	1	2	3	4	5	6	7	8	9	10	11	12
Class size	1	2	2	1	3	3	1	2	2	1	3	3
A_1^+	1	1	1	1	1	1	1	1	1	1	1	1
A_2^+	1	1	1	1	-1	-1	1	1	1	1	-1	-1
B_1^+	1	-1	1	-1	1	-1	1	-1	1	-1	1	-1
B_2^+	1	-1	1	-1	-1	1	1	-1	1	-1	-1	1
E_1^+	2	1	-1	-2	0	0	2	1	-1	-2	0	0
E_2^+	2	-1	-1	2	0	0	2	-1	-1	2	0	0
A_1^-	1	1	1	1	1	1	-1	-1	-1	-1	-1	-1
A_2^-	1	1	1	1	-1	-1	-1	-1	-1	-1	1	1
B_1^-	1	-1	1	-1	1	-1	-1	1	-1	1	-1	1
B_2^-	1	-1	1	-1	-1	1	-1	1	-1	1	1	-1
E_1^-	2	1	-1	-2	0	0	-2	-1	1	2	0	0
E_2^-	2	-1	-1	2	0	0	-2	1	1	-2	0	0

for H_2O-benzene, B_1^+ or B_2^+ for D_2O-benzene, and B_1 or B_2 for HDO-benzene [7].

First, we will calculate the nuclear spin statistics. The irreducible representations of the nuclear spin representation, Γ^{nuc}, are determined by taking the sum of spin statistics for each irreducible representation $\{A_1^+, A_2^+, \ldots, E_2^-\}$. Following Balasubramanian's method [4], the nuclear spin statistics for the A_1^+ state, $P^{A_1^+}$, is calculated. The first step is to classify the operation in terms of cycles: E = (1)(2)(3)(4)(5)(6)(7)(8) = x_1^8, that is, there are 8 cycles of length 1, and for (135)(246) = (135)(246)(7)(8) = $x_3^2 \cdot x_1^2$, that is, 2 cycles of length 3 and 2 cycles of length 1, and so on. Balasubramanian shows that in order to calculate the spin statistics, one needs only to substitute in x the number of spin states possible for each species exchanged. For C_6H_6-H_2O, we are concerned only with H which has 2 possible spin states, $-\frac{1}{2}$ and $\frac{1}{2}$, hence x=2. Using the equation given by Balasubramanian,

$$P^{\Gamma} = \frac{1}{(grouporder)} \sum_{operations} \chi_{operations} \cdot (classsize) \cdot x_1^{b_1} \cdot x_2^{b_2} \cdots x_n^{b_n},$$

$$\begin{aligned} P^{A_1^+} &= \frac{1}{24}(1 \cdot 1 \cdot 2^8 + 1 \cdot 2 \cdot 2^3 + 1 \cdot 2 \cdot 2^4 + 1 \cdot 1 \cdot 2^5 + 1 \cdot 3 \cdot 2^5 \\ &+ 1 \cdot 3 \cdot 2^6 + 1 \cdot 1 \cdot 2^7 + 1 \cdot 2 \cdot 2^2 + 1 \cdot 2 \cdot 2^3 + 1 \cdot 1 \cdot 2^4 + 1 \cdot 3 \cdot 2^4 + 1 \cdot 3 \cdot 2^5) \end{aligned}$$

When the P^{Γ}'s are calculated for all Γ, we have for benzene-H_2O,

$$\begin{aligned}\Gamma^{nuc} &= 39A_1^+ + 3A_2^+ + 9B_1^+ + 21B_2^+ + 27E_1^+ + 33E_2^+ \\ &+ 13A_1^- + A_2^- + 3B_1^- + 7B_2^- + 9E_1^- + 11E_2^-\end{aligned}$$

Now, for D_2O-benzene, the H's on benzene have two possible spin states, and the D's on water have three possible spin states, i.e., x_{bz}=2 and x_w=3. This yields, for example, E=(1)(2)(3)(4)(5)(6)(7)(8)=$x_{bz}^6 \cdot x_w^2$, and (135)(246)=(135)(246)(7)(8)=$x_{bz}^2 \cdot x_w^2$. Thus,

$$\begin{aligned}P^{A_1^+} &= \frac{1}{24}(2^6 \cdot 3^2 + 2 \cdot 2 \cdot 3^2 + 2 \cdot 2^2 \cdot 3^2 + 2^3 \cdot 3^2 + 3 \cdot 2^3 \cdot 2^2 \\ &+ 3 \cdot 2^4 \cdot 3^2 + 2^6 \cdot 3 + 2 \cdot 2 \cdot 3 + 2 \cdot 2^2 \cdot 3 + 2^3 \cdot 3 + 3 \cdot 2^3 \cdot 3 + 3 \cdot 2^4 \cdot 3) \\ &= 78\end{aligned}$$

The nuclear spin statistics obtained for D_2O-benzene is therefore:

$$\begin{aligned}\Gamma^{nuc} &= 78A_1^+ + 6A_2^+ + 18B_1^+ + 42B_2^+ + 54E_1^+ + 66E_2^+ \\ &+ 39A_1^- + 3A_2^- + 9B_1^- + 21B_2^- + 27E_1^- + 33E_2^-\end{aligned}$$

The next step is to determine the representations for the rotational wavefunction, Γ^{rot}. By considering the benzene to be the rotating frame, we can use the Γ^{rot} of benzene derived by Wilson [7]. These are the same as those given by Gotch and Zwier [5], Γ^{rot}=A_1^+ for k=0, J=even; Γ^{rot}=A_2^+ for k=0, J=odd; Γ^{rot}=E_1^+ for k=6n$\pm$1; Γ^{rot}=E_2^+ for k=6n$\pm$2; Γ^{rot}=B_1^++B_2^+ for k=6n$\pm$3; and Γ^{rot}=A_1^++A_2^+ for k=6n$\pm$6.

The representation for the torsional motion, Γ^{tor}, can be determined by examining the transformation of the internal rotation coordinate, ϕ. In chapter 3, ϕ is shown as the rotation of benzene, but actually, it is the relative angle between benzene and water. Here, it is taken as the internal rotation angle of water against the benzene frame. These transformations are summarized in Gotch and Zwier's character table [5, 6]. For the $m = 0$ state, E gives the character $e^{im\phi} = e^0 = 1$. (123456) gives $e^{i \cdot 0 \cdot (\phi - \pi/3)} = e^0 = 1$. Similar calculations with the remaining operations show that the

characters for m=0 correspond to characters of A_1^+. Similarly, the Γ^{tor} designations for $m = \pm 1$, $m = \pm 2$, and $m = \pm 3$ were determined and found to match those given by Gotch and Zwier, i.e., $m = \pm 1$ is E_1^-, $m = \pm 2$ is E_2^+, and $m = \pm 3$ is $(B_1^- + B_2^-)$.

Finally, we simply need to take the direct product, $\Gamma^{int} = \Gamma^{nuc} \otimes \Gamma^{tor} \otimes \Gamma^{rot}$. For example, in $m = 0$, k=0, J=odd case, $\Gamma^{int} = \Gamma^{nuc} \otimes A_1^+ \otimes A_1^+ = \Gamma^{nuc} \otimes A_2^+$. Multiplication rules are given in Tables .2, .3. The only B_2^- and B_1^- terms in the direct product are $7B_2^- + 3\ B_1^-$. Thus, the statistical weight of this state is 10. Likewise, $m = 0$, k=0, J=even gives similar results. $m = 0$, k=6n±1 has 11 each of B_2^- and B_1^- terms, giving the statistical weight of 22. The statistical weights for benzene-H_2O are obtained by continuing the arithmetic:

$m = 0, k = 0, J = even$	10
$m = 0, k = 0, J = odd$	10
$m = 0, k = 6n \pm 1$	22
$m = 0, k = 6n \pm 2$	18
$m = 0, k = 6n \pm 3$	28
$m = 0, k = 6n \pm 6$	20

The results obtained for $m = 1$ states are slightly different from that given by Gotch and Zwier.

$k = 0, J = even$	33
$k = 0, J = odd$	33
$k = 6n \pm 1$	57
$k = 6n \pm 2$	75
$k = 6n \pm 3$	54
$k = 6n \pm 6$	66

Table .2: Direct product multiplication rules used in this appendix. The rules are calculated by taking the direct product character, for example, $B_1^+ \otimes E_1^-$ has characters $2\ -1\ -1\ 2\ 0\ 0\ -2\ 1\ 1\ -2\ 0\ 0$ which is the character of E_2^-. For further explanation, consult Cotton.

Γ^1	Γ^2	$\Gamma^1 \otimes \Gamma^2$
A_1^+	E_1^-	E_1^-
A_2^+	E_1^-	E_1^-
B_1^+	E_1^-	E_2^-
B_2^+	E_1^-	E_2^-
E_1^+	E_1^-	$A_1^- + A_2^- + E_2^-$
E_2^+	E_1^-	$B_1^- + B_2^- + E_1^-$
A_1^-	E_1^-	E_1^+
A_2^-	E_1^-	E_1^+
B_1^-	E_1^-	E_2^+
B_2^-	E_1^-	E_2^+
E_1^-	E_1^-	$A_1^+ + A_2^+ + E_2^+$
E_2^-	E_1^-	$B_1^+ + B_2^+ + E_1^+$
A_1^+	A_1^-	A_1^-
A_2^+	A_1^-	A_2^-
B_1^+	A_1^-	B_1^-
B_2^+	A_1^-	B_2^-
E_1^+	A_1^-	E_1^-
E_2^+	A_1^-	E_2^-
A_1^-	A_1^-	A_1^+
A_2^-	A_1^-	A_2^+
B_1^-	A_1^-	B_1^+
B_2^-	A_1^-	B_2^+
A_1^+	A_2^-	A_2^-
A_2^+	A_2^-	A_1^-
B_1^+	A_2^-	B_2^-
B_2^+	A_2^-	B_1^-
E_1^+	A_2^-	E_1^-
E_2^+	A_2^-	E_2^-
A_2^-	A_2^-	A_1^+
B_1^-	A_2^-	B_2^+
B_2^-	A_2^-	B_1^+

Table .3: Direct product table continued.

Γ^1	Γ^2	$\Gamma^1 \otimes \Gamma^2$
A_1^+	E_2^-	E_2^-
A_2^+	E_2^-	E_2^-
B_1^+	E_2^-	E_1^-
B_2^+	E_2^-	E_1^-
E_1^+	E_2^-	$B_1^- + B_2^- + E_1^-$
E_2^+	E_2^-	$A_1^- + A_2^- + E_2^-$
B_1^-	E_2^-	E_1^+
B_2^-	E_2^-	E_1^+
A_1^+	B_1^-	B_1^-
A_2^+	B_1^-	B_2^-
A_1^+	B_2^-	B_2^-
A_2^+	B_2^-	B_1^-
E_2^+	E_1^-	$B_1^- + B_2^- + E_1^-$
E_2^-	E_1^-	$B_1^+ + B_2^+ + E_1^+$

Bibliography

[1] P.R. Bunker. *Molecular Symmetry and Spectroscopy.* Academic Press, New York, NY, 1979.

[2] F.A. Cotton. *Chemical Applications of Group Theory.* Wiley-Interscience, New York, NY, 1963.

[3] Jr. E.B. Wilson. The Statistical Weights of the Rotational Levels of Polyatomic Molecules, Including Methane, Ammonia, Benzene, Cyclopropane and Ethylene. *J. Chem. Phys.*, 3:276, 1935.

[4] K. Balasubramanian. Generating Functions for the Nuclear Spin Statistics of Nonrigid Molecules. *J. Chem. Phys.*, 75:4572, 1981.

[5] A.J. Gotch and T.S. Zwier. Multiphoton Ionization Studies of Clusters of Immiscible Liquids: 1. C_6H_6-$(H_2O)_n$, n=1,2. *J. Chem. Phys.*, 95:3388, 1992.

[6] Albert Joseph Gotch. *Probing Solute/Solvent Interactions: A Study of Benzene-Small Molecule van der Waals' Complexes.* Ph.D. thesis, Purdue University, Purdue, IN, December 1991.

Appendix E: Fitting programs

This appendix describes several computer codes used in this thesis. The first set of codes to be described are the spectral fitting programs. Then, routines used to fit *ab initio* potentials are listed. Lastly, input files for structural fitting programs are given.

Spectral fitting routine

The spectral fitting routines used were derivations of "AFITSPEC.F" written by Roger Bumgarner. The general flow chart of the program is show in Figure .4. This is a least square fitting program with the Hamiltonian entered in the subroutine called "FSUB".

Following is a copy of the code used to fit Ar-D_2O and Ar-DOH spectra. The "FSUB" routine of the program specific to Ar-water is placed at the end.

```
C JACOB FITTING PROGRAM RENAMED FITSPEC FOR APPLICATION TO FITTING
C MICROWAVE TRANSITIONS
      IMPLICIT REAL*8(A-H,O-Z)
      REAL*8 JACOB
      CHARACTER*79 TITLE1,TITLE2,TITLE3,infile,outfile,tofday,AFILE
      CHARACTER*15 PNAMES,VNAMES
      CHARACTER*1 HOW,IHOW,YES
      DIMENSION ALPHA(21,1),DELTAA(21,1),Y(400),YO(400),YP(400),
     1JACOB(400,21),TJACOB(21,400),W(400),XINV(21,21),PNAMES(21),
     2AINC(21),HOW(21),EVECT(400,1),TEMP(21,400),V(21,21),ASAVE(21),
     3DSAVE(21),IQNUMS(400,10),CORRM(21,21),ALLVAR(21),VNAMES(21),
     4IFFIT(21),WO(400)
C THIS VERSION ALLOWS 21 PARAMETERS AND 400 DATA PT. MAX.
C PROGRAM TO PERFORM GENERALIZED NON-LINEAR LEAST SQUARES FIT BY THE JACOBIAN
C METHOD. SEE HYUNYONG KIM, J. CHEM. ED., VOL.47, pp. 120-122 (1970).
C ALLVAR IS THE MATRIX OF VARIABLES SENT TO THE SUBROUTINE FSUB FOR
C CALCULATION OF THE Y VALUES. ALPHA IS THE MATRIX OF PARAMETERS OUT OF
C ALLVAR WHICH ARE ACTUALLY BEING FIT, DELTAA IS THE MATRIX OF CORRECTIONS
C TO THE PARAMETERS, Y IS THE MATRIX CONTAINING THE DATA AS READ IN, YO
C IS THE MATRIX CONTAINING THE CALCULATED VALUES CORRESPONDING TO Y, WITH
C THE CURRENT VALUES OF ALPHA, YP IS THE MATRIX CONTAINING CALCULATED Y'S
C FOR USE IN CALCULATING THE DERIVATIVES, JACOB IS THE JACOBIAN MATRIX
C CONTAINING THE DERIVATIVE OF EACH Y WITH RESPECT TO EACH PARAMETER,
C TJACOB IS JACOB'S TRANSPOSE, W IS THE MATRIX CONTAINING THE WEIGHTS OF
```

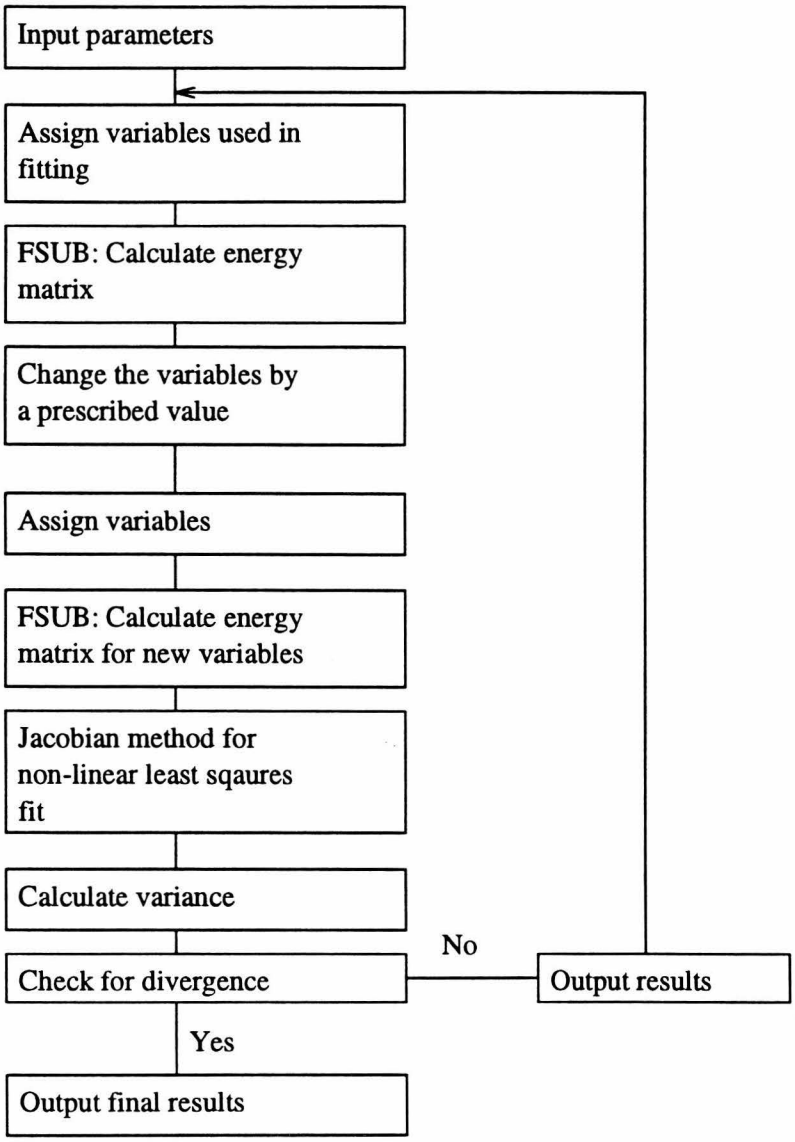

Figure .4: General flow chart for the spectral fitting program

```
C EACH Y, as used in the fit.  WO is the matrix containing the uncertainties
C of the data points.
C XINV IS A MATRIX USED FOR STORING THE INVERSE OF JACOB*TJACOB
C PNAMES IS A MATRIX CONTAINING THE NAMES OF THE PARAMETERS IN ALPHA, AINC
C IS THE MATRIX CONTAINING THE INCREMENTS TO USE ON ALPHA WHEN CALCULATING
C THE DERIVATIVES, HOW IS A MATRIX TO INDICATE HOW TO CALCULATE AINC,
C EVECT IS THE ERROR VECTOR ORC Y-YO, TEMP IS A TEMPORARY MATRIX NEEDED IN
C THE CALCULATIONS, V IS THE VARIANCE-COVARIANCE MATRIX AND CORRM IS THE
C MATRIX OF CORRELATION COEFFICIENTS.
C MODIFIED 4/21/88 TO GET WEIGHTING CORRECT FOR CALCULATION OF STD.
C DEVIATIONS OF PARAMETERS.
C Modified 5-13-91 to: 1)read in uncertainties rather than weights
C 2) allow for variable input and output filenames 3) tag the output
C file with the time and date 4) calculate the std dev. of the overall
C fit properly and report the average ratio of the calculated deviation
C relative to the uncertainty.  REB
C Modified 5-15-91 to print output for asymbd7 input
C Modified 5-17-91 to include diagonal L distortion constants and to
C allow for J's up to 50.
C Modified 8-17-91 to output final fit in tex table format if desired
C
C  SET MAX. NUMBER OF PARAMETERS AND DATA PTS. POSSIBLE W/ ABOVE DIMENSIONS
      MAXPS=21
      MAXDPS=400
C    OPEN  INPUT FILE AND OUTPUT FILE
      IIN = 7
      IOUT = 8
      IAOUT=2
      ibout=3
      IASW=0
      itbl=0
      write(*,*) 'Input name of input file?'
      READ(*,*)infile
      WRITE(*,*)
      write(*,*) 'Input name of output file?'
      READ(*,*) outfile
      write(*,*)
      write(*,*) 'Do you want an input file for asymbd7?'
      write(*,*) '(Y,y or N,n) '
      read(*,*)YES
      write(*,*)
      IF ((YES.EQ.'Y').OR.(YES.EQ.'y')) THEN
          IASW=1
          write(*,*)'Input name of file for asymbd7 input file?'
          read(*,*) AFILE
          OPEN(IAOUT,FILE=AFILE)
      endif
      write(*,*)
      write(*,*) 'Do you want a separate file with the final '
      write(*,*)'output in TEX format? (Y,y or N,n)'
      read(*,*)YES
      write(*,*)
      IF ((YES.EQ.'Y').OR.(YES.EQ.'y')) THEN
          itbl=1
```

```
          write(*,*)'Input name of file for table file?'
          read(*,*) AFILE
          OPEN(ibout,FILE=AFILE)
       endif

       OPEN(IIN,FILE=infile)
       OPEN(IOUT,FILE=outfile)
       CALL FDATE(tofday)
       write(IOUT,*)tofday
       write(IOUT,*)
C

C INITIALIZATION
C
       SSOLD=1.0D16
       KOUNT=0
       Z=0.0D0
       DO 30 I=1,MAXPS
          DSAVE(I)=Z
          ASAVE(I)=Z
          ALLVAR(I)=Z
          IFFIT(I)=0
          ALPHA(I,1)=Z
          DELTAA(I,1)=Z
          AINC(I)=Z
          DO 10 J=1,MAXPS
             V(I,J)=Z
  10         XINV(I,J)=Z
          DO 20 J=1,MAXDPS
             TEMP(I,J)=Z
             JACOB(J,I)=Z
  20         TJACOB(I,J)=Z
  30   CONTINUE
       DO 40 J=1,MAXDPS
          W(J)=Z
          W0(J)=Z
          EVECT(J,1)=Z
          Y(J)=Z
          Y0(J)=Z
          YP(J)=Z
          DO 40 I=1,10
  40         IQNUMS(J,I)=0
C
C INPUT SECTION
C DATA FILE SHOULD CONSIST OF THE FOLLOWING:
C LINES 1-3 TITLE LINES 79 CHARS OR LESS EACH
C LINE 4: THE NUMBER OF CYCLES THE FIT SHOULD RUN - INTEGER FREE FORMAT
C LINE 5: THE NUMBER OF VARIABLES TO BE FIT,"NVARS" - INTEGER FREE FORMAT
C         NOTE- THIS INCLUDES BOTH THE FIXED AND FIT VARIABLES.
C
C NVARS LINES
C  EACH LINE CONTAINING FIVE ITEMS;
C   1) THE PARAMETER NAME (15 CHARS OR LESS),
C   2) THE INITIAL VALUE OF THE PARAMETER - REAL FREE FORMAT;
```

```
C   3) HOW TO INCREMENT THE PARAMETER - IF AN P IS HERE, THE PARAMETER WILL
C BE INCREMENTED A PROPORTIONAL AMOUNT FOR TAKING THE DERVIVATIVE. IF AN F
C IS HERE, THE PARAMETER WILL BE INCREMENTED BY A FIXED AMOUNT. 1 CHARACTER.
C   4) THE FRACTION OR FIXED AMMOUNT TO INCREMENT THE PARAMETER WHEN
C CALCULATING DERIVATIVES. REAL - FREE FORMAT.
C   5) A 1 TO INDICATE THAT THIS VARIABLE WILL BE FIT. OTHERWISE, VARIABLE
C WILL BE HELD FIXED TO THE VALUE INPUT - INTEGER FREE FORMAT
C
C THE NUMBER OF DATA PTS. "NDPTS" AND THE NUMBER OF QUANTUM NUMBERS "NQNUMS"
C FOR EACH DATA POINT - 2 INTEGERS FREE FORMAT
C
C NDPTS LINES
C EACH LINE CONTAINS FOUR ITEMS;
C   1) THE DATA POINT - REAL FREE FORMAT
C   2) NQNUMS MANY QUANTUM NUMBERS - INTEGERS FREE FORMAT
C   3) A Multiplicative number for the weight - REAL FREE FORMAT
C   4) The uncertainty of the data point - REAL FREE FORMAT
C      Weights of the data point in the fit will be calculated
C      as  #3*1/(#4*#4). i.e. as the inverse square of the uncertainty
C      times the multiplicative factor.
C
      READ(IIN,*)TITLE1
      READ(IIN,*)TITLE2
      READ(IIN,*)TITLE3
      WRITE(IOUT,1)TITLE1,TITLE2,TITLE3
      WRITE(IOUT,*)' THE FOLLOWING VARIABLES WERE FIXED DURING THE FIT '
      WRITE(IOUT,51)
      READ(IIN,*)KMAX
      READ(IIN,*)NVARS
      NPARMS=0
C READ IN VARIABLES AND ASSIGN FIT ONES TO ALPHA
      DO 50 I=1,NVARS
         READ(IIN,*) VNAMES(I),ALLVAR(I),IHOW,AINCR,IFFIT(I)
         IF( IFFIT(I).EQ.1) THEN
            NPARMS=NPARMS+1
            PNAMES(NPARMS)=VNAMES(I)
            ALPHA(NPARMS,1)=ALLVAR(I)
            HOW(NPARMS)=IHOW
            AINC(NPARMS)=AINCR
         ELSE
            WRITE(IOUT,61) VNAMES(I),ALLVAR(I)
         ENDIF
  50  CONTINUE
      WRITE(IOUT,*)
      READ(IIN,*) NDPTS,NQNUMS
      DO 60 I=1,NDPTS
         READ(IIN,*) Y(I),(IQNUMS(I,J),J=1,NQNUMS),FACTW,WO(I)
  60     W(I)=FACTW*1.0D0/(WO(I)*WO(I))
C CALCULATE YO
  65  CALL ASSIGN(MAXPS,ALLVAR,ALPHA,VNAMES,PNAMES,NVARS,NPARMS,
     1IFFIT)
      CALL FSUB(MAXPS,MAXDPS,NDPTS,NPARMS,ALLVAR,YO,IQNUMS)
C CALCULATE JACOBIAN MATRIX "JACOB" AND ITS TRANSPOSE
      DO 80 J=1,NPARMS
```

```
         IF(HOW(J).EQ.'F') THEN
            DELA=AINC(J)
         ELSE
            DELA=AINC(J)*ALPHA(J,1)
         ENDIF
         IF(DELA.EQ.0.0D0) DELA=1.0D-6
         ALPHA(J,1)=ALPHA(J,1)+DELA
         CALL ASSIGN(MAXPS,ALLVAR,ALPHA,VNAMES,PNAMES,NVARS,NPARMS,
     1   IFFIT)
         CALL FSUB(MAXPS,MAXDPS,NDPTS,NPARMS,ALLVAR,YP,IQNUMS)
         ALPHA(J,1)=ALPHA(J,1)-DELA
         DO 70 I=1,NDPTS
            JACOB(I,J)=(YP(I)-YO(I))/DELA
  70        TJACOB(J,I)=JACOB(I,J)*W(I)
  80  CONTINUE
C CALCULATE ERROR VECTOR
      DO 90 I=1,NDPTS
  90     EVECT(I,1)=Y(I)-YO(I)
C
C DO PRESCRIBED MATRIX OPERATIONS
C12345678912345678921234567893123456789412345678951234567896123456789712345678
      CALL MMULT(MAXPS,MAXDPS,MAXDPS,MAXPS,MAXPS,MAXPS,NPARMS,NDPTS,
     1NPARMS,TJACOB,JACOB,XINV)
      CALL MTRXIN(MAXPS,XINV,NPARMS)
      CALL MMULT(MAXPS,MAXPS,MAXPS,MAXDPS,MAXPS,MAXDPS,NPARMS,NPARMS,
     1NDPTS,XINV,TJACOB,TEMP)
      CALL MMULT(MAXPS,MAXDPS,MAXDPS,1,MAXPS,1,NPARMS,NDPTS,1,TEMP,
     1EVECT,DELTAA)
C CALCULATE VARIANCE OF OVERALL FIT and the average ratio of the
C calculated deviation relative to the expected uncertainty
      SS=0.0D0
      averel=0.0D0
      DO 100 I=1,NDPTS
      averel=averel+DABS( Y(I)-YO(I) )/WO(I)
 100     SS=SS+(Y(I)-YO(I))*(Y(I)-YO(I))
      SS=SS/(DBLE(NDPTS)-DBLE(NPARMS))
      averel=averel/NDPTS
      SDEV=DSQRT(SS)
C CALCULATE THE VARIANCE-COVARIANCE MATRIX.
      DO 110 I=1,NPARMS
         DO 110 II=1,NPARMS
 110        V(I,II)=SS*XINV(I,II)
C CHECK FOR DIVERGENCE
      IF(SS.GT.SSOLD) GO TO 1000
C RESET NO DIVERGENCE SWITCH
      IDIV=0
C THIS IS CONVERGING BUT NOT YET DONE
      SSOLD=SS
      CALL OUTPUT(Y,YO,ALPHA,KOUNT,SDEV,V,MAXDPS,MAXPS,NDPTS,NPARMS,
     1PNAMES,IQNUMS,NQNUMS,W,WO,averel)
C CORRECT ALPHAS BUT SAVE ALPHA'S AND CORRECTIONS IN CASE A DAMPENED FIT
C IS DESIRED ON NEXT CYCLE
      DO 120 I=1,NPARMS
         ASAVE(I)=ALPHA(I,1)
```

```
         DSAVE(I)=DELTAA(I,1)*0.1D0
  120 ALPHA(I,1)=ALPHA(I,1)+DELTAA(I,1)
C CHECK FOR TOO MANY ITERATIONS
      IF(KOUNT.EQ.KMAX) GO TO 1200
      KOUNT=KOUNT+1
C RE-ITERATE FOR NEW ALPHAS
      GO TO 65
C
C SECTION FOR  DIVERGENCE - WILL ATTEMPT DAMPENED FIT
C CHECK TO SEE IF DAMPENED FIT HAS BEEN ATTEMPTED ON PREVIOUS CYCLE
 1000 IF(IDIV.NE.0) GO TO 1300
      IDIV=1
      WRITE(IOUT,*)
      WRITE(IOUT,*) ' ***** CAUTION ATTEMPTING DAMPENED FIT! ***** '
      DO 1010 I=1,NPARMS
 1010    ALPHA(I,1)=ASAVE(I)+DSAVE(I)
      GO TO 65
C
C TOO MANY ITERATIONS SECTION
C
 1200 WRITE(IOUT,31) KMAX
      GO TO 1500
C
C DIVERGENT EVEN AFTER DAMPENED FIT
C
 1300 WRITE(IOUT,*) ' FIT STOPPED DUE TO DIVERGENCE EVEN THOUGH ',
     1'DAMPENED FIT HAS BEEN TRIED.'
      WRITE(IOUT,*)
C Re-correct alphas back to values prior to attempting dampened
C fit
      DO 1310 I=1,NPARMS
 1310    ALPHA(I,1)=ASAVE(I)
         CALL ASSIGN(MAXPS,ALLVAR,ALPHA,VNAMES,PNAMES,NVARS,NPARMS,
     1   IFFIT)
C
C DONE DONE DONE - ALL DONE SECTION - DONE DONE DONE
C
C CALCULATE  AND OUTPUT CORRELATION MATRIX
 1500 DO 1505 I=1,NPARMS
         DO 1505 J=1,NPARMS
 1505       CORRM(I,J)=DSQRT((V(I,J)*V(I,J))/(V(I,I)*V(J,J)))
      WRITE(IOUT,*)
      WRITE(IOUT,*) ' CORRELATION MATRIX '
      WRITE(IOUT,*)
      DO 1507 I=1,NPARMS
 1507 WRITE(IOUT,11)PNAMES(I),(CORRM(I,J),J=1,NPARMS)
      WRITE(IOUT,*)
      WRITE(IOUT,41)
      write(IOUT,*)
      CALL FDATE(tofday)
      write(IOUT,*)tofday
      write(IOUT,*)
C      DO 1510 I=1,NPARMS
C         DO 1510 J=1,NDPTS
```

```
C 1510        WRITE(IOUT,21)Y(J),ALPHA(I,1),JACOB(J,I)
C
C  Output file for asymbd7 (if requested)
      IF(IASW.EQ.0) goto 2115
      X=0.0
      YY=1.0
      Z=2.0
      A=3.0
      B=4.0
      WRITE(IAOUT,71)ALLVAR(1),X,X,ALLVAR(1)
      WRITE(IAOUT,71)ALLVAR(2),X,X,ALLVAR(2)
      WRITE(IAOUT,71)ALLVAR(3),X,X,ALLVAR(3)
      WRITE(IAOUT,71)ALLVAR(7),X,X,ALLVAR(7)
      WRITE(IAOUT,71)ALLVAR(8),X,X,ALLVAR(8)
      WRITE(IAOUT,71)ALLVAR(13),X,X,ALLVAR(13)
      WRITE(IAOUT,71)ALLVAR(14),X,X,ALLVAR(14)
      WRITE(IAOUT,71)ALLVAR(15),X,X,ALLVAR(15)
      WRITE(IAOUT,71)ALLVAR(4),Z,X,ALLVAR(4)
      WRITE(IAOUT,71)ALLVAR(5),YY,YY,ALLVAR(5)
      WRITE(IAOUT,71)ALLVAR(6),X,Z,ALLVAR(6)
      WRITE(IAOUT,71)ALLVAR(9),A,X,ALLVAR(9)
      WRITE(IAOUT,71)ALLVAR(10),Z,YY,ALLVAR(10)
      WRITE(IAOUT,71)ALLVAR(11),YY,Z,ALLVAR(11)
      WRITE(IAOUT,71)ALLVAR(12),X,A,ALLVAR(12)
      WRITE(IAOUT,71)ALLVAR(16),B,X,ALLVAR(16)
      WRITE(IAOUT,71)ALLVAR(17),A,YY,ALLVAR(17)
      WRITE(IAOUT,71)ALLVAR(18),Z,Z,ALLVAR(18)
      WRITE(IAOUT,71)ALLVAR(19),YY,A,ALLVAR(19)
      WRITE(IAOUT,71)ALLVAR(20),X,B,ALLVAR(20)
c ***** final output in TEX table format*******
 2115 if(itbl.eq.0) stop
      write(ibout,*)'\\vfill \\eject'
      write(ibout,*)'\\baselineskip=12pt'
      write(ibout,*)'\\noindent'
      write(ibout,*)'Table xxx. Your title here'
      write(ibout,*)'\\vskip 12pt'
      write(ibout,*)'$$'
      write(ibout,*)'\\table'
c234567891123456789212345678931234567894123456789523456789623456789712
      write(ibout,*)
     1'\\tablespec {\\r \\r \\r \\r \\r \\r \\r \\r \\r}'
      write(ibout,*)'\\body{'
      write(ibout,*)'\\hline'
      write(ibout,216)
      write(ibout,*)'\\hline'
      write(ibout,*)'\\hline'
      do 2000 i=1,ndpts
         resid=Y(I)-Y0(I)
         unc=W0(i)
         if(unc.ge.10.0d0) then
           iunc=unc
           write(ibout,211) (IQNUMS(I,J), J=1,6),
     1     Y(i),unc, Y0(i),resid
         endif
```

```
          if((unc.ge.1.0d0).and.(unc.lt.10.0d0)) then
            iunc=10*unc
            write(ibout,212)
     1      (IQNUMS(I,J), J=1,6), Y(i),iunc, YO(i),resid
          endif
          if((unc.ge.0.1d0).and.(unc.lt.1.0d0)) then
            iunc=100*unc
            write(ibout,213)
     1      (IQNUMS(I,J), J=1,6), Y(i),iunc, YO(i),resid
          endif
          if((unc.ge.0.01d0).and.(unc.lt.0.1d0)) then
            iunc=1000*unc
            write(ibout,214)
     1      (IQNUMS(I,J), J=1,6), Y(i),iunc, YO(i),resid
          endif
          if((unc.ge.0.001d0).and.(unc.lt.0.01d0)) then
            iunc=10000*unc
            write(ibout,215)
     1      (IQNUMS(I,J), J=1,6), Y(i), iunc, YO(i),resid
          endif
 2000 continue
          write(ibout,*)'\\hline'
          write(ibout,*)'}'
          write(ibout,*)'\\endtable'
          write(ibout,*)'$$'
  211  format('|',i2,'|',i2,'|',i2,'|',i2,'|',i2,'|',i2,'|',i2,
     1 '|',f16.0,'(',i5,')|',f16.0,'|',f5.0,'|\\end')
  212  format('|',i2,'|',i2,'|',i2,'|',i2,'|',i2,'|',i2,'|',i2,
     1 '|',f16.1,'(',i2,')|',f16.1,'|',f5.1,'|\\end')
  213  format('|',i2,'|',i2,'|',i2,'|',i2,'|',i2,'|',i2,'|',i2,
     1 '|',f16.2,'(',i2,')|',f16.2,'|',f5.2,'|\\end')
  214  format('|',i2,'|',i2,'|',i2,'|',i2,'|',i2,'|',i2,'|',i2,
     1 '|',f16.3,'(',i2,')|',f16.3,'|',f6.3,'|\\end')
  215  format('|',i2,'|',i2,'|',i2,'|',i2,'|',i2,'|',i2,'|',i2,
     1 '|',f16.4,'(',i2,')|',f16.4,'|',f7.4,'|\\end')
  216  format('|J$\'\'$|K$_P\'\'$|K$_O\'\'$|J$\'$|',
     1'K$_P\'$|K$_O\'$|Obs. (MHz)|Calc. (MHz)|O-C (MHz)|\\end')
C ************************************************************
c
    1  FORMAT(/A79,/A79,/A79/)
   11  FORMAT(1X,A15,15F8.4)
   21  FORMAT(1X,F20.10,1X,G20.10,1X,F15.5)
   31  FORMAT(1X,/' FIT STOPPED BECAUSE',I3,' ITERATIONS HAVE BEEN',
     1' COMPLETED. FIT MAY NOT',/' YET HAVE CONVERGED TO THE BEST',
     2' POSSIBLE VALUES.')
   41  FORMAT(8X,'DATA PT.',12X,'PARAMETER',12X,'DERIVATIVE')
   51  FORMAT(//' VARIABLE',15X,' FIXED AT ')
   61  FORMAT(1X,A15,3X,G20.10)
   71  FORMAT(1X,G20.10,2F4.1,G20.10)
       END
c--------------------->End of main body<-----------------
c-------------------->Called subroutines<--------------
       SUBROUTINE OUTPUT(Y,YO,ALPHA,KOUNT,SDEV,V,MAXDPS,MAXPS,NDPTS,
      1NPARMS,PNAMES,IQNUMS,NQNUMS,W,WO,averel)
```

```
      IMPLICIT REAL*8(A-H,O-Z)
      CHARACTER*15 PNAMES
C2345678911234567892123456789312345678941234567895123456789612345678971 23
      DIMENSION Y(MAXDPS),YO(MAXDPS),ALPHA(MAXPS,1),V(MAXPS,MAXPS)
      DIMENSION PNAMES(MAXPS),IQNUMS(MAXDPS,10),W(MAXDPS),WO(maxdps)
      IIN = 7
      IOUT = 8
      WRITE(IOUT,1) KOUNT
      DO 10 I=1,NPARMS
         SDA=DSQRT(V(I,I))
  10     WRITE(IOUT,11)I,PNAMES(I),ALPHA(I,1),SDA
         WRITE(IOUT,21)SDEV
         WRITE(IOUT,51)averel
         WRITE(IOUT,31)
      DO 20 I=1,NDPTS
         RESID=Y(I)-YO(I)
  20  WRITE(IOUT,41)Y(I),WO(I),W(I),YO(I),RESID,
     1 (IQNUMS(I,J),J=1,NQNUMS)
   1  FORMAT(1X,'************************************************',
     1'*****************************'
     2//' ITERATIVE CYCLE # ',I2//'  #  PNAME',20X,'VALUE',15X,
     3 'STD. DEV.')
  11  FORMAT(1X,I2,2X,A15,2X,G20.10,2X,G20.10)
  21  FORMAT(//1X,' STD. DEV. OF OVERALL FIT= ',G30.5)
  31  FORMAT(//6X,'DATA POINT',3X,' Uncert. ',1x, ' WT. ',7X,
     1 'CALC',15X,'RESID',6X,'QUANT. NOS.')
  41  FORMAT(1X,F15.4,1X,F8.3,1X,G8.2,1X,F15.4,1X,F15.4,10I3)
  51  FORMAT(1X,'Ave error relative to uncertainty = ',G30.5//)
      RETURN
      END
C
C------------------------>>>><<<<<-----------------
      SUBROUTINE ASSIGN(MAXPS,ALLVAR,ALPHA,VNAMES,PNAMES,NVARS,NPARMS,
     1IFFIT)
C SUBROUTINE TO ASSIGN THE FIT VARIABLES "ALPHA" TO THE VARIABLES USED
C IN THE FUNCTION (OR CALLED BY ) FSUB.
      IMPLICIT REAL*8(A-H,O-Z)
      CHARACTER*15 VNAMES,PNAMES
      DIMENSION VNAMES(MAXPS),PNAMES(MAXPS),ALLVAR(MAXPS),
     1ALPHA(MAXPS,1),IFFIT(MAXPS)
      NUMP=0
      DO 10 I=1,NVARS
         IF(IFFIT(I).EQ.1) THEN
            NUMP=NUMP+1
            ALLVAR(I)=ALPHA(NUMP,1)
         ENDIF
   10 CONTINUE
      RETURN
      END
c----------------------->>>>><<<<<---------------------
      SUBROUTINE MMULT(NDAR,NDAC,NDBR,NDBC,NDCR,NDCC,NAR,NAC,
     1NBC,A,B,C)
C SUBROUTINE TO POST MULTIPLY MATRIX A BY MATRIX B AND STORE THE RESULT
C IN MATRIX C. NDxR AND NDxC ARE THE DIMENSIONS IN THE MAIN PROGRAM OF
```

```
C OF THE ROW AND COLUMN OF THE x MATRIX. NAR, NAC, AND NBC ARE THE NUMBER
C OF A ROWS, A COLUMNS AND B COLUMNS TO BE MULTIPLIED. OF COURSE THE NUMBER
C OF B ROWS MUST EQUAL THE NUMBER OF A COLUMNS FOR PROPER MULTIPLICATION.
C ALSO NOTE THAT THE DIMENSION OF THE PRODUCT C IS (NAR,NBC).
      IMPLICIT REAL*8(A-H,O-Z)
      DIMENSION A(NDAR,NDAC),B(NDBR,NDBC),C(NDCR,NDCC)
      DO 10 I=1,NAR
         DO 10 J=1,NBC
            C(I,J)=0.0D0
            DO 10 K=1,NAC
               C(I,J)=C(I,J)+A(I,K)*B(K,J)
   10 CONTINUE
      RETURN
      END
C----------------------->>>>><<<<<-----------------------
      SUBROUTINE MTRXIN(MDIM,A,N)
      IMPLICIT REAL*8(A-H,O-Z)
      DIMENSION A(MDIM,MDIM),IPV(50,3)
C    INITIALIZATION
      DO 1 J=1,N
    1 IPV(J,3)=0
C    SEARCHFOR PIVOT ELEMENT
      DO 3 I=1,N
         AMAX=0.0D0
         DO 6 J=1,N
            IF(IPV(J,3)-1)7,6,7
    7       DO 5 K=1,N
               IF(IPV(K,3)-1)9,5,9
    9          IF(AMAX-DABS(A(J,K)))11,5,5
   11 IROW=J
               ICOLUM=K
               AMAX=DABS(A(J,K))
    5       CONTINUE
    6 CONTINUE
      IPV(ICOLUM,3)=IPV(ICOLUM,3)+1
      IPV(I,1)=IROW
      IPV(I,2)=ICOLUM
C    INTERCHANGE ROWS TO PUT PIVOT ELEMENT ON DIAGONAL
      IF(IROW-ICOLUM)16,17,16
   16 DO 20 L=1,N
         SWAP=A(IROW,L)
         A(IROW,L)=A(ICOLUM,L)
   20 A(ICOLUM,L)=SWAP
C    DIVIDE PIVOT ROW BY PIVOT ELEMENT
   17 PIVOT=A(ICOLUM,ICOLUM)
      A(ICOLUM,ICOLUM)=1.0D0
      DO 23 L=1,N
   23 A(ICOLUM,L)=A(ICOLUM,L)/PIVOT
C    REDUCE THE NON PIVOT ROWS
      DO 3 L1=1,N
         IF(L1-ICOLUM)26,3,26
   26    T=A(L1,ICOLUM)
         A(L1,ICOLUM)=0.0D0
         DO 29 L=1,N
```

```
   29    A(L1,L)=A(L1,L)-A(ICOLUM,L)*T
    3 CONTINUE
C   INTERCHANGE THE COLUMNS
      DO 31 I=1,N
         L=N-I+1
      IF(IPV(L,1)-IPV(L,2))34,31,34
   34    JROW=IPV(L,1)
         JCOLUM=IPV(L,2)
         DO 32 K=1,N
            SWAP=A(K,JROW)
            A(K,JROW)=A(K,JCOLUM)
            A(K,JCOLUM)=SWAP
   32    CONTINUE
   31 CONTINUE
      RETURN
      END
c
c------------------------>>>>><<<<<-----------------------
      SUBROUTINE HDIAG(A,N,NDIM,IEGEN,IORD,EIVR)
C
C A=MATRIX TO BE DIAGONALIZED
C NDIM=DIMENSION OF A
C N=DIMENSION OF SUBMATRIX TO BE DIAGONALIZED
C IEGEN=0 IF BOTH EIGENVALUES AND EIGENVECTORS ARE DESIRED
C       1 IF ONLY EIGENVALUES ARE DESIRED
C IORD=0 IF NO ORDERING OF EIGENVALUES OR VECTORS IS DESIRED
C          (ORDER IN = ORDER OUT)
C      1 IF ORDERING BY SIZE OF EIGENVALUES IS DESIRED
C EIVR=TRANSFORMATION MATRIX (MATRIX OF EIGENVECTORS)
C
C*****THIS ROUTINE USES A VARIABLE THRESHOLD JACOBI METHOD
C*****IT GIVES VERY GOOD EIGENVALUES AND EIGENVECTORS
C*****THE ROUTINE IS MUCH FASTER THAN THE OLD HDIAG ROUTINE WRITTEN
C*****AT M.I.T. THAT USES THE JACOBI METHOD BUT NOT THE VARIABLE
C*****THRESHOLD TECHNIQUE THAT IS APPLIED HERE
C MODIFIED FOR USE ON IBM PC M.S.FORTRAN BY R.BUMGARNER- AUG. '85.
      IMPLICIT REAL*8(A-H,O-Z)
      DIMENSION A(NDIM,NDIM),EIVR(NDIM,NDIM)
      IF(N.GT.0) GOTO 1
      EIVR(1,1)=1.0
      RETURN
    1 IF(IEGEN.GT.0) GOTO 102
      DO 101 J=1,N
      DO 100 I=1,N
  100 EIVR(I,J)=0.0
  101 EIVR(J,J)=1.0

C        FIND THE ABSOLUTELY LARGEST ELEMENT OF A

  102 ATOP=0.
      DO 111 I=1,N
      DO 111J=I,N
      IF(ATOP.GE.ABS(A(I,J))) GOTO 111
      ATOP=ABS(A(I,J))
```

```
  111 CONTINUE
      IF(ATOP)109,109,113
  109 RETURN

C        CALCULATE THE STOPPING CRITERION -- DSTOP

  113 AVGF=FLOAT(N*(N-1))*.55
      D=0.0
      DO 114 JJ=2,N
      DO 114 II=2,JJ
      S=A(II-1,JJ)/ATOP
  114 D=S*S+D
      DSTOP=(1.E-06)*D

C        CALCULATE THE THRESHOLD, THRSH
C
      THRSH = SQRT(D/AVGF)*ATOP
C
C        START A SWEEP
C
  115 IFLAG=0
      DO 130 JCOL=2,N
      JCOL1=JCOL-1
      DO 130 IROW=1,JCOL1
      AIJ=A(IROW,JCOL)
C
C        COMPARE THE OFF-DIAGONAL ELEMENT WITH THRSH
C
      IF(ABS(AIJ).LE.THRSH) GOTO 130
      AII=A(IROW,IROW)
      AJJ=A(JCOL,JCOL)
      S=AJJ-AII
C
C        CHECK TO SEE IF THE CHOSEN ROTATION IS LESS THAN THE ROUNDING ERROR.
C        IF SO , THEN DO NOT ROTATE.
C
      IF(ABS(AIJ).LE.(1.0E-09*ABS(S))) GOTO 130
      IFLAG=1
C
C        IF THE ROTATION IS VERY CLOSE TO 45 DEGREES, SET SIN AND COS
C        TO 1/(ROOT 2).
C
      IF((1.0E-10*ABS(AIJ)).LT.ABS(S)) GOTO 116
      S=.707106781
      C=S
      GO TO 120
C
C        CALCULATION OF SIN AND COS FOR ROTATION THAT IS NOT VERY CLOSE
C        TO 45 DEGREES
C
  116 T=AIJ/S
      S=0.25/SQRT(0.25+T*T)
C
C        COS = C ,  SIN= S
```

```
C
      C=SQRT(0.5+S)
      S=2.*T*S/C
C
C        CALCULATION OF THE NEW ELEMENTS OF MATRIX A
C
  120 DO 121 I=1,IROW
      T=A(I,IROW)
      U=A(I,JCOL)
      A(I,IROW)=C*T-S*U
  121 A(I,JCOL)=S*T+C*U
      I2=IROW+2
      IF(I2.GT.JCOL) GOTO 123
      CONTINUE
      DO 122 I=I2,JCOL
      T=A(I-1,JCOL)
      U=A(IROW,I-1)
      A(I-1,JCOL)=S*U+C*T
  122 A(IROW,I-1)=C*U-S*T
  123 A(JCOL,JCOL)=S*AIJ+C*AJJ
      A(IROW,IROW)=C*A(IROW,IROW)-S*(C*AIJ-S*AJJ)
      DO 124 J=JCOL,N
      T=A(IROW,J)
      U=A(JCOL,J)
      A(IROW,J)=C*T-S*U
  124 A(JCOL,J)=S*T+C*U
C
C        ROTATION COMPLETED.
C        SEE IF EIGENVECTORS ARE WANTED BY USER
C
      IF(IEGEN.GT.0) GOTO 126
      DO 125 I=1,N
      T=EIVR(I,IROW)
      EIVR(I,IROW)=C*T-EIVR(I,JCOL)*S
  125 EIVR(I,JCOL)=S*T+EIVR(I,JCOL)*C
C
C        CALCULATE THE NEW NORM D AND COMPARE WITH DSTOP
C
  126 CONTINUE
      S=AIJ/ATOP
      D=D-S*S
      IF(D.GE.DSTOP) GOTO 129
C
C        RECALCULATE DSTOP AND THRSH TO DISCARD ROUNDING ERRORS
C
      D=0.
      DO 128 JJ=2,N
      DO 128 II=2,JJ
      S=A(II-1,JJ)/ATOP
  128 D=S*S+D
      DSTOP=(1.E-06)*D
  129 THRSH=SQRT(D/AVGF)*ATOP
  130 CONTINUE
      IF(IFLAG.NE.0) GOTO 115
```

```
C
C     ARRANGE THE EIGENVALUES IN THE ORDER OF INCREASING ENERGY.
C     ARRANGE THE EIGENVECTORS IN THE SAME ORDER.
C
      IF(IORD.EQ.0) RETURN
      NU=N
      DO 11 I=1,N
      IF(I.GE.NU)    RETURN
      AMIN=A(I,I)
      DO 10 J=I,NU
      IF(A(J,J).GE.AMIN)    GO TO 10
C     IF IEGEN IS -1,EXCUDE UNCONVERGED EIGENVALUES FROM THIS ORDERING.
      TE=ABS(EIVR(N,J))+ABS(EIVR(N-1,J))
      IF((TE.GT..05).AND.(IEGEN.EQ.-1))   GO TO 15
      II=I
      AMIN =A(J,J)
      A(J,J)=A(I,I)
      A(I,I)=AMIN
 16   DO 12 K=1,N
      TEMP=EIVR(K,II)
      EIVR(K,II)=EIVR(K,J)
 12   EIVR(K,J)=TEMP
      GO TO 10
 15   AM=A(J,J)
      A(J,J)=A(NU,NU)
      A(NU,NU)=AM
      II=NU
      NU=NU-1
      GO TO 16
 10   CONTINUE
 11   CONTINUE
      RETURN
      END
c-------------------------------->>> FSUB <<<<-----------
c This subroutine may be used to fit transitions from ground state to
c Coriolis coupled upper states.  It can be easily modified to make it
c work for more than one ground states and/or more than two upper states.
c Written by Sakae Suzuki, in attempt to fit ArD2O data. June 21, 1990.
      subroutine fsub(maxps,maxdps,ndpts,nparms,
     1                      allvar,y,iqnums,ifcmhz,jmax)
      implicit real*8(a-h,o-z)
      real*8 lg,ls,lp
      dimension allvar(maxps),y(maxdps),eivr(100,100),
     1          iqnums(maxdps,10),h(100,100)
c The quantum numbers entered are
c     j(grd.st.), 0=sig or 1 =pi, j(upp.st.)
cFollowing distortion const.'s are used.
      bg=allvar(1)
      dg=allvar(2)
      hg=allvar(3)
      lg=allvar(4)
      vs=allvar(5)
      bs=allvar(6)
      ds=allvar(7)
```

```
      hs=allvar(8)
      ls=allvar(9)
      vp=allvar(10)
      bp=allvar(11)
      dp=allvar(12)
      hp=allvar(13)
      lp=allvar(14)
      vpm=allvar(10)
      bpm=allvar(11)
      dpm=allvar(17)
      hpm=allvar(18)
      lpm=allvar(19)
      beta=allvar(20)
c Make the matrix to be diagonalized
      z=0.0d0
      do 15 i=1, 2*jmax+2
        do 10 j=1, 2*jmax+2
   10     h(i,j)=z
   15     continue
c First make the sigma state block matrix
      do 20 j=1,jmax+1
      xj=dble(j-1)
      one=1.0d0
      h(j,j)=vs+bs*xj*(xj+one)-ds*(xj*(xj+one))**2+hs*(xj*(xj+one))**3
     1         +ls*(xj*(xj+one))**4
      h(j,jmax+1+j)=beta*(dsqrt(xj*(xj+one)))
c Next, make the pi state block matrix
        h(jmax+1+j,j)=h(j,jmax+1+j)
   20 h(jmax+1+j,jmax+1+j)=vp+bp*(xj*(xj+one)-one)-dp*(xj*(xj+one)-one)**2
     1         +hp*(xj*(xj+one)-one)**3+lp*(xj*(xj+one)-one)**4
c Done making the matrix
c Get the matrix diagonalized using hdiag.
      ndim=100
      msize=jmax*2+2
      iegen=1
      iord=0
      call hdiag(h,msize,ndim,iegen,iord,eivr)
c Now calculate y using the diagonalized matrix.
      do 100 i=1,ndpts
c calculate ground state energy, gse
         j=iqnums(i,1)
         xj=dble(j)
         gse=bg*xj*(xj+one)-dg*(xj*(xj+one))**2+hg*(xj*(xj+one))**3
     1       +lg*(xj*(xj+one))**4
c calculate transition energy for pi- states
         if (iqnums(i,2).eq.2) then
            j=iqnums(i,3)
            xj=dble(j)
            ae=vpm+bpm*(xj*(xj+one)-one)-dpm*(xj*(xj+one)-one)**2
     1        +hpm*(xj*(xj+one)-one)**3+lpm*(xj*(xj+one)-one)**4
            y(i)=dabs(ae-gse)
            goto 100
         end if
c calculate transition energy for pi+ states
```

```
        j=iqnums(i,3)
        if (iqnums(i,2).eq.1) then
                              j=jmax+2+j
                              else
                              j=j+1
        end if
c i.e., if the level is pi, then values from the second block of the
c matrix must be used.
        y(i)=dabs(h(j,j)-gse)
  100   continue
      return
      end
```

The following is a sample input file used to fit the Ar-DOH $\Sigma^+ \rightarrow \Pi^{+/-}$ transitions. The descriptions of the input items are given in as comments in the code above and as comments to the right in the input file below.

```
'ArDOH SIGMA+ -> PI+/-'          | title
''                               | title
''                               | title
7                                | number of iterations
20                               | number of variables
1                                | 1 indicates that the units are in MHz
'BG  ', 6136.44,'P',1.0E-4,0     | BG=Variable name, 6136.44=value
'DG  ', 0.034273,'P',1.0E-4,0    | 'P'=proportional variable change
'HG  ',0.0,'P',1.0E-4,0          | 1.0E-4.0=proportionality of change
'LG  ', 0.0       ,'P',1.0E-4,0 | 0 since BG is not fit in this run,
'VS  ', 640000.0,'P',1.0E-4,1    | 1 if it is fit in this run.
'BS  ', 6100,'P',1.0E-4,1
'DS  ', 0.03,'P',1.0E-4,1
'HS  ', 0.0 ,'P',1.0E-4,0
'LS  ',0.0,'P',1.0E-4,0
'VP  ', 604911.6,'P',1.0E-4,0
'BP  ', 2889.944,'P',1.0E-4,0
'DP  ',0.087,'P',1.0E-4,0
'HP  ',-1.595540295e-5,'P',1.0E-4,0
'LP  ',0.0,'P',1.0E-4,0
'vpm ',630000.0,'P',1.0e-4,0
'bpm ',6100.0,'P',1.0e-4,0
'dpm ',0.03,'P',1.0e-4,0
'hpm ',0.0,'P',1.0e-4,0
'lpm ',0.0,'P',1.0e-4,0
'BETA ',000.0,'F',1.0,0
14,3                          | Data entries, quantum numbers.
731150.74,6,0,7,1,1           | Data point, three quantum numbers,
718857.34,5,0,6,1,1           | weighting factor, uncertainty.
706556.4,4,0,5,1,1
694247.88,3,0,4,1,1
681943.38,2,0,3,1,1
669638.42,1,0,2,1,1
```

```
657337.9,0,0,1,1,1
620488.8,2,0,1,1,1
608227.16,3,0,2,1,1
595977.02,4,0,3,1,1
583737.9,5,0,4,1,1
571512.06,6,0,5,1,1
547085.88,8,0,7,1,1
534884.66,9,0,8,1,1
```

FSUB for the benzene-water microwave data

The benzene-water ground state data were fit using an asymetric top program, but the result indicated that the complex behaved as a symmetric top. The following is the FSUB subroutine used to fit asymetric top microwave data.

```
      SUBROUTINE FSUB(MAXPS,MAXDPS,NDPTS,NPARMS,ALLVAR,Y,IQNUMS)
      IMPLICIT REAL*8(A-H,O-Z)
      INTEGER EINDEX,OFFSET
      DIMENSION ALLVAR(MAXPS),Y(MAXDPS),IQNUMS(MAXDPS,10)
      DIMENSION E(2602)
      AEFF=ALLVAR(1)
      BEFF=ALLVAR(2)
      CEFF=ALLVAR(3)
      DELTJ=ALLVAR(4)
      DELTJK=ALLVAR(5)
      DELTK=ALLVAR(6)
      DELJ=ALLVAR(7)
      DELK=ALLVAR(8)
      HJ=ALLVAR(9)
      HJK=ALLVAR(10)
      HKJ=ALLVAR(11)
      HK=ALLVAR(12)
      SHJ=ALLVAR(13)
      SHJK=ALLVAR(14)
      SHK=ALLVAR(15)
      XLJ=ALLVAR(16)
      XLJJK=ALLVAR(17)
      XLJK=ALLVAR(18)
      XLKKJ=ALLVAR(19)
      XLK=ALLVAR(20)
      JMIN=51
      JMAX=0
      DO 10 I=1,NDPTS
          IF(JMIN.GT.IQNUMS(I,1)) JMIN=IQNUMS(I,1)
          IF(JMIN.GT.IQNUMS(I,4)) JMIN=IQNUMS(I,4)
          IF(JMAX.LT.IQNUMS(I,1)) JMAX=IQNUMS(I,1)
   10     IF(JMAX.LT.IQNUMS(I,4)) JMAX=IQNUMS(I,4)
      IF(JMIN.LT.1) JMIN=1
      OFFSET=(JMIN)*(JMIN)-1
C      WRITE(*,*) ' CALLING DASYME '
      CALL DASYME(JMIN,JMAX,AEFF,BEFF,CEFF,DELTJ,DELTJK,
     1DELTK,DELJ,DELK,HJ,HJK,HKJ,HK,SHJ,SHJK,SHK,
     2XLJ,XLJJK,XLJK,XLKKJ,XLK,E,ME)
      DO 20 I=1,NDPTS
         J=IQNUMS(I,1)
         KP=IQNUMS(I,2)
         KO=IQNUMS(I,3)
         EINDEX=(J+1)**2-J+KP-KO-OFFSET
         EG=E(EINDEX)
         J=IQNUMS(I,4)
         KP=IQNUMS(I,5)
```

```
         KO=IQNUMS(I,6)
         EINDEX=(J+1)**2-J+KP-KO-OFFSET
         EU=E(EINDEX)
   20    Y(I)=DABS(EU-EG)
      RETURN
      END
      SUBROUTINE DASYME(JMIN,JMAX,AEFF,BEFF,CEFF,DELTJ,DELTJK,
     1DELTK,XELJ,XELK,HJ,HJK,HKJ,HK,XHJ,XHJK,XHK,
     2XLJ,XLJJK,XLJK,XLKKJ,XLK,E,ME)
      IMPLICIT REAL*8(A-H,O-Z)
      DIMENSION H(102,102),EIVR(102,102),E(2602)
C SUBROUTINE TO CALCULATE ENERGIES OF NON-RIGID ASYMMETRIC TOPS USING
C WATSON'S DISTORTION PARAMETERS. FOR SPECIFIC METHOD USED SEE:
C WATSON, J. CHEM. PHYS., VOL.48,4517 (1968) , " VIBRATIONAL SPECTRA
C AND STRUCTURE", EDITED BY DURIG,SECTION BY WATSON . THE MATRIX
C ELEMENTS ARE TAKEN FROM COOK,DE LUCIA AND HELMINGER, J. MOL. SPECT.,
C VOL 41,123-136,(1972) WITH THE FOLLOWING CHANGES TO MAKE THEM CONSISTENT
C WITH WATSON'S  A-REDUCED HAMILTONIAN. *****ALL SMALL H'S AND SMALL
C DELTA'S ARE REVERSED IN SIGN ****** ! I.E. THIS PROGRAM IS CORRECT FOR
C WATSON'S A-REDUCED HAMILTONIAN. TO MAKE IT CONSISTENT WITH COOK ET.AL.,
C REVERSE THE SIGNS OF THEIR SMALL H'S AND SMALL DELTA'S BEFORE INPUT.
C (ABC)EFF ARE THE EFFECTIVE ROTATIONAL CONSTANTS (SCRIPT IN COOK'S TEXT).
C DELT(J,JK,K) ARE THE CAP DELTAS WHILE DEL(J,K) ARE THE SMALL DELTAS.
C H(J,JK,KJ,K) ARE THE CAP H'S WHILE SH(J,JK,K) ARE THE SMALL H'S.
C H IS THE MATRIX USED FOR THE HAMILTONIAN SIZED FOR JMAX=40
C EIVR IS THE CORRESPONDING EIGENVECTOR MATRIX. E IS THE MATRIX WHERE
C THE ENERGIES ARE STORED AFTER CALCULATION.
C ROGER BUMGARNER 5/6/87
      NDIM=102
      IEGEN=1
      IORD=1
C FILL-IN MATRIX OF ENERGIES AND QUANTUM NOS W/  0(0,0) VALUE AND
C INITIALIZE MATRICES
      DO 2 I=1,NDIM
         DO 2 II=1,NDIM
            EIVR(I,II)=0.0D0
   2  H(I,II)=0.0D0
      DO 3 I=1,2602
   3     E(I)=0.0D0
C ME IS THE INDEX USED FOR STORING THE ENERGIES IN E.
      ME=1
      IF (JMAX.GT.50) THEN
         WRITE (*,*) 'VALUE OF JMAX EXCEEDS THE MAXIMUM VALUE FOR THE '
         WRITE (*,*) 'CURRENT DIMENSIONS OF THE MATRICES. JMAX SET=50 '
         JMAX=50
      ENDIF
      IF(JMIN.LE.0) JMIN=1
      XKAPPA=(2.0D0*BEFF-AEFF-CEFF)/(AEFF-CEFF)
C PROLATE TOP CASE
      IF (XKAPPA.LT.0.0D0) THEN
         XR=BEFF
         YR=CEFF
         ZR=AEFF
      ENDIF
```

```
C OBLATE TOP CASE
      IF (XKAPPA.GE.0.0D0) THEN
         XR=AEFF
         YR=BEFF
         ZR=CEFF
      ENDIF
C MATRIX ELEMENTS IN HAMIL ARE WRITTEN IN COOK'S FORM SO WILL
C CORRECT CONSTANTS TO A-REDUCED FORM RATHER THAN SCREWING WITH
C PREVIOUSLY WRITTEN "GOOD" CODE
      DELJ=-XELJ
      DELK=-XELK
      SHJ=-XHJ
      SHJK=-XHJK
      SHK=-XHK
C  J-LOOP
      DO 50 J=JMIN,JMAX
         NUMKS=2*J+1
         M=0
C INITIALIZE (OR RE-INITIALZE) H MATRIX TO ZERO'S. M=IS MATRIX INDEX
C TO BE USED FOR VALUES OF K
         DO 5 I=1,NUMKS
            DO 4 II=1,NUMKS
               H(I,II)=0.0D0
   4        CONTINUE
   5     CONTINUE
C  K-LOOP
         DO 20 IK=1,NUMKS
            K=IK-J-1
            M=M+1
            MP=M-1
C  KPRIME-LOOP
            DO 10 IKP=IK,NUMKS
               KP=IKP-J-1
               MP=MP+1
               H(M,MP)=AHAMIL(XR,YR,ZR,DELTJ,DELTJK,
     1         DELTK,DELJ,DELK,HJ,HJK,HKJ,HK,SHJ,SHJK,SHK,
     2         XLJ,XLJJK,XLJK,XLKKJ,XLK,J,K,KP)
               H(MP,M)=H(M,MP)
C END K' LOOP
  10        CONTINUE
C END K-LOOP
  20     CONTINUE
         CALL HDIAG(H,NUMKS,NDIM,IEGEN,IORD,EIVR)
C NOTE: EIGENVALUES COME BACK ORDERED, SO KP AND KO ASSIGNMENTS CAN
C BE MADE ON THE BASIS OF THIS ORDERING.
         DO 30 IK=1,NUMKS
            ME=ME+1
            E(ME)=H(IK,IK)
  30     CONTINUE
C END J-LOOP
  50  CONTINUE
      RETURN
      END
      FUNCTION AHAMIL(XR,YR,ZR,DELTJ,DELTJK,
```

```
     1DELTK,DELJ,DELK,HJ,HJK,HKJ,HK,SHJ,SHJK,SHK,
     2XLJ,XLJJK,XLJK,XLKKJ,XLK,J,K,KP)
      IMPLICIT REAL*8(A-H,O-Z)
      AHAMIL=0.0D0
      KCHK=IABS(K-KP)
      IF( (KCHK.NE.2).AND.(K.NE.KP) ) RETURN
      SXY=0.5D0*(XR+YR)
C DIAGONAL TERMS
      IF(K.EQ.KP) AHAMIL=SXY*P(1,J)+(ZR-SXY)*PZ(1,K)-DELTJ*P(2,J)-
     1DELTJK*PPZ(1,1,J,K)-DELTK*PZ(2,K)+HJ*P(3,J)+HJK*PPZ(2,1,J,K)+
     2HKJ*PPZ(1,2,J,K)+HK*PZ(3,K)+XLJ*P(4,J)+XLJJK*PPZ(3,1,J,K)+
     3XLJK*PPZ(2,2,J,K)+XLKKJ*PPZ(1,3,J,K)+XLK*PZ(4,K)
C OFF DIAGONAL BY TWO TERMS
      IF(KCHK.EQ.2) THEN
         B0=(XR-YR)/(2.0D0*ZR-XR-YR)
         AHAMIL=(ZR-SXY)*(-B0*PPM(0,J,K))-2.0D0*DELJ*PPM(1,J,K)-
     1   DELK*PPZPM(0,1,J,K)+2.0D0*SHJ*PPM(2,J,K)+SHJK*
     2   PPZPM(1,1,J,K)+SHK*PPZPM(0,2,J,K)
      ENDIF
      RETURN
      END
C FUNCTIONS TO CALCULATE MATRIX ELEMENTS OF ANG. MOM. OPERATORS
C (P**2N)*(PZ**2M)
      FUNCTION PPZ(N,M,J,K)
      IMPLICIT REAL*8(A-H,O-Z)
      XJ=J
      XK=K
      PPZ=((XJ*(XJ+1.0D0))**N)*XK**(2*M)
      RETURN
      END
C (P**2N)*(PMINUS**2)
      FUNCTION PPM(N,J,K)
      IMPLICIT REAL*8(A-H,O-Z)
      XJ=J
      PPM=-0.5D0*(XJ*(XJ+1))**N*FPLS(J,K)
      RETURN
      END
C FPLUS FUNCTION
      FUNCTION FPLS(J,K)
      IMPLICIT REAL*8(A-H,O-Z)
      J1=J*(J+1)
      K1=K*(K+1)
      K2=(K+1)*(K+2)
      XJ1=J1
      XK1=K1
      XK2=K2
      FPLS=DSQRT((XJ1-XK1)*(XJ1-XK2))
      RETURN
      END
C (P**2N)*(PZ**2M)*PMINUS**2
      FUNCTION PPZPM(N,M,J,K)
      IMPLICIT REAL*8(A-H,O-Z)
      XJ=J
      XK=K
```

```
      PPZPM=-0.5D0*(XJ*(XJ+1.0D0))**N*(XK**(2*M)+(XK+2.0D0)**(2*M))*
     1 FPLS(J,K)
      RETURN
      END
C P**2N
      FUNCTION P(N,J)
      IMPLICIT REAL*8(A-H,O-Z)
      XJ=J
      P=(XJ*(XJ+1.0D0))**N
      RETURN
      END
C PZ**2M
      FUNCTION PZ(M,K)
      IMPLICIT REAL*8(A-H,O-Z)
      XK=K
      PZ=XK**(2*M)
      RETURN
      END
```

The following is a sample input file used to fit the benzene-water microwave data. Not all 68 data points are listed.

```
' FIT OF Benzene Water Spectrum '
' '
' '
15
15
'A      ',2809.0,'F',0.00001,0
'B      ',1994.85,'F',0.0000001,1
'C      ',1994.81,'F',0.0000001,1
'DELTJ ',0.358000237E-02,'F',0.00000001,1
'DELTJK',0.3791584325E-01,'F',0.00000001,1
'DELTK ',0.0,'F',0.001,0
'delJ  ',0.0,'F',0.001,0
'delK  ',0.0,'F',0.001,0
'HJ    ',0.0,'F',0.000001,0
'HJK   ',0.0,'F',0.000001,0
'HKJ   ',0.0,'F',0.000001,0
'HK    ',0.0,'F',0.000001,0
'hJ    ',0.0,'F',0.000001,0
'hJK   ',0.0,'F',0.000001,0
'hK    ',0.0,'F',0.000001,0
68,6           |68 data points, 6 quantum numbers
39834.082,10,8,2,9,8,1,1.0,1.0    |This data list is truncated and do not
39834.082,10,8,3,9,8,2,1.0,1.0    |contain all 68 data points.
39845.2,10,7,3,9,7,2,1.0,1.0
39845.2,10,7,4,9,7,3,1.0,1.0
39854.996,10,6,4,9,6,3,1.0,1.0
39854.996,10,6,5,9,6,4,1.0,1.0
39863.36,10,5,5,9,5,4,1.0,1.0
```

```
39863.36,10,5,6,9,5,5,1.0,1.0
39870.20,10,4,6,9,4,5,1.0,1.0
39870.20,10,4,7,9,4,6,1.0,1.0
39875.52,10,3,7,9,3,6,1.0,1.0
            .
            .
            .
```

FSUB for the benzene-water FIR data

The benzene-water VRT band was fit to a Hamiltonian that included l-type doubling and a symmetric top hamiltonian for the ground and upper state. The following is the FSUB subroutine used for fitting the benzene-water 19.5 cm^{-1} VRT transition.

```
      SUBROUTINE FSUB(MAXPS,MAXDPS,NDPTS,NPARMS,ALLVAR,Y,IQNUMS)
      IMPLICIT REAL*8(A-H,O-Z)
c     INTEGER EINDEX,OFFSET
      DIMENSION ALLVAR(MAXPS),Y(MAXDPS),IQNUMS(MAXDPS,10)
      AEFF=ALLVAR(1)
      BEFF=ALLVAR(2)
      CEFF=ALLVAR(3)
C THIS TAKES CARE OF THE CASE WHEN WE HAVE PROLATE TOP
      DJ=ALLVAR(4)
      DJK=ALLVAR(5)
      DK=ALLVAR(6)
C HERE WE START THE FIRST UPPER STATE CONSTANTS
      AEFFu=ALLVAR(7)
      BEFFu=ALLVAR(8)
      CEFFu=ALLVAR(9)
      zeta=ALLVAR(10)
      evib=ALLVAR(11)
      DJl=ALLVAR(12)
      DJu=ALLVAR(13)
      DJKl=ALLVAR(14)
      DJKu=ALLVAR(15)
      xHJl=ALLVAR(16)
      xHJu=ALLVAR(17)
      xHJJKl=ALLVAR(18)
      xHJJKu=ALLVAR(19)
      DKl=ALLVAR(20)
      DKu=ALLVAR(21)
      xHJKKl=ALLVAR(22)
      xHJKKu=ALLVAR(23)
c
cHere we start the calculation of the symmetric top
      DO 10 I=1,NDPTS
c**first calculate the lower state(ground state) energy
xl=iqnums(I,1)
xj=iqnums(I,2)
xk=iqnums(I,3)
xm=iqnums(I,4)
EV=0.0d0
xm=0.0d0
xHJKK=0.0d0
xHJ=0.0d0
xHJJK=0.0d0
c
        EG=energy(AEFF,BEFF,DJ,DJK,
     1zeta,xHJ,xHJJK,DK,xHJKK,
     1EV,xl,xj,xk)
```

```
c**second, calculate the upper state (vibration with l-type) energy
xl=iqnums(I,5)
xj=iqnums(I,6)
xk=iqnums(I,7)
xm=iqnums(I,8)
xm=0.0d0
        EV=evib
xq=2.0d0*BEFFu**2/evib
c
if(xl.lt.0.0d0) then
EU=energy(AEFFu,BEFFu,DJu,DJKu,
     1zeta,xHJu,xHJJKu,DKu,xHJKKu,
     1EV,xl,xj,xk)
xpee=pee(xj,xk,xl,zeta,AEFFu,BEFFu,xq)
else
EU=energy(AEFFu,BEFFu,DJl,DJKl,
     1zeta,xHJl,xHJJKl,DKl,xHJKKl,
     1EV,xl,xj,xk)
if(xk.eq.1.0d0) then
xpee=xl*0.5d0*xj*(xj+1)*xq
else
xpee=pee(xj,xk,xl,zeta,AEFFu,BEFFu,xq)
endif
endif
EU=EU+xpee
Y(I)=dabs(EU-EG)
   10 continue
      RETURN
      END
c*******************************
      FUNCTION energy(AEFF,BEFF,DJ,DJK,
     1zeta,xHJ,xHJJK,DK,xHJKK,
     1EV,xl,xj,xk)
      IMPLICIT REAL*8(A-H,O-Z)
C Only symmetric top is admissible in this program.
      energy=EV+(BEFF-DJK*xk**2)*xj*(xj+1.0d0)+(AEFF-BEFF)*xk**2
     1       -DJ*xj**2*(xj+1.0d0)**2
     1       -xHJ*xJ**3*(xJ+1.0d0)**3-xHJJK*xJ**2*(xJ+1)**2*xK**2
     1       -xHJKK*xJ*(xJ+1)*xK**4
     1       -2.0d0*zeta*AEFF*xk*xl-DK*xK**4
     1       +2.0d0*((2.0d0*DJ+DJK)*xj*(xj+1)
     1       +(2.0d0*DK+DJK)*xK**2)*xK*xl*zeta
      RETURN
      END
c******************
FUNCTION pee(xj,xk,xl,zeta,AEFF,BEFF,q)
IMPLICIT REAL*8(A-H,O-Z)
sign=xl*xk
zero=0.0d0
if(sign.lt.zero) then
sign=-1.0d0
else
sign=1.0d0
endif
```

```
quotient=8.0d0*(xk-sign)*((1-(zeta))*AEFF-BEFF)
pee=sign*(xj*(xj+1)-xk*(xk-sign))*(xj*(xj+1)-
     1(xk-sign)*(xk-sign*2.0d0))*q**2
pee=pee/quotient
RETURN
END
```

The following is a sample input file used to fit the benzene-water FIR data.

```
' bw fit using ljkldep.f '
' assume symmetric top, and l-type doubling  '
' '
6
23
'A      ',2736.863866,'F',0.00001,1
'B      ',1912.063781,'F',0.0000001,1
'C      ',0.0,'F',0.0000001,0
'DJ     ',0.4908498237E-02,'F',0.0001,1
'DJK    ',0.3999750214E-01,'F',0.0001,1
'DK     ',0.0,'F',0.0001,1
'AU     ',2720.661331,'F',0.0001,1
'BU     ',1872.530593,'F',0.0001,1
'CU     ',0.0,'F',0.001,0
'zeta   ',0.87549,'F',0.001,0
'evib   ',581141.8353,'F',0.01,1
'DJL    ',-0.2614592159E-01,'F',0.00001,1
'DJU    ',0.9377751027E-02,'F',0.00001,1
'DJKL   ',-0.6489334815,'F',0.001,1
'DJKU   ',0.2852940657,'F',0.001,1
'HJl    ',0.00,'F',0.0001,0
'HJu    ',0.0,'F',0.001,0
'HJJKl  ',0.0,'F',0.00001,0
'HJJKu  ',0.0,'F',0.00001,0
'DKl    ',3.665586141,'F',0.001,1
'DKu    ',4.087836510,'F',0.00001,1
'HJKKl  ',0.0,'F',0.000001,0
'HJKKu  ',0.0,'F',0.000001,0
75,8
583280.000, 0, 2, 2, 0,-1, 2, 1, 0, 1.0, 1.0
583035.000, 0, 3, 2, 0,-1, 3, 1, 0, 1.0, 1.0
582709.000, 0, 4, 2, 0,-1, 4, 1, 0, 1.0, 1.0
582306.000, 0, 5, 2, 0,-1, 5, 1, 0, 1.0, 1.0
581824.000, 0, 6, 2, 0,-1, 6, 1, 0, 1.0, 1.0
581264.000, 0, 7, 2, 0,-1, 7, 1, 0, 1.0, 1.0
575796.000, 0, 2, 2, 0,-1, 1, 1, 0, 1.0, 1.0
571809.000, 0, 3, 2, 0,-1, 2, 1, 0, 1.0, 1.0
567741.000, 0, 4, 2, 0,-1, 3, 1, 0, 1.0, 1.0
563593.000, 0, 5, 2, 0,-1, 4, 1, 0, 1.0, 1.0
559368.000, 0, 6, 2, 0,-1, 5, 1, 0, 1.0, 1.0
```

FSUB for the $(D_2O)_3$ data

The $(D_2O)_3$ data obtained at Caltech was combined with the 98 cm^{-1} band obtained by Saykally group to obtain a fit. The following FSUB subroutine was used to simultaneously fit the two bands with a common ground state.

```
      SUBROUTINE FSUB(MAXPS,MAXDPS,NDPTS,NPARMS,ALLVAR,Y,IQNUMS)
      IMPLICIT REAL*8(A-H,O-Z)
      INTEGER EINDEX,OFFSET
      DIMENSION ALLVAR(MAXPS),Y(MAXDPS),IQNUMS(MAXDPS,10)
      DIMENSION E(2602),EL(2602),EUU(2602)
      AEFF=ALLVAR(1)
      BEFF=ALLVAR(2)
      if (AEFF.EQ.0.0D0) AEFF=BEFF
c this takes care of the case when we deal with A=B, oblate top
c which D20 trimer is.
      CEFF=ALLVAR(3)
      IF (CEFF.EQ.0.0D0) CEFF=BEFF
C THIS TAKES CARE OF THE CASE WHEN WE HAVE PROLATE TOP
      DELTJ=ALLVAR(4)
      DELTJK=ALLVAR(5)
      DELTK=ALLVAR(6)
C HERE WE START THE FIRST UPPER STATE CONSTANTS
      AEEFU=ALLVAR(7)
      BEFFU=ALLVAR(8)
      if (AEFFU.EQ.0.0D0) AEFFU=BEFFU
      CEFFU=ALLVAR(9)
      IF (CEFFU.EQ.0.0D0) CEFFU=BEFFU
      DELTJU=ALLVAR(10)
      DELTJKU=ALLVAR(11)
      DELTKU=ALLVAR(12)
C EUP IS THE VIBRATIONAL ENERGY FOR THE FIRST UPPER STATE
      EUP=ALLVAR(13)
C EU2 IS THE VIBRATIONAL ENERGY FOR THE SECOND UPPER STATE
      EU2=ALLVAR(14)
C HERE WE START THE SECOND UPPER STATE CONSTANTS
      AEFF2=ALLVAR(15)
      BEFF2=ALLVAR(16)
      CEFF2=ALLVAR(17)
      IF (AEFF2.EQ.0.0D0) AEFF2=BEFF2
      IF (CEFF2.EQ.0.0D0) CEFF2=BEFF2
      DELTJ2=ALLVAR(18)
      DELTJK2=ALLVAR(19)
      DELTK2=ALLVAR(20)
      ELO=0.0D0
C  JUST TO MAKE THE FUNCTION CALLING HAPPY, WE NEED TO DEFINE THE
C FOLLOWING TERMS
      DELJ=0.0D0
      DELK=0.0D0
      HJ=0.0D0
      HJK=0.0D0
      HKJ=0.0D0
```

```
      HK=0.0D0
      SHJ=0.0D0
      SHJK=0.0D0
      SHK=0.0D0
      XLJJK=0.0D0
      XLJK=0.0D0
      XLKKJ=0.0D0
      XLK=0.0D0
      JMIN=51
      JMAX=0
      DO 10 I=1,NDPTS
          IF(JMIN.GT.IQNUMS(I,2)) JMIN=IQNUMS(I,2)
          IF(JMIN.GT.IQNUMS(I,6)) JMIN=IQNUMS(I,6)
          IF(JMAX.LT.IQNUMS(I,2)) JMAX=IQNUMS(I,2)
   10     IF(JMAX.LT.IQNUMS(I,6)) JMAX=IQNUMS(I,6)
      IF(JMIN.LT.1) JMIN=1
      OFFSET=(JMIN)*(JMIN)-1
C      WRITE(*,*) ' CALLING DASYME '
C FIRST CALCULATE THE ENERGY LEVEL FOR GROUND STATE, EL
      CALL DASYME(JMIN,JMAX,AEFF,BEFF,CEFF,DELTJ,DELTJK,
     1DELTK,DELJ,DELK,HJ,HJK,HKJ,HK,SHJ,SHJK,SHK,
     2ELO,XLJJK,XLJK,XLKKJ,XLK,EL,ME)
C SECOND, CALCULATE THE ENERGY LEVEL FOR THE FIRST UPPER STATE
C E.
      CALL DASYME(JMIN,JMAX,AEFFU,BEFFU,CEFFU,DELTJU,DELTJKU,
     1DELTKU,DELJU,DELKU,HJ,HJK,HKJ,HK,SHJ,SHJK,SHK,
     2EUP,XLJJK,XLJK,XLKKJ,XLK,E,ME)
C LASTLY, CALCULATE THE ENERGY LEVEL FOR THE SECOND VIBRATIONALLY
C EXCITED STATE, EUU.
      CALL DASYME(JMIN,JMAX,AEFF2,BEFF2,CEFF2,DELTJ2,DELTJK2,
     1DELTK2,DELJ,DELK,HJ,HJK,HKJ,HK,SHJ,SHJK,SHK,
     2EU2,XLJJK,XLJK,XLKKJ,XLK,EUU,ME)
      DO 20 I=1,NDPTS
         J=IQNUMS(I,2)
         KP=IQNUMS(I,3)
         KO=IQNUMS(I,4)
         EINDEX=(J+1)**2-J+KP-KO-OFFSET
         EG=EL(EINDEX)
C  NOTE THAT THE LOWER STATE IS ALWAYS THE GROUND STATE IN THIS PROGRAM
         IV2=IQNUMS(I,5)
         J=IQNUMS(I,6)
         KP=IQNUMS(I,7)
         KO=IQNUMS(I,8)
         EINDEX=(J+1)**2-J+KP-KO-OFFSET
         IF (IV2.EQ.1) EU=E(EINDEX)
         IF (IV2.EQ.2) EU=EUU(EINDEX)
         IF (IV2.EQ.0) EU=EL(EINDEX)
   20    Y(I)=DABS(EU-EG)
      RETURN
      END
      SUBROUTINE DASYME(JMIN,JMAX,AEFF,BEFF,CEFF,DELTJ,DELTJK,
     1DELTK,XELJ,XELK,HJ,HJK,HKJ,HK,XHJ,XHJK,XHK,
     2EV,XLJJK,XLJK,XLKKJ,XLK,E,ME)
      IMPLICIT REAL*8(A-H,O-Z)
```

```
      DIMENSION H(102,102),EIVR(102,102),E(2602)
C SUBROUTINE TO CALCULATE ENERGIES OF NON-RIGID ASYMMETRIC TOPS USING
C WATSON'S DISTORTION PARAMETERS. FOR SPECIFIC METHOD USED SEE:
C WATSON, J. CHEM. PHYS., VOL.48,4517 (1968) , " VIBRATIONAL SPECTRA
C AND STRUCTURE", EDITED BY DURIG,SECTION BY WATSON . THE MATRIX
C ELEMENTS ARE TAKEN FROM COOK,DE LUCIA AND HELMINGER, J. MOL. SPECT.,
C VOL 41,123-136,(1972) WITH THE FOLLOWING CHANGES TO MAKE THEM CONSISTENT
C WITH WATSON'S  A-REDUCED HAMILTONIAN. *****ALL SMALL H'S AND SMALL
C DELTA'S ARE REVERSED IN SIGN ****** ! I.E. THIS PROGRAM IS CORRECT FOR
C WATSON'S A-REDUCED HAMILTONIAN. TO MAKE IT CONSISTENT WITH COOK ET.AL.,
C REVERSE THE SIGNS OF THEIR SMALL H'S AND SMALL DELTA'S BEFORE INPUT.
C (ABC)EFF ARE THE EFFECTIVE ROTATIONAL CONSTANTS (SCRIPT IN COOK'S TEXT).
C DELT(J,JK,K) ARE THE CAP DELTAS WHILE DEL(J,K) ARE THE SMALL DELTAS.
C H(J,JK,KJ,K) ARE THE CAP H'S WHILE SH(J,JK,K) ARE THE SMALL H'S.
C H IS THE MATRIX USED FOR THE HAMILTONIAN SIZED FOR JMAX=40
C EIVR IS THE CORRESPONDING EIGENVECTOR MATRIX. E IS THE MATRIX WHERE
C THE ENERGIES ARE STORED AFTER CALCULATION.
C ROGER BUMGARNER 5/6/87
      NDIM=102
      IEGEN=1
      IORD=1
C FILL-IN MATRIX OF ENERGIES AND QUANTUM NOS W/  0(0,0) VALUE AND
C INITIALIZE MATRICES
      DO 2 I=1,NDIM
         DO 2 II=1,NDIM
            EIVR(I,II)=0.0D0
   2  H(I,II)=0.0D0
      DO 3 I=1,2602
   3     E(I)=0.0D0
C ME IS THE INDEX USED FOR STORING THE ENERGIES IN E.
      ME=1
      IF (JMAX.GT.50) THEN
         WRITE (*,*) 'VALUE OF JMAX EXCEEDS THE MAXIMUM VALUE FOR THE '
         WRITE (*,*) 'CURRENT DIMENSIONS OF THE MATRICES. JMAX SET=50 '
         JMAX=50
      ENDIF
      IF(JMIN.LE.0) JMIN=1
      XKAPPA=(2.0D0*BEFF-AEFF-CEFF)/(AEFF-CEFF)
C PROLATE TOP CASE
      IF (XKAPPA.LT.0.0D0) THEN
         XR=BEFF
         YR=CEFF
         ZR=AEFF
      ENDIF
C OBLATE TOP CASE
      IF (XKAPPA.GE.0.0D0) THEN
         XR=AEFF
         YR=BEFF
         ZR=CEFF
      ENDIF
C MATRIX ELEMENTS IN HAMIL ARE WRITTEN IN COOK'S FORM SO WILL
C CORRECT CONSTANTS TO A-REDUCED FORM RATHER THAN SCREWING WITH
C PREVIOUSLY WRITTEN "GOOD" CODE
      DELJ=-XELJ
```

```
      DELK=-XELK
      SHJ=-XHJ
      SHJK=-XHJK
      SHK=-XHK
C  J-LOOP
      DO 50 J=JMIN,JMAX
         NUMKS=2*J+1
         M=0
C INITIALIZE (OR RE-INITIALZE) H MATRIX TO ZERO'S. M=IS MATRIX INDEX
C TO BE USED FOR VALUES OF K
         DO 5 I=1,NUMKS
            DO 4 II=1,NUMKS
               H(I,II)=0.0D0
   4        CONTINUE
   5     CONTINUE
C  K-LOOP
         DO 20 IK=1,NUMKS
            K=IK-J-1
            M=M+1
            MP=M-1
C  KPRIME-LOOP
            DO 10 IKP=IK,NUMKS
               KP=IKP-J-1
               MP=MP+1
               H(M,MP)=AHAMIL(XR,YR,ZR,DELTJ,DELTJK,
     1         DELTK,DELJ,DELK,HJ,HJK,HKJ,HK,SHJ,SHJK,SHK,
     2         EV,XLJJK,XLJK,XLKKJ,XLK,J,K,KP)
c note: at the beginning of the line 2, the variable XLJ was removed
               H(MP,M)=H(M,MP)
C END K' LOOP
  10        CONTINUE
C END K-LOOP
  20     CONTINUE
         CALL HDIAG(H,NUMKS,NDIM,IEGEN,IORD,EIVR)
C NOTE: EIGENVALUES COME BACK ORDERED, SO KP AND KO ASSIGNMENTS CAN
C BE MADE ON THE BASIS OF THIS ORDERING.
         DO 30 IK=1,NUMKS
            ME=ME+1
            E(ME)=H(IK,IK)
  30     CONTINUE
C END J-LOOP
  50  CONTINUE
      RETURN
      END
      FUNCTION AHAMIL(XR,YR,ZR,DELTJ,DELTJK,
     1DELTK,DELJ,DELK,HJ,HJK,HKJ,HK,SHJ,SHJK,SHK,
     2EV,XLJJK,XLJK,XLKKJ,XLK,J,K,KP)
      IMPLICIT REAL*8(A-H,O-Z)
      AHAMIL=0.0D0
      KCHK=IABS(K-KP)
      IF( (KCHK.NE.2).AND.(K.NE.KP) ) RETURN
C DIAGONAL TERMS
      IF(K.EQ.KP) AHAMIL=EV+YR*P(1,J)+(ZR-YR)*PZ(1,K)-DELTJ*P(2,J)-
     1DELTJK*PPZ(1,1,J,K)-DELTK*PZ(2,K)
```

```
      RETURN
      END
C FUNCTIONS TO CALCULATE MATRIX ELEMENTS OF ANG. MOM. OPERATORS
C (P**2N)*(PZ**2M)
      FUNCTION PPZ(N,M,J,K)
      IMPLICIT REAL*8(A-H,O-Z)
      XJ=J
      XK=K
      PPZ=((XJ*(XJ+1.0D0))**N)*XK**(2*M)
      RETURN
      END
C (P**2N)*(PMINUS**2)
      FUNCTION PPM(N,J,K)
      IMPLICIT REAL*8(A-H,O-Z)
      XJ=J
      PPM=-0.5D0*(XJ*(XJ+1))**N*FPLS(J,K)
      RETURN
      END
C FPLUS FUNCTION
      FUNCTION FPLS(J,K)
      IMPLICIT REAL*8(A-H,O-Z)
      J1=J*(J+1)
      K1=K*(K+1)
      K2=(K+1)*(K+2)
      XJ1=J1
      XK1=K1
      XK2=K2
      FPLS=DSQRT((XJ1-XK1)*(XJ1-XK2))
      RETURN
      END
C (P**2N)*(PZ**2M)*PMINUS**2
      FUNCTION PPZPM(N,M,J,K)
      IMPLICIT REAL*8(A-H,O-Z)
      XJ=J
      XK=K
      PPZPM=-0.5D0*(XJ*(XJ+1.0D0))**N*(XK**(2*M)+(XK+2.0D0)**(2*M))*
     1 FPLS(J,K)
      RETURN
      END
C P**2N
      FUNCTION P(N,J)
      IMPLICIT REAL*8(A-H,O-Z)
      XJ=J
      P=(XJ*(XJ+1.0D0))**N
      RETURN
      END
C PZ**2M
      FUNCTION PZ(M,K)
      IMPLICIT REAL*8(A-H,O-Z)
      XK=K
      PZ=XK**(2*M)
      RETURN
      END
```

The following is a sample input file used with the above fitting program.

```
' D2O trimer lines, using threesym.f'
' Both Berkeley and Caltech lines '
' 43 cm-1 lines are corrected for shifts'
10
20
'A      ',0.0,'F',0.00001,0
'B      ',5796.175201,'F',0.0000001,1
'C      ',3088.457654,'F',0.0000001,1
'DELTJ  ',0.2544919988E-01,'F',0.00000001,1
'DELTJK',-0.2782223533E-01,'F',0.00000001,1
'DELTK  ',0.0,'F',0.001,0
'AU     ',0.0,'F',0.001,0
'BU     ',5792.255036,'F',0.001,1
'CU     ',3100.327694,'F',0.000001,1
'DELTJU',0.1408074394E-01,'F',0.000001,1
'DELTJKU',-0.3743947377E-01,'F',0.000001,1
'DELTKU',0.0,'F',0.001,0
'EUP    ',1232142.018,'F',0.000001,1
'EU2    ',2940936.079,'F',0.000001,1
'A2     ',0.0,'F',0.00001,0
'B2     ',5796.175201,'F',0.0000001,1
'C2     ',3088.457654,'F',0.0000001,1
'DELTJ2',0.2544919988E-01,'F',0.00000001,1
'DELTJK2',-0.2782223533E-01,'F',0.00000001,1
'DELTK2',0.0,'F',0.001,0
105,8
1243725.78,0,0,0,0,1,1,1,0,1.0,1.0    | Ground state to the lower excited
1255305.42,0,1,1,0,1,2,2,0,1.0,1.0    | state.
1278434.88,0,3,3,0,1,4,4,0,1.0,1.0
1289986.94,0,4,4,0,1,5,5,0,1.0,1.0
1313062.40,0,6,6,0,1,7,7,0,1.0,1.0
1324585.34,0,7,7,0,1,8,8,0,1.0,1.0
              .
              .
              .
2955983.0000,0,1,0,1,2,2,0,2,1.0,1.0    | Ground state to the upper excited
2925866.0000,0,2,0,2,2,1,0,1,1.0,1.0    | state.
2920441.0000,0,2,1,1,2,1,1,0,1.0,1.0
2919683.0000,0,3,0,3,2,2,0,2,1.0,1.0
2914237.0000,0,3,2,2,2,2,2,1,1.0,1.0
2913501.0000,0,4,0,4,2,3,0,3,1.0,1.0
2897158.0000,0,4,3,1,2,3,3,0,1.0,1.0
2896366.0000,0,5,3,3,2,4,3,2,1.0,1.0
              .
              .
              .
```

Programs to fit the *ab initio* potentials

FSUB routines were also written to fit *ab initio* potentials. For example, to fit a radial potential, the following FSUB routine was combined with the non-linear least squares fit program used above.

```
c Subroutine to fit potential terms to ab-initio (or other) pointwise potential
c Potential is expanded as V=De(1-exp(-a(R-Re)))^2 (Morse function)
      subroutine fsub(maxps,maxdps,ndpts,nparms,allvar,y,iqnums,
     1ifcmhz,R)
      implicit real*8(a-h,o-z)
      implicit integer(i-n)
      dimension allvar(maxps),y(maxdps),iqnums(maxdps,10)
      dimension R(maxdps)
      De=allvar(1)
      a=allvar(2)
      R1=allvar(3)
      do 20 i=1,ndpts
          Rp=R(i)
          y(i)=0.0d0
          b=-a*(Rp-R1)
          v=DEXP(b)
              y(i)=De*((1-v)**2.0d0)
   20 continue
      return
      end
```

Angular coordinates were fit with the following expansion:

$$V = \sum_n \frac{V_n}{2}(1 - cos(n\theta))^2.$$

The FSUB routine which incorporates this is as follow:

```
c Subroutine to fit potential terms to ab-initio (or other) pointwise potential
c Potential is expanded as V=sum[Vn/2*(1-cos(n*theta))]
      subroutine fsub(maxps,maxdps,ndpts,nparms,allvar,y,iqnums,
     1ifcmhz,theta)
      implicit real*8(a-h,o-z)
      implicit integer(i-n)
      dimension allvar(maxps),y(maxdps),iqnums(maxdps,10)
      dimension theta(maxdps)
c  v1=allvar(1)
c  v2=allvar(2)
c  v3=allvar(3)
c  v4=allvar(4)
c  v5=allvar(5)
c  v6=allvar(6)
```

```
c etc. can do up to v10
      do 20 i=1,ndpts
          th=theta(i)*2.0d0*3.1415926d0/360.0d0
          y(i)=0.0d0
          do 10 j=1,10
              xn=dble(j)
              y(i)=y(i)+(allvar(j)/2.0d0)*(1.0d0-dcos(xn*th))
   10     continue
   20 continue
      return
      end
```

A sample input file for the latter is given below. The comments in parentheses indicate the input format.

```
'Fit of  Vns to MP2 pot'
' with BSSE correction'
'benzene h2o, for the chi angle '
10
10
0
'v1',10.0,'P',0.00001,1  | Vn term,initial value,'P',delta value,1
'v2',1.0,'P',0.00001,1   | 'P' means that the Vn term will be changed
'V3', 0.0,'P',0.00001,0  | proportionally according to the delta value.
'V4', 0.0,'P',0.00001,0  | 'F' would indicate that Vn should be changed
'V5',0.0,'P',0.00001,0   | by a fixed value, delta value, at each step.
'V6',0.0,'P',0.00001,0
'V7',0.0,'P',0.01,0
'V8',0.0,'P',0.01,0
'V9',0.0,'P',0.01,0
'V10',0.0,'P',0.01,0
21,1                     | Number of entries,1
607.351,1,'n',1.0,19.99  | Energy,1,'n',1.0,angle
480.176,1,'n',1.0,17.99  | Only Energy and angle values
372.74,1,'n',1.0,15.99   | should be changed.
280.65,1,'n',1.0,13.99
201.72,1,'n',1.0,11.99
138.13,1,'n',1.0,9.99
87.703,1,'n',1.0,7.99
48.24,1,'n',1.0,5.99
24.118,1,'n',1.0,3.99
6.577,1,'n',1.0,1.99
0.0,1,'n',1.0,0.0
6.577,1,'n',1.0,-1.99
24.118,1,'n',1.0,-3.99
48.24,1,'n',1.0,-5.99
87.703,1,'n',1.0,-7.99
138.13,1,'n',1.0,-9.99
201.72,1,'n',1.0,-11.99
280.65,1,'n',1.0,-13.99
```

```
372.74,1,'n',1.0,-15.99
480.176,1,'n',1.0,-17.99
607.351,1,'n',1.0,-19.99
```

One often needs to predict vibrational frequencies based on these one-dimensional potential. A program written by R.E. Bumgarner, called "driver.f" was often used in conjunction with the results of the above fitting routines.

```
      implicit real*8(a-h,o-z)
      implicit integer(i-n)
      dimension e(202,202),eivr(202,202),p1(3),p2(3)
      character*79  title
      character*24 stime
      open(9,file='driver.in',status='old')
      open(10,file='driver.out',status='new')
      call fdate(stime)
      write(10,*)stime
      read(9,*) title
      write(10,*) title
      ndim=202
      read(9,*)xi,xi2
      read(9,*)v1,v2,v3
      read(9,*)v4,v5,v6
      read(9,*)mmax
      write(10,11) xi,xi2
   11 format(1x,'Moments of inertia amu-ang squared',f14.8,1x,f14.8)
      write(10,*)
      write(10,*) ' Potential terms'
      write(10,21) v1,v2,v3
   21 format(1x,'V1= ',g12.6,' V2= ',g12.6,' V3= ',g12.6)
      write(10,31) v4,v5,v6
   31 format(1x,'V4= ',g12.6,' V5= ',g12.6,' V6= ',g12.6)
      iunit=0
      call introt(xi,v1,v2,v3,v4,v5,v6,mmax,e,
     1eivr,ndim,iunit,p1,p2,s)
      sp1=(e(2,2)-e(1,1))*29.9792458d0
      write(10,*)
      write(10,*) 'Splitting between lowest states for first'
      write(10,41)sp1
   41 format(1x,'moment of inertia = ',g20.10)
      write(10,*)
      write(10,*)' Expectation values '
c234567891123456789212345678931234567894123456789512345678961234567897 12
      do 10 j=1,2
         write(10,51)j,p1(j),p2(j)
   10 continue
   51 format(1x,'state ',i3,' P1= ',g20.10,' P2= ',g20.10)
      delp1=p1(2)-p1(1)
      delp2=p2(2)-p2(1)
      write(10,52) delp1,delp2
```

```
   52 format(1x,'Delta P1 = ',f15.8,'  Delta P2 = ',f15.8)
      write(10,53)s
   53 format(1x,'Sin transition element = ',f15.8)
      write(10,*)
      write(10,61)
   61 format(1x,'First ten energy levels for first M.O.I.')
      do 40 i=1,10
   40 write(10,71) e(i,i)
   71 format(1x,g20.10)
c Section for second moment of inertia
      write(10,*)
      write(10,*)
      write(10,*)
      call introt(xi2,v1,v2,v3,v4,v5,v6,mmax,e,
     1eivr,ndim,iunit,p1,p2,s)
      sp1=(e(2,2)-e(1,1))*29.9792458d0
      write(10,*)
      write(10,*)
      write(10,*) 'Splitting between lowest states for second'
      write(10,81)sp1
   81 format(1x,'moment of inertia= ',g20.10)
      write(10,*)
      write(10,*)' Expectation values '
c234567891123456789212345678931234567894123456789512345678961234567897l2
      do 70 j=1,2
         write(10,51)j,p1(j),p2(j)
   70 continue
      delp1=p1(2)-p1(1)
      delp2=p2(2)-p2(1)
      write(10,52) delp1,delp2
      write(10,53)s
      write(10,*)
      write(10,91)
   91 format(1x,'First ten energy levels for second M.O.I.')
      do 80 i=1,10
   80 write(10,71) e(i,i)
      end
c------------------------------>>>>>><<<<<<--------------------
      SUBROUTINE INTROT(XI,V1,V2,V3,V4,V5,V6,MMAX,E,
     1 EIVR,NDIM,IUNIT,P1,P2,S)
      IMPLICIT REAL*8(A-H,O-Z)
      IMPLICIT INTEGER(I-N)
C234567891123456789212345678931234567894123456789512345678961234567897l2
C subroutine to calculate energies of an internal rotor
C XI is the internal rotor's moment of inertia in amu-
C angstrom^2 V1,V2 etc. are the std. potential energy terms
C i.e. barrier heights of the n-fold potential terms, MMAX is
C is the maximum M over which the basis set is extended, IUNIT
C is a switch telling what units the potential terms are given in
C for now, they must be given in cm-1
      DIMENSION E(NDIM,NDIM),EIVR(NDIM,NDIM),P1(3),P2(3)
C     OPEN(8,FILE='introt.out',STATUS='NEW')
      NSIZE=2*MMAX+1
      IF(NSIZE.GT.(NDIM-1)) THEN
```

```
         MMAX=INT((NDIM-2)**.5)
         NSIZE=NDIM-1
      ENDIF
C convert xi to MHz
      B=505379.0631D0/XI
C convert to cm-1
      BCM=(B/1000.0D0)/29.9792458D0
C SET UP HAMILTONIAN
      DO 20 I=1,NSIZE
         M=INT(I/2)*(-1)**I
         XM=DBLE(M)
         EK=XM*XM*BCM
c diagonal term
         E(I,I)=EK+(V1+V2+V3+V4+V5+V6)/2.0D0
         DO 10 IP=I+1,NSIZE
             MP=INT(IP/2)*(-1)**IP
             MDEL=IABS(MP-M)
c off diagonal terms
             E(I,IP)=0.0D0
             IF(MDEL.GT.6) GOTO 10
             IF(MDEL.EQ.1) E(I,IP)=-V1/4.0D0
             IF(MDEL.EQ.2) E(I,IP)=-V2/4.0D0
             IF(MDEL.EQ.3) E(I,IP)=-V3/4.0D0
             IF(MDEL.EQ.4) E(I,IP)=-V4/4.0D0
             IF(MDEL.EQ.5) E(I,IP)=-V5/4.0D0
             IF(MDEL.EQ.6) E(I,IP)=-V6/4.0D0
             E(IP,I)=E(I,IP)
  10    CONTINUE
  20  CONTINUE
      CALL HDIAG(E,NSIZE,NDIM,0,1,EIVR)
c calculate P1(cos) and P2(cos) for the two lowest eigenstates
          S=0.0D0
      DO 60 J=1,2
           P1(J)=0.0D0
           P2(J)=0.0D0
          DO 50 I=1,100
             M=INT(I/2)*(-1)**I
             DO 40 IP=1,100
                MP=INT(IP/2)*(-1)**IP
                ICHK=ABS(M-MP)
                ICHK2=M-MP
                IF(ICHK.EQ.1) P1(J)=P1(J)+0.5D0*EIVR(I,J)*EIVR(IP,J)
                IF(ICHK.EQ.0) P2(J)=P2(J)+0.25D0*EIVR(I,J)*EIVR(IP,J)
                IF(ICHK.EQ.2) P2(J)=P2(J)+0.375D0*EIVR(I,J)*EIVR(IP,J)
         IF((ICHK2.EQ.1).AND.(J.EQ.1)) S=S+0.5D0*EIVR(I,1)*EIVR(IP,2)
         IF((ICHK2.EQ.-1).AND.(J.EQ.1)) S=S-0.5D0*EIVR(I,1)*EIVR(IP,2)
  40        CONTINUE
  50    CONTINUE
  60 continue
     RETURN
     END
```

The input file for driver.f is as follow:

```
'bzwt, water bending against benzene'
201.64,218.86
19600.73178,0.0,0.0
0.0,0.0,0.0
80
```

The first line is the title of the fit. The second line lists the moments of inertia for two isotopomers along the vibration/torsional motion under consideration. Units are in Amu·$\AA^2$. The next two lines list V_n, three on each line, beginning with $n = 1$. The last line gives the maximum m, the internal rotation quantum number, to be used in the fit.

A useful conversion number is that between a rotational constant in MHz to moment of inertia in $Amu \cdot \AA^2$:

$$I_{(Amu)} = \frac{505379.0631 MHz \cdot Amu \cdot \AA^2}{rotational\ constant}$$

where 505379.0631 $MHz \cdot Amu \cdot \AA^2 = \frac{\hbar}{4\pi}$.

STRFTQ

A program originally written by R.H. Schwendeman (a description is given in *Critical Evaluation of Chemical and Physical Structural Information*, edited by D.R. Lide, Jr., and M.A. Paul, National Academy of Sciences, Washington, D.C., 1974), and later modified by F. Lovas at the National Institute of Standard and Technology is used to fit structures to rotational constants. There are several copies of the manual in the Blake lab. The details of the input parameters are given in the manual. An input file used to fit benzene-water is given below, followed by a brief explanation. Blank lines noted below are used to differentiate sections in the input file, and thus, are necessary.

```
17   Benzne-H2O/D2O
 0  0.        0.0       0.0     0.000
 1 12.        0.0       0.0     1.400
 2 12.       60.0       0.0     1.400
 3 12.      120.0       0.0     1.400
 4 12.      120.0       0.0     1.400
 5 12.      120.0       0.0     1.400
 6 12.      120.0       0.0     1.400
 2  1.      180.0       0.0     1.080
 3  1.      240.0       0.0     1.080
 4  1.      240.0       0.0     1.080
 5  1.      240.0       0.0     1.080
 6  1.      240.0       0.0     1.080
 7  1.      240.0       0.0     1.080
 1  0.       90.0      90.0     3.323
14 16.       90.0      90.0     0.067
15  1.       52.3       0.0     0.958
15  1.      307.7       0.0     0.958
16  2.      17  2.
16  2.      17  1.
  <--------blank line
    0.     1994.833  1994.833
    0.     1912.068  1912.068
    0.     1956.357  1956.357
 0 0.      0 0.      0 0.
 0 0.      0 0.      0 0.
 0 0.      0 0.      0 0.
 0 0.      0 0.      0 0.
 0 0.      0 0.      0 0.
 0 0.      0 0.      0 0.
 0 0.      0 0.      0 0.
 0 0.      0 0.      0 0.
 0 0.      0 0.      0 0.
 0 0.      0 0.      0 0.
 0 0.      0 0.      0 0.
```

```
 0 0.       0 0.       0 0.
 0 0.       0 0.       0 0.
 0 0.       2 1.       1 1.
 2 1.       0 0.       0 0.
 0 0.       0 0.       0 0.
 0 0.       0 0.       0 0.
 1 2 5
 1 3 6
 2 2 5
 2 3 6
 3 2 5
 3 3 6
                              <----------blank line
 11415
122313
```

The first line gives the number of particles used to describe the structure, i.e., the number includes the "dummy" atoms. The orientations and bond lengths are specified by: the particle(B) to which this atom(A) is attached; the atomic number of (A); the angle with particle(B) to which this atom(A) is attached and the particle(C) to which (B) is attached; the dihedral angle between (A), (B), (C), and with (B), (C), and (D), where (D) is the particle to which (C) is attached; and the bond length between (A) and (B). Thus, we see that the first carbon atom is attached to the first particle which is a dummy atom. Since the dummy atom is attached to nothing, only the bond length is defined. The first hydrogen atom is attached to the first carbon atom which is in turn attached to the dummy atom. After the coordinates are entered, two lines without intervening space, "16 2. 17 2." and "16 2. 17 1." are entered to indicate that the particle 16 and 17 are replaced by deuterium in the first isotopomer, and particle 16 is replaced by deuterium and particle 17 is replaced by hydrogen in the second isotopomer. A space line is followed by A, B, and C rotational constants for the three isotopomers. Then the coordinates that are allowed to vary for the fit are indicated. The third coordinate, i.e., bond length, of particle 14 is allowed to change first, and then the dihedral angle of particle 14 and the angle of particle 15 are allowed to change. The value "1." indicates that the angles on 14 and 15 are changed with the same sign. The next set of three numbers indicates that for isotopomer 1, the B rotational constant should be fit, and the next set of three indicates that the C rotational constant should be fit, also. It is the same for the

second and third isotopomers. After the space line, two lines are entered to control the output of the fit.

Appendix F: *Gaussian 92* and DMC

Gaussian 92

Detailed instructions for *Gaussian 92* are given in the manual. Following are four input files used for the benzene-water calculations.

The first input file is for the full optimization of all degrees of freedom, both inter- and intramolecular, for benzene-water, followed by a frequency calculation. The manual indicates that the frequency calculation should be done only on fully optimized structure at the same level of optimization calculation. Since frequency calculation requires a large amount of disk space, we can only run it at the Hartree-Fock level. For a full optimization without frequency prediction, the keywork "HF" was replaced with "MP2=direct" for a second order Moller-Plesset perturbation theory calculation. For the full optimization at this MP2 level presented in Chapter 4, only the intermolecular coordinates were optimized to reduce the calculation time. The designation of the checkpoint file, "%chk=/gaus/scr/bzwthf.chk", is necessary to link the geometry from the optimization calculation to the frequency calculation. For full optimization and frequency calculation, all the interatomic relationships must be independent variables. For example, if all the C-H distances were given as a single variable, say "ch", then the frequency calculation will fail. However, for a frequency calculation, there must not be any more or less than 3N-6 variables for non-linear molecules, or 3N-5 variables for linear molecules. Thus, in this input file for benzene-water dimer, of the 48 relation-variables, there are only 39 variables that are allowed to vary in the calculation.

```
$RunGauss
%chk=/gaus/scr/bzwthf.chk
# HF 6-31g** SCF=Direct FOPT MaxDisk=90000000
<-----------------blank line
Fully optimized structure at HF level.
  <-----------------blank line
0,1
C1
C2  C1 cc2
C3  C2 cc3  C1  full3
```

```
C4  C3 cc4  C2  full4   C1 cis4
C5  C4 cc5  C3  full5   C2 cis5
C6  C5 cc6  C4  full6   C3 cis6
H1  C1 ch1  C2  full7   C3 trans1
H2  C2 ch2  C3  full8   C4 trans2
H3  C3 ch3  C4  full9   C5 trans3
H4  C4 ch4  C5  full10  C6 trans4
H5  C5 ch5  C6  full11  C1 trans5
H6  C6 ch6  C1  full12  C2 trans6
X1  C1 cc   C2  half    C3 cisx1
X2  X1 xx   C1  right1  C2 right2
O   X2 ox   X1  atilt   C1 thirty
X3  O  one  X2  right3  X1 cisx3
H7  O  oh1  X2  hoh2    X3 right4
H8  O  oh2  H7  hoh     X2 cish8
<----------------blank line
xx    3.1668
atilt 179.1688
thirty 16.0338
cc    1.3974
cc2    1.3974
cc3    1.3974
cc4    1.3974
cc5    1.3974
cc6    1.3974
ch1    1.0826
ch2    1.0826
ch3    1.0826
ch4    1.0826
ch5    1.0826
ch6    1.0826
oh1    0.958
oh2    0.958
full3  119.9955
full4  119.9955
full5  119.9955
full6  119.9955
full7  119.9955
full8  119.9955
full9  119.9955
full10  119.9955
full11  119.9955
full12  119.9955
half   59.9934
hoh2   52.3
hoh   104.6
cis4     0.0337
cis5     0.0337
cis6     0.0337
trans1 180.1801
trans2 180.1801
trans3 180.1801
trans4 180.1801
trans5 180.1801
```

```
trans6 180.1801
<----------------blank line
cisx1   0.0337
cisx3   0.0337
cish8   0.0337
one     1.00
ox      0.067
right1  90.08
right2  90.08
right3  90.08
right4  90.08
<---------------blank line
--Link1--
%chk=/gaus/scr/bzwthf.chk
# HF 6-31g** SCF=Direct freq geom=checkpoint guess=check MaxDisk=90000000
<---------------blank line
Frequency for the fully optimized structure
<---------------blank line
0,1
```

The second input sample is for scanning a variable. In this input file, the variable "right1" is varied in 10 steps from 70.01° by 2.0° each step. Thus, the energy calculation will be made for "right1" at 70.01, 72.01, 74.01, ... 90.01. The remaining variables are fixed.

```
$RunGauss
# MP2=DIRECT 6-31g** SCF=DIRECT SCAN MaxDisk=90000000
<--------------blank line
Scan bz-wt ang  for 10 times at MP2 level. second z-matrix
<--------------blank line
0,1
C1
C2  C1 cc2
C3  C2 cc3  C1  full3
C4  C3 cc4  C2  full4   C1 cis4
C5  C4 cc5  C3  full5   C2 cis5
C6  C5 cc6  C4  full6   C3 cis6
H1  C1 ch1  C2  full7   C3 trans1
H2  C2 ch2  C3  full8   C4 trans2
H3  C3 ch3  C4  full9   C5 trans3
H4  C4 ch4  C5  full10  C6 trans4
H5  C5 ch5  C6  full11  C1 trans5
H6  C6 ch6  C1  full12  C2 trans6
X1  C1 cx   C2  half    C3 cisx1
X2  X1 xx   C1  right1  C2 right2
O   X2 ox   X1  theta   C1 phi
H7  O  oh1  X2  hoh1    X1 psi
H8  O  oh2  X2  hoh2    H7 cish1
```

```
<--------------blank line
right1  70.01 10 2.0
<--------------blank line
cx      1.3974
xx  3.1658
theta 168.2484
phi 18.1013
psi     101.198
cc2     1.3974
cc3     1.3974
cc4     1.3974
cc5     1.3974
cc6     1.3974
ch1     1.0826
ch2     1.0826
ch3     1.0826
ch4     1.0826
ch5     1.0826
ch6     1.0826
oh1     0.958
oh2     0.958
full3   119.9955
full4   119.9955
full5   119.9955
full6   119.9955
full7   119.9955
full8   119.9955
full9   119.9955
full10   119.9955
full11   119.9955
full12   119.9955
half    60.0
hoh2    52.3
cis4      0.0337
cis5      0.0337
cis6      0.0337
trans1 180.
trans2 180.
trans3 180.
trans4 180.
trans5 180.
trans6 180.
cisx1    0.0001
cish1    180.
ox       0.067
right2   90.
hoh1    52.3
```

The third input file is for a counterpoise correction for each of the points calculated using the above input file. In the last three lines, atoms number 13, 14 and 15, which

are the oxygen atom and two hydrogens, are set to nuclear charges of zero, effectively removing the electrons from the three atoms. Thus, the orbitals for water remain but there are no electrons, i.e., they are "ghost" atoms. The "massage" keyword allows this specification.

```
$RunGauss
# MP2=DIRECT 6-31g** SCF=DIRECT SCAN MaxDisk=90000000 massage
<------------blank line
Scan bz-wt ang  for 10 times at MP2 level. second z-matrix
<------------blank line
0,1
C1
C2  C1 cc2
C3  C2 cc3  C1  full3
C4  C3 cc4  C2  full4   C1 cis4
C5  C4 cc5  C3  full5   C2 cis5
C6  C5 cc6  C4  full6   C3 cis6
H1  C1 ch1  C2  full7   C3 trans1
H2  C2 ch2  C3  full8   C4 trans2
H3  C3 ch3  C4  full9   C5 trans3
H4  C4 ch4  C5  full10  C6 trans4
H5  C5 ch5  C6  full11  C1 trans5
H6  C6 ch6  C1  full12  C2 trans6
X1  C1 cx   C2  half    C3 cisx1
X2  X1 xx   C1  right1  C2 right2
O   X2 ox   X1  theta   C1 phi
H7  O  oh1  X2  hoh1    X1 psi
H8  O  oh2  X2  hoh2    H7 cish1
<------------blank line
right1  70.01 10 2.0
<------------blank line
cx     1.3974
xx  3.1658
theta 168.2484
phi 18.1013
psi    101.198
cc2    1.3974
cc3    1.3974
cc4    1.3974
cc5    1.3974
cc6    1.3974
ch1    1.0826
ch2    1.0826
ch3    1.0826
ch4    1.0826
ch5    1.0826
ch6    1.0826
oh1    0.958
oh2    0.958
full3  119.9955
full4  119.9955
```

```
full5  119.9955
full6  119.9955
full7  119.9955
full8  119.9955
full9  119.9955
full10  119.9955
full11  119.9955
full12  119.9955
half   60.0
hoh2   52.3
cis4     0.0337
cis5     0.0337
cis6     0.0337
trans1 180.
trans2 180.
trans3 180.
trans4 180.
trans5 180.
trans6 180.
cisx1   0.0001
cish1   180.
ox      0.067
right2  90.
hoh1   52.3
<------------blank line
13 0 0.
14 0 0.
15 0 0.
```

The fourth input file is also for counterpoise correction. This time, all the benzene atoms are specified as having a nuclear charge of zero. A scan similar to the previous two files was attemped, but failed. Thus, each scan point was made into a single point calculation. The following file is for the first point in the scan.

```
$RunGauss
# MP2=DIRECT 6-31g** SCF=DIRECT MaxDisk=90000000 massage
<-------------blank line
Scan bz-wt ang  for 10 times at MP2 level. second z-matrix
<-------------blank line
0,1
C1
C2  C1 cc2
C3  C2 cc3  C1  full3
C4  C3 cc4  C2  full4   C1 cis4
C5  C4 cc5  C3  full5   C2 cis5
C6  C5 cc6  C4  full6   C3 cis6
H1  C1 ch1  C2  full7   C3 trans1
H2  C2 ch2  C3  full8   C4 trans2
H3  C3 ch3  C4  full9   C5 trans3
```

```
H4  C4 ch4  C5  full10  C6 trans4
H5  C5 ch5  C6  full11  C1 trans5
H6  C6 ch6  C1  full12  C2 trans6
X1  C1 cx   C2  half    C3 cisx1
X2  X1 xx   C1  right1  C2 right2
O   X2 ox   X1  theta   C1 phi
H7  O  oh1  X2  hoh1    X1 psi
H8  O  oh2  X2  hoh2    H7 cish1
<------------blank line
right1  70.01
cx     1.3974
xx  3.1658
theta 168.2484
phi 18.1013
psi    101.198
cc2    1.3974
cc3    1.3974
cc4    1.3974
cc5    1.3974
cc6    1.3974
ch1    1.0826
ch2    1.0826
ch3    1.0826
ch4    1.0826
ch5    1.0826
ch6    1.0826
oh1    0.958
oh2    0.958
full3  119.9955
full4  119.9955
full5  119.9955
full6  119.9955
full7  119.9955
full8  119.9955
full9  119.9955
full10  119.9955
full11  119.9955
full12  119.9955
half   60.0
hoh2   52.3
cis4     0.0337
cis5     0.0337
cis6     0.0337
trans1 180.
trans2 180.
trans3 180.
trans4 180.
trans5 180.
trans6 180.
cisx1   0.0001
cish1   180.
ox      0.067
right2  90.
hoh1   52.3
```

```
<---------------blank line
1 0 0.
2 0 0.
3 0 0.
4 0 0.
5 0 0.
6 0 0.
7 0 0.
8 0 0.
9 0 0.
10 0 0.
11 0 0.
12 0 0.
```

DMC calculations

A detailed description of the use of QCLUSTER, a diffusion Monte Carlo simulation program package, is given in the manual written by Pablo Sandler. Copies of the manual are available in the Blake group as well as from Pablo Sandler who can be contacted at sandler@cold.fh.huji.ac.il. A brief flow chart describing the steps and output from the QCLUSTER is given in Figure .5.

The programs reside on the two IBM RISC workstations in the Blake lab. On "gavot", the QCLUSTER directory is under the /home/guest directory. On "mazurka", it is in /gaus/sakaetemp. The necessary steps to run QCLUSTER will be described using the benzene-water case as an example.

Three files in `QCLUSTER/SRC_ALL` must be edited to produce the executable file for QCLUSTER. These files are psips.inc, Makefile, and a file that includes the potential energy functions (pesbw.f for benzene-water). The psips.inc file defines the parameters of the fit. Normally, it only needs to be edited once to change the number of atoms, "NatMAX", unless one wishes to change other variables. In the case of benzene-water, NatMAX was set to 15.

```
      parameter  (Npsips=4000,Nmax=Npsips+200,NatMAX=15,
     +     NmolMAX=4,NdimMAX=NmolMAX*9+3)
```

Next, the potential energy function must be defined. The file for benzene-water, pesbw.f, is as follows:

```
      function vpes(conf)
      implicit double precision (a-h,o-z)
      include 'psips.inc'
      dimension    conf(NmolMAX*NatMAX,3),x(3),y(3),z(3),
     +             w(3,3),wrot(3,3),bcm(3),vparam(7)
      data  vparam /2.884d-3, 6.32488, 1.0901, 4.6175d-3, 3.337d-4,
     +  8.94d-2, 0.0d0 /
c                      De,Re,alpha,V1/2,V2/2, V1chi/2,V2chi/2
      ax = 0.d0
      ay = 0.d0
      do i=1,3
         x(i) = conf(1,i) - conf(4,i)
         ax = ax + x(i)**2
         y(i) = conf(2,i) - conf(6,i)
         ay = ay + y(i)**2
```

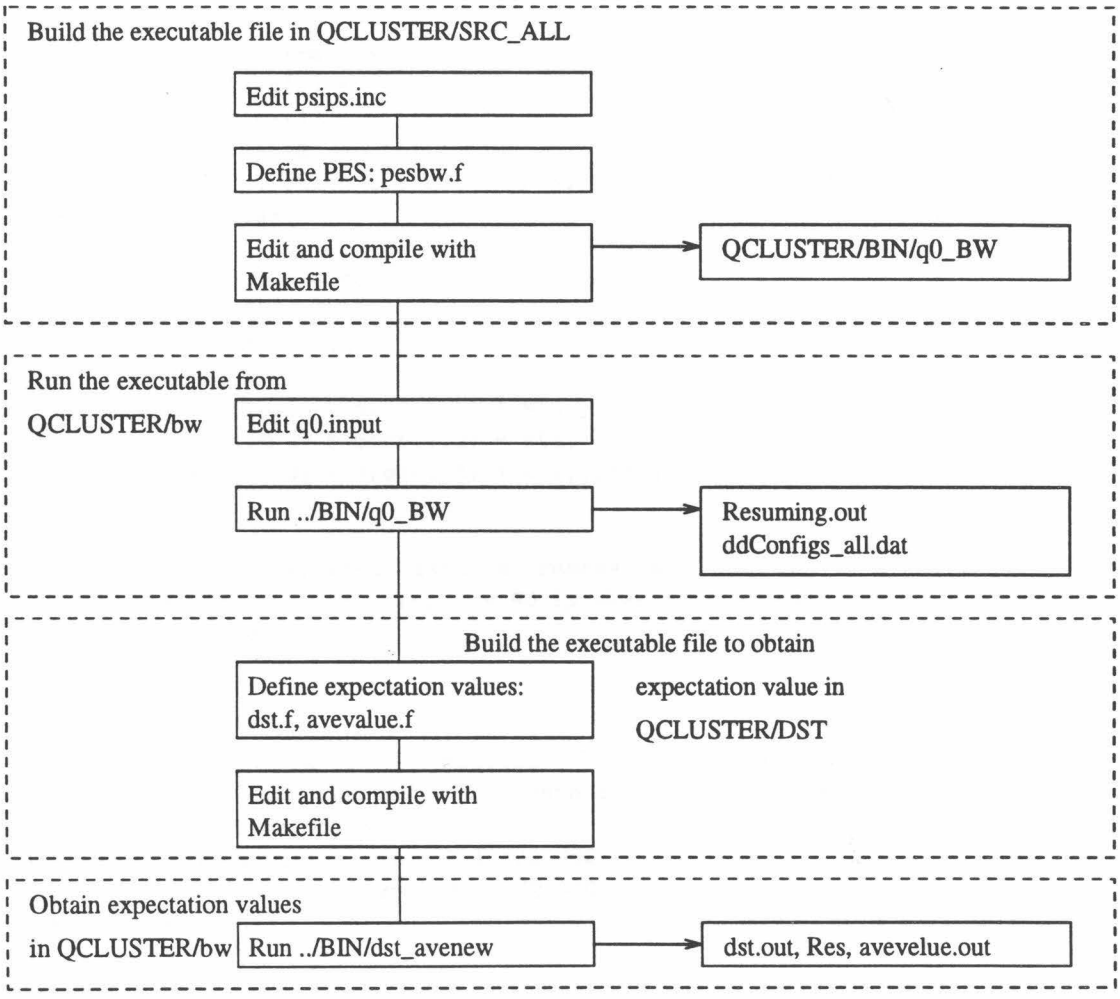

Figure .5: QCLUSTER flow chart

```
         bcm(i) = (conf(1,i) + conf(4,i))/2.0d0
      end do
      ax = sqrt(ax)
      ay = sqrt(ay)
      do i=1,3
         x(i) = x(i)/ax
         y(i) = y(i)/ay
         do j=1,3
            w(i,j) = conf(12+i,j) - bcm(j)
         end do
      end do
      rmorse=0.0d0
      do i=1,3
rmorse=rmorse+w(2,i)**2
      end do
      rmorse = sqrt(rmorse)
      z(1) = x(2)*y(3) - x(3)*y(2)
      z(2) = x(3)*y(1) - x(1)*y(3)
      z(3) = x(1)*y(2) - x(2)*y(1)
c Define wrot(i,j) which are the coordinate for water in the benzene
c coordinate system.
      do i=1,3
         wrot(i,1) = 0.d0
         wrot(i,2) = 0.d0
         wrot(i,3) = 0.d0
         do j=1,3
            wrot(i,1) = wrot(i,1) + w(i,j)*x(j)
            wrot(i,2) = wrot(i,2) + w(i,j)*y(j)
            wrot(i,3) = wrot(i,3) + w(i,j)*z(j)
         end do
      end do
c Find chi.  by using bz-O distance, rmorse, and then the bz-O distance
c along the z axis, zlbo.  angle = 90 is what is defined as chi=0.
zlbo=abs(wrot(2,3))
achi=zlbo/rmorse
chi=acos(achi)
achi2=2.0d0*chi
c Find theta.  Locate the H-H midbond.  Take the angle between the vector
c to the midbond and the projection onto axis normal to benzene plane
c and colinear with Oxygen.
hhx=wrot(2,1)-(wrot(1,1)+wrot(3,1))/2.0d0
hhy=wrot(2,2)-(wrot(1,2)+wrot(3,2))/2.0d0
zoh=abs(wrot(2,3))
xyzoh=abs(wrot(1,3)+wrot(3,3))/2.0d0
hhz=zoh-xyzoh
xlohh=hhx**2+hhy**2+hhz**2
xlohh=sqrt(xlohh)
atheta=hhz/xlohh
theta=acos(atheta)
atheta2=2.0d0*theta
c Calculate the energies.
      em = exp(-vparam(3)*( rmorse-vparam(2) ))
      vmorse =  vparam(1)*( em*(em-2) )
```

```
      vtheta = vparam(4)*(1-atheta) + vparam(5)*(1-atheta2) +
     + 4.83d-5

vchi=vparam(6)*(1.0d0-achi)+vparam(7)*(1.0d0-achi2)

      vpes = vmorse + vtheta + vchi
      return
      end
```

Writing this file may be time consuming. In the case of benzene-water, the arbitrary Cartesian coordinate system used to define the benzene-water structure was first changed to a benzene-centered coordinate system. Various potential terms were defined with respect to this coordinate system. Test the potential function to make sure it compiles. Type "xlf -c pesbw.f" in the benzene-water case.

The last file to edit in this directory is Makefile. Two items which need to be edited are in the first and the last line. In the first line, the entry "pesbw.o" must be changed to the name of a new potential function one wishes to use. In the last line, "`../BIN/q0_BW`" must be changed to "../BIN/(*executable filename*)". The following is an example of a Makefile.

```
OBJS0 = qrw.o wrw.o wrwd.o dwconf.o inigra.o pesbw.o

LIB = ../LIBNUM2/librand.a

# SGI - indy
#FFLAGS =  -Olimit 2700 -O -sopt -col120 -mips2
#FORT = f77

# HP
#FFLAGS =  +es

# IBM 6000
FFLAGS = -O3
FORT = xlf

q0_BW: $(OBJS0)
$(FORT)   -o ../BIN/q0_BW $(FFLAGS) $(OBJS0) $(LIB)
```

Once this is done, give the command "make" in the `QCLUSTER/SRC_ALL` directory. An executable file will be created as QCLUSTER/BIN/(*executable filename*). (Or `QCLUSTER/BIN/q0_BW` for benzene-water.)

After the executable is ready, the input file can be created. The input file should be located in QCLUSTER/(*directory of your choice*), (QCLUSTER/bw), and should be called q0.input. An example for benzene-water is given below. Details of this file are given in the manual. When the input file is ready, type "../BIN/(*executable filename*)", or "`../BIN/q0_BW`". This produces several output files in the working directory (QCLUSER/bw): Resuming.out is where the results are printed, and `ddConfigs_all.dat` is where the information necessary to obtain expectation values are stored. Depending on the number of iterations, defined as the variable "iseed" in QCLUSTER, this step may take anywhere from tens of minutes to tens of hours.

```
2
ASY 12
12.0 0.7 1.212 0.0
12.0 1.4 0.0 0.0
12.0 0.7 -1.212 0.0
12.0 -0.7 -1.212 0.0
12.0 -1.4 0.0 0.0
12.0 -0.7 1.212 0.0
1.00783 1.240 2.1473 0.0
1.00783 2.48 0.0 0.0
1.00783 1.24 -2.1473 0.0
1.00783 -1.24 -2.1473 0.0
1.00783 -2.48 0.0 0.0
1.00783 -1.24 2.1473 0.0
ASY 3
1.00783 0.768516 -0.52853 0.0
15.994910 0.000009 0.066601 0.0
1.00783 -0.768584 -0.528418 0.0
<-------------blank line
0.0 0.0 4.2
0.5 0.5 0.5
<-------------blank line
4.0d10
2.45d10 4.35d10
60.0 500
30.0 500
<-------------blank line
2
1
```

The first line gives the number of molecules. The second line indicates that the first molecule is an asymmetric top with 12 atoms. The benzene Cartesian coordinates are given. The second molecule is an asymmetric top with 3 atoms. Following the coordinates and one blank line, the location of the initial gaussian distribution of

particles is given. Three initial random numbers are also provided. The lines "60.0 500" and "30.0 500" command the simulation to first run 500 steps with 60 time units for each step, and then average for 500 steps with 30 time units for each step. The number of generations the simulation will keep track is 2 and the number of iterations is 1.

The last step is to obtain expectation values by editing or creating files in the QCLUSTER/DST directory. For example, dst.f and avevalue.f contain codes necessary to calculate rotational constants, a radial distribution function, and angular distribution functions. Again, the first line and the last line of Makefile must be edited to refer to the correct object files and names. Once this is done, type "make" which will creat an executable (`dst_avenew`) in the QCLUSTER/BIN directory. In order to obtain the expectation values, return to the working directory (QCLUSTER/bw) and run the executable (`../BIN/dst_avenew`). The expectation values will be printed in files specified by the codes (Res and avevalue.out). The dst.f, avevalue.f and the Makefile are printed below.

```
c ------>> dst.f, calculate distribution functions <<-----------
      program dst
      parameter (NatALL=18)
      implicit   double precision (a-h,o-z)
      character*3 type
      dimension  rsys(NatALL,3),rintc(NatALL,3),
     +  ddconf(NatALL*3),
     +  dmass(NatALL),aCLvec(3),bCLvec(3),cCLvec(3),
     +  rrbw(201),rtheta(91),rchi(91),rphi(91)
      data       UnitMass /1822.9321/ !1amu = m(12C)/me a.u. ~ 1822 a.u.
      data       pi /3.14159265359/
      data       ams /1.e-10/
      data       Bohr /5.2918e-11/ !m
      data       Hartree /2.195e5/ !1/cm
      data       speedli /2.99792e10/ !cm/sec

      open(9,file='dst.input',status='old')
      open(20,file='ddConfigs_all.dat',status='old',form='unformatted')
      open(30,file='Res',status='unknown')
open(40,file='avevalue.out')
 103  format(a3,i6)

      read(20)NCcyc
      read(9,*)Nruns
      NCall = Nruns*NCcyc
      read(9,*)Nmol
```

```
      Natoms = 0
      do imol=1,Nmol
         read(9,103)type,NatTMP
         if (imol.eq.1) Nfirst=NatTMP
         Natoms = Natoms + NatTMP
      end do
      if (Natoms.gt.NatALL) then
         print*,'our system has more atoms than permited'
         print*,'change the NatALL parameter'
         stop
      end if
      close(9)

      open(10,file='masses.dat',status='old')
      do iat=1,Natoms
         read(10,*)dmass(iat)
         dmass(iat) = dmass(iat)*UnitMass
      end do

      open(3,file='1stmol_rot.dat',status='unknown')
      do iref=1,Nfirst
         read(3,*)(rsys(iref,kkm),kkm=1,3)
      end do
      close(3)

      Nrel = Natoms-Nfirst

      sum = 0.d0
      arTOT = 0.d0
      brTOT = 0.d0
      crTOT = 0.d0

      do icyc=1,NCall
         read(20)Ndd
         do m=1,Ndd
               read(20)(ddconf(ik),ik=1,Nrel*3),dd
               dd = dd/NCall
               sum = sum + dd

c--------------> calculating principal axis and rotatinal constants
               do iat=Nfirst+1,Natoms
                  iatTMP = iat - Nfirst
                  do ic=1,3
                     rsys(iat,ic) = ddconf((iatTMP-1)*3+ic)
                  end do
               end do
               call inertm(rsys,dmass,NatALL,Natoms,rintc,ai,bi,ci,
     +                        aCLvec,bCLvec,cCLvec)
               arTOT = arTOT + 0.5*dd/ai
               brTOT = brTOT + 0.5*dd/bi
               crTOT = crTOT + 0.5*dd/ci
c-------->Add any properties you want to average right here! rsys
c--------> are the atom locations.
c avevalue will return R, theta and chi.
```

```
call avevalue(rsys,NatALL,rbw,theta,chi,phi)
rbw=rbw*Bohr
rbw=rbw*1e10*50
irbw=int(rbw)-140
if((irbw.ge.0).and.(irbw.le.200)) then
rrbw(irbw)=rrbw(irbw)+dd
endif
c-------> Now for theta, we need to weight for the volume
c-------> element.
deg=3.14d0/180.0d0
theta=theta*0.5d0*180.0d0/3.14d0
itheta=int(theta)
abt=itheta*2.0d0
abt=sqrt(abt*abt)
abt=abt*deg
abt2=abt+2.0d0*deg
c        abt's are absolute values of theta, vthew is the
c        volume element weight
vthew=(0.556d0*sin(abt2))**2-(0.556d0*sin(abt))**2
if((itheta.ge.0).and.(itheta.le.90)) then
rtheta(itheta)=rtheta(itheta)+dd/vthew
endif
c-------> Similar volume weighting for chi coordinate.
chi=chi*180.d0/3.14d0
ichi=int(chi)
abchi=ichi*1.0d0
abchi=sqrt(abchi*abchi)
abchi=abchi*deg
abchi1=abchi+deg
vweight=(rbw*sin(abchi1))**2-(rbw*sin(abchi))**2
if((ichi.ge.0).and.(ichi.le.90))then
rchi(ichi)=rchi(ichi)+dd/vweight
endif
c--------> Do the phi coordinate to make sure that
c--------> it's flat.
phi=phi*180.0d0/3.14d0*0.25d0+45.0d0
iphi=int(phi)
if((iphi.ge.0).and.(iphi.le.90))then
rphi(iphi)=rphi(iphi)+dd
endif
c---------------------->>>end of new average properties.
         end do
      end do
      close(20)
c-----------> calculate the sum of dd for each coordinate
c-----------> without weighting factor, each sum of dd should
c-----------> = 1.0
totrrbw=0.0d0
do is=0,200
totrrbw=totrrbw+rrbw(is)
end do
totrtheta=0.0d0
totrchi=0.0d0
totrphi=0.0d0
```

```
avetheta=0.0d0
do isum=0,90
totrtheta=totrtheta+rtheta(isum)
totrchi=totrchi+rchi(isum)
totrphi=totrphi+rphi(isum)
xsum=isum*2.0d0
avetheta=avetheta+xsum*rtheta(isum)
end do
avetheta=avetheta/totrtheta
c-----> output
629   format(a5,f10.2,a5)
      write(30,*)' Total Probability on averaging = ',sum
      write(30,*)('-',i=1,60)
      write(30,*)' Rotational Constants '
      write(30,*)('-',i=1,60)
      write(30,629)' A = ',arTOT*speedli*1e-6*Hartree,' MHz'
      write(30,629)' B = ',brTOT*speedli*1e-6*Hartree,' MHz'
      write(30,629)' C = ',crTOT*speedli*1e-6*Hartree,' MHz'
      write(30,*)
write(40,*)'rbw'
do i=0,200
write(40,*)i,rrbw(i)
end do
write(40,*)'totrrbw=',totrrbw
write(40,*)'theta'
do i=0,90
write(40,*)i,rtheta(i)
end do
write(40,*)'totrtheta=',totrtheta
write(40,*)'average theta=',avetheta
write(40,*)'chi'
do i=0,90
write(40,*)i,rchi(i)
end do
write(40,*)'totrchi=',totrchi
write(40,*)'phi'
do i=0,90
iphi=(i-45)*4
write(40,*)iphi,rphi(i)
end do
write(40,*)'totrphi=',totrphi
close(40)
      end



c--------->>>avevalue.f, calculate R, theta, chi, phi <<--------------
      subroutine avevalue(rsys,NatALL,rbw,theta,chi,phi)
      implicit double precision (a-h, o-z)
      dimension rsys(NatALL,3),x(3),y(3),z(3),w(3,3),wrot(3,3),bcm(3)

c This function is called by dst.f.  This is used to calculate the
c position variables, R(b-w), theta, chi.
```

```
c First, define axes.
      ax = 0.d0
      ay = 0.d0
      do i=1,3
         x(i) = rsys(1,i) - rsys(4,i)
         ax = ax + x(i)**2
         y(i) = rsys(2,i) - rsys(6,i)
         ay = ay + y(i)**2
         bcm(i) = (rsys(1,i) + rsys(4,i))/2.0d0
      end do
      ax = sqrt(ax)
      ay = sqrt(ay)
c Define w(i,j), water position relative to benzene-cm
      do i=1,3
         x(i) = x(i)/ax
         y(i) = y(i)/ay
         do j=1,3
            w(i,j) = rsys(12+i,j) - bcm(j)
         end do
      end do
c Find rbw, bz-cm to water-O distance.
      rbw=0.0d0
      do i=1,3
rbw=rbw+w(2,i)**2
      end do
      rbw = sqrt(rbw)
c Find unit vector z(x',y',z') in the benzene frame from the lab frame
c x',y',z'.
      z(1) = x(2)*y(3) - x(3)*y(2)
      z(2) = x(3)*y(1) - x(1)*y(3)
      z(3) = x(1)*y(2) - x(2)*y(1)
c Define wrot(i,j) which are the coordinate for water in the benzene
c coordinate system.
      do i=1,3
         wrot(i,1) = 0.d0
         wrot(i,2) = 0.d0
         wrot(i,3) = 0.d0
         do j=1,3
            wrot(i,1) = wrot(i,1) + w(i,j)*x(j)
            wrot(i,2) = wrot(i,2) + w(i,j)*y(j)
            wrot(i,3) = wrot(i,3) + w(i,j)*z(j)
         end do
      end do
c Find chi.  by finding bz-O distance, xlbo, and then the bz-O distance
c along the z axis, zlbo.  angle = 90 is what is defined as chi=0.
c But bz-O distance is rbw found above.
zlbo=abs(wrot(2,3))
achi=zlbo/rbw
chi=acos(achi)
c Find theta.  Locate the H-H midbond.  Take the angle between the vector
c to the midbond and the projection onto axis normal to benzene plane
c and colinear with Oxygen.
hhx=wrot(2,1)-(wrot(1,1)+wrot(3,1))/2.0d0
hhy=wrot(2,2)-(wrot(1,2)+wrot(3,2))/2.0d0
```

```
zoh=abs(wrot(2,3))
xyzoh=abs(wrot(1,3)+wrot(3,3))/2.0d0
hhz=zoh-xyzoh
xlohh=hhx**2+hhy**2+hhz**2
xlohh=sqrt(xlohh)
atheta=hhz/xlohh
theta=acos(atheta)
c Find phi by looking at the first hydrogen against the X and Y axes
c defined by benzene.
h1x=wrot(1,1)
h1y=wrot(1,2)
aphi=h1x/sqrt(h1x**2+h1y**2)
phi=acos(aphi)
if (h1y.lt.0.0d0) then
phi=-1.0d0*phi
endif
      return
      end
```

The Makefile contains:

```
OBJS10 = dst.o avevalue.o

LIB = ../LIBNUM2/librand.a

# IBM-AIX
FFLAGS =  -O3
FORT = xlf

# HP
#FFLAGS =  -O +es
#FFLAGS =  -C +es

dst: $(OBJS10)
$(FORT)   -o ../BIN/dst_avenew $(FFLAGS) $(OBJS10) $(LIB)
```

Appendix G: PI theory for $(D_2O)_3$

This appendix details the derivation of the permutation inversion (PI) group G_{48} for the water trimer. The PI group for water trimer was first described as G_{96} by Pugliano and Saykally [1], but later re-evaluated to be G_{48}. The following derivation was accomplished with much help from Jennifer Loeser at University of California at Berkeley; she was particularly helpful in the determination of G_{48} character table.

Several PI groups will be examined, beginning with the most simple case, and compared to the observed quartet pattern. Once the PI group, character table and the spin statistics are worked out, the selection rules will be evaluated. In each step, the expected spectral patterns will be compared with that observed until a PI group that refects the measurements is found. The reader is also refered to the PI group G_{96} of $(D_2O)_3$ is worked out by Balasubramanian and Dyke [2].

I will begin by assuming a cyclic structure. This will aid in visualizing the operations in the group. As seen in Figure .6, the oxygen atoms are labeled A, B, and C. The hydrogen atoms attached to A are 1 and 2, those attached to B are 3 and 4, and those attached to C are 5 and 6. The next assumption about the structure is that the "flipping" motion is very facile, leading to a symmetric top with three-fold symmetry. One such three-fold symmetric structure is a planar structure. We will, therefore, use the planar structure as the reference geometry. The point group for the planar structure is $C_{3h}=\{E, C_3, C_3^2, \sigma_h, S_3, S_3^5\}$. The corresponding PI group is $C_{3h(M)}$ = { E, (ACB)(153)(246), (ABC)(135)(246), E*,(ACB)(153)(264)*, (ABC)(135)(246)*}, where the operations have been written in corresponding order. The character table for this flipping symmetric top can be found in Cotton under C_{3h} and is reproduced below(Table .4).

We will evaluate the spin statistics based on this PI group and character table, and determine if flipping motion alone can account for the splitting in our $(D_2O)_3$ spectra. There are several ways to calculate spin statistics, but a simple method

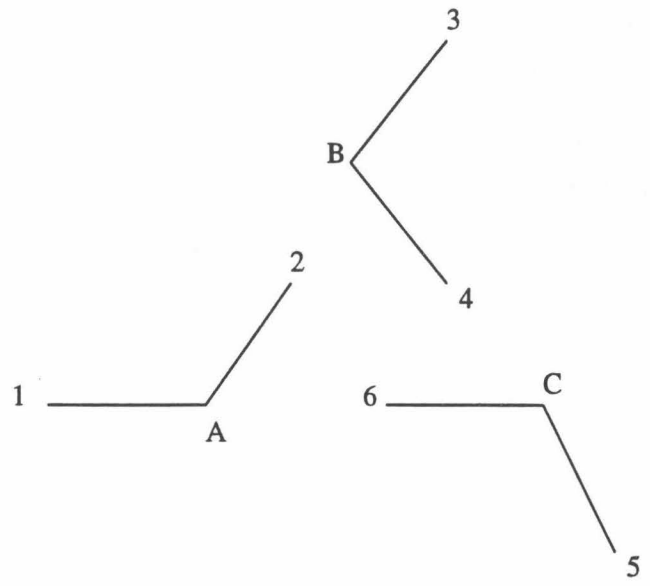

Figure .6: Water trimer in its planar structure and labeling convention used.

Table .4: C_{3h} character table. The notations under JL are those used by J.Loeser and by Liu *et al* [3]. e=exp($2\pi i/3$)

	Operation	E	C_3	C_3^2	σ_h	S_3	S_3^5
JL	Class Size	1	1	1	1	1	1
A_1'	A'	1	1	1	1	1	1
A_2'	E'	1	e	e^*	1	e	e^*
A_3'		1	e^*	e	1	e^*	e
A_1''	A''	1	1	1	-1	-1	-1
A_2''	E''	1	e	e^*	-1	-e	$-e^*$
A_3''		1	e^*	e	-1	$-e^*$	-e

described by K. Balasubramanian will be used in this derivation [4]. Balasubramanian's method works as follows: Spin statistics for a state with A′ symmetry $=P^{A_1'}=\frac{1}{order}\sum^{operations} g\chi(x_1^a x_2^b x_3^c \ldots)$ where g is the class size of an operation, χ is the character for that operation, and x_i^a denotes a cycle of length i and a multiples. For example, an operation (12) is a cycle of length 2, hence, x_2^1. An operation (12)(345) consists of a cycle of length 2, and a cycle of length 3, hence, $x_2^1 x_3^1$. An operation (12)(34) consists of two cycles of length 2, hence, x_2^2. Since the spin statistics come only from the hydrogen atoms, we don't have to worry about the cycles involving oxygen atoms. In $C_{3h(M)}$, E=(1)(2)(3)(4)(5)(6) has x_1^6, (ACB)(153)(264) is x_3^2, and so forth. Using Balasubramanian's equation, we have

$$P^{A_1'} = \frac{1}{6}(x_1^6 + x_3^2 + x_3^2 + x_1^6 + x_3^2 + x_3^2).$$

Now, we only need to substitute the number of spins possible for a molecule of concern to x_i^a. A detailed derivation of this equation is given by Balasubramanian. For $(D_2O)_3$, the number of spins possible for deuterium is 3, i.e., 1 and 0 and -1. For H, it is 2, i.e., -1/2 and 1/2, so

$$P^{A_1'} = \frac{1}{6}(3^6 + 3^2 + 3^2) \cdot 2 = 249.$$

Like wise, for A_2',

$$P^{A_2'} = \frac{1}{6}(1 \cdot 3^6 + e^{2i\pi/3}2^2 + e^{-2i\pi/3}3^2) \cdot 2 = 1/3(3^6 + 3^2(-1)) = 240.$$

Doing the same arithmetic gives us $P^{A_3'} = 240, P^{A_1''} = 0, P^{A_2''} = 0, and P^{A_3''} = 0.$

Now the spacial symmetry must be calculated. For the $(D_2O)_3$ case, we need

(space symmetry) $\times$ (spin symmetry) = A' or A''.

space symmetry	$\times$	*spin symmetry*	=	*overall*	*Stat. Wt.*
A_1'		A_1'		A_1'	249
A_2'		A_3'		A_1'	240
A_3'		A_2'		A_1'	240
A_1''		A_1'		A_1''	249
A_2''		A_3'		A_1''	240
A_3''		A_2'		A_1''	240

The A_2' and A_3' form E', and A_2'' and A_3'' form E'', so there should be four states with spin weights of 249, 480, 249, 480. The spectrum does not agree with this pattern.

Next, we will examine the "clockwise-counter clockwise" (cw-ccw) motion with the "flipping" motion. We must combine the $C_{3h(M)}$ group with the cw-ccw motions consisting of the following operations:{ (AB)(13)(24), (AC)(15)(26), (BC)(35)(46), (AB)(13)(24)*, (AC)(15)(26)*, (BC)(35)(46)* }. We obtain the following:

New operations	*Isomorphic with*	D_{3h}
E	$\rightarrow$	E
$(ACB)(153)(264), (ABC)(135)(246)$	$\rightarrow$	$2C_3$
$(AB)(13)(24), (AC)(15)(26), (BC)(35)(46)$	$\rightarrow$	$3C_2$
E^*	$\rightarrow$	σ_h
$(ACB)(153)(264)^*, (ABC)(135)(246)^*$	$\rightarrow$	$2S_3$
$(AB)(13)(24)^*, (AC)(15)(26)^*, (BC)(35)(46)^*$	$\rightarrow$	$3\sigma_v$

The character table including the cw-ccw motion and the flipping motion is, thus, simply obtained from Cotton under D_{3h} (Table .5) [5].

Using the character table, we can calculate the spin weights as before. The order of this group is 12, i.e., it is G_{12}.

$$P^{A_1'} = \frac{1}{12}(3^6 + 2 \cdot 3^2 + 3 \cdot 3^2 \cdot 3^2) \cdot 2 = 165.$$

Table .5: D_{3h} character table

D_{3h}	E	C_3	C_2	σ_h	S_3	σ_v
Class size	1	2	3	1	2	3
A_1'	1	1	1	1	1	1
A_2'	1	1	-1	1	1	-1
E'	2	-1	0	2	-1	0
A_1''	1	1	1	-1	-1	-1
A_2''	1	1	-1	-1	-1	1
E''	2	-1	0	-2	1	0

$$P^{A_2'} = \frac{1}{12}(3^6 + 2 \cdot 3^2 - 3 \cdot 3^2) \cdot 2 = 84.$$

$$P^{E'} = \frac{1}{12}(2 \cdot 3^6 - 2 \cdot 3^2) \cdot 2 = 240.$$

$$P^{A_1''} = 0,$$

$$P^{A_2''} = 0,$$

and

$$P^{E''} = 0.$$

When the spacial symmetry are taken in to consideration, we have:

space symmetry	×	*spin symmetry*	=	*overall*	*Stat. Wt.*
A_1'		A_1'		A_1'	165
A_2'		A_2'		A_1'	84
E'		E'		$A_1' + A_2' + E'$	240
A_1''		A_1'		A_1''	165
A_2''		A_2'		A_1''	84
E''		E'		$A_1'' + A_2'' + E''$	240

Again, these spin statistics do not explain the quartet pattern in the spectra.

Next, consider the "C_2" motion, which involves rotating the water subunits about their C_2 axes. This motion produces the following operations: {E, (12), (34), (56), (12)(34), (12)(56), (34)(56), (12)(34)(56)}. The "C_2" motion is a direct product of

Table .6: C_3 character table

C_3	E	(ABC) C_3	(ACB) C_3^2
A_1	1	1	1
A_2	1	e	e*
A_3	1	e*	e

three monomer C_2 motions, (12), (34) and (56). The direct product $C_2 \otimes C_2 \otimes C_2$ has the same elements as given above. This is a more complicated motion in that it is no longer described by simple rotations and mirror images. It can be described only as a PI group. Since Bunker [6] does not have a character table for the direct product of the C_{3h} and "C_2", we will have to derive it. We will proceed by ignoring the inversion half of C_{3h}, i.e., we will consider the direct product of the group C_3 and "C_2" (see Table .6 for C_3 character table). This reduces the arithmetic necessary. To obtain the full character table for $C_{3h} \otimes$ "C_2", which includes the inversion, we only need to expand the smaller character table of $C_3 \otimes$ "C_2", denoted as R, as follows:

$C_{3h} \otimes$ "C_2"		
	R	R
	R	$-R$

The direct product of $C_3 \otimes$ "C_2" contains:

$\{E$,
$(ACB)(153)(264)$, $(ABC)(135)(246)$,
(12), $(ACB)(153)(264)(12)$, $(ABC)(135)(246)(12)$,
(34), $(ACB)(153)(264)(34)$, $(ABC)(135)(246)(34)$,
(56), $(ACB)(153)(264)(56)$, $(ABC)(135)(246)(56)$,
(12)(34), $(ACB)(153)(264)(12)(34)$, $(ABC)(135)(246)(12)(34)$,
(12)(56), $(ACB)(153)(264)(12)(56)$, $(ABC)(135)(246)(12)(56)$,
(34)(56), $(ACB)(153)(264)(34)(56)$, $(ABC)(135)(246)(34)(56)$,
(12)(34)(56), $(ACB)(153)(264)(12)(34)(56)$, $(ABC)(135)(246)(12)(34)(56)\}$

These operations need to be rewritten to eliminate duplication, and to simplify the notation. For example, the operation (ACB)(153)(264)(12) is the same as (ACB)(153264). The list of unique operations for $C_3 \otimes$ "C_2" is as follows:

$$
\begin{array}{lll}
\{E, & (ACB)(153)(264), & (ABC)(135)(246), \\
(12), & (ACB)(153264), & (ABC)(135246), \\
(34), & (ACB)(154263), & (ABC)(146235), \\
(56), & (ACB)(164253), & (ABC)(136245), \\
(12)(34), & (ACB)(154)(263), & (ABC)(146)(235), \\
(12)(56), & (ACB)(164)(253), & (ABC)(136)(245), \\
(34)(56), & (ACB)(163)(254), & (ABC)(145)(236), \\
(12)(34)(56), & (ACB)(163254), & (ABC)(145236)\}
\end{array}
$$

There are 24 operations, and 48 operations after including inversion.

Now, we need to find the character table for this group. The operations must be sorted into classes before the character table can be constructed. By definition, two operations A and B are in the same class if there is another operation, C, in the group such that $C^{-1}AC=B$ [5]. We also know that the operations in a given class have the same cycles. Thus, one may make preliminary guesses and classify the operations in the following sets:

$$Set\ a = \{E\},$$

$$Set\ b = \{(ACB)(153)(264), (ACB)(154)(263), (ACB)(164)(253), (ACB)(163)(254)\},$$

$$Set\ c = \{(ABC)(135)(246), (ABC)(146)(235), (ABC)(136)(245), (ABC)(145)(236)\},$$

$$Set\ d = \{(12)(34), (12)(56), (34)(56)\},$$

$$Set\ e = \{(12)(34)(56)\},$$

$$Set\ f = \{(ACB)(163254), (ACB)(153264), (ACB)(154263), (ACB)(164253)\},$$

$$Set\ g = \{(ABC)(145236), (ABC)(135246), (ABC)(146235), (ABC)(136245)\},$$

$$Set\ h = \{(12), (34), (56)\}.$$

These guesses can be checked using a pair of operations which are inverse to each other. For example, (ABC)(135)(246) is an inverse of (ACB)(153)(264). For the operation (12), [(ABC)(135)(246)](12)[(ACB)(153)(264)] = (34). Thus, (12) and (34) are in the same class. Similar arithmetic will show that the guesses above are correct. There are 8 classes with class sizes 1, 1, 3, 3, 4, 4, 4 and 4. This is the same class structure as tetrahedral point group. Here, we are tempted to assume that the correct character table is that of T_h point group (see Table .7). However, it should be derived.

Table .7: The character table for the point group T_h. The sets of operations are noted with the shorthand defined in the text.

	T_h	a	b	c	d	e	f	g	h
JL	Class Size	1	4	4	3	1	4	4	3
A'_1	A	1	1	1	1	1	1	1	1
A'_2	A	1	e	e*	1	1	e	e*	1
A'_3	A	1	e*	e	1	1	e*	e	1
B''_1	A	1	1	1	1	-1	-1	-1	-1
B''_2	A	1	e	e*	1	-1	-e	-e*	-1
B''_3	A	1	e*	e	1	-1	-e*	-e	-1
F_B	T	3	0	0	-1	3	0	0	-1
F_A	T	3	0	0	-1	-3	0	0	1

The notations under JL are the those used by J. Loeser.

The lengthy derivation of the complete $C_3 \otimes$"C_2" character table was obtained with much assistance from Jennifer Loeser at the University of California at Berkeley.

The derivation is split into two parts. First, the character table for the direct product "C_2"=$C_2 \otimes C_2 \otimes C_2$ is obtained. Then the $C_3 \otimes$"C_2" character table is calculated.

Each C_2 has the following character table:

C_2	E	$C_2 = (12)$
A	1	1
B	1	-1

The direct product will have the elements {E, (12), (34), (56), (12)(34), (12)(56), (34)(56), (12)(34)(56)}, as found above, and representations

$$A \otimes A \otimes A,$$

$$A \otimes A \otimes B, A \otimes B \otimes A, B \otimes A \otimes A,$$

$$A \otimes B \otimes B, B \otimes A \otimes B, B \otimes B \otimes A,$$

$$B \otimes B \otimes B.$$

Characters for these representations are obtained by simple arithmetic. For A⊗A⊗B, the character under operation E=(E, E, E) is $1 \cdot 1 \cdot 1 = 1$, under (12)=((12), E, E) is $1 \cdot 1 \cdot 1 = 1$, under (34)=(E, (34), E) is $1 \cdot 1 \cdot 1 = 1$, under (12)(34)=((12), (34), E) is $1 \cdot 1 \cdot 1 = 1$, under (56)=(E, E, (56)) is $1 \cdot 1 \cdot -1 = -1$, under (12)(56)=((12), E, (56)) is $1 \cdot 1 \cdot -1 = -1$, under (34)(56)=(E, (34), (56)) is $1 \cdot 1 \cdot -1 = -1$, and under (12)(34)(56) is $1 \cdot 1 \cdot -1 = -1$. Similarly, when all the representations are calculated, we find the character table for "C_2" (see Table .8).

Table .8: Character table for the direct product $C_2 \otimes C_2 \otimes C_2$.

"C_2"	E	(12)	(34)	(12)(34)	(56)	(12)(56)	(34)(56)	(12)(34)(56)
A⊗A⊗A	1	1	1	1	1	1	1	1
B⊗B⊗B	1	-1	-1	1	-1	1	1	-1
A⊗A⊗B	1	1	1	1	-1	-1	-1	-1
A⊗B⊗A	1	1	-1	-1	1	1	-1	-1
B⊗A⊗A	1	-1	1	-1	1	-1	1	-1
A⊗B⊗B	1	1	-1	-1	-1	-1	1	1
B⊗A⊗B	1	-1	1	-1	-1	1	-1	1
B⊗B⊗A	1	-1	-1	1	1	-1	-1	1

To obtain $C_3 \otimes$"C_2", we perform similar arithmetic. For the direct products of $A \otimes A \otimes A \otimes A_n$ $(n = 1, 2, 3)$ and $B \otimes B \otimes B \otimes A_n$ $(n = 1, 2, 3)$, we obtain the results summarized in Table .9.

We note that A⊗A⊗B and A⊗B⊗A and B⊗A⊗A are the same except that the water, which has B symmetry, is changed among them. These are degenerate and

Table .9: One-dimensional characters of $C_3 \otimes$ "C_2"

	a	b	c	d	e	f	g	h
$A \otimes A \otimes A \otimes A_1$	1	1	1	1	1	1	1	1
$A \otimes A \otimes A \otimes A_2$	1	e*	e	1	1	e*	e	1
$A \otimes A \otimes A \otimes A_3$	1	e	e*	1	1	e	e*	1
$B \otimes B \otimes B \otimes A_1$	1	1	1	1	-1	-1	-1	-1
$B \otimes B \otimes B \otimes A_2$	1	e*	e	1	-1	-e*	-e	-1
$B \otimes B \otimes B \otimes A_3$	1	e	e*	1	-1	-e	-e*	-1

compose a three-dimensional representation. The characters of the direct product for each one of these with A_n $(n = 1, 2, 3)$ are given in Table .10.

Table .10: Characters for each of the AAB type three-dimensional representations.

	a	b	c	d	e	f	g	h
$A \otimes A \otimes B \otimes A_1$	1	1	1	1	-1	1	1	1
$A \otimes A \otimes B \otimes A_2$	1	e*	e	1	-1	e*	e	1
$A \otimes A \otimes B \otimes A_3$	1	e	e*	1	-1	e	e*	1
$A \otimes B \otimes A \otimes A_1$	1	1	1	-1	-1	1	1	1
$A \otimes B \otimes A \otimes A_2$	1	e*	e	-1	-1	e*	e	1
$A \otimes B \otimes A \otimes A_3$	1	e	e*	-1	-1	e	e*	1
$B \otimes A \otimes A \otimes A_1$	1	1	1	-1	-1	-1	-1	-1
$B \otimes A \otimes A \otimes A_2$	1	e*	e	-1	-1	-e*	-e	-1
$B \otimes A \otimes A \otimes A_3$	1	e	e*	-1	-1	-e	-e*	-1
Total	9	0	0	-3	-9	0	0	3

The sum of the character under each operation is (9 0 0 -3 -9 0 0 3). Since the degeneracy is 3, we divide this total by three to get the character for one of the representations and find (3 0 0 -1 -3 0 0 1), which is the same pattern for T under T_h or F_A in the JL notation (see Table .7). Similar exercises show that the other three degenerate representations from "C_2" yield the characters for F_B under the JL notation. Thus, we see that the $C_3 \otimes$ "C_2" character table is isomorphic with T_h. The G_{48} character table can then be generated by forming a matrix

G_{48}		
	T_h	T_h
	T_h	$-T_h$

Using the character table, we can determine the spin statistics as we did for the other two test cases, namely

$$P^{A_1} = 3^6 + 3 \cdot 3^5 + 3 \cdot 3^4 + 3^3 + 4 \cdot 3^2 + 4 \cdot 3^2 + 4 \cdot 3 + 4 \cdot 3 = 76.$$

$$P^{A_1} = 3^6 + 3 \cdot 3^5 + 3 \cdot 3^4 + 3^3 + 4 \cdot 3^2 \cdot e + 4 \cdot 3^2 \cdot e^* + 4 \cdot 3 \cdot e + 4 \cdot 3 \cdot e^* = 70.$$

Likewise, we find $P^{A_3} = 70$, $P^{B_1} = 11$, $P^{B_2} = 8$, $P^{B_3} = 8$, $P^{F_A} = 108$, $P^{F_B} = 54$. This set of spin statistics can reproduce the intensity patterns seen in the spectra, that is, there are more than four branches possible, whereas in the previous two cases, there was no way to obtain four states with the given spin statistics.

We must now construct the correlation table to see if the G_{24} group, or with inversion, G_{48}, can reproduce the quartet intensity pattern. To do this, we investigate the correlation between C_{3h} and G_{48}. In the C_{3h} group, different K states have different irreducible representations [7]. The "C_2" motion splits each K state. We must now determine how each irreducible representation in C_{3h} splits to give the irreducible representations in G_{48}. In order to test if the A_1^+ in G_{48} correlates with A_1' in C_{3h}, we use the following equation:

$$a_{A_1'}^{A_1^+} = \frac{1}{6} \sum_{operations} \chi^{\Gamma_{A_1^+}}[operation]\chi^{\Gamma_{A_1'}}[operation] = \frac{1}{6}(1 \cdot 1 + 1 \cdot 1 + 1 \cdot 1) \cdot 2 = 1.$$

This shows that A_1^+ in G_{48} correlates with A_1' in C_{3h}. Similarly, we can test whether A_1^+ in G_{48} correlates with A_2' in C_{3h}.

$$a_{A_2'}^{A_1^+} = \frac{1}{6}(1 \cdot 1 + e \cdot 1 + e^* \cdot 1) \cdot 2 = 0.$$

This shows that A_1^+ in G_{48} does **not** correlate with A_2' in C_{3h}. A series of similar tests show the following correlations:

$$
\begin{aligned}
G_{48} &\leftrightarrow C_{3h} \\
A_1^+ &\leftrightarrow A_1' \\
A_2^+ &\leftrightarrow A_2' \\
A_3^+ &\leftrightarrow A_3' \\
B_1^+ &\leftrightarrow A_1' \\
B_2^+ &\leftrightarrow A_2' \\
B_3^+ &\leftrightarrow A_3' \\
F_A^+ &\leftrightarrow A_1', A_2', A_3' \\
F_B^+ &\leftrightarrow A_1', A_2', A_3' \ , \\
A_1^- &\leftrightarrow A_1'' \\
A_2^- &\leftrightarrow A_2'' \\
A_3^- &\leftrightarrow A_3'' \\
B_1^- &\leftrightarrow A_1'' \\
B_2^- &\leftrightarrow A_2'' \\
B_3^- &\leftrightarrow A_3'' \\
F_A^- &\leftrightarrow A_1'', A_2'', A_3'' \\
F_B^- &\leftrightarrow A_1'', A_2'', A_3''
\end{aligned}
$$

or for the reverse correlations,

$$
\begin{aligned}
A_1' &\leftrightarrow A_1^+, B_1^+, F_A^+, F_B^+ \\
A_2' &\leftrightarrow A_2^+, B_2^+, F_A^+, F_B^+ \\
A_3' &\leftrightarrow A_3^+, B_3^+, F_A^+, F_B^+ \\
A_1'' &\leftrightarrow A_1^-, B_1^-, F_A^-, F_B^- \\
A_2'' &\leftrightarrow A_2^-, B_2^-, F_A^-, F_B^- \\
A_3'' &\leftrightarrow A_3^-, B_3^-, F_A^-, F_B^-
\end{aligned}
$$

In the C_{3h} point group, rotations corresponding to $K_c = 0, \pm 3, \pm 6, \ldots$, must have

a character under (ACB) and (ABC) equal to 1 [7]. This is only true for A_1' and A_1''. Thus, for $(D_2O)_3$, the $K_c = 0, \pm 3, \pm 6, \ldots$ states have, after being split by the "C_2" motion, spin statistics of A_1=76, B_1=11, F_A=108 and F_B=54. For $K_c \neq 0, \pm 3, \pm 6, \ldots$, A_2 and A_3 are the appropriate irreducible representations. Thus, the spin statistics for these states are, A_2 or A_3 = 70, B_2 or B_3 = 8, F_A=108 and F_B=54. Most telling difference is between the weakest and the strongest line with a factor of ~10 difference. In the G_{96} assignment made by Pugliano and Saykally [1], the largest difference in the spin statistics was a factor of 3.5. After more careful measurements, the spin statistic patterns of G_{48} matched the intensity patterns observed [3].

The final order of business is to establish the selection rules. For a dipole-allowed transition, we require $\Gamma^+ \Leftrightarrow \Gamma^-$. This means that in C_{3h}, we permit $A' \Leftrightarrow A''$, $A' \Leftrightarrow E''$, $A'' \Leftrightarrow E'$, and $E' \Leftrightarrow E''$. This can be checked as follows: For $A' \Leftrightarrow A''$, pick from G_{48} notations the A_1^+ correlating to A′ and A_1^- correlating to A″, for which $A_1^+ \otimes A_1^- = A_1^-$. This is an anti-symmetric representation, and so is allowed. Another example may be $E' \Leftrightarrow E''$ in C_{3h}, or $F_A^+ \Leftrightarrow F_A^-$ in G_{48}. The direct product $F_A^+ \otimes F_A^-$ contains the A_1^- representation when it is reduced. Similar checks of the various states are used to determine the selection rules presented in Chapter 5.

In terms of the notation by M. Schütz, m corresponds to the pseudorotation of the trimer about the oblate top axis. The rotation about the oblate top axis is described by K_c. Thus, the selection rules for the corresponding m states are the same as those for K_c given above.

Bibliography

[1] N. Pugliano and R.J. Saykally. Measurement of Quantum Tunneling Between Chiral Isomers of the Cyclic Water Trimer. *Science*, 257:1937, 1992.

[2] K. Balasubramanian and T. Dyke. Nuclear Spin Species, Statistical Weights, and Correlation Tables for Weakly Bound Van Der Waals Complexes. *J. Phys. Chem.*, 88:4688, 1984.

[3] K. Liu, M.J. Elrod, J.G. Loeser, J.D. Cruzan, N. Pugliano, M.G. Brown, J. Rzepiela, and R.J. Saykally. Far-IR Vibration-Rotation Tunneling Spectroscopy of the Water Trimer. *Faraday Dis.*, 97:35, 1994.

[4] K. Balasubramanian. Generating Functions for the Nuclear Spin Statistics of Nonrigid Molecules. *J. Chem. Phys.*, 75:4572, 1981.

[5] F.A. Cotton. *Chemical Applications of Group Theory.* Wiley-Interscience, New York, NY, 1963.

[6] P.R. Bunker. *Molecular Symmetry and Spectroscopy.* Academic Press, New York, NY, 1979.

[7] Jr. E.B. Wilson. The Statistical Weights of the Rotational Levels of Polyatomic Molecules, Including Methane, Ammonia, Benzene, Cyclopropane and Ethylene. *J. Chem. Phys.*, 3:276, 1935.